Book of Abstracts

Vancouver, BC, Canada

Dear Participants,

The 8th Pacific Rim Conference on Rheology will be held in Vancouver, on the Point Grey campus of the University of British Columbia (UBC)[1], May 15 – 19, 2023. It will host discussions on rheological research in fundamental and traditional areas of rheology, non-Newtonian fluid mechanics, nano-technology, biomaterials and special technical sessions directed at natural resource industries.

The conference is a joint effort of the Canadian Society of Rheology and the University of British Columbia. The organizing committee welcomes the participants to enjoy the diverse talks on various topics related to rheology and fluid mechanics, engage in friendly discussions with their peers, all while experiencing the beautiful landscapes of UBC and western Canada. We encourage young scientists to have discussions with world-class experts and use this unique opportunity for networking.

We wish to thank all who have contributed organising this event: plenary speakers, exhibitors, contributing universities, research institutes and companies, and participants.

Secretary General: Prof. Ian A. Frigaard, University of British Columbia, Canada.

Technical Committee Chair: Prof. Savvas G. Hatzikiriakos, University of British Columbia, Canada.

Conference Secretary: Dr. Marjan Zare, University of British Columbia, Canada.

Conference Manager: Dr. Mariana Carrasco-Teja, University of British Columbia, Canada.

Abstracts Editor: Dr. Rodrigo S. Mitishita, University of British Columbia, Canada.

Honorary Conference Chair: Prof. A. Jeffrey Giacomin, Queen's University, Canada

[1] *UBC Point Grey Campus is on the unceded Traditional Territory of the xʷməθkʷəy̓əm (Musqueam) People*

Contents

Local Organizing Committee

Abdellah Ajii	(Polytechnique Montreal)	Xi Li	(McMaster University)
Neil Balmforth	(University of British Columbia)	Giovanniantonio Natale	(University of Calgary)
John R. de Bruyn	(University of Western Ontario)	Mark Pawlik	(University of British Columbia)
Gwynn Elfring	(University of British Columbia)	Arun Ramchandran	(University of Toronto)
James Feng	(University of British Columbia)	Denis Rodrigue	(Laval University)
John Frostad	(University of British Columbia)	Joerg Rottler	(University of British Columbia)
Jeffrey Giacomin	(Queen's University, Canada)	Sean Sanders	(University of Alberta)
Dana Grecov	(University of British Columbia)	Marjan Zare	(University of British Columbia)
Marie-Claude Heuzey	(Polytechnique Montreal)	Mohammad Taghavi	(Laval University)
Reghan J. Hill	(McGill University)	Anthony Wachs	(University of British Columbia)
Bern Klein	(University of British Columbia)		

Sponsors and Exhibitors

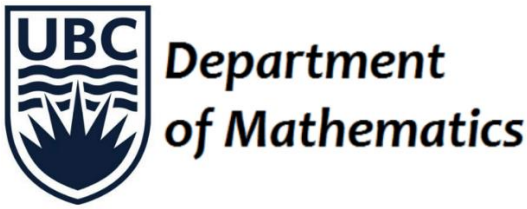

Technical Committee and Symposia

G1. POLYMER SOLUTIONS AND MELTS	**Kyu Hyun**	**(Pusan National University, Korea)**
	Ravi Jagadeeshan	(Monash University, Australia)
	Chen-Yang Liu	(The Chinese Academy of Sciences, China)
G2. INDUSTRIAL RHEOLOGY IN POLYMER PROCESSING	Abdellah Ajii	(Polytechnique Montreal, Canada)
	Joung Sook Hong	(Seoul National University, Korea)
	Denis Rodrigue	(Laval University, Canada)
G3. BLENDS, COMPOSITES AND NANOCOMPOSITES	Yumi Matsumiya	(Kyoto University, Japan)
	Yihu Song	(Zhejiang University, China)
	Wei Yu	(Shanghai Jiao Tong University, China)
G4. SUSPENSIONS AND COLLOIDS	Sarah Hormozi	(Cornell University, USA)
	Anthony Wachs	(University of British Columbia, Canada)
G5. EMULSIONS, FOAMS AND BUBBLES	Reghan James Hill	(McGill University, Canada)
	Arun Ramchandran	(University of Toronto, Canada)
	Marjan Zare	(University of British Columbia, Canada)
G6. SELF-ASSEMBLY AND FLOW-INDUCED SYSTEMS/GELS	Michel Cloitre	(ESPCI, France)
	Takamasa Sakai	(Tokyo University, Japan)
	Kenji Urayama	(Kyoto University, Japan)
G7. BIOMATERIALS AND BIOLOGICAL SYSTEMS	Nicky Eshtiaghi	(RMIT University, Australia)
	Dana Grecov	(University of British Columbia, Canada)
	Jason Stokes	(University of Queensland, Australia)
G8. SOLIDS, GLASSES AND GRANULAR SYSTEMS	George Petekidis	(University of Crete, Greece)
	Dimitris Vlassopoulos	(University of Crete, Greece)
G9. ACTIVE MATTER	Gwynn Elfring	(University of British Columbia, Canada)
	Giovanniantonio Natale	(University of Calgary, Canada)
G10. NON-NEWTONIAN FLUID MECHANICS AND STABILITY	Ruri Hidema	(Kobe University, Japan)
	Li Xi	(McMaster University, Canada)
	Miguel Moyers-Gonzalez	(University of Canterbury, New Zealand)
G12. RHEOLOGY IN THE OIL AND GAS INDUSTRY	Paulo Souza Mendes	(PUC-Rio, Brazil)
	Sean Sanders	(University of Alberta, Canada)
	Mohammad Taghavi	(Laval University, Canada)
G13. RHEOLOGY IN THE MINING INDUSTRY	Leopoldo Gutierrez	(University of Concepcion, Chile)
	Marek Pawlik	(University of British Columbia, Canada)
	Anthony Stickland	(University of Melbourne, Australia)
S2. HIROSHI WATANABE – HONORARY SYMPOSIUM	Savvas G. Hatzikiriakos	(University of British Columbia, Canada)
	Youngdon Kwon	(Sung Kyun Kwan University, Korea)
	Yuichi Masubuchi	(Nagoya University, Japan)

Conference Program

Monday & Tuesday, May 15 and 16, 2023

Monday May 15, 2023
Social Events: Casual Evening and Registrations - The Nest, Level 4 (6:00 PM - 9:00 PM)

Tuesday May 16, 2023		
Plenary Presentation - GEOG 100 (9:00 AM - 10:00 AM) - Chair: Dimitris Vlassopoulos		
Time	**Title**	**Presenter**
9:00 AM	PLENARY: What we learn about yielding from recovery rheology	ROGERS, Simon

Coffee Break - Lounge at MATH 125/126 (10:00 AM - 10:30 AM)

Biomaterials and Biological Systems - GEOG 100 (10:30 AM - 12:10 PM) - Chair: Yaman Boluk		
Time	**Title**	**Presenter**
10:30 AM	Poroelastic Modelling Reveals The Cooperation Between Two Mechanisms For Albuminuria	XU, Zela
10:50 AM	Hydrodynamics and rheology of fluctuating, semiflexible, inextensible, and slender filaments in Stokes flow	DONEV, Aleksandar
11:10 AM	Tribology and rheology of hyaluronic acid based cellulose nanocrystal suspensions	BOSE, Akshai
11:30 AM	Self-organized cable formation and force transmission in an active vertex model for biological tissues	QIU, Mingfeng
11:50 AM	No Talk Scheduled	

Blends, Composites and Nanocomposites - GEOG 212 (10:30 AM - 12:10 PM) - Chair: Reghan Hill		
Time	**Title**	**Presenter**
10:30 AM	Study of the stability of electrical and rheological properties of electrically conductive composites with co-continuous morphology	STRUGOVA, Daria
11:10 AM	Should we keep choosing nano-sized particles to kinetically stabilize co-continuous blends?	SHAH, Rajas
11:30 AM	Rheological and conductive properties of injection- and compression-molded carbon nanotube polymer composites	SLEMENIK PERŠE, Lidija
11:50 AM	No talk scheduled	

Rheology in the Oil and Gas Industry - GEOG 200 (10:30 AM - 12:10 PM) - Chair: Paulo de Souza Mendes		
Time	**Title**	**Presenter**
10:30 AM	KEYNOTE: Assessment of Critical Conditions Required for Effective Hole Cleaning in Horizontal Wells - Effects of Fluid Rheological Properties and Near Wall Turbulence on the Particle Removal From Bed Deposits	KURU, Ergun
11:10 AM	Primary cementing of horizontal wells: laminar displacement flows in obstructed eccentric annuli	ALISHAHI, Marzieh
11:30 AM	Cementing displacement flows of shear-thinning fluids in horizontal wells, with and without casing rotation	RENTERIA, Alondra
11:50 AM	Displacement flows of shear thinning fluids in a vertical annulus	ZHANG, Ruizi

Suspensions and Colloids - GEOG 147 (10:30 AM - 12:10 PM) - Chair: Sarah Hormozi		
Time	**Title**	**Presenter**
10:30 AM	Non-Brownian suspensions in pressure-driven flow: numerical simulations with frame-invariant sub-grid corrections	ORSI, Michel
10:50 AM	Finite system size correction in microrheological analysis under periodic boundary conditions : a direct numerical simulation approach	NAKAYAMA, Yasuya
11:10 AM	Lubrication force between two approaching cylinders in a Bingham fluid	WACHS, Anthony
11:30 AM	Cross Flow Filtration of Viscoplastic Suspensions, a Robust Mathematical Model	IZADI, Mahdi
11:50 AM	Imparting extensibility to jammed colloidal inks for direct-ink-writing printability	SAENGOW, Chaimongkol

Lunch - Lounge at MATH 125/126 (12:10 PM - 12:50 PM)

Plenary Presentation - MATH 100 (12:50 PM - 1:50 PM) - Chair: Paulo de Souza Mendes		
Time	**Title**	**Presenter**
12:50 PM	Sludge rheology and its applications in sludge treatment processes	ESHTIAGHI, Nicky

Biomaterials and Biological Systems – MATH 104 (2:00 PM - 3:40 PM) - Chair: Dana Grecov		
Time	**Title**	**Presenter**
2:00 PM	KEYNOTE: Bioprinting of collagen hydrogels in supported gel environment	BOLUK, Yaman
2:40 PM	Effects of gelation concentration on cyclic deformation behavior of polysaccharide hydrogels	HORINAKA, Jun-ichi
3:00 PM	Tendon fascicle-inspired collagen multifilament bundle produced by multi-pin contact drawing of an aqueous collagen-polyethylene oxide solution	YAGHOOBI, Hessameddin
15:20	Effect of homogenization of raw milk on the physical properties of aged cheese	KANEDA, Isamu

Blends, Composites and Nanocomposites - MATH 203 (2:00 PM - 3:40 PM) - Chair: Denis Rodrigue		
Time	**Title**	**Presenter**
2:00 PM	Formulating adhesives with aminated polyolefins for low surface energy substrate	ZHANG, Ziyue
2:20 PM	Conformational relaxation of styrene-butadiene rubbers having a different microstructure but the same composition at hydrophilic and hydrophobic interface	TANEDA, Hidenobu
2:40 PM	Shape memory and mechano-rheological properties of amine containing polyethylene/polycaprolactone blend	GUSTOWSKI, Jan
3:00 PM	Rheological Evaluation of Polyhydroxyalkanoates (PHAs) through Constitutive Equation Modelling	BEHZADFAR, Ehsan
3:20 PM	Development of Biodegradable and Antiviral Surgical Face Masks from Poly(lactic acid) and Poly(dimethyl siloxane)-based Polyhydroxyurethanes	YOUNES, Georges

Rheology in the Oil and Gas Industry - GEOG 200 (2:00 PM - 3:40 PM) - Chair: Ida Karimfazli		
Time	**Title**	**Presenter**
2:00 PM	Research on stability of electrorheological effect of waxy crude oil	XIE, Yiwei
2:20 PM	Impact of oil composition on electrorheological effect of waxy crude oil	LI, Hongying
2:40 PM	Significance of volume shrinkage on yielding charecteristics of waxy oil	SHINDE, Sachin
3:00 PM	Wall-slip effects on flow restart in a plugged waxy crude oil pipeline	SANYAL, Aniruddha
3:20 PM	Flow restart mechanism in a multiphase gelled pipeline	TIKARIHA, Lomesh

Suspensions and Colloids - GEOG 147 (2:00 PM - 3:40 PM) - Chair: Anthony Wachs		
Time	**Title**	**Presenter**
2:00 PM	KEYNOTE: The Role of Rolling Resistance in the Rheology of Wizarding Quidditch Ball Suspensions	HORMOZI, Sarah
2:40 PM	Adjuvanted silica suspensions: from particles contact properties to rheology	CHATEAU, Xavier
3:00 PM	Rheology of High Performace Cement-Based Materials For Use in Additive Manufacturing	MARTYS, Nicos
3:20 PM	Exploring the interplay between interparticle forces, rheology, and tribology in nanoclay-based nanolubricants	MARTÍN ALARCÓN, Leonardo

Coffee Break - Lounge at MATH 125/126 (3:40 PM - 4:10 PM)

Biomaterials and Biological Systems - MATH 104 (4:10 PM - 5:50 PM) - Chair: Nicky Eshtiaghi		
Time	**Title**	**Presenter**
4:10 PM	Reversal motion of E-coli bacteria in nematic liquid crystals	GORAL, Martyna
4:30 PM	Diffusion of lipid nanoparticles through airway mucus	ROKHFOROUZ, Mohammad Reza
4:50 PM	Oscillatory microfluidic thromboelastograph (micro-TEG) analysis of whole blood coagulation and fibrinolysis	SHIN, SeHyun
5:10 PM	Scale-dependent rheology of synovial fluid lubricating macromolecules	MARTÍN ALARCÓN, Leonardo
5:30 PM	Rheology of corn stover slurries undergoing dilute-acid pretreatment	SAMANIUK, Joseph

Blends, Composites and Nanocomposites - MATH 203 (4:10 PM - 5:50 PM) - Chair: Savvas Hatzikiriakos		
Time	**Title**	**Presenter**
4:10 PM	Rheology of biocomposites	RODRIGUE, Denis
4:30 PM	How morphological and rheological properties of PLA/MWCNT nanocomposites are affected by molecular weight, stereo configuration of PLA, and processing	CARREAU, Pierre
4:50 PM	Compatibilized polylactide/polyamide 11 (PLA/PA11) blends containing multiwall carbon nanotubes: morphology, rheology, electrical and mechanical properties	MOUSAVI, Zeinab
5:10 PM	Why is the pyane effect missing higher harmonics?	WANG, Xiaorong
5:30 PM	Effect of inorganic filler on rheological properties and morphology of polylactic acid(pla)/low-density polyethylene(ldpe) blends	KIM, Min Chan

Rheology in the Oil and Gas Industry - GEOG 200 (4:10 PM - 5:50 PM) - Chair: Ergun Kuru		
Time	**Title**	**Presenter**
4:10 PM	KEYNOTE: Normal stresses at the yielding point	DE SOUZA MENDES, Paulo
4:50 PM	Continuous Monitoring of Yield Stress and Solid Fraction of a Solid Suspension Using a Microfluidic Yield Rheometer	KAVISHVAR, Durgesh
5:10 PM	Hercshel-Bulkley parameter evaluation of oil-based drilling fluids	SAASEN, Arild
5:30 PM	An algebraic thixotropic elasto-viscoplastic model for describing pre-yielding and post-yielding behaviour	KUMAR, Lalit

Suspensions and Colloids - GEOG 147 (4:10 PM - 5:50 PM) - Chair: Gwynn Elfring		
Time	**Title**	**Presenter**
4:10 PM	KEYNOTE: Rheology of active colloids: motility-induced shear-thickening	LÖWEN, Hartmut
4:50 PM	Densitaxis of swimming microorganisms	SHAIK, Vaseem
5:10 PM	Hydrodynamic interactions of active matter near boundaries	ABTAHI, Seyed Arman
5:30 PM	Dynamics of 2D colloidal crystals in the presence of localized internal stresses created by active particles	JOHN, Jacob

Poster Session: Welcome Reception & Poster Session - Sage Bistro (7:00 PM - 10:00 PM)		
Board	**Title**	**Presenter**
	Advances in cone-plate rheometers for busy labs	MOONAY, David
	Active particles crossing sharp viscosity gradients	GONG, Jiahao
	effect of the temperature on the rheological behaviors of lithium-ion batteries anode slurry	김, 예슬
	Rheological differences in anode slurries caused by shape difference between natural and synthetic graphite	KIM, Yeeun
	Two-step yielding behavior of concentrated lithium-ion battery anode slurry	PARK, Jun Dong
	Jamming mechanisms of dilute fibre suspensions under dead-end and cross-flow conditions	VILLALBA CHEHAB, Miguel Esteban
	Diagnosing the state of the battery slurries using a machine learning technique	KANG, Seunghoon
	Rheology and drag reduction and engineering applications of novel oil-phase suspended polyacrylamide slicker water fracturing fluids	LU, Yongjun
	Rheology and self-assembly of carboxylated cellulose nanocrystals	HALLMAN, Madeleine
	Impact of extent of digestion on the shear rheological behaviour of anaerobic digested sludge	ESHTIAGHI, Nicky
	Measuring transient extensional viscosity using filament stretching on an ARES-G2 rheometer	CHEN, Tianhong
	Deformational vorticity in constitutive equations: the co-rigid rotational Maxwell model	MISCHEL, Cody
	Development of extensional rheometer using parallel disk ring	MINEYAMA, Yukihiro
	Optimization of the drag-reducing effect by controlling the preparation conditions of additives	SAEKI, Takashi
	Effects of relaxation time of polymer solutions on the spatio-temporal fluctuation in a two-dimensional flow	FUKUSHIMA, Kengo
	Rheological method to investigate pseudolayer compression elastic constant and the dynamics of the twist-bend nematic liquid crystal	PRAVEEN KUMAR, Mylapalli
	Predicticting the rate of cement plug failure	CHARABIN, Scott
	Microrheology of polyelectrolyte solutions in the semidilute entangled regime	MATSUMOTO, Atsushi
	Gelatinization of individual starch granules	MO, Lanxin
	Effect of asphaltene on the rheological properties of bitumen	PIETTE, Jourdain
	Evaluation of the liquid holdup in a stratified gas-liquid inclined pipeline according to the herschel–bulkley fluid model	XU, Jingyu
	Effect of carbon nanotubes CNTS) dispersity in ag/polydimethylsiloxan (PMDS) composite conductors	JEONG, EunHui
	Influence of viscosity hierarchy on density-unstable fluid-fluid displacement in vertical concentric annuli	GHORBANI, Maryam
	Dynamic viscoelasticity and spinning behavior of an organogelator, PMDA-R, dissolved in various oils	KAIDE, Aya
	Capillary imbibition in a diverging flexible channel	BOUDINA, Mouad

Wednesday, May 17, 2023

Wednesday May 17, 2023		
Plenary Presentation - GEOG 100 (9:00 AM - 10:00 AM) - Chair: Ralph Colby		
Time	**Title**	**Presenter**
9:00 AM	Comparison of viscoelastic and dielectric properties of type-a chain: experimental attempt for deeper understanding of polymer rheology	WATANABE, Hiroshi
Coffee Break - Lounge at MATH 125/126 (10:00 AM - 10:30 AM)		
Blends, Composites and Nanocomposites - GEOG 212 (10:30 AM - 12:10 PM) - Chair: Xiaorong Wang		
Time	**Title**	**Presenter**
10:30 AM	KEYNOTE: Role of network compressibility on the complex conductivity of structured polyelectrolyte hydrogels	HILL, Reghan
11:10 AM	Ultrasound effect on dispersion and distribution of graphitic materials inside different pdms	DEMARQUETTE, Nicole
11:30 AM	Fluid composites as alternatives to solid electrical components	GONZALEZ-GARCIA, Lola
11:50 AM	The rheological properties of hot melt adhesives doped with carbon nanotubes	LATKO-DURAŁEK, Paulina
Hiroshi Watanabe – Honorary Symposium - GEOG 100 (10:30 AM - 12:10 PM) - Chair: Yuichi Masubuchi		
Time	**Title**	**Presenter**
10:30 AM	KEYNOTE: response of block copolymer electrolytes to ionic current	BALSARA, Nitash P.
11:10 AM	Glass transition and entanglement in semiflexible conjugated polymer melts	COLBY, Ralph
11:30 AM	Nano rheology of glassy materials using dielectric molecular probe	INOUE, Tadashi
11:50 AM	Profile of Hiroshi Watanabe	INOUE, Tadashi MATSUMIYA, Yumi
Rheology in the Oil and Gas Industry - GEOG 200 (10:30 AM - 12:10 PM) - Chair: Masoud Daneshi		
Time	**Title**	**Presenter**
10:30 AM	Drift flux modeling of gas release in oil sand tailing ponds	HAJIEGHRARY, Omid
10:50 AM	Rheology of fresh cement paste as affected by cellulose nanofibres and superplasticizer	BINDIGANAVILE, VIVEK
11:10 AM	Defying gravity: the fluid mechanics of off-bottom plug placement	KARIMFAZLI, Ida
11:30 AM	Rheological behavior of mature fine tailings	MALMIR, Amir
11:50 AM	Investigations on methane hydrate formation, dissociation, and viscosity in gas-water-sand system	SONG, Shangfei
Lunch - Lounge at MATH 125/126 (12:10 PM - 12:50 PM)		

Plenary Presentation - MATH 100 (12:50 PM - 1:50 PM)		
Time	**Title**	**Presenter**
12:50 PM	Coating process for battery electrode	NAM, Jaewook

Hiroshi Watanabe – Honorary Symposium - MATH 104 (2:00 PM - 3:40 PM) - Chair: Yumi Matsumiya		
Time	**Title**	**Presenter**
2:00 PM	Viscoelastic properties of bidisperse linear polymers under elongational flow	EVELYNE, van Ruymbeke
2:20 PM	Dual slip-link simulation study on stretch-orientation-induced reduction of friction in bi-disperse blends	TANIGUCHI, Takashi
2:40 PM	Elongation viscosity of a poly(styrene-b-2-vinylpyridine) block copolymer forming spherical microphage-separated structure	DOI, Yuya
3:00 PM	Primitive chain network simulations for non-linear rheology of monodisperse polystyrene melts with friction change and violation of the fluctuation-dissipation theorem.	MASUBUCHI, Yuichi
3:20 PM	Universality of polymer melts	LIU, Chen-Yang

Non-Newtonian Fluid Mechanics and Stability - GEOG 200 (2:00 PM - 3:40 PM) - Chair: Shinji Tamano		
Time	**Title**	**Presenter**
2:00 PM	KEYNOTE: computational rod climbing and dipping dependent upon normal stresses	KWON, Youngdon
2:40 PM	Alignment of wormlike micelles under shear flow: Comparison with polymers	KOIDE, Yusuke
3:00 PM	Effect of viscosity contrast in structure -rheology relationship in sheared lamellar mesophase in 3D	PAL, Arkaprava
3:20 PM	Molecular dynamics simulation of the behavior of thin lubrication film	LIU, Dongjie

Self-assembly and Flow-induced Systems/Gels - MATH 203 (2:00 PM - 3:40 PM) - Chair: Qian Chen		
Time	**Title**	**Presenter**
2:00 PM	Simulation of Competition between Reaction and Relaxation in Gelation Kinetics	UNEYAMA, Takashi
2:20 PM	Diversity in strain-induced crystallization of natural rubber by biaxial elongation	SAKURAI, Shinichi
2:40 PM	Quantifying the Enhancement Effect of Strain Induced Crystallization on Tearing Energy by Edge Crack Test Method	TSUNODA, Katsuhiko
3:00 PM	Revealing the correlation between strain-induced crystallization and local strain field around the crack-tip of natural rubber	MAI, Thanh-Tam
3:20 PM	Cluster formations of terminal groups of polyisoprenes in natural rubbers: Molecular dynamics simulation study	TAKASHI, Taniguchi

Suspensions and Colloids - GEOG 147 (2:00 PM - 3:40 PM) - Chair: Hartmut Löwen		
Time	**Title**	**Presenter**
2:00 PM	KEYNOTE: Shear thickening in dense suspensions of rigid rods	PETEKIDIS, George
2:40 PM	Flow-induced structural change of cathode slurry during storage and its mechanism	PARK, Jeong Hoon
3:00 PM	Practical rheometry for suspensions and other fun complex systems	MOONAY, David
3:20 PM	Yield and flow in aggregated particulate suspsensions in water	STICKLAND, Anthony SCALES, Peter

Coffee Break - Lounge at MATH 125/126 (3:40 PM - 4:10 PM)

Hiroshi Watanabe – Honorary Symposium – MATH 104 (4:10 PM - 5:50 PM) - Chair: Tadashi Inoue		
Time	**Title**	**Presenter**
4:10 PM	Rheo-dielectric behavior of unentangled poly (butadiene oxide) under steady shear	MATSUMIYA, Yumi
4:30 PM	Experimental study on phase separation dynamics of unentangled polymer blend with dynamic asymmetry	SATO, Takeshi
4:50 PM	Simulation study of unentangled polymers under fast flow	TAKIMOTO, Jun-ichi
5:10 PM	Molecular Dynamics Simulations for Viscosity Growth and Conformations of Unentangled Polymers under Shear Flow	UNEYAMA, Takashi
5:30 PM	No talk scheduled.	

Non-Newtonian Fluid Mechanics and Stability - GEOG 200 (4:10 PM - 5:50 PM) - Chair: Li Xi		
Time	**Title**	**Presenter**
4:10 PM	KEYNOTE: Psychorheology: toward understanding how we experience viscous and viscoelastic materials	MARTIN, Jeffrey
4:50 PM	Modelling drop mobility on lubricated surfaces using a ternary free energy lattice Boltzmann algorithm	OROZCO-FUENTES, Sirio
5:10 PM	Analysis of pulsatile flows of complex fluids in two-dimensional channels	PARK, Nayeon
5:30 PM	Solving the closure problem for dilute polymer solutions	ANSUMALI, Santosh

Self-assembly and Flow-induced Systems/Gels - MATH 203 (4:10 PM - 5:50 PM) - Chair: Kenji Urayama		
Time	**Title**	**Presenter**
4:10 PM	KEYNOTE: Relationships between viscoelastic relaxation and network connectivity in transient networks with well-controlled network structures	KATASHIMA, Takuya
4:50 PM	Phantom chain simulations for tetra and tri-branched networks	MASUBUCHI, Yuichi
5:10 PM	Negative energy elasticity in polymer gel elasticity	SAKAI, Takamasa
5:30 PM	Universal Equation of State of Osmotic Pressure for Polymer Gels	YASUDA, Takashi

Suspensions and Colloids - GEOG 147 (4:10 PM - 5:50 PM) - Chair: Chaimongkol Saengow		
Time	**Title**	**Presenter**
4:10 PM	Influences of shape of molecular weight distribution on tensile properties of polyethylene solids	KIDA, Takumitsu
4:30 PM	Linking multiscale rheology to performance of hierarchically structured pem fuel cell catalyst layer	LEE, Min-Hyung Markus
4:50 PM	Inertial flow of immersed elastic capsules through a corner	HUET, Damien
5:10 PM	Slip Behaviour and Thixotropy of Kaolinite and Mature Fines Tailings	PIETTE, Jourdain
5:30 AM	Z-shaped dejamming phase diagram of colloidal gels	XIA, Bin

Social Events: Pub Night & Karaoke (7:00 PM - Late)

Thursday, May 18, 2023

Thursday May 18, 2023		
Plenary Presentations: JNNFM Walters Award Lecture – GEOG 100 (9:00 AM - 10:00 AM) - Chair: Ian Frigaard		
Time	**Title**	**Presenter**
9:00 AM	Viscoplastic Fingers and Fractures in a Hele-Shaw Cell	BALL, Thomasina
Coffee Break - Lounge at MATH 125/126 (10:00 AM - 10:30 AM)		
Emulsions, Foams and Bubbles - GEOG 147 (10:30 AM - 12:10 PM) - Chair: Marjan Zare		
Time	**Title**	**Presenter**
10:30 AM	Controlled Collision of Hele-Shaw Droplets in Extensional Flow Using a Six-Port Microfluidic Device	RAZZAGHI, Aysan
10:50 AM	Bubbles in Yield Stress Fluids: Link between the Rheology and Stability of Bubbles	DANESHI, Masoud
11:10 AM	Preparation and properties of conductive foams via high internal phase emulsion	LEE, Seong Jae
11:30 AM	Shear-triggered Coalescence	MASHAYEKHI, Alireza
11:50 AM	A New Instrument for Interfacial Dilational Rheology	HUANG, Yun-Han
Hiroshi Watanabe – Honorary Symposium - GEOG 100 (10:30 AM - 12:10 PM) - Chair: Youngdon Kwon		
Time	**Title**	**Presenter**
10:30 AM	KEYNOTE: Rheology modification of polymeric networks via loop threading	VLASSOPOULOS, Dimitris
11:10 AM	Time-Strain Separability and Inseparability in Multiaxial Stress Relaxation of Polymer Gels with Permanent and Transient Crosslinks	URAYAMA, Kenji
11:30 AM	Intriguing melting behavior of the natural rubber crystal formed by strain-induced crystallization	SAKURAI, Shinichi
11:50 AM	Have you ever listened to the sound of the fluid?	AHN, Kyung Hyun
Non-Newtonian Fluid Mechanics and Stability - GEOG 200 (10:30 AM - 12:10 PM) - Chair: Miguel Moyers-Gonzalez		
Time	**Title**	**Presenter**
10:30 AM	Rheological effects on purely-elastic flow asymmetries in the cross-slot geometry	YOKOKOJI, Arisa
10:50 AM	Flow of a wormlike micellar solution over a long cavity	HILLEBRAND, Fabian
11:10 AM	Effects of channel length in expansion parts on flow regimes of polymer solution in consecutive abrupt contraction-expansion channels	HIDEMA, Ruri
11:30 AM	Instabilities in immiscible multi-layer viscous shear flows in the presence of interfacial slip	KATSIAVRIA, Anna
11:50 AM	Effect of ultrasound fields on asphaltene-laden w/o interfaces: a microrheology approach	KHALESI MOGHADDAM, Razie
Self-assembly and Flow-induced Systems/Gels - GEOG 212 (10:30 AM - 12:10 PM) - Chair: Takamasa Sakai		
Time	**Title**	**Presenter**
10:30 AM	KEYNOTE: Nonlinear Rheology of Concentrated Poly(vinyl alcohol)/Borax Aqueous Solution	CHEN, Quan
11:10 AM	Hystereses In One-dimensional Compression Of A Poroelastic Hydrogel	XU, Zelai
11:30 AM	Nonlinear rheology of entangled wormlike micelles: a slip-spring simulation study	SATO, Takeshi
11:50 AM	Coupling a ionic surfactant and a drug salt: equilibrium characteristic parameters & strain hardening in start-up flow	GRIZZUTI, Nino
Lunch - Lounge at MATH 125/126 (12:10 PM - 1:50 PM)		

Emulsions, Foams and Bubbles - GEOG 147 (2:00 PM - 3:40 PM) - Chair: Arun Ramchandran		
Time	**Title**	**Presenter**
2:00 PM	KEYNOTE: Squeezing of a concentrated emulsion with surfactant through a periodic porous medium	ZINCHENKO, Alexander
2:40 PM	The effect of surface viscosity on droplet breakup and relaxation under extensional flow	NARSIMHAN, Vivek
3:00 PM	Flow and instability induced by bubbles rising in a two-layer fluid system	ZARE, Marjan
3:20 PM	Dynamics and mixing of trapped droplets	ROURE, Gesse

Non-Newtonian Fluid Mechanics and Stability - GEOG 200 (2:00 PM - 3:40 PM) - Chair: Ian Frigaard		
Time	**Title**	**Presenter**
2:00 PM	Gas propagation through porous media filled with yield-stress fluid	POURZAHEDI, Ali
2:20 PM	Localization of stirring flows: the effect of the yield stress	DANESHVAR GARMROODI, Mohammad Reza
2:40 PM	Thin-film flow of a Bingham fluid over topography with a temperature dependent rheology	MOYERS, Miguel
3:00 PM	Damping of surface waves by a floating viscoplastic plate	WANG, Xuemeng
3:20 AM	No talk scheduled.	

Polymer Solutions and Melts - MATH 104 (2:00 PM - 3:40 PM) - Chair: Benjamin Yavitt		
Time	**Title**	**Presenter**
2:00 PM	Advanced polymer rheology based on rheo-optical tools and a dual motor device	LAEUGER, Joerg
2:20 PM	Universal diffusion of dendrimers in semidilute solutions of linear polymers	JAGADEESHAN, Ravi
2:40 PM	The Effect of the Solvent Dielectric Constant on the Conformation and Dynamics of Polyelectrolytes in Solution	MATSUMOTO, Atsushi
3:00 PM	Recent advances in polymer viscoelasticity from general rigid bead-rod theory	GIACOMIN, Alan Jeffrey
3:20 PM	Improvement of Heat Resistance using Physical Aging in Polystyrene Injection Moldings	TAO, Kosaku

Self-assembly and Flow-induced Systems/Gels - MATH 203 (2:00 PM - 3:40 PM) - Chair: Takuya Katashima		
Time	**Title**	**Presenter**
2:00 PM	Effect of salt concentration and flow rate on clogging dynamics in the single micro-pore	KIM, Dae Yeon
2:20 PM	Star-polymer-DNA gels showing predictable stress relaxation behavior	LI, Xiang
2:40 PM	Observation of flow birefrengence in dynamic squeeze flow	KATO, Manabu
3:00 PM	SAXS, SANS and Spectroscopy Study on High Tunability of a Block Copolymer by Strongly Selective Solvents	OKAMOTO, Shigeru
3:20 PM	No talk scheduled	

Social Events: Buses to Downtown Vancouver - Mathematics & Geography Buildings (4:30 PM - 6:30 PM)
Social Events: Cruise Dinner on the Magic Spirit (6:30 PM – 11:00 PM)

Friday, May 19, 2023

Friday May 19, 2023		
Plenary Presentations: GEOG 100 (9:00 AM - 10:00 AM)		
Time	**Title**	**Presenter**
9:00 AM	Substrate colonization by an emulsion drop prior to spreading	RAMACHANDRAN, Arun
Coffee Break - Lounge at MATH 125/126 (10:00 AM - 10:30 AM)		
Industrial Rheology in Polymer Processing - GEOG 200 (10:30 AM - 12:10 PM) - Chair: Jourdain Piette		
Time	**Title**	**Presenter**
10:30 AM	Rheology-Driven Continuous In-Melt Separation of PET/PE Blends and Laminates: A Novel Approach to Recycling	MAIA, Joao
10:50 AM	Experimental Validation of Viscosity Homogenization Treatment System for Waste Plastic Recycling	ENDO, Hiroki
11:10 AM	Development of composite via secondary polymer-induced particle aggregation and destruction of its particle aggregation during 3d printing	HONG, JOUNG SOOK
11:30 AM	Analysis of operating limits of vacuum-assisted slot die coating of herschel-bulkley fluids	LEE, Myungjae
11:50 AM	No talk scheduled.	
Non-Newtonian Fluid Mechanics and Stability - GEOG 100 (10:30 AM - 12:10 PM) - Chair: Ruri Hidema		
Time	**Title**	**Presenter**
10:30 AM	KEYNOTE: Effect of local relaxation time on drag reduction in turbulent boundary layer flow of viscoelastic fluids	TAMANO, Shinji
11:10 AM	Turbulent drag reduction with flexible and rigid polymer solutions: from low to maximum drag reduction	MITISHITA, Rodrigo
11:30 AM	Relating elastoinertial turbulence to the phenomenology of polymer drag reduction	XI, Li
11:50 AM	No talk scheduled	
Polymer Solutions and Melts – GEOG 212 (10:30 AM - 12:10 PM) - Chair: Ravi Jagadeeshan		
Time	**Title**	**Presenter**
10:30 AM	KEYNOTE: Modular material properties in bimodal blends of amine functionalized polyolefins	YAVITT, Benjamin
11:10 AM	Linear Viscoelastic Properties of Comb-Shaped Ring Polystyrenes	DOI, Yuya
11:30 AM	Application of a robust self-healing experimental protocol for associating polymers	MORADINIK, Nafiseh
11:50 AM	No talk scheduled	
Rheology in the Mining Industry - GEOG 147 (10:30 AM - 12:10 PM) - Chair: Masoud Daneshi		
Time	**Title**	**Presenter**
10:30 AM	Rheological characterization of suspensions generated from copper ores o varying mineralogical features at grinding conditions	GUTIERREZ, Leopoldo
10:50 AM	Quantifying the effects of fines and clays on mineral tailings dewatering	STICKLAND, Anthony
11:10 AM	Modelling high-pressure dewatering rolls for mineral tailings	EKANAYAKE, Nilanka
11:30 AM	Influence of fluid type in the transition from spray to roping in hydrocyclones	BETANCOURT, Fernando
11:50 AM	No talk scheduled	
Closing Remarks - MATH 100 (12:15 PM - 12:45 PM)		

List of abstracts

Tuesday, May 16, 2023

Plenary Presentation - GEOG 100 (9:00 AM - 10:00 AM)

8TH PACIFIC RIM CONFERENCE ON RHEOLOGY, May 15-19, 2023

What we learn about yielding from recovery rheology

Simon A. Rogers

Chemical and Biomolecular Engineering, University of Illinois at Urbana-Champaign, Urbana, IL, USA (sarogers@illinois.edu)

ABSTRACT

Yield stress fluids are often thought about in a piecewise manner as behaving like elastic solids below the yield stress and like generalized Newtonian liquids above it. Accurate determination of the yield stress is therefore crucial to understanding and predicting the behaviour of yield stress fluids such as inks for 3D printing, foods and cosmetics, muds and soils, and many industrially and biologically relevant materials. Despite the centrality of the yield stress concept, there exist multiple methods by which researchers determine 'the' yield stress, and they can provide values that are orders of magnitude apart. Such discrepancies have even led to some asking the question of whether the yield stress exists at all.

In this work we study a series of yield stress fluids using recovery rheology concepts, where strain is decomposed into recoverable and unrecoverable components, and present evidence that yielding takes place gradually over a wider range of stresses than previously thought. It is shown that the overshoot in the loss modulus that has often been used as a measure of yielding is due to the acquisition of unrecoverable strain. It's shown how these measurements led to the development of a model that describes spatially heterogeneous yielding in a mean-field manner and how accurately this model predicts the rheology of simple yield stress fluids.

In more complex materials, responses are observed with two overshoots in the loss modulus, a phenomenon often referred to as "double yielding". It is shown that these dual features are really a combination of two distinct processes, only one if which is yielding. New protocols inspired by recovery concepts are also used to show that small amounts of flow occur below the yield stress determined by a Herschel-Bulkley fit to steady-shear flow measurements in a predictable manner as a function of stress amplitude, angular frequency, and applied stress phase angle. Relations are presented that show how these measures can be used to determine the contribution to the loss modulus from unrecoverable plastic deformations, providing some of the same information as the full iteratively performed recovery tests, but in a fraction of the time.

Recovery rheology therefore adds nuance to our understanding of yield stress fluids by highlighting the continuous nature of yielding and providing a general set of methods by which reliable and consistent yielding information can be rapidly obtained.

8TH PACIFIC RIM CONFERENCE ON RHEOLOGY, May 15-19, 2023

POROELASTIC MODELLING REVEALS THE COOPERATION BETWEEN TWO MECHANISMS FOR ALBUMINURIA

Zelai Xu[1], Pengtao Yue[2] and James J. Feng[1]

[1]University of British Columbia, Vancouver, Canada
[2]Virginia Tech, Blacksburg, United States of America

ABSTRACT

Albuminuria occurs when albumin leaks abnormally into the urine. Its mechanism remains unclear. A gel-compression hypothesis attributes the glomerular barrier to compression of the glomerular basement membrane (GBM) as a gel layer. Loss of podocyte foot processes (FPs) would allow the gel layer to expand circumferentially, enlarge its pores and leak albumin into the urine. To test this hypothesis, we develop a poroelastic model of the GBM. It predicts GBM compression in healthy glomerulus and GBM expansion in the diseased state, essentially confirming the hypothesis. However, by itself, the gel compression and expansion mechanism fails to account for two features of albuminuria: the reduction in filtration flux and the thickening of the GBM. A second mechanism, the constriction of flow area at the slit diaphragm downstream of the GBM, must be included. The cooperation between the two mechanisms produces the amount of increase in GBM porosity expected *in vivo* in a mutant mouse model, and also captures the two *in vivo* features of reduced filtration flux and increased GBM thickness. Finally, the model supports the idea that in the healthy glomerulus, gel compression helps maintain a roughly constant filtration flux under varying filtration pressure.

METHODOLOGY

The function of the kidney relies on microvascular filtration units known as glomeruli (Fig. 1a). To clarify mechanism of albuminuria, a gel compression hypothesis[1] has been proposed to explain the change of permeability between a healthy GBM and a diseased one. We have built the following model to testify the hypothesis. In view of recent studies of the mechanics of basement membranes[2,3], we represent the GBM as a poroelastic gel layer composed of an elastic network and aqueous solvent. we omit the endothelial cells owing to their limited contribution to the size selective filtration, and focus on the GBM and FPs. Fig. 1(b) depicts a quarter of the glomerular capillary, and the computational domain is an annular sector delineated by the two arcs Γ_1 and Γ_2. The filtration flow is driven by the pressure difference between P_1 at Γ_1 and $P = 0$ in the urinary space downstream of the FPs. The flow inside the lumen is inertialess Stokes flow along the radial direction. The GBM is a layer of poroelastic gel, with initially constant fluid and solid volume fractions. As the GBM is deformed by the flow, its volume fraction may vary in time and along the radial direction.

The details of the poroelastic theory and numerical method can be find in our previous studies[4,5].

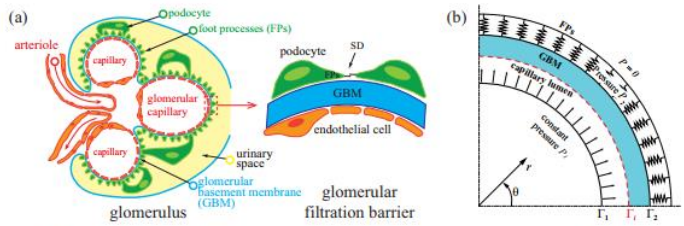

Figure 1: (a) Schematics showing the glomerular filtration barrier in the kidney. Each glomerulus encloses a network of capillaries through which the blood is filtered. The capillary wall consists of a fenestrated endothelium on the inside, a glomerular basement membrane (GBM) and podocytes on the outside. The liquid filtrate passes through the endothelium and the GBM, and flows out through the slit diaphragm (SD) between the foot processes (FPs) of the podocytes into the urinary space. (b) The computational domain is between the arcs Γ_1 and Γ_2. The red dashed line Γ_i represents the interface between the blood in the capillary lumen and the GBM. The filtration is driven by a constant pressure P_1 on Γ_1 and the flow direction is indicated by the array of arrows. The buttressing effect of the FPs is represented by elastic springs pushing on the exit of the domain Γ_2.

To reflect the morphological changes due to FP effacement, we focus on two features. The first is the weakening of the buttress force on the downstream surface of the GBM. The second is the effect of shortened and narrowed SD on restricting the filtration flux. We model the FP buttressing force by elastic springs that resist normal displacement of the GBM's outer surface Γ_2 with a radial normal stress by an elastic coefficient E. The viscous flow across the SD requires a pressure drop which is assumed to be proportional to the local fluid velocity with a friction coefficient μ_D. For the diseased state, E should decrease while μ_D would increase according to the experimental observation[6].

RESULTS

We present here only the most salient results of the study, and a more comprehensive description can be found in our recent paper[7]. Fig. 2 compares the steady-state shape of GBM for the healthy glomerulus and for a diseased glomerulus with softened E and elevated μ_D. The values of E and μ_D for healthy and diseased state have been determined from experimental literature and our own modeling. We can observe the dilation of the capillary and the more porous GBM in the diseased state. These are primarily caused by the softening of FP and also consistent with the gel compression hypothesis and experimental observation by Butt *et al.*[6]. Additionally, we found the thickening of GBM and lower filtration flux. We attribute these two characteristics to the shorting SD, represented by an elevated μ_D. Both were observed in the experiment, but were not explained by the gel compression hypothesis alone. Most interestingly, the shorting SD increases the porosity of the GBM further, which could lead to more serious albuminuria. In summary, the softening FPs and the shortening SD both contribute to the albuminuria.

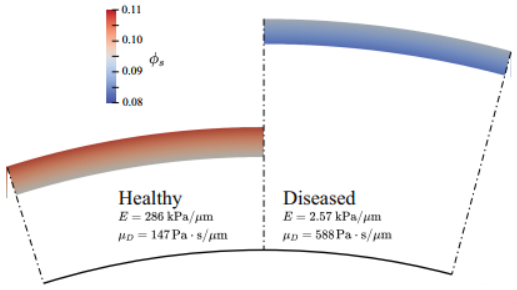

Figure 2: Combined effects of reducing the buttressing modulus E and raising the SD friction coefficient μ_D. Comparison of the GBM morphology and the volume fraction ϕ_s contours.

REFERENCES

.

1. Fissell, W. H.; Miner, J. H. What Is the Glomerular Ultrafiltration Barrier? JASN 2018, 29 (9), 2262–2264.
2. Li, H.; Zheng, Y.; Han, Y. L.; Cai, S.; Guo, M. Nonlinear Elasticity of Biological Basement Membrane Revealed by Rapid Inflation and Deflation. Proc. Natl Acad. Sci. USA 2021, 118 (11), e2022422118.
3. Khalilgharibi, N.; Mao, Y. To Form and Function: On the Role of Basement Membrane Mechanics in Tissue Development, Homeostasis and Disease. Open Biol. 2021, 11 (2), 200360.
4. Xu, Z.; Zhang, J.; Young, Y.-N.; Yue, P.; Feng, J. J. Comparison of Four Boundary Conditions for the Fluid-Hydrogel Interface. Phys. Rev. Fluids 2022, 7 (9), 093301.
5. Li, L.; Zhang, J.; Xu, Z.; Young, Y.-N.; Feng, J. J.; Yue, P. An Arbitrary Lagrangian-Eulerian Method for Simulating Interfacial Dynamics between a Hydrogel and a Fluid. Journal of Computational Physics 2022, 451, 110851.
6. Butt, L.; Unnersjö-Jess, D.; Höhne, M.; Edwards, A.; Binz-Lotter, J.; Reilly, D.; Hahnfeldt, R.; Ziegler, V.; Fremter, K.; Rinschen, M. M.; Helmstädter, M.; Ebert, L. K.; Castrop, H.; Hackl, M. J.; Walz, G.; Brinkkoetter, P. T.; Liebau, M. C.; Tory, K.; Hoyer, P. F.; Beck, B. B.; Brismar, H.; Blom, H.; Schermer, B.; Benzing, T. A Molecular Mechanism Explaining Albuminuria in Kidney Disease. Nat Metab 2020, 2 (5), 461–474.
7. Xu, Z.; Yue, P.; Feng, J. J. Poroelastic Modelling Reveals the Cooperation between Two Mechanisms for Albuminuria. J. R. Soc. Interface. 2023, 20 (198), 20220634.

Hydrodynamics and rheology of fluctuating, semiflexible, inextensible, and slender filaments in Stokes flow

Aleksandar Donev[1], Ondrej Maxian[1], Brennan Sprinkle[1,2]

[1]Department of Mathematics, Courant Institute, New York University, New York, NY 10012
[2]Department of Applied Mathematics and Statistics, Colorado School of Mines, Golden, CO 80401

ABSTRACT

Every animal cell is filled with a cytoskeleton, a dynamic gel made of inextensible filaments / bio-polymers, such as microtubules, actin filaments, and intermediate filaments, all suspended in a viscous fluid. Similar suspensions of elastic filaments or polymers are widely used in materials processing. Numerical simulation of such gels is challenging because the filament aspect ratios are very large.

We have recently developed new methods for rapidly computing the dynamics of non-Brownian and Brownian inextensible slender filaments in periodically-sheared Stokes flow[1,2,4]. We apply our formulation to a permanently[1] and dynamically cross-linked actin mesh[3] in a background oscillatory shear flow. We find that nonlocal hydrodynamics can change the visco-elastic moduli by as much as 40% at certain frequencies, especially in partially bundled networks[3,4].

I will focus on accounting for bending thermal fluctuations of the filaments by first establishing a mathematical formulation and numerical methods for simulating the dynamics of stiff but not rigid Brownian fibers in Stokes flow.[4] I will emphasize open questions for the community such as whether there is a continuum limit of the Brownian contribution to the stress tensor from the filaments.

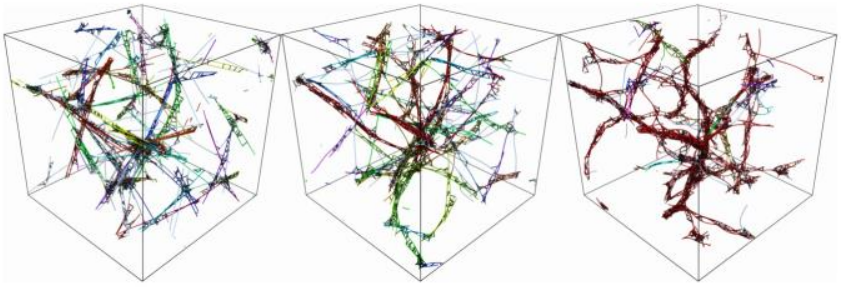

Figure 1: Bundling in a dynamically-cross-linked gel of Brownian actin filaments with decreasing persistence length from left to right.

ACKNOWLEDGEMENTS

This work is supported in part by the U.S. National Science Foundation under grant DMS-2052515.

REFERENCES

1. O. Maxian et al, Integral-based spectral method for inextensible slender fibers in Stokes flow,. *Phys. Rev. Fluids*, 6:014102, 2021
2. O. Maxian et al,. Hydrodynamics of a twisting, bending, inextensible fiber in Stokes flow, *Phys. Rev. Fluids*, 7:074101, 2022
3. O. Maxian et al, Interplay between Brownian motion and cross-linking controls bundling dynamics in actin networks, *Biophysical J.*, 121:1230–1245, 2022.
4. O. Maxian et al., Bending fluctuations in semiflexible, inextensible, slender filaments in Stokes flow: towards a spectral discretization, ArXiv:2301.11123, submitted to *J. Chem. Phys.*, 2023.

TRIBOLOGY AND RHEOLOGY OF HYALURONIC ACID BASED CELLULOSE NANOCRYSTAL SUSPENSIONS

Akshai Bose[1], Behzad Zakani[1,2] and Dana Grecov[1,2]

[1]Dept. of Mechanical Engineering, University of British Columbia, Vancouver, Canada
[2]UBC Bioproducts Institute, University of British Columbia, Vancouver, Canada

ABSTRACT

Hyaluronic acid (HA) is an unbranched mucopolysaccharide with repeating units of N-acetylglucosamine and glucuronic acid glycosidic linkage. Due to the biomechanical properties of HA, it is used in a wide range of biomedical applications, especially as a friction or viscosity modifier. The current study investigates the microstructural, tribological and rheological properties of HA based cellulose nanocrystals (CNC) suspensions.

The microstructural characterization of the CNC suspensions was performed using a polarized optical microscope (POM). The POM images revealed the presence of chiral nematic domains of CNCs where their size increase with an increase in CNC concentration (due to the intermolecular hydrogen bonding (H-bond) between the CNCs). The tribological measurements were performed using a pin-on-disk tribometer. Using a steel-steel tribo-pair, results showed a reduction in the coefficient of friction and wear with the addition of only 0.5 wt.% CNC to HA. The energy-dispersive X-ray spectroscopy (EDX) revealed that the addition of CNCs reduced the surface corrosion of the tribo-pair. At higher CNC concentrations, the COF value tends to increase, due to the abrasive behaviour of the large CNC agglomerates. Rheological measurements were performed using a rotational rheometer. The steady shear viscometry data of HA/CNC suspensions exhibited shear thinning behaviour at lower shear rates due to the alignment of CNC agglomerates along the shear direction. The frequency sweep data revealed that the solid-like viscoelastic behaviour (storage modulus greater than loss modulus) of HA/CNC suspension increased with an increase in CNC concentration. The HA/CNC suspension with CNC concentration of 1 wt % and more exhibit yielding behaviour. The yield stress of the suspensions increases with CNC concentration. These findings may serve as an initial step in developing HA/CNC-based rheology or tribology modifiers for different biomedical and pharmaceutical applications.

SELF-ORGANIZED CABLE FORMATION AND FORCE TRANSMISSION IN AN ACTIVE VERTEX MODEL FOR BIOLOGICAL TISSUES

Mingfeng Qiu[1], Vincent Hakim[1] and Francis Corson[1]

[1]Laboratoire de Physique de l'Ecole Normale Supérieure,
CNRS, ENS, Université PSL, Sorbonne Université, Université de Paris,
75005 Paris, France

Biological tissues, as complex materials, have been receiving increased interest in recent years. An important example is an epithelial monolayer, a single layer of packed cells. This type of tissue lines the surfaces of animal organs and plays fundamental roles in life. In a commonly used approach, termed the vertex model[1,2], an epithelial monolayer is described by a network of active edges representing boundaries between neighbouring cells (**Fig. 1** right). Biologically, each edge represents bundled polymeric filaments (actin) crosslinked by molecular motors (myosin). These edges actively contract and sustain tension, which is thus transmitted throughout the tissue. Vertex models display intriguing rheology, transitioning between solid and fluid states as cell parameters change[3].

The mechanical response of epithelial tissues involves interactions of many elements. Traditionally it is believed that genes and biochemistry instruct mechanics. Recently, it is becoming clear that mechanics feeds back onto and drives gene expression and biochemical signalling[4,5], but how mechanical feedback affects tissue behaviour remains poorly understood.

Inspired by experimental observation, we propose a vertex model with a coarse-grained description of passive edge viscoelasticity as well as active molecular motor activities. The model incorporates a known feedback loop in which edge tension regulates motor recruitment (**Fig. 1** left). We study the emergent response of this type of tissues to external forces using both theory and computations. Through a mechanical instability caused by the feedback, a tissue can become patterned with long focused paths consisting of chains of strongly contracting edges spanning many cells (**Fig. 1** right). We characterize the properties of such contractile cables.

Our theory provides a potential explanation for the formation and refinement of actomyosin cables, which are ubiquitous in the development of organisms and whose origins are largely unclear. From the physics point of view, the spontaneous contractile paths offer mechanisms for long-range force transmission, highlighting novel mechanical states in active materials.

References

1. Honda H., Description of cellular patterns by Dirichlet domains: the two-dimensional case, *J Theor Biol*, **72**, 523-543, 1978.

2. Farhadifar R., Roper J.-C., Aigouy B., Eaton S., Julicher F., The influence of cell mechanics, cell-cell interactions, and proliferation on epithelial packing, *Curr Biol*, **17**, 2095-2104, 2007.

8TH PACIFIC RIM CONFERENCE ON RHEOLOGY, May 15-19, 2023

NONLINEAR RHEOLOGY OF RUBBER VULCANIZATES NANOCOMPOSITES

Yihu Song[1,2]
[1]MOE Key Laboratory of Macromolecular Synthesis and Functionalization, Department of Polymer Science and Engineering, Zhejiang University, Hangzhou 310027, China
[2]Shanxi-Zheda Institute of New Materials and Chemical Engineering, Taiyuan 030000, China.

ABSTRACT

Nanoparticles significantly reinforce rubber materials while they also enhance the dissipation and strain softening behaviours of the nanocomposites, the latter being characterized by nonlinear Payne effect. For a long time, formation of filler networks mediated by rubber-filler interfacial interactions is assigned to the major reinforcement mechanism beyond the hydrodynamic effect and breakdown of filler network mediated by chains slippage and desorption from the filler nanoparticles is thought to account for the Payne effect. We show that the filler amplifies microscopic deformation and therefore reinforces the rubber phase depending on the dynamics of the rubber, which is well accounted for by the time-concentration superpositioning principle.[1-4] We show that the neat rubber vulcanizates exhibit nonlinear dynamic rheology that determines the Payne effect of vulcanizates nanocomposites. The filler amplifies the microscopic deformation and promotes softening of the rubber phase, which is well accounted for by the concentration-concentration superpositioning principle. We realize that many studies ignoring the viscoelasticity of the rubber matrices and simplifying the matrices to "the carrier of the particle network" give deceptively misleading conclusions being far away from guiding the industry to manufacture high-performance nanocomposites. We develop several strategies to optimize the reinforcement, dissipation and strain softening behaviours of rubber nanocomposites based on regulation of the nonideally crosslinked network of the rubber matrices in addition to improvement of filler dispersion and interfacial interaction.

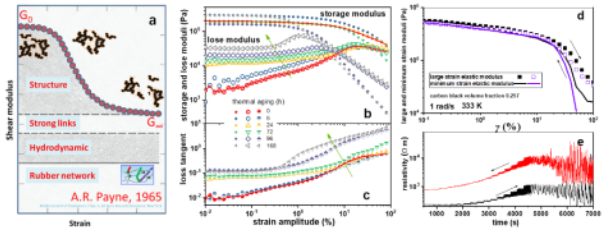

ACKNOWLEDGEMENTS

The work was supported by the National Natural Science Foundation of China (U1908221) and Shanxi-Zheda Institute of Advanced Materials and Chemical Engineering (2021SZ-TD002).

REFERENCES

1. Fan, X., Xu, H., Zhang, Q., Song, Y., Zheng, Q. Polymer 2019, 167, 109
2. Song, Y., Zheng, Q. Prog. Mater. Sci. 2016, 84, 1
3. Sun, J., Song, Y., Zheng, Q., Tan, H., Yu, J., Li, H. J. Polym. Sci. Part B Polym. Phys. 2007, 45, 2594
4. Xu, H., Xia, X., Hussain, M., Song, Y., Zheng, Q. Polymer 2018,156, 222

STUDY OF THE STABILITY OF ELECTRICAL AND RHEOLOGICAL PROPERTIES OF ELECTRICALLY CONDUCTIVE COMPOSITES WITH CO-CONTINUOUS MORPHOLOGY

D. Strugova, E. David, N.R. Demarquette

École de Technologie Supérieure – ÉTS, Montréal, Québec H3C 1K3, Canada

ABSTRACT

Polymer blends presenting a co-continuous morphology have raised more and more interest due to their potential application as conductive materials when used with electrically conductive fillers, such as carbonaceous nanoparticles[1-3]. These materials have a wide range of potential applications, including electronics, sensors, and energy storage devices. The conductivity of these composites can be adjusted by varying the concentration and type of filler used as well as the morphology of the matrix. The unique structure of co-continuous blends, allows for efficient distribution of the conductive filler throughout the material, making it possible to achieve a drastic reduction of the percolation threshold concentration, which is the point at which the material becomes electrically conductive[1, 4]. This is achieved when the filler is located within one of the phases or at the interface between the two polymers forming the co-continuous morphology resulting in a double percolation. This reduces the amount of filler required to reach the percolation threshold and thus making the material more cost-effective. However, during processing, the composites are subjected to deformation, which can alter their morphology and electrical properties. Understanding the behavior of these materials under different loading conditions is important.

In this study, the linear viscoelastic properties of co-continuous polypropylene/polystyrene blends filled with multiwall carbon nanotubes (PP/PS/MWCNT) have been investigated. PP/PS/MWCNT composites with different concentrations of MWCNT (0 to 5 wt.%) have been prepared by melt mixing. The rheological, electrical, and morphological properties of the obtained samples were then characterized. The samples were subjected to a sequence of small amplitude oscillatory shear (SAOS), a steady shear (simulating flow), and a recovery step. This test design was used to evaluate the morphology before and after applied deformation, and deformation + recovery. The evolution of electrical properties was investigated during applied deformation and recovery using a rheometer coupled with an impedance-meter. The SAOS response was fitted to a model, which considers the contribution of filler network elasticity of filled composites to the dynamic modulus[4]. This was done in order to evaluate the change of morphology undergone by the different samples when subjected to a deformation step prior to and after the recovery.

It was shown that the addition of even a very low amount of MWCNT refined the co-continuous morphology of the PP/PS blend. In addition, it was shown that MWCNT stabilized the morphology of a co-continuous blend once added at a certain concentration, even when significant deformation was applied. The co-continuous morphology was also refined during the recovery step. Electrical conductivity presented similar behavior. It was not only recovered to its initial values but even increased one order of magnitude.

REFERENCES

1. Strugova, D.; Ferreira Junior, J. C.; David, É.; Demarquette, N. R., Ultra-Low Percolation Threshold Induced by Thermal Treatments in Co-Continuous Blend-Based PP/PS/MWCNTs Nanocomposites. *Nanomaterials-Basel* **2021,** *11* (6), 1620.

2. Kurusu, R. S.; Helal, E.; Moghimian, N.; David, E.; Demarquette, N., The role of selectively located commercial graphene nanoplatelets in the electrical properties, morphology, and stability of EVA/LLDPE blends. *Macromolecular Materials and Engineering* **2018,** *303* (9), 1800187.

3. Chen, Y.; Yang, Q.; Huang, Y.; Liao, X.; Niu, Y., Influence of phase coarsening and filler agglomeration on electrical and rheological properties of MWNTs-filled PP/PMMA composites under annealing. *Polymer* **2015,** *79*, 159-170.

4. Strugova, D.; David, É.; Demarquette, N. R., Linear viscoelasticity of PP/PS/MWCNT composites with co-continuous morphology. *J Rheol* **2022,** *66* (4), 671-681.

Should we keep choosing nano-sized particles to kinetically stabilize co-continuous blends?

Rajas Sudhir Shah[1], Steven Bryant[1,2], and Milana Trifkovic [1]

[1]Department of Chemical and Petroleum Engineering, Schulich School of Engineering, University of Calgary, Calgary, Canada
[2]Canada Excellence Research Chair in Materials Engineering for Unconventional Oil Reservoirs, University of Calgary, Calgary, Canada

ABSTRACT

Filling co-continuous polymer blends with solid particles has proven to improve their structural stability. Such composites further demonstrate improved functionality, making them an attractive choice of material in a wide range of applications. These objectives are achieved by trapping and percolating the particles either in one of the polymer phases or at the polymer-polymer interface. Localization is dependent on the thermodynamics and geometric properties of the particles, polymers and processing conditions employed. It has been widely reported for spherical particles that particles with smaller sizes are the most effective in preventing the coarsening of co-continuous structures. However, processing composites with nanoparticles is not trivial due their tendency to aggregate, caused be colloidal interactions. As such, they require chemical surface modification to be effective. Tuning surface properties often involve complex, costly, toxic treatments and are usually useful on a case-by-case basis. Another crucial factor considered in reported studies is the requirement of monodisperse particles, which again is not trivial to achieve on an industrial scale. To tackle these issues, we approach this study with two critical questions in mind: How is microstructural stability dependent on the size of pristine particle? How does particle size distribution affect it? We perform in-situ high-temperature confocal rheology studies to assess the effect of particle size on the extent of particle agglomeration, particle migration across the interface, and its consequence on coarsening of polymer blends filled with pristine silica particles. This enabled characterization of coarsening kinetics by relating the evolving 3D microstructure to the time dependence of the macroscopic flow behavior with rheological measurements.

We began by investigating the dynamics of five different silica particles with diameter ranging from 5 nm to 490 nm filled polypropylene (PP) and poly(ethylene-co-vinyl acetate) (EVA) co-continuous blend which is known to breakdown into droplet-matrix blend during coarsening when not filled with particles. While particle size does not play a role on blend stability when particles are thermodynamically driven to their preferred polymer phase, a striking effect is achieved when particles are kinetically trapped at the interface. We find that the interparticle interaction, driven by smaller interparticle distance governs their extent of agglomeration and consequently their ability to stabilize co-continuous morphology. Strikingly, the largest (490 nm) particles are more effective in suppressing coarsening than 5 nm and 60 nm particles, while 140 nm and 250 nm particles are

most effective. Furthermore, we demonstrate that migration of primary particles of any size is influenced by the interplay of interfacial folding during melt blending and Laplacian pressure exerted by a highly curved, newly created, interface. On the other hand, the large agglomerates localized in the thermodynamically preferred polymer phase.

In the second part of the study, we introduce the most effective particles (140 nm and 250 nm) in the blends under different loading ratios to simulate polydispersity in four different blends based on PP (or polyethylene, PE) and EVA. Different grades of PP (or PE) and EVA are carefully chosen as model polymers blends with different properties, viz., zero shear viscosity, interfacial tension, and viscosity ratio between components under processing conditions and at rest. As such the driving force (ratio between interfacial tension and viscosity, Γ/η) for coarsening in these blends is different. We find that polydispersity in particle size do not negatively affect the blend stability, it can be used as an additional tuning parameter. The efficacy of the particles to suppress the coarsening is dependent on the zero-shear viscosity of the blends. Lower viscosity blends can coarsen to a greater extent before particles can percolate at the interface. Further, the increase of elasticity in blends has a dependence on final blend morphology, and Γ/η ratio. Blend with lowest Γ/η ratio has higher interfacial area and hence the corresponding network of particles formed on the interface are weaker yielding a lower growth in elasticity. As such, the blend elasticity is determined to be more susceptible to the morphology of blends than component properties. Blends of medium interfacial tension and viscosity achieved optimal structural stability and enhancement in elasticity. These results extend our fundamental understanding of the stabilization of co-continuous morphology in polymer blends by particles, providing promising new avenues for fundamental studies and applications alike.

RHEOLOGICAL AND CONDUCTIVE PROPERTIES OF INJECTION- AND COMPRESSION-MOLDED CARBON NANOTUBE POLYMER COMPOSITES

Alen Oseli[1], Tanja Tomković[2], Savvas G. Hatzikiriakos[2], Lidija Slemenik Perše[1]

[1]University of Ljubljana, Faculty for Mechanical Engineering, Ljubljana, Slovenia
[2]The University of British Columbia, Department of Chemical and Biological Engineering, Vancouver, Canada

ABSTRACT

In the present study we show that carbon nanotube network formation and morphology play significant roles on the rheological, mechanical, and electrical properties of polymer-based nanocomposites. Results show that the formed network is in majority constructed of nanotube bundles, which geometrically entangle at a critical volume fraction ϕ_{cv} (geometrical percolation threshold). The geometrical entanglement of carbon nanotubes significantly affects the rheological performance regardless of the network morphology which improves the mechanical properties. On the other hand, nanotube configuration affects the electrical performance even if the network is not fully established (below ϕ_{cv}). In this case, random configuration moves the transition from isolator to conductor ϕ_{cv}^{e} (electrical percolation threshold) to much lower nanotube content and profoundly improves the conductivity of the nanocomposite.

INTRODUCTION

Carbon nanotubes-CNTs are widely accepted as exceptional nanofillers with superior strength and effective electron transfer, which can be utilized to improve functional performance of host materials. They establish randomly connected network within polymers, where they serve as mechanical reinforcement or conductive pathway, which can be used in numerous cutting-edge technologies[1]. Nevertheless, the functional performance of such materials mainly depends on network formation and its morphology. CNT network in polymer-based nanocomposites is generally established in melt and governs the properties of such materials in solid state. Within this research we focus on the rheological properties and electrical conductivity of CNT polymer-based nanocomposites.

Up to date there are numerus research works reporting on the improvement of mechanical properties with the addition of CNTs. Recent studies in this field observed percolation event in mechanical properties, explaining that particle interactions additionally reinforce the material[2]. However, none of these studies explicitly correlate the improvements with network formation and its morphology. Furthermore, since the effective electron transfer is one of the key features of CNTs, extensive research has already been conducted on electrical conductivity of such nanocomposites[3]. While there are some reports that geometrical entanglement of CNTs is a key

factor for the establishment of conductive network, there are others showing that randomness in CNT configuration increases the probability to enable electron transfer. Therefore, the aim of the present research was to investigate network formation, its morphology, and their effects on the rheological and conductive properties of CNT polymer-based nanocomposites.

EXPERIMENTAL PART

Low-density polyethylene-LDPE was used as matrix material, while single-walled carbon nanotubes-SWCNTs were selected as nanofiller. Nanocomposites preparation process was performed in three phases: (i) the preparation of SWCNT/LDPE mixtures with uniformly dispersed nanofiller in the matrix material by using twin-screw extrusion; the preparation of the samples with different network morphologies by (ii) injection molding (aligned network configuration) and (iii) compression molding (random network configuration). The morphology of SWCNT network was investigated by plasma etching technique coupled with SEM. The SWCNT network formation and growth was observed through rheological analysis, i.e., complex viscosity η*, viscoelastic storage G'(ω) and loss G"(ω) modulus as a function of frequency ω. Tests were conducted at constant temperature (150°C) in the linear viscoelastic regime by using a modular rotational rheometer MCR 302 (Anton Paar, Austria) coupled with plate-plate sensor system (PP25, 1 mm gap). Electrical conductivity was investigated by utilizing custom build 4-wire and 2-wire DC measurement rig. In the measured voltage range, all samples showed Ohmic behavior, thus the specific conductivity σ was determined from the linear slope of the *I-U* curves.

RESULTS AND DISCUSSION

From the rheological tests, the frequency dependency of the relative viscosity ($\eta_{rel} = \eta'/\eta_m$; η' - real part of complex viscosity, η_m - viscosity of matrix material) was determined. Two regimes can be observed (Fig. 1a): dilute and semi-dilute regime, separated by the critical volume fraction ϕ_{cv} indicating SWCNT network development. Below ϕ_{cv} (in the dilute regime) no particle interactions are present and SWCNT bundles behave as individual entities, mainly interacting with the host material. The mechanical reinforcement can be understood as a transfer of external load from host material to nanoparticles. However, above ϕ_{cv} (in the semi-dilute regime), the bundles form randomly connected network, where interactions by adjacent rods become significant. Bellow ϕ_{cv}, where bundles are unconstrained, two configurations were obtained, namely the aligned configuration formed in injection molding samples and the random configuration formed in compression molding samples. However, those configurations provide no particular change in the rheological behavior η_{rel}. Above ϕ_{cv}, the movement of the bundles is constrained and randomly connected network is formed regardless of the process method used, resulting in approximately the same mechanical reinforcement.

The electrical conductivity σ of nanocomposites was normalized to relative conductivity as $\sigma_{rel} = \sigma/\sigma_m$, ($\sigma_m$ is electrical conductivity of matrix material, Fig. 1b). The most interesting and significant finding of this work is that the electrical percolation threshold ϕ_{cv}^e distinctly differs and is not associated with the geometrical percolation ϕ_{cv}; moreover, it may occur at considerably lower concentrations. Below ϕ_{cv} the aligned configuration of injection molded samples does not allow the charge transfer, while the random configuration of compression molded samples allows the charge transfer although the network has not been fully established.

8TH PACIFIC RIM CONFERENCE ON RHEOLOGY, May 15-19, 2023

Assessment of Critical Conditions Required for Effective Hole Cleaning in Horizontal Wells - Effects of Fluid Rheological Properties and Near Wall Turbulence on the Particle Removal From Bed Deposits

Ergun Kuru

University of Alberta, Edmonton, Canada

ABSTRACT

Hole cleaning is a complex process as there are many variables affect cuttings removal (e.g. drilling fluid type, density, flow rate and rheological properties, cuttings size, hole inclination angle, drill pipe rotation speed and eccentricity). Among these variables, the drilling fluid flow rate and rheological properties are the most critical ones as they have strong influence on hole cleaning while at the same time, field control of these variables can be managed conveniently. Understanding the fluid/particle interaction, in particular, how drilling fluid velocity and rheological characteristics affect particle removal from bed deposits is, therefore, key to the design and development of optimum hydraulics program for effective hole cleaning.

Despite significant progress made in drilling fluids, tools, and field practices, along with more than 50 years of university and industry research, field experience indicates that hole cleaning is still a major problem on most highly inclined and horizontal wells.

As part of the systematic efforts to develop a unified theory of hole cleaning, a comprehensive research study has been conducted at the University of Alberta, which has two major components: i-) experimental investigation of the near bed turbulence and how it would relate to particle removal from bed deposits (i.e. fluid velocity effect); ii-) experimental investigation of how the critical conditions (i.e., flow rate, shear stress) for the particle removal from bed deposits changes with fluid shear dependent viscosity and viscoelastic properties (i.e., fluid rheological characteristics effect).

In this talk, I will present some of the results from our experimental investigations of the effects of fluid rheological properties and near wall turbulence on the particle removal from bed deposits in horizontal wells. Within the light of experimental results from the our studies along with the most recent findings in the sediment transport field, I will also discuss the inadequacies and unjustified assumptions currently used for mechanistic and semi-mechanistic (empirical) hole cleaning models and suggest alternative solutions to these shortcomings.

PRIMARY CEMENTING OF HORIZONTAL WELLS: LAMINAR DISPLACEMENT FLOWS IN OBSTRUCTED ECCENTRIC ANNULI

Marzieh Alishahi[1], Rodrigo Mitishita[2], Ian A. Frigaard[1,2]

[1]Department of Mechanical Engineering, University of British Columbia, Vancouver, Canada
[2]Department of Mathematics, University of British Columbia, Vancouver, Canada

ABSTRACT

Primary cementing is an operation performed during the construction of an oil well. The aim is to displace the drilling mud with a cement slurry along the gap between the rock formation and the steel casing. Difficulty arises because the gap is small, because the in-situ fluids (drilling muds) have a yield stress, and because the steel casing is rarely concentric in horizontal wells. Additional difficulties to the displacement include the presence of other geometrical irregularities along the length of the well such as the presence of washouts, keyseats and breakouts (see Renteria *et al.*[1] for more details) and also left over rock cuttings from drilling.

The motivation of this work is the study of displacement flows in a partially obstructed, eccentric annular space, which may be caused by a consolidated cuttings bed in the narrow side of the annulus. Recently, Mitishita *et al.*[2] experimentally investigated turbulent displacements of a Carbopol solution (yield stress fluid) in both an unobstucted and obstructed annulus, with the eccentricity $e = 0.5$ and 0.7. The addition of the obstruction was mostly detrimental at low eccentricities, with a significant amount of Carbopol left behind downstream of the obstruction. Furthermore, lowering the Reynolds number (while still in the turbulent flow regime) generally resulted in lower displacement efficiencies. However, other investigations resulted in less conclusive findings about efficiency of turbulent *vs* laminar displacements[2,3], without taking well irregularities into account.

We expand the previous experiments of Mitishita *et al.*[4] by focusing on laminar displacement flows in obstructed, eccentric annuli. These types of flows have only been studied briefly by 3D simulations[5], but not in experiments. To address this gap, we perform displacement flow experiments with Carbopol solutions as a displaced fluid. To achieve laminar Reynolds numbers in our large scale flow loop, xanthan gum solutions at high concentrations are used as displacing fluids. The rheology of the fluids is characterized with a Malvern Kinexus Ultra+ rheometer. Experimental measurements include pressure drop, flow rate and direct visualization of the displacement flows with high-resolution cameras. Our results serve as a comparison to the results of Mitishita *et al.*[4], while provinding an initial benchmark for numerical simulations of such flows.

REFERENCES

1. Renteria A., Sarmadi P., Thompson C., Frigaard I.A. Effects of wellbore irregularity on primary cementing of oil wells, Part 1: large scale effects. *J. Pet. Sci. Eng.*, **208**, 109581, 2022.

2. Maleki A., Frigaard I.A. Comparing laminar and turbulent primary cementing flows. *J. Pet. Sci. Eng.*, **30**, 123101, 2018.

3. Maleki A., Frigaard I.A. Turbulent displacement flows in primary cementing of oil and gas wells. *Phys. Fluids*, **177**, 808-821, 2019.

4. Mitishita R.S., Waldal N., Vogl A., Frigaard I.A. Turbulent displacement flows of viscoplastic fluids in obstructed eccentric annuli experiments *Phys. Fluids*, **34**, 053114, 2022.

5. Mitishita R.S., Sarmadi P., Waldal N., Vogl A., Frigaard I.A. Primary Cementing of Horizontal Wellbores With Solid Cutting Beds, International Conference on Offshore Mechanics and Arctic Engineering, Hamburg, Germany, ASME, 2022.

CEMENTING DISPLACEMENT FLOWS OF SHEAR-THINNING FLUIDS IN HORIZONTAL WELLS, WITH AND WITHOUT CASING ROTATION

Alondra Renteria[1] and Ian A. Frigaard[1]

[1]University of British Columbia, Vancouver, Canada

ABSTRACT

Results from a laboratory experimental study of displacement flows in an eccentric horizontal annulus are presented. The fluids are shear-thinning or Newtonian, with density differences. The scenario represents a typical horizontal well cementing setup. In general terms, we find that having a viscosity stable configuration (more stable fluid displacing less stable fluid) produces better displacements. However, now the effective viscosity ratio between fluids can vary at different locations around the annulus and with the imposed flow rate. Thus for example, we demonstrate how a flow rate increase can improve displacement by shear-thinning the displaced fluid. Casing rotation (i.e. rotating the inner cylinder), has been found to be effective at improving the displacement, but in the case of adverse viscosity ratios, displacement from the annulus walls remains poor. Lastly, it is noted that these reported effects of fluid rheology are mostly secondary to the dominant competition between eccentricity and buoyancy.

DISPLACEMENT FLOWS OF SHEAR THINNING FLUIDS IN A VERTICAL ANNULUS

Ruizi Zhang[1], Ian A. Frigaard[1,2]

[1] Department of Mechanical Engineering, University of British Columbia, 2054-6250 Applied Science Lane, Vancouver, BC, Canada V6T 1Z4
[2] Department of Mathematics, University of British Columbia, 1984 Mathematics Road, Vancouver, BC, Canada, V6T 1Z2

ABSTRACT

Displacement flows occur in construction of oil and gas wells, when the drilling mud is replaced with a cement slurry all along the annular gap between the steel casing and newly exposed rock formation. A complete and durable layer of cement that seals hydraulically, is the foremost goal of the primary cementing job. Failure to seal the well causes gas leakage, which may come from the target reservoir or an intermediate zone. There is acute current interest in such leakage due to greenhouse gas (GHG) emission implications, both environmentally and politically. Thus, a better understanding of all cementing processes is necessary and important, especially focusing on the rheology and mechanics of fluids.

To properly design, execute and evaluate a primary cement job, one must first understand the rheological properties of the fluids. Drilling muds and cement slurries are typically described as generalized Newtonian fluids, often with a yield stress and some shear thinning behaviour. In our previous studies[1,2,3,4], both experimental and computational directions have been followed, using Newtonian fluid pairs for simplicity. Amongst the main results is the general understanding that having a positive ratio of displacing to displaced fluid viscosity is beneficial in reducing the amount of dispersion within the annular gap. By extension, this implies that rheology does affect displacement, and our aim here is to understand the simplest such scenarios, where the fluids are shear-thinning. Are there practical situations in which rheology has a dominant effect on the displacement, or is it always secondary?

In this work, we present both experimental and computational results of displacement flows in a vertical eccentric annulus, using combinations of shear thinning and Newtonian fluids, as is representative of cement-preflush or preflush-mud pairings. In experimental study, Xanthan gum (XG) is used as the shear-thinning fluid. Glycerol and sugar are used to change the density and viscosity of the fluids. A high-resolution Malvern Kinexus Ultra+ rheometer with parallel plates is employed to characterize the XG solutions, and the result can be fitted to the Power-law model. The experiments were carried out in a dimensionally scaled laboratory set-up[4]. As comparisons, we ran a series 3-D numerical simulations by solving the full Navier-Stokes equations and concentration advection equation. A power law model is used for non-Newtonian

fluids. We have found that using shear thinning fluids yields similar flow trends as the Newtonian fluids, if other parameters are maintained the same. The buoyancy force and eccentricity are still dominant in controlling the displacement efficiency. The shear thinning rheology starts to play a secondary role when the flow rate increases, but is still not distinct from that of purely viscous flows.

REFERENCES

1. Renteria, A.; Frigaard, I. A. Primary cementing of horizontal wells. Displacement flows in eccentric horizontal annuli. Part 1. Experiments. *Journal of Fluid Mechanics*, **905**, A7, 2020. https://doi:10.1017/jfm.2020.713.
2. Sarmadi, P.; Renteria, A.; Frigaard, I. A. Primary cementing of horizontal wells. Displacement flows in eccentric horizontal annuli. Part 2. Computations. *Journal of Fluid Mechanics*, **915**, A83, 2021. https://doi:10.1017/jfm.2021.158.
3. Zhang, R.; Frigaard, I. A. Primary cementing of vertical wells: Displacement and dispersion effects in narrow eccentric annuli. *Journal of Fluid Mechanics*, **947**, A32, 2022. https://doi:10.1017/jfm.2022.626.
4. Zhang, R; Jung, H; Renteria, A; Frigaard, I. A. Experimental Study of Displacement Flows in a Vertical Eccentric Annulus. In *proceedings of the ASME 2022 41st International Conference on Ocean, Offshore and Arctic Engineering*, V010T11A051, June 5–10, 2022. https://doi.org/10.1115/OMAE2022-78621.

8TH PACIFIC RIM CONFERENCE ON RHEOLOGY, May 15-19, 2023

NON-BROWNIAN SUSPENSIONS IN PRESSURE-DRIVEN FLOW: NUMERICAL SIMULATIONS WITH FRAME-INVARIANT SUB-GRID CORRECTIONS

Michel Orsi[1,2], Laurent Lobry[1] and François Peters[1]

[1]Université Côte d'Azur, CNRS, Institut de Physique de Nice (INPHYNI), France
[2]Benjamin Levich Institute and Department of Chemical Engineering,
CUNY City College of New York, New York, New York 10031

INTRODUCTION

Significant progress in the understanding of the rheology of non-Brownian suspensions has been made during the last decade [1], particularly thanks to the consideration of direct interactions between particles [2,3,4]. Discrete simulations that take into account both these direct interactions and the hydrodynamic ones have played an important role. However, many fundamental questions are still open, often involving heterogeneous flows characterized by a spatially variable volume fraction and shear rate. The simulation of this type of flow requires special treatment.

METHOD

We use the Fictitious Domain Method (FDM) implemented in the OpenFOAM toolbox [5]. In this particle-scale approach, the mesh is Cartesian, regular and fixed, and the Navier-Stokes equations are solved over the whole simulation domain. A specific force density is applied in order to impose the rigidity of the particles. When two particles move at a small distance from each other, a lubrication flow occurs. If the inter-particle distance is smaller than the mesh grid size, this flow cannot be calculated by the solver and sub-grid corrections must therefore be introduced to fully take into account the missing forces and stresses. Classically, the sub-grid corrections are implemented for a linear flow and involve the particle velocity relative to the ambient flow and the local strain rate [2]. In the case of a heterogeneous flow, this formulation is no longer suitable as it requires the local strain rate to be evaluated at each position, at the cost of significant practical problems. We propose a new formulation for which we can remove the terms involving the ambient flow, making it possible to express the stresses on the particles only in terms of a function of the particles velocities, while maintaining the frame-indifference of this relation [5].

RESULTS

Using this new formulation for the sub-grid corrections, we present simulation results of frictional suspensions in a plane Poiseuille flow, investigating different values of the volume fraction. As observed in earlier experimental and numerical works [6,7,8], shear-induced particle migration toward

the center of the channel is observed, resulting in a variable volume fraction profile and a blunted velocity profile across the channel (see Figure 1). The results are compared to a modified version of the Suspension Balance Model (SBM) [9,10]. Finally, a detailed local balance of the contact and hydrodynamic stresses, including the fluid pressure, is performed.

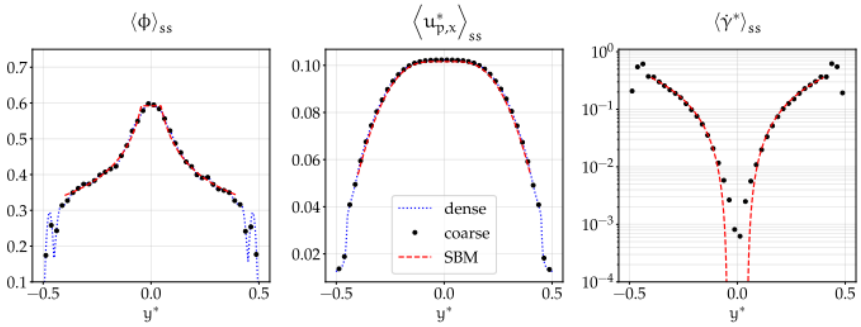

Figure 1: Steady-state results for $\phi_0 = 0.40$ and comparison with a modified version of the SBM. Coarsely- and densely-discretized profiles across the channel ($y^* = y/L$, being y the direction of the gradient of the velocity, and L the channel width): (left) volume fraction, (center) particle velocity, and (right) shear rate.

ACKNOWLEDGEMENTS

This work was supported by the French National Agency (ANR) under the program Blanc AMARHEO (ANR-18-CE06-0009-01). This work was also supported by the French government, through the UCAJEDI Investments in the Future project managed by the National Research Agency (ANR) under reference number ANR-15-IDEX-01.

REFERENCES

1. Guazzelli É., Pouliquen O, Rheology of dense granular suspensions, *Journal of Fluid Mechanics*, **852**, 2018.

2. Gallier S., Lemaire E., Peters F., Lobry L., Rheology of sheared suspensions of rough frictional particles, *Journal of Fluid Mechanics*, **757**, 514–549, 2014.

3. Mari R., Seto R., Morris J.F., Denn M.M., Shear thickening, frictionless and frictional rheologies in non-Brownian suspensions, *Journal of Rheology*, **58(6)**, 1693–1724, 2014.

4. Peters F., Ghigliotti G., Gallier S., Blanc F., Lemaire E., Lobry L., Rheology of non-Brownian suspensions of rough frictional particles under shear reversal: A numerical study, *Journal of Rheology*, **60(4)**, 715–732., 2016.

5. Orsi M., Lobry L., Peters F., Frame-invariant sub-grid corrections to the Fictitious Domain Method for the simulation of particulate suspensions in nonlinear flows using OpenFOAM, *Journal of Computational Physics*, **474**, 2023.

6. Lyon M.K., Leal L.G., An experimental study of the motion of concentrated suspensions in two-dimensional channel flow. Part 1. Monodisperse systems, *Journal of Fluid Mechanics*, **363**, 25–56, 1998.

7. Yeo K., Maxey M.R., Numerical simulations of concentrated suspensions of monodisperse particles in a Poiseuille flow, *Journal of Fluid Mechanics*, **682**, 491–518, 2011.

8. Rashedi A., Sarabian M., Firouznia M., Roberts D., Ovarlez G., Hormozi S., Shear-induced migration and axial development of particles in channel flows of non-Brownian suspensions, *AIChE Journal*, **66(12)**, e17100, 2020.

9. Nott P.R., Guazzelli E., Pouliquen O., The suspension balance model revisited, *Physics of Fluids*, **23(4)**, 043304, 2011.

10. Badia A., D'Angelo Y., Peters F., Lobry L., Frame-invariant modeling for non-Brownian suspension flows, *Journal of Non-Newtonian Fluid Mechanics*, **309**, 104904, 2022.

FINITE SYSTEM SIZE CORRECTION IN MICRORHEOLOGICAL ANALYSIS UNDER PERIODIC BOUNDARY CONDITIONS : A DIRECT NUMERICAL SIMULATION APPROACH

Yasuya Nakayama[1], Yuki Matsuoka[2], Toshihisa Kajiwara[1]

[1]Dept. Chemical Engineering, Kyushu University, Fukuoka 819-0395, Japan
[2]Corporate Engineering Center, Sumitomo Bakelite Co., Ltd., Shizuoka 426-0041, Japan

ABSTRACT

To investigate the Brownian motion of particles suspended in viscoelastic fluids, stochastic Smoothed Profile method (SPm) as a direct numerical simulation is developed by extending deterministic SPm for suspensions in viscoelastic media. To solve the viscoelastic flow driven by thermal fluctuations in the suspending medium, the random stress in the fluid momentum equation as well as the random driving force for the conformation tensor in the Oldroyd-B model are incorporated according to the fluctuating hydrodynamics and fluctuating viscoelasticity formalisms. Thermal equilibrium and dynamical properties calculated by numerical simulations successfully reproduce the analytic predictions, validating the direct simulation for the coupled fluctuating Navier.Stokes and Oldroyd-B equations, and for the coupling between the stochastic viscoelastic medium and particles. As an application of the stochastic SPm, we investigate a finite system size effect under periodic boundary conditions (PBC) on the passive microrheological relationship between the mean-square displacement (MSD) of a Brownian particle and the medium dynamic modulus. Comparing the modulus microrheologically calculated from MSD with the input one reveals that the effect of periodic image cell interaction appears not only in the long-time diffusive regime but also in the short-time region. A frequency-dependent finite system size correction is implemented by phenomenologically extending the long-time diffusive regime correction, allowing the passive microrheology analysis under PBCs. This result can be directly applied to other different mesoscale numerical simulations including coarse-grained molecular dynamics and dissipative particle dynamics.

ACKNOWLEDGEMENTS

The numerical calculations were mainly carried out using the computer facilities at the Research Institute for Information Technology at Kyushu University. This work was supported by Grants-in-Aid for Scientific Research (JSPS KAKENHI) under Grant No. JP18K03563.

Lubrication force between two approaching cylinders in a Bingham fluid

Xavier Chateau[1] and Anthony Wachs[2]

[1]Ecole des Ponts ParisTech, Champs-sur-Marne, France
[2]University of British Columbia, Vancouver, Canada

ABSTRACT

We examine the problem of two circular cylinders immersed in a Bingham fluid approaching each other at zero Reynolds number. The goal of this study is to understand how lubrication forces manifest in the small gap between the cylinders as a function of the Bingham number. We consider both (i) the case of purely normal lubrication force when the relative position vector and the velocity vector of both cylinders are aligned and (ii) the case with normal and tangential lubrication forces when this alignment is broken.

We select a large enough flow domain such that the assumption of two cylinders immersed in an infinite domain is reasonably satisfied and the spurious influence of the boundary conditions at the limit of the finite size domain is minimal in the case of small Bingham numbers. The flow domain is therefore a simple and large rectangle and the two cylinders are located close to its center. We compute the two-dimensional steady flow solution for a set of cylinder positions and cylinder velocities. The set of governing equations comprise the Stokes equations and the Bingham constitutive law, combined to Dirichlet conditions imposed on the velocity field over all boundaries of the flow domain. While the magnitude of the cylinder velocities is not a relevant parameter, we coherently set it to a value such that the corresponding Reynolds number is indeed very small and representative of Stokes flow conditions. The solution is obtained by an Augmented Lagrangian algorithm or a FISTA algorithm that both solve the Bingham model without any regularization [1]. We use a boundary fitted Finite Element discretization scheme with either P1-P2-P1DC or P1-P1isoP2-P0isoP2 elements for pressure, velocity and strain rate tensor components, respectively, combined to adaptive unstructured mesh refinement to capture the details of the flow field and the yield surfaces as accurately as possible [3]. The code is implemented on the FreeFEM++ platform [2] and is validated through comparisons with results published in the literature on other similar flow configurations [3].

We discuss the computed results in terms of flow field, yielded/unyielded regions and magnitude of the lubrication force. Given that our computed results fully resolve the flow in the thin lubrication gap, we are also in a position to compare them to approximate analytical solutions previously published in the literature [4]. The findings of this work also contribute to extend our understanding of the role of lubrication in dense suspensions of rigid particles in a yield stress fluid.

Cross Flow Filtration of Viscoplastic Suspensions, a Robust Mathematical model

Mahdi Izadi[1,2], Ian A. Frigaard[1,2], Seyed Mohammad Taghavi[3]

[1]Department of Mechanical Engineering, University of British Columbia, BC, Canada, V6T 1Z4
[2] Department of Mathematics, University of British Columbia, Vancouver, Canada, V6T 1Z2
[3] Department of Chemical Engineering, Laval University, Quebec, Canada G1V 0A6

The flow of suspension in conduits with large aspect ratios has always been a topic of pivotal importance in a wide range of applications, including but not limited to cardiovascular flows, slurry transport, filtration, etc. Rheological complexities of suspensions, such as its dependency on the volume fraction of solids, possibility of formation of solid cake, and the migration of particles have challenged researchers in their studies. In addition, the presence of particles modifies local strain rates and shear rate, subsequently, which necessitates meticulousness for if the suspending fluid has shear-dependent rheology. Besides, as the carrying fluid exhibits yield stress behavior,the possibility of plug formation may affect the flwo characteristics, such as shear-induced migration of particles, which necessitates a proper track down of yield surface.

The occurrence of cross-flow filtration, in which only the liquid content can pass through the walls, makes the dynamics of the solid phase, and so the suspension, and also the yield surface more complicated.

This paper proposes a mathematical model for the cross-flow filtration of viscoplastic suspensions, in a continuum framework. Using the Suspension Balance Model and homogenization approach, we consider the particle migration, and local shear effects, respectively. Our model takes the transition from suspension flow into a packed bed formation and the possibility of interstitial flow into account.

We base our model on Transversal Flow Equilibrium (TFE) to accurately depict the yield surface, while considering the effect of the reduction of the flow-rate due to the filtration. TFE allows considering the plug area as strictly unyileded.

Different in-flow conditions, including constant flow rate and pressure, are explored in this model, allowing the exploration of various phenomena such as dispersion and stoppage mechanisms.

This paper investigates the flow and penetration of a viscoplastic suspension in a long permeable parallel/converging plate geometry under different conditions, and discusses the effect of different parameters on the penetration length and time, and the stoppage mechanisms in various scenarios over relevant ranges.

References

[1] Hormozi S. and Frigaard IA. Dispersion of solids in fracturing flows of yield stress fluids. *Journal of Fluid Mechanics 830.* (2017) **47**: 93–137.

IMPARTING EXTENSIBILITY TO JAMMED COLLOIDAL INKS FOR DIRECT-INK-WRITING PRINTABILITY

Chaimongkol Saengow[1], Samya Sen[2,6], Joaquin Yus[3], Kelly M. Chang[1,5]
Amy J. Wagoner Johnson[1,2,3,4] and Randy H. Ewoldt[1,2]

[1]Beckman Institute for Advanced Science and Technology, University of Illinois Urbana-Champaign, Urbana, Illinois 61801, USA
[2]Department of Mechanical Science and Engineering, University of Illinois Urbana-Champaign, Urbana, Illinois 61801, USA
[3]Carl R. Woese Institute for Genomic Biology, University of Illinois Urbana-Champaign, Urbana, Illinois 61801, USA
[4]Carle Illinois College of Medicine, University of Illinois Urbana-Champaign, Urbana, Illinois 61801, USA
[5]Department of Materials Science of Engineering, University of Illinois Urbana-Champaign, Urbana, Illinois 61801, USA
[6]Department of Materials Science and Engineering, Stanford University, Stanford, California 94305, USA

ABSTRACT

We introduce and test the hypothesis that extensional rheology, as well as yield stress, are the two key rheological properties [1] for jammed colloidal inks used in direct-write 3D printing of implantable lattice-structured bone scaffolds (**Fig. 1.**). Guided by prior observations that yield stress fluids can be engineered with high extensibility [2], and that higher extensibility of emulsion-based yield stress fluids enabled more robust printing [3], we describe an experimental study of these paste-like materials that varies ink formulation and flow conditions to map printability to these rheological properties. The inks consist of an aqueous suspension of hydroxyapatite particles (the main mineral of bone), irregularly shaped and sized 1-10μm, which creates a cementitious paste-like yield-stress fluid. To induce capillarity for better bone growth, we add sacrificial polymethyl methacrylate beads (PMMA, 5.96 ± 2.00μm in diameter) to create microporosity in the final scaffolds. This baseline formulation of ink is difficult to print due to brittle filament rupture if the nozzle speed is not closely matched to the average velocity of the extruded ink. We examine two methods to tune extensibility and yield stress: (i) incorporating polymer additives, and (ii) modulating electrostatic particle interaction. Hydroxypropyl methylcellulose serves as the polymer additive, tested at different loading. Polyacrylic acid and polyethylenimine coat the particles with negative and positive charge, respectively, to modulate yield stress. By mapping printability to the rheological design requirements of extensibility and yield stress, our results show how modulating these two key rheological properties can improve printability.

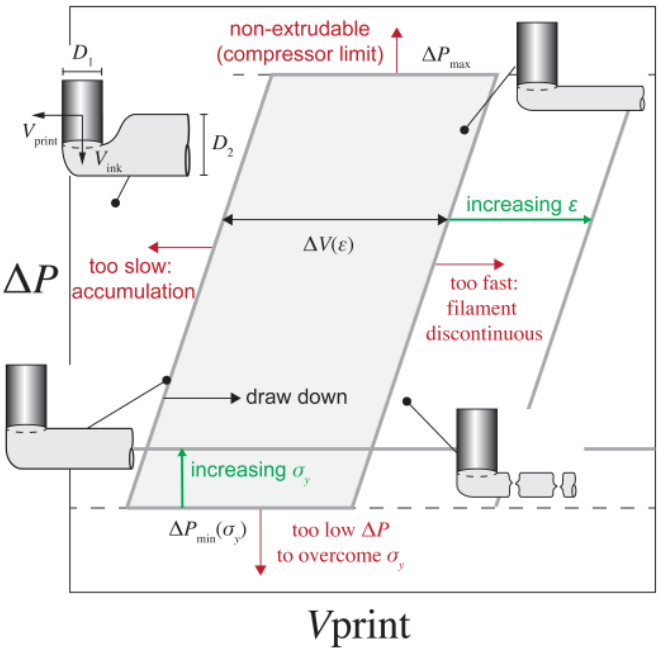

Figure 1: Printability map of direct-ink writing of lattice scaffolds shows four important regimes, depending on the two characteristic speeds: (i) ink accumulation when $V_{\text{print}} < V_{\text{ink}}$ yielding $D_1 < D_2$; (ii) equi-dimentional, $V_{\text{print}} = V_{\text{ink}}$, $D_1 = D_2$; (iii) rod thinning, $V_{\text{print}} > V_{\text{ink}}$, , $D_1 > D_2$; and (iv) rod discontinuous $V_{\text{print}} \gg V_{\text{ink}}$. The rod thinning window can be widened by extensibility.

REFERENCES

1. Ewoldt, R. H.; Saengow, C. Designing Complex Fluids. Annu. Rev. Fluid Mech., **54**, 413–441, 2022. https://doi.org/10.1146/annurev-fluid-031821-104935.
2. Nelson, A. Z.; Bras, R.; Liu, J.; Ewoldt, R. H. Extending Yield-Stress Fluid Paradigms. *J. Rheol.* **61(1)**, 357–369, 2018. https://doi.org/10.1122/1.5003841.
3. Rauzan, B. M.; Nelson, A. Z.; Ewoldt, R. H.; Nuzzo R. G. Particle-Free Emulsions for 3D Printing Elastomers. *Adv. Funct. Mater.* **28(21)**, 1707032, 2018. http://doi.org/10.1002/adfm.201707032

Plenary Presentation - MATH 100 (12:50 PM - 1:50 PM)

8TH PACIFIC RIM CONFERENCE ON RHEOLOGY, May 15-19, 2023

SLUDGE RHEOLOGY AND ITS APPLICATIONS IN SLUDGE TREATMENT PROCESSES

Nicky Eshtiaghi[1]
[1]RMIT University, Australia

ABSTRACT

Sludge rheology is important for the design and operation of sludge treatment processes in terms of process optimisation and maintenance cost reduction. Sludge rheology has a significant impact on the performance of pumps, anaerobic digesters, dewaterability equipment, mixers, and heat exchangers.

A large portion of the total energy consumption in any sludge treatment plants is used for pumping sludge within the treatment processes. The efficient operation of sludge pumps requires an accurate calculation of friction losses for which sludge rheological parameters is an important parameter. Rheological parameters change as composition changes due to season, origin and treatment process. Furthermore, the type of selected rheological model and data fitting process impact on the pressure drop calculation. A validated pressure drops calculation toolkit was developed with up to 10% errors against actual data collected both at industrial scale and a pilot plant of sludge pumping system in a range of solid concentrations of sludge.

Anaerobic digesters are used to treat sludge and produce biogas. The rheology of the sludge can affect the digestion process, as it can impact the ability of microorganisms to break down the organic matter in the sludge. Sludge with high viscosity may have a lower biodegradability, resulting in a longer retention time within the digester, which can increase the size and cost of the digester. Additionally, the rheology of the sludge can impact the efficiency of the mixing within the digester, affecting the biogas production and overall treatment performance. The impact of the extent of digestion in terms of the volatile solids destruction on rheological properties in semi-continuous pilot digesters is also presented. Experimental results from this study indicate that higher volatile solids destruction leads to increased difficulty to flow and dewater. Since rheological behaviour is interlinked with chemical organic content (COD) of sludge, On-line rheometers can be used to monitor this process performance indicator (COD) rather than conducting offline time consuming chemical tests.

There is still much to be learned about the complex interactions between different components in sludge, and that new measurement techniques will be needed to improve our understanding of sludge rheology and its applications in sludge treatment processes.

8TH PACIFIC RIM CONFERENCE ON RHEOLOGY, May 15-19, 2023

BIOPRINTING OF COLLAGEN HYDROGELS IN A SUPPORTED GEL ENVIRONMENT

Yaman Boluk[1*], Xiaoyi Lan[1], and Adetola Adesida[2,3]

[1]Department of Civil and Environmental Engineering, Faculty of Engineering, University of Alberta, Edmonton, AB, Canada
[2]Department of Surgery, Divisions of Orthopedic Surgery & Surgical Research, Faculty of Medicine & Dentistry, Li Ka Shing Centre for Health Research Innovation, University of Alberta, Edmonton, AB, Canada
[3]Department of Surgery, Division of Otolaryngology, Faculty of Medicine & Dentistry, Li Ka Shing Centre for Health Research Innovation, University of Alberta, Edmonton, AB, Canada

ABSTRACT

The challenge of 3D printing soft hydrogels such as live cell-embedded collagens in tissue engineering is to build complex structures while keeping overhanging features intact. Those requirements can be met by extruding "weak" printable hydrogels directly into the bath of a supporting gel. The supporting gel prevents the collapse or deformation of the printed object under its weight. Once the printing is completed, the object is cured, removed from the support bath, and rinsed off. This sacrificial supporting gel has to be removed easily after 3D printing. Supporting baths, based on crosslinked polyacrylic copolymer microgels, granular gels, silica nanoparticle suspensions, nano clay suspensions, hydrophilic poly(ethylene oxide) (PEO) (PluronicTM) are reviewed. The design of an appropriate supporting hydrogel bath poses several challenges. The supporting gel has to behave like Bingham plastic, not yielding until a threshold shear force is reached. In the meantime, its yield stress, τ_y has to be low enough to accommodate nozzle movement. Besides supporting the deposited printing gel, the support bath must exhibit a high plateau shear elastic modulus, G ′. In addition, those viscoelastic properties have been thermo-reversible. Our group has prepared and printed live cell-laden collagens in gelatin support baths for engineered nasal cartilage applications, which can potentially replace and reduce donor-site morbidities associated with native cartilage grafts taken from other anatomical sites for reconstructive nasal surgeries. In those studies, complex objects are printed in support gels with delicate structures.

FREEFORM PRINTING MODEL

In a typical freeform printing in a gel process, a filament drop is extruded from the dispensing needle with a release speed of V and dragged to a horizontal distance equal to the step distance with a path speed of v_o. This step-by-step horizontal movement of filament extrudate in the support gel bath can be modeled as shown in Figure 1.

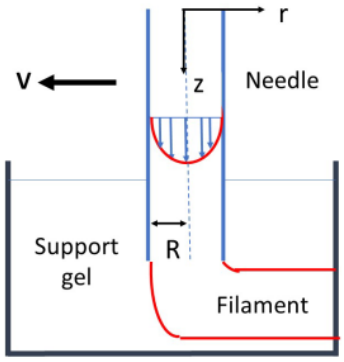

Fgure 1: Filament depostion in a gel bath

EFECTS OF GELATION CONCENTRATION ON CYCLIC DEFORMATION BEHAVIOR OF POLYSACCHARIDE HYDROGELS

Jun-ichi Horinaka[1], Souma Ogawa[1], Hiroshi Takagaki[1], Tomoya Tanaka[1] and Toshikazu Takigawa[1]

[1] Kyoto University, Kyoto, Japan

ABSTRACT

Cyclic deformation behavior of κ-carrageenan and agarose hydrogels have been examined to elucidate the relationship between the network structures of polysaccharide hydrogels and their mechanical properties. Regarding the gelation mechanism on the molecular level, it has been commonly reported that these polysaccharides dissolved in water tends to transform the chain conformation from random-coil to helix on decreasing temperature and a piece of hydrogel appears successively by the aggregation of the helical chains to be crosslinks of the gel above a critical concentration. However, there is a decisive difference in the interaction between aggregated helices. In the case of κ-carrageenan, an anionic polysaccharide, the aggregation of the helical chains becomes stable by the shielding effect of counter-cation species on the electrostatic repulsion between anionic helices. On the other hand, helices of agarose, a neutral polysaccharide, aggregates via hydrogen bonding. Hydrogels have been prepared at different gelation concentrations, and then the stress-strain curves during four cyclic deformations have been measured at the same network concentration. It has been found that Young's modulus for κ-carrageenan hydrogels is higher for the gel prepared at 5 gL^{-1} (C05) compared to that for the gel prepared at 30 gL^{-1} (C30) [1] and that the relation between Young's modulus and the gelation concentration is opposite for agarose hydrogels. C30 shows almost linear relation between the stress and the strain like an ideal rubber, while a residual strain appears in each cyclic deformation for C05, as shown in Fig.1. The extent of the residual strain depends on the maximum strain and the deformation speed, indicating that C05 deforms plastically to some extent. The residual strain for C05 decreases gradually even after a cyclic deformation and disappears in the case of a small strain as if there were a memory of the structure. Qualitatively-similar difference in the cyclic deformation behavior has been obtained for agarose hydrogels. Optical investigations of the hydrogels have been also carried out to explain the effects of the gelation concentration on the mechanical properties based on the network structure specific to the polysaccharides.

TENDON FASCICLE-INSPIRED COLLAGEN MULTIFILAMENT BUNDLE PRODUCED BY MULTI-PIN CONTACT DRAWING OF AN AQUEOUS COLLAGEN-POLYETHYLENE OXIDE SOLUTION

Hessameddin Yaghoobi[1,2], John Frampton[2,3] and Laurent Kreplak[1,2]

[1]Department of Physics & Atmospheric Science, Dalhousie University, Halifax, Nova Scotia, B3H 4R2, Canada
[2]School of Biomedical Engineering, Dalhousie University, Halifax, Nova Scotia, B3H 4R2, Canada
[3]Department of Biochemistry & Molecular Biology, Dalhousie University, Halifax, Nova Scotia, B3H 4R2, Canada

ABSTRACT

Polyethylene oxide (PEO)-collagen monofilaments are prepared using multi-pin contact drawing, which is a bio-friendly and cost-effective method that uses an entangled polymer fluid to aid in monofilament formation[1]. Using this bottom-up approach, thousands of monofilaments containing well-aligned collagen triple helices are assembled into a structure that recapitulates the architecture of a tendon fascicle. In this approach, a series of hydration steps are applied to remove the PEO, and promote the self-assembly of the collagen triple helices into fibrils within each monofilament, while preserving the hierarchical structure of the collagen multifilament bundle. Attenuated total reflectance Fourier-transform infrared (ATR-FTIR) spectroscopy and wide-angle X-ray scattering (WAXS) are used to confirm the presence and alignment of collagen triple helices in the resulting collagen multifilament bundle. Scanning electron microscopy (SEM) reveals that each monofilament contains collagen fibrils with a diameter around 15 nm. Small angle X-ray scattering (SAXS) patterns are consistent with fibrils containing microfibrils, with the characteristic D-band spacing observed *in vivo*. However, these microfibrils are axially staggered by one-sixth of the D-band spacing. This is a well-known polymorphic form of collagen that has been observed *in vitro*[2], albeit at significantly lower collagen concentration than what is used here. These polymorphic collagen fibrils can be effectively crosslinked with ultraviolet (UV) radiation in the dry state giving rise to collagen multifilament bundles with an average ultimate tensile strength (UTS) of 38.5 MPa, which is comparable to that of wet spun, glutaraldehyde crosslinked collagen multifilaments (40 MPa)[3], and also to that of rat tail tendon fibers (39 MPa)[4]. The effect of UV crosslinking on the chemical and molecular structure of collagen multifilament bundles is also demonstrated through ATR-FTIR spectroscopy and WAXS, which shows that the triple-helical structure of the collagen molecule remains unchanged. This fabrication method leverages extensional flow for molecular alignment, decouples the molecular alignment from the molecular assembly, recapitulates the structure of a tendon and offers tunability in tensile properties, using only

collagen molecules and no other chemical additives in addition to PEO, which is removed during the hydration process.

REFERENCES

1. Verma, S. K.; Yaghoobi, H.; Slaine, P.; Baldwin, S. J.; Rainey, J. K.; Kreplak, L.; Frampton, J. P. Multi-Pin Contact Drawing Enables Production of Anisotropic Collagen Fiber Substrates for Alignment of Fibroblasts and Monocytes. *Colloids Surfaces B Biointerfaces*, **215**, 2022. https://doi.org/10.1016/j.colsurfb.2022.112525.
2. Harris, J. R.; Reiber, A. Influence of Saline and pH on Collagen Type I Fibrillogenesis in Vitro: Fibril Polymorphism and Colloidal Gold Labelling. *Micron*, **38(5)**, 513–521, 2007. https://doi.org/10.1016/j.micron.2006.07.026.
3. Tonndorf, R.; Aibibu, D.; Cherif, C. Collagen Multifilament Spinning. *Mater. Sci. Eng. C*, **106**, 2020. https://doi.org/10.1016/j.msec.2019.110105.
4. Kato, Y. P.; Christiansen, D. L.; Hahn, R. A.; Shieh, S. J.; Goldstein, J. D.; Silver, F. H. Mechanical Properties of Collagen Fibres: A Comparison of Reconstituted and Rat Tail Tendon Fibres. *Biomaterials*, **10 (1)**, 38–42, 1989. https://doi.org/10.1016/0142-9612(89)90007-0

EFFECT OF HOMOGENIZATION OF RAW MILK ON THE PHYSICAL PROPERTIES OF AGED CHEESE

Isamu Kaneda[1], , Sasara Kaneko[1], Takashi Tochihara[1] and Masato Ohnuma[2]

[1]Rakuno Gakuen University, Hokkaido, Japan
[2]Hokkaido University, Hokkaido, Japan

ABSTRACT

The art of cheese production is a sophisticated technology that has been refined over many years of experience. However, it is well known that the characteristics of the final product vary depending on the characteristics of the raw milk and the conditions during production. Such problems indicate that maintaining a constant product quality is a difficult task even today. Our research is focused on the question of how the condition of the milk influences the physical properties of cheese. Generally the production of aged cheese does not involve homogenization of the raw milk, because such shear stress on the milk affects to the mechanical properties of cheese. However, the reason of the phenomenon is still unknown. Therefore we investigated the effect of homogenization of raw milk on the physical properties of aged cheeses.

In this p aper, Gouda-type cheese was produced by relatively low pressure homogenization (2-4 MPa) of raw milk, and rheological properties were examined immediately after production and throughout the 8-weeks ripening period. The fracture strength of homogenized cheese immediately after production was lower than the control. During the ripening period, the fracture strength reached a minimum around 10 days and then converged to a constant value which was dependent on the homogenization strength (Fig.1). Linear viscoelastic properties were also examined throughout the ripening period to obtain information on the structure of the cheese. The mechanical spectrum of the cheese can be analysed with a weak-gel model (Eq.1).

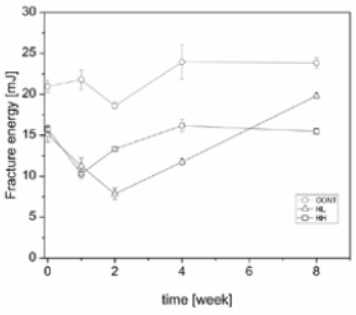

Fig.1. Changes in fracture energy during the ripening period for each sample. Circles, triangles, and squares denote the results for CONT(non homogenized), HL (2MPa), and HH(4MPa), respectively.

$$G^* = A_f \omega^{1/z} \quad (1)$$

The coordination number (z) in this model is a parameter of the degree of filling of the hypothetical flow unit in the system, and this parameter is considered to represent structural information at the colloidal level. Fig. 2 shows the transition of z during the ripening process. It was found that the structure at the colloidal level changes discontinuously around 10 days of ripening. Nanostructures in the cheese during the ripening period were also examined by SAXS measurements. We found that the behaviour of structures a few nanometers in diameter, which we believe to be colloidal calcium phosphate (CCPs), changed around 10 days of aging, and this phenomenon was thought to correspond to a discontinuous change in mechanical properties around 10 days of aging.

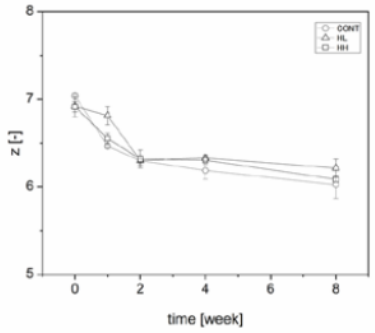

Fig.2. Change in coordination number during the ripening period for each sample. Circles, triangles, and squares denote the results for CONT (non homogenized) , HL (2MPa), and HH (4MPa), respectively.

Reports of studies tracking rheological properties during the cheese ripening process are rare, and we hope that the results of this study will encourage more thought about the events that are occurring in cheese during ripening.

ACKNOWLEDGEMENTS

This work was supported by JSPS KAKENHI Grant Number 20H02926

8TH PACIFIC RIM CONFERENCE ON RHEOLOGY, May 15-19, 2023

Formulating adhesives with aminated polyolefins for low surface energy substrate

Z. Zhang[1], B.M. Yavitt[1,2,3], B. Kaur[2], D.J. Gilmour[2,4], L.L. Schafer[2], S.G. Hatzikiriakos[1]

[1] Department of Chemical and Biological Engineering, University of British Columbia, Vancouver, B.C, Canada, V6T 1Z3

[2] Department of Chemistry, University of British Columbia, Vancouver, B.C, Canada, V6T 1Z1

[3] Department of Chemical Engineering, University of Cincinnati, Cincinnati, OH, USA

[4] a2o Advanced Materials Inc., Vancouver, B.C, Canada, V6T 1Z1

ABSTRACT

Non-polar polyolefins are catalytically functionalized with amine substituents to yield polar polymers with dynamic associative interactions[1]. Aminated polyolefins (APO) display self-healing ability and impressive adhesive properties on many commodity polyolefins and poly(tetrafluoroethylene) (PTFE)[1]. The potential for APO to be used as an adhesive material is limited by its low mechanical strength. The addition of commercial polyolefin tackifiers is found to increase the mechanical properties while maintaining the unique properties of APO. APO was blended with additive at different mass ratios. Rheological, mechanical and adhesion properties of the formulations were collected to gain insight into the wide parameter space and the impact of polymer chain dynamics on the adhesive performance. Potential candidates for general-use of these hot-melt adhesive systems were selected based on the optimized rheology, mechanical and adhesive results.

REFERENCES

(1) Gilmour, D. J.; Tomkovic, T.; Kuanr, N.; Perry, M. R.; Gildenast, H.; Hatzikiriakos, S. G.; Schafer, L. L. Catalytic Amine Functionalization and Polymerization of Cyclic Alkenes Creates Adhesive and Self-Healing Materials. *ACS Appl. Polym. Mater.* **2021**, *3* (5), 2330–2335. https://doi.org/10.1021/acsapm.1c00158.

CONFORMATIONAL RELAXATION OF STYRENE-BUTADIENE RUBBERS HAVING A DIFFERENT MICROSTRUCTURE BUT THE SAME COMPOSITION AT HYDROPHILIC AND HYDROPHOBIC INTERFACE

Hidenobu Taneda[1], Kosuke Fujino[2], Daisuke Kawaguchi[1,2] and Keiji Tanaka[1,2]

[1]Center for Polymer Interface and Molecular Adhesion Science,
Kyushu University, Fukuoka, Japan
[2]Department of Applied Chemistry, Kyushu University, Fukuoka, Japan

ABSTRACT

The orientational relaxation of poly(styrene-*r*-butadiene) (SBR) chains at solid interfaces were examined by sum-frequency generation spectroscopy (SFG) with the molecular-level depth resolution. To tackle an effect of interaction between segments and substrate on the interfacial mobility of chains, SBRs having different microstructures but the same composition, were prepared on hydrophilic and hydrophobic quartz substrates. At a hydrophilic interface, SFG signal intensity from phenyl groups decreased with increasing temperature and the temperature dependence markedly changed at a characteristic temperature (T_c). The T_c, in which chains start to structurally relax, was ca. 150 K higher than the bulk glass transition temperature. It is likely that 1,2- and 1,4-butadiene are energetically comparable to each other for the quartz surface. On the other hand, the T_c was not discerned at a hydrophobic interface. This makes it clear that the orientational relaxation was markedly suppressed possibly due to the stronger interaction between chain segments and hydrophobic surface.

INTRODUCTION

Polymer nanocomposites, in which inorganic nanofillers are dispersed, show better mechanical and dielectric properties than the neat polymer matrix. The improvement of the properties strongly depends on the aggregation states and molecular motion of chains at the interface with the filler. So far, based on sum-frequency generation (SFG) spectroscopy, we reported that adsorbed polymer chains in direct contact with the solid surface were frozen in mobility up to a temperature far above the bulk glass transition temperature (T_g^b), depending

on the interaction between them.[1-3] Given that the interaction became stronger, the reinforcement effect should be more effective, leading to better mechanical properties. The objective of this study is to obtain better understanding of how the interaction between polymer and solid surface impacts the polymer mobility at the interface.

EXPERIMENTAL SECTION

As samples, poly(styrene-*r*-butadiene) (SBR) composed of constant styrene (St) content (22–24 mol%) and varying 1,2- and 1,4-butadiene (1,2- and 1,4-Bd) contents were used. Table 1 shows a number-average molecular weight (M_n), molecular weight distribution (M_w/M_n), T_g^b and the molar ratio of St and 1,2-Bd of the samples. As hydrophilic and hydrophobic substrates, fused quartz without/with a chloro(decyl)dimethylsilane (DDS) coating monolayer was used. SBR films were prepared on the substrates by a spin-coating method from toluene solutions. Then, SBR films prepared onto a quartz prism and a quartz window were adhered in the surface-to-surface geometry at (T_g^b + 80) K under vacuum for 24 h. SFG spectra were collected with visible and tunable infrared beams traveling through a prism and overlapping at the SBR/solid interface. The measurements were carried out with a polarization combination of *ssp* (SF output, visible input and infrared input).

Table 1: Characteristics of SBRs.

Sample	M_n	M_w/M_n	T_g^b / K	St in SBR / mol%	1,2-Bd in Bd / mol%
SBR28	200k	1.08	233	22	28
SBR44	190k	1.04	245	22	44
SBR69	160k	1.10	266	24	69

RESULTS AND DISCUSSION

Figure 1(a) shows SFG spectra for SBR28, SBR44 and SBR69 films at the quartz substrate. A peak observed at 2,846 cm^{-1} was assigned to the symmetric C-H stretching vibration of methylene groups (CH_2s). A peak observed at 2,905 cm^{-1} could be assigned to the anti-symmetric C-H stretching vibration of methylene groups (CH_2as) and/or the C-H vibration

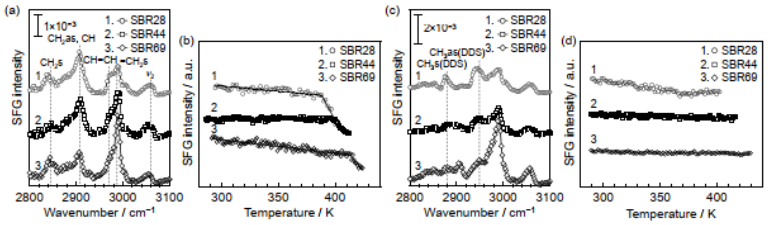

Figure 1: SFG spectra for SBR28, SBR44 and SBR69 at (a) quartz and (c) DDS-treated quartz interface, respectively. Temperature dependence of SFG peak intensity of ν_2 mode in phenyl group at (b) quartz and (d) DDS-treated quartz interfaces, respectively.

of methyne groups (CH). Peaks at 2,972 and 2,988 cm^{-1} were assigned to the C-H stretching vibration of vinylene groups (CH=CH) in 1,4-Bd and the C-H stretching vibration of vinyl methylene groups in 1,2-Bd (=CH_2s), respectively. Also, a peak at 3,060 cm^{-1} was originated from the ν_2 mode of phenyl groups. Taking into account that SFG signals can be obtained from functional groups orientated at the interface, the above results indicate that the local conformation of SBR chains was ordered at the quartz interface even at a temperature above the T_g^b. Also, it is noteworthy that the signal intensity for =CH_2s increased with increasing 1,2-Bd content in SBR.

To examine the orientational relaxation of SBR at the interface, the signal intensity of the ν_2 mode was chased during the heating process. Figure 1(b) shows temperature dependence of signal intensity at 3,060 cm^{-1}. In the case of SBR28, the intensity gradually decreased with increasing temperature, and the slope remarkably changed at 388 K, at which the local conformation of interfacial chains started to alter. This characteristic temperature T_c was comparable to those based on the SFG signals from CH=CH and =CH_2s. Thus, it seems most likely that the orientational randomization resulted from the segmental motion of SBR chains. The difference between T_c and T_g^b was approximately 150 K. This makes it clear that the mobility of SBR chains was strongly suppressed in close proximity to the quartz interface. A similar trend was also observed for SBR44 and SBR69.

To examine how the surface chemistry of the substrate impacts the interfacial mobility, similar experiments were conducted at the hydrophobic DDS-treated quartz interface. Figure 1(c) shows SFG spectra for the SBR films at the DDS-treated quartz interface. In addition to the peaks originated from SBR, peaks assignable to the symmetric and anti-symmetric C-H stretching vibration of methyl groups (CH_3s, CH_3as) for DDS were observed. Figure 1(d) shows the relationship between temperature and peak intensity of the ν_2 mode. Although a gradual decrease in the SFG intensity was discerned, the slope remained almost changed. This means that the orientational relaxation of SBR chains at the interface did not occur within the temperature range employed. A possible explanation for this finding is that the interfacial relaxation was not allowed due to the stronger interaction between SBR chains and the hydrophobic surface. Thus, it can be claimed that the interaction of segments with a solid surface strongly impacts the segmental mobility at the interface.

ACKNOWLEGEMENTS

This work was supported by the JST-Mirai Program (JPMJMI18A2).

REFERENCES

1. Zuo, B.; Inutsuka, M.; Kawaguchi, D.; Wang. X.; Tanaka, K. Conformational Relaxation of Poly(styrene-*co*-butadiene) Chains at Substrate Interface in Spin-Coated and Solvent-Cast Films. *Macromolecules* **2018**, *51*, 2180-2186.
2. Zuo, B.; Inutsuka, M.; Kawaguchi, D.; Wang. X.; Tanaka, K. Conformational Relaxation of Poly(styrene-*co*-butadiene) Chains at Substrate Interface in Spin-Coated and Solvent-Cast Films. *Macromolecules* **2018**, *51*, 2180-2186.
3. Nguyen, H. K.; Sugimoto, S.; Konomi, A.; Inutsuka, M.; Kawaguchi, D.; Tanaka, K. Dynamics Gradient of Polymer Chains near a Solid Interface. *ACS Marco Lett.* **2019**, *8*, 1006-1011.

SHAPE MEMORY AND MECHANO-RHEOLOGICAL PROPERTIES OF AMINE CONTAINING POLYETHYLENE/POLYCAPROLACTONE BLEND.

Jan S. Gustowski,[†] Benjamin M. Yavitt,[‡] Savvas G. Hatzikiriakos,[‡] Laurel L. Schafer[†]

[†]Department of Chemistry, University of British Columbia, Vancouver, British Columbia V6T 1Z4, Canada

[‡]Department of Chemical and Biological Engineering, University of British Columbia, Vancouver, British Columbia V6T 1Z3, Canada

jgustowski@chem.ubc.ca

ABSTRACT

Biodegradable polymers can potentially reduce global plastic waste generation.[1] Therefore, the incorporation of compostable polymers into manufacturing streams is highly desired. To date biodegradable polymers are limited in their application due to relatively poorer mechanical properties compared to those of commercial polyolefins and other commodity polymers.[2,3] Blending biodegradable polymers with other polymers is a practical strategy for developing materials with superior mechanical properties.[4] Herein, we report the blending of biodegradable polymers with aminated polyethylene (APE) previously developed.[5] The intrinsic hydrogen-bonding ability of the APE[6], coupled with the hydrogen bond accepting capability of biodegradable polyesters, is exploited to access miscible polymer blends that could also be useful for the compatibilization of otherwise immiscible commodity polymers. APE is blended with commercially available polycaprolactone (PCL) at various compositions. Films are processed by compounding and extrusion. The thermal properties of the blended materials are investigated by differential scanning calorimetry (DSC) together with rheological tests to investigate the miscibility and processability of the blends. Composition-dependent single point T_gs and lowering crystallinity levels provide the indication of formation of highly miscible blend. Tensile tests (TT) were used to probe the mechanical properties of the newly generated blended materials. APE is known to exhibit self-healing and exceptional adhesive properties.[5] One the other hand, pure APE does not possess any shape memory properties. Surprisingly, blending it with PCL results in a polymer mixture which changes its shape upon exposure to an external stimulus and returns to its original shape by a simple heat treatment.

Rheological Evaluation of Polyhydroxyalkanoates (PHAs) through Constitutive Equation Modelling

Hadis Torabi[1,2], Hadis Zarrin[1] and Ehsan Behzadfar[1,2]

[1]Chemical Engineering Department, Toronto Metropolitan University (formerly Ryerson University), Toronto, ON, M5B 2K3 Canada
[2]Sustainable Polymers Research Lab (SPRL), The Creative School, Toronto Metropolitan University (formerly Ryerson University), Toronto, ON, M5B 2K3 Canada

ABSTRACT

The processing of biobased, biodegradable polymers inherits rheological challenges due to the thermal instability of their molecular structure[1]. Polyhydroxyalkanoates (PHA) is one of these biobased, biodegradable polymers that is emerging in different applications such as food packaging. To meet the packaging needs for foods, PHAs must be designed to achieve better processability, and better performance. PHAs undergo thermal degradation as early as they start to melt. In order to understand how temperature and possible thermal degradation, influence the rheological behaviour of PHAs, Eickhoff and Harrison[2] investigated the dynamic rheology of PHA resins over time. The complex viscosity of the resins with two different molecular weights starts dropping after a short period of time. This viscosity reduction is more pronounced for the PHA polymers with higher molecular weights with a higher concentration of the 3-hydroxyhexanoate comonomer in their structure, indicating a greater rate of degradation. A similar observation was reported by Conrad.[3] They reported that higher valerate content contributes to higher viscosity values but makes the resin more susceptible to thermal degradation. To overcome these challenges, PHAs have been blended with other polymers, such as polylactic acid (PLA), to produce different products used in various applications. Bousfield[4] found that the composition of the PHA/PLA blend had an impact on its complex viscosity values. They showed that in comparison to 25 wt.% PLA and 75 wt.% PHA, 75 wt.% PLA and 25 wt.% PHA had higher complex viscosity.[4] Moreover, almost no shear thinning was observed in those compositions. Zhao *et al.*[5] reported that PHA/PLA blends with 90 wt.% PHA and 10 wt.% PLA exhibited much lower complex viscosity, storage modulus and loss modulus than the blend containing 70 wt.% PHA and 30 wt.% PLA at 140 °C.[5] Zembouai *et al.*[6] showed an increase in the complex viscosity of the PHA with valerate content, and PLA blend as PLA concentration increased. They demonstrated that the complex viscosity of PHA with valerate content and PLA blends follow the mixing rule with some discrepancies.[6] However, there is not a comprehensive study investigating the influence of the structural changes, which are inevitable during most processing, on the rheological properties and final product performance.

In this study, the rheological behaviour of PHA, in pure forms and hybrid forms with PLA, has been investigated. Dynamic, shear and extensional rheology were employed to analyze the rheological properties in a wide range of stress fields with different levels of deformation. The

generalized Maxwell model, a combination of spring and dashpot elements, was used to represent the relaxation modulus of the studied resins. Time-temperature superposition and constitutive modelling were applied to model the obtained rheological data. Also, different damping functions were used to examine the nonlinearity in viscoelastic response as a function of deformation levels. Our results showed that the rheological properties of PHA are very susceptible to temperature and residence time at high temperatures. We found that even short residence times of two minutes at the temperature of 200 °C have substantially influenced the morphology and rheological responses of PHA and PLAs containing 10 wt.% of PHA hybrid materials. The rheological data at different temperatures indicated that PHA decreases PLA/PHA's viscosity to values lower than the volumetric average values, implying PHA's contribution in changing the chain interactions within PLA morphology. However, the presence of PHA did not influence the shear-thinning behaviour of PLA. The K-BKZ constitutive equation was shown to represent the rheological properties of the resins accurately. Damping functions such as Marruci and Wagner successfully predicted the nonlinearity of the rheological properties beyond linear viscoelastic region (LVE). Also, the extensional viscosity data revealed the reduced viscosity values for the hybrid materials to levels below the average values lower than the volumetric average values, pointing to the changes in the molecular interactions of PLA in the presence of PHA. This study reflects on the effect of processing conditions on the rheological behaviour of PHAs as biobased, biodegradable polymers and their hybrid materials in emerging markets.

ACKNOWLEDGEMENTS

The authors acknowledge the financial support from Toronto Metropolitan University, Natural Sciences and Engineering Research Council of Canada (NSERC), MITACS, Canada Foundation for Innovation (CFI), and Ontario Research Fund (ORF) programs.

REFERENCES

(1) Chile, L.-E.; Kaser, S. J.; Hatzikiriakos, S. G.; Mehrkhodavandi, P. Synthesis and Thermorheological Analysis of Biobased Lignin-Graf t-Poly(Lactide) Copolymers and Their Blends. **2018**. https://doi.org/10.1021/acssuschemeng.7b02866.

(2) Eickhoff, J.; Harrison, G. M. The Shear, Extensional and Degradation Rheology of Renewable Resource Polymers. In *Global Plastics Environmental Conference*; 2006.

(3) Conrad, J. D. The Rheology and Processing of Renewable Resource Polymers, 2009, Vol. 454. https://doi.org/10.1063/1.2964497.

(4) Bousfield, G.; Carreau, P. J.; Heuzey, M.-C.; Demarquette, N.; Ecole polytechnique (Montréal, Q. D. de génie chimique. Effect of Chain Extension on Rheology and Tensile Properties of PHB and PHB-PLA Blends. *PhDT* **2014**, 93.

(5) Zhao, H.; Bian, Y.; Li, Y.; Dong, Q.; Han, C.; Dong, L. Bioresource-Based Blends of Poly(3-Hydroxybutyrate-Co-4-Hydroxybutyrate) and Stereocomplex Polylactide with Improved Rheological and Mechanical Properties and Enzymatic Hydrolysis. *J. Mater. Chem. A* **2014**, *2* (23), 8881–8892. https://doi.org/10.1039/C4TA01194E.

(6) Zembouai, I.; Kaci, M.; Bruzaud, S.; Benhamida, A.; Corre, Y. M.; Grohens, Y. A Study of Morphological, Thermal, Rheological and Barrier Properties of Poly(3-Hydroxybutyrate-Co-3-Hydroxyvalerate)/Polylactide Blends Prepared by Melt Mixing. *Polym. Test.* **2013**, *32* (5), 842–851. https://doi.org/10.1016/J.POLYMERTESTING.2013.04.004.

DEVELOPMENT OF BIODEGRADABLE AND ANTIVIRAL SURGICAL FACE MASKS FROM POLY(LACTIC ACID) AND POLY(DIMETHYLSILOXANE)-BASED POLYHYDROXYURETHANES

Georges R. Younes[1] and Abdellah Ajji[1]

[1]Chemical Engineering Department, École Polytechnique de Montréal, Montreal, Canada

ABSTRACT

The COVID-19 outbreak urged the use of personal protective equipment (PPE) by society and healthcare workers around the world. [1] Among the different PPE, surgical face masks have been imposed by governments of different countries, including Canada, to be worn in the workplace, schools, and other closed spaces, as COVID-19 is a viral respiratory disease, which gets transmitted through saliva droplets and bioaerosols emitted by breathing, talking, sneezing, and coughing. [2] This restriction has led to an increase in demand of surgical face masks, and it is estimated that the world population is using and throwing away 3.7 billion face masks every day. [3] In fact, most of the commercial surgical face masks are disposable. They are made of non-woven fabrics of synthetic polymers, mainly poly(propylene) and poly(acrylonitrile), by means of different polymer processing methods, such as electrospinning. [3, 4] Because they are disposable, environmental concerns were raised against their excessive consumption since they are seen as a new source of plastic waste that could potentially pollute the soil and water resources. [3, 5] Also, their filtration efficiency gradually decreases, [6] and they become contaminated hosts of different viruses and microorganisms causing a health threat to the person wearing the mask, especially if they are healthcare professionals. [7] As a result, the scientific community has recently recommended the preparation of sustainable and high-performance surgical face masks with multifunctional properties. [3, 8, 9] Hence, the development of biodegradable face masks with antiviral and antimicrobial activities would resolve the environmental and health issues associated with conventional surgical face masks. [3, 9, 10]

In this work, poly(lactic acid) (PLA) is being blended with a poly(dimethylsiloxane)-based polyhydroxyurethane (PDMS-PHU) to prepare biodegradable surgical face masks. PLA is a known biopolymer for its outstanding physical and mechanical properties, but it suffers from poor ductility and impact toughness. Polyhydroxyurethanes (PHUs), on the other hand, constitute a promising class of non-isocyanate polyurethanes whose monomers can be bio-sourced. In fact, PHUs do not contain isocyanates, which are toxic base monomers of conventional polyurethanes, and they are prepared from the polyaddition of dicarbonates with diamines. [11] The PHUs herein are synthesized from a sugar derived dicarbonate and a PDMS-

based diamine. The PDMS soft segments are expected to provide the PLA matrix with the necessary flexibility and toughness to be processed and electrospun, whereas, it is anticipated that the hydroxyl groups dangling from the PHU backbone would bridge between the two polymer phases through hydrogen bonding. [11, 12] Different PLA/PDMS-PHU blend ratios are studied, and their thermal, rheological, mechanical, morphological, and microstructural properties are examined. Owing to the hydrophobic and biocompatibility nature of PDMS, the antimicrobial properties of the developed blends are assessed as well against different kinds of bacteria. Indeed, the hydrophobic character of PDMS allows the formation of anti-biofouling surface that prevents bacterial adhesion. [13]

At a later stage, it will be attempted to melt or solvent electrospin fibers from those blends while incorporating natural agents extracted from aloe vera plants and brown algae; aloe vera extract and laminarin, respectively, which showed antiviral activities against different pathogens. [14, 15] After optimizing the electrospinning process, the resulting non-woven textiles will be tested for their antimicrobial and antiviral properties.

REFERENCES

1. Cook, T. M. Personal protective equipment during the coronavirus disease (COVID) 2019 pandemic - a narrative review. *Anaesthesia* **2020,** 75 (7), 920-927 DOI: 10.1111/anae.15071.

2. Cheng, V. C.; Wong, S. C.; Chuang, V. W.; So, S. Y.; Chen, J. H.; Sridhar, S.; To, K. K.; Chan, J. F.; Hung, I. F.; Ho, P. L.; Yuen, K. Y. The role of community-wide wearing of face mask for control of coronavirus disease 2019 (COVID-19) epidemic due to SARS-CoV-2. *J Infect* **2020,** 81 (1), 107-114 DOI: 10.1016/j.jinf.2020.04.024.

3. Babaahmadi, V.; Amid, H.; Naeimirad, M.; Ramakrishna, S. Biodegradable and multifunctional surgical face masks: A brief review on demands during COVID-19 pandemic, recent developments, and future perspectives. *Sci Total Environ* **2021,** 798, 149233 DOI: 10.1016/j.scitotenv.2021.149233.

4. Ju, J. T. J.; Boisvert, L. N.; Zuo, Y. Y. Face masks against COVID-19: Standards, efficacy, testing and decontamination methods. *Adv Colloid Interface Sci* **2021,** 292, 102435 DOI: 10.1016/j.cis.2021.102435.

5. Aragaw, T. A. Surgical face masks as a potential source for microplastic pollution in the COVID-19 scenario. *Mar Pollut Bull* **2020,** 159, 111517 DOI: 10.1016/j.marpolbul.2020.111517.

6. Zhang, R.; Xu, Q.; Bai, S.; Hai, J.; Cheng, L.; Xu, G.; Qin, Y. Enhancing the filtration efficiency and wearing time of disposable surgical masks using TENG technology. *Nano Energy* **2021,** 79, 105434 DOI: 10.1016/j.nanoen.2020.105434.

7. Zhiqing, L.; Yongyun, C.; Wenxiang, C.; Mengning, Y.; Yuanqing, M.; Zhenan, Z.; Haishan, W.; Jie, Z.; Kerong, D.; Huiwu, L.; Fengxiang, L.; Zanjing, Z. Surgical masks as source of bacterial contamination during operative procedures. *J Orthop Translat* **2018,** 14, 57-62 DOI: 10.1016/j.jot.2018.06.002.

8. Karmacharya, M.; Kumar, S.; Gulenko, O.; Cho, Y.-K. Advances in Facemasks during the COVID-19 Pandemic Era. *ACS Applied Bio Materials* **2021,** 4 (5), 3891-3908 DOI: 10.1021/acsabm.0c01329.

9. Seidi, F.; Deng, C.; Zhong, Y.; Liu, Y.; Huang, Y.; Li, C.; Xiao, H. Functionalized Masks: Powerful Materials against COVID-19 and Future Pandemics. *Small* **2021**, e2102453 DOI: 10.1002/smll.202102453.

10. Karim, N.; Afroj, S.; Lloyd, K.; Oaten, L. C.; Andreeva, D. V.; Carr, C.; Farmery, A. D.; Kim, I. D.; Novoselov, K. S. Sustainable Personal Protective Clothing for Healthcare Applications: A Review. *ACS Nano* **2020,** 14 (10), 12313-12340 DOI: 10.1021/acsnano.0c05537.

11. Younes, G. R.; Marić, M. Bio-based Thermoplastic Polyhydroxyurethanes Synthesized from the Terpolymerization of a Dicarbonate and Two Diamines: Design, Rheology, and Application in Melt Blending. *Macromolecules* **2021,** 54 (21), 10189-10202 DOI: 10.1021/acs.macromol.1c01640.

12. Shi, W.; Chen, Z. Mechanical, rheological, and crystallinity properties of polylactic acid/polyethylene glycol-polydimethylsiloxane copolymer blends by melt blending. *Journal of Applied Polymer Science* **2022,** 140 (4), DOI: 10.1002/app.53346.

13. Miranda, I.; Souza, A.; Sousa, P.; Ribeiro, J.; Castanheira, E. M. S.; Lima, R.; Minas, G. Properties and Applications of PDMS for Biomedical Engineering: A Review. *J Funct Biomater* **2021,** 13 (1), DOI: 10.3390/jfb13010002.

14. Ng, Y. C.; Kim, Y. W.; Ryu, S.; Lee, A.; Lee, J.-S.; Song, M. J. Suppression of norovirus by natural phytochemicals from Aloe vera and Eriobotryae Folium. *Food Control* **2017,** 73, 1362-1370 DOI: 10.1016/j.foodcont.2016.10.051.

15. Ahmadi, A.; Zorofchian Moghadamtousi, S.; Abubakar, S.; Zandi, K. Antiviral Potential of Algae Polysaccharides Isolated from Marine Sources: A Review. *Biomed Res Int* **2015,** 2015, 825203 DOI: 10.1155/2015/825203.

8TH PACIFIC RIM CONFERENCE ON RHEOLOGY, May 15-19, 2023

RESEARCH ON STABILITY OF ELECTRORHEOLOGICAL EFFECT OF WAXY CRUDE OIL

Yiwei Xie[1], Hongying Li[1], Miaomiao Xu[1,2] and Jinjun Zhang[1]

[1]National Engineering Research Center of Oil and Gas Pipeline Transportation Safety /MOE Key Laboratory of Petroleum Engineering/Beijing Key Laboratory of Urban Oil & Gas Distribution Technology/China University of Petroleum, Beijing 102249, China
[2]CNOOC Gas Pipelining Limited, Haikou 570105, China

ABSTRACT

Applying a high-voltage electric field to a waxy oil may improve its cold flowability dramatically based on its electrorheological effect. However, the stability of the electrorheological effect and its influencing factors are not well understood. The effect of the electric field strength and shear after the removal of the electric field on the stability of the electrorheological effect was investigated. The results show that the electrorheological effect of crude oil is gradually weakened after the removal of the electric field, the higher the field strength, the longer the duration time of the modification effect. The shear after the removal of the electric field would accelerate the weakening of the modification effect of oil with low liquid phase viscosity and small colloidal particle size but can provide additional flowability improvement of oil with high liquid phase viscosity and large colloidal particle size. Impedance test showed that charged particles would absorb on the surface of wax particles under electric treatment, and gradually diffuse back to the bulk phase after the removal of the electric field. Both the electric field strength and shear affect the stability by affecting the adsorption and diffusion of charged particles. This study deepened the understanding of the stability of the electrorheological effect and provided guidance for engineering applications.

INTRODUCTION

Exposure to a high-voltage electric field may improve the cold flowability of a waxy oil significantly thanks to the electrorheological effect of the oil. The oil viscosity may be reduced by as much as 80% or higher, and the yield stress may be depressed by 90% by imposing an electric field with the intensity of 0.2~5 kV/mm on crude oil just for seconds. Tao found that the viscosity reduction of electrically-treated oil decreased from 82% to 34% after standing for 24 h at constant temperature [1]. Li indicated that the modification effect induced by the electric field would gradually disappear with the extension of time, but the shear is conducive to maintaining the modification effect [2]. It can be found that previous studies all ignored the

influence of electric treatment conditions and oil composition on the stability of the electrorheological effect.

EXPERIMENTAL SECTION

The rheological and impedance in-situ integrated measuring device was used in this study. The device is composed of a stress-controlled HAAKE MARS III rheometer with an electrorheological module, a frequency response analyzer, a high-voltage power supply, and a water bath. The rheometer can be connected with the impedance analyzer to test the viscosity and impedance of oil samples in situ before and after electric treatment.

RESULTS AND DISCUSSIONS

To explore the influence of electric field strength on the modification effect of crude oils after the removal of the electric field, four waxy oils were treated under different field strengths (2~5 kV/mm) for 90 s at the temperature of 3°C above their pour point respectively. The results are shown in **Fig. 1**. It can be seen that for the four oil samples, the viscosity reduction was increased with the increasing field strength, and the modification effect can maintain longer under static condition.

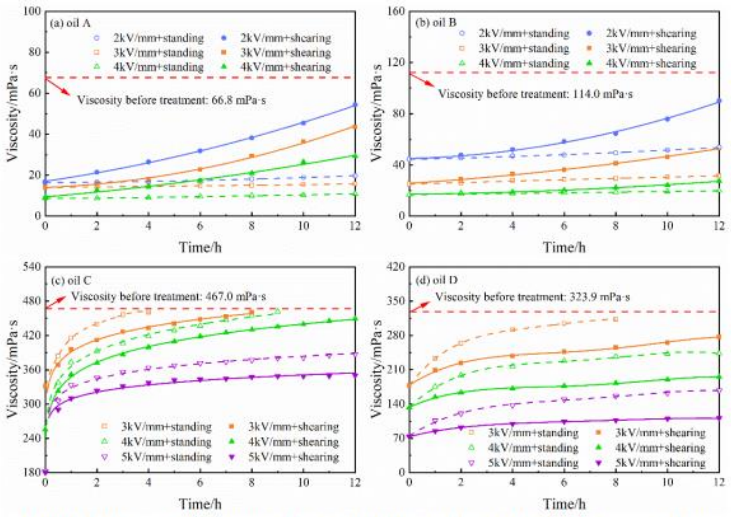

Figure 1: Changes of viscosity of the treated oils after the removal of the electric field

However, compared with the static condition, the shear stability of the four oils had opposite performances. The efficacy of the electric treatment of oil A and oil B can be sustained for a longer time under static condition. The viscosity reduction of oil A was 78% after an electric field with 3 kV/mm was applied, and the viscosity of treated oil was almost unchanged

after standing for 12 h, however, the viscosity reduction was just remained 35% after shearing at 10 s^{-1} for 12 h. For oil C and oil D, shearing at 10 s^{-1} preserved the efficacy of the electric treatment.

To examine the impacts of high shear on the stability of electric modification, the electrically-treated oil sample was sheared at a rate of 600 s^{-1} for 300 s after the electric field was removed. The shear rate imposed on the sample was then lowered to 10 s^{-1}, at which the viscosity was measured. **Table 1** shows the equilibrium viscosity of the waxy oil with different shear histories.

Table 1: Viscosity of waxy crude oils under various treatment condition at 10 s^{-1}

treatment condition	viscosity（mPa·s）			
	oil A	oil B	oil C	oil D
without treatment	66.78	114.00	467.00	323.90
after electric treatment	14.14	25.34	330.63	177.41
shearing at 600 s^{-1} after treatment	29.71	49.38	265.47	145.60

Our previous study has shown that interfacial polarization, i.e., charged particle accumulation on the wax particle surface, is the primary mechanism of the electrorheological behavior of waxy oils [3]. In this study, the impedance characteristics of four oil samples under different conditions were measured. The results showed that the impedance of waxy crude oils increased significantly after electric treatment, indicating that some charged colloidal particles such as resins and asphaltenes had accumulated on the surface of wax particles upon the application of the electric field. After the removal of an electric field, the impedance of treated oil decreased gradually with the extension of time, which means the charged particles gradually diffuse back to the bulk fluid, and thus the viscosity and impedance gradually recover. Moreover, the electric field strength and shear affect the stability by affecting the adsorption and diffusion of charged particles.

ACKNOWLEDGEMENTS

The authors gratefully acknowledge the National Natural Science Foundation of China (No.51534007, No. 52174066) for providing financial support.

REFERENCES

1. Tao, R. J.; Tang, H. Reducing viscosity of paraffin base crude oil with electric field for oil production and transportation. *Fuel*, **118**, 69–72, 2014. https://doi.org/http://doi.org/10.1016/j.fuel.2013.10.056.
2. Li, H. Y.; Li, Z. X.; Xie, Y. W.; Guo, W.; Huang, Q.; Chen, C. H.; Ma, C. B,; Xu, M. M.; Han, S. P.; Zhang, J. J. Impacts of shear and thermal histories on the stability of waxy crude oil flowability improvement by electriv treatments. *J. Petrol. Sci. Eng*, **204**, 108764, 2021. https://doi.org/10.1016/j.petrol.2021.108764.
3. Chen, C. H.; Zhang, J. J.; Xie, Y. W.; Huang, Q.; Ding, Y. F.; Zhuang, Y.; Xu, M. M.; Han, S. P.; Li, Z. X.; Li, H. Y. An investigation to the mechanism of the electrorheological behaviors of waxy oils. *Chem. Eng. Sci*, **239**, 116646, 2021. https://doi.org/ 10.1016/j.ces.2021.116646.

IMPACT OF OIL COMPOSITION ON ELECTRORHEOLOGICAL EFFECT OF WAXY CRUDE OIL

Hongying Li[1], Yiwei, Xie[1], Qian Huang[1,2] Chaoyue Zhang[1], Yang Su[1], and Jinjun Zhang[1]

[1]National Engineering Research Center of Oil and Gas Pipeline Transportation Safety /MOE Key Laboratory of Petroleum Engineering/Beijing Key Laboratory of Urban Oil & Gas Distribution Technology/China University of Petroleum, Beijing 102249, China
[2] China Petroleum Engineering and Planning Institute

ABSTRACT

Electric field treatment is a novel approach to improve the cold flowability of waxy oil, and its basic physical principle is negative electrorheological effect of waxy oil. The electrorheological effect of different crude oils varies greatly. In this work, the electrorheological effect of 8 waxy crude oils with various resin and asphaltene content (4%-23%) are investigated. It is found that for crude oils with lower resin and asphaltene content (less than 5%), the viscosity reduction induced by electric field increased first and then decreased with the increase of precipitated wax. For the crude oil with medium resin and asphaltene content, the viscosity reduction increases monotonically with the increase of precipitated wax. However, for crude oil with higher content of resin and asphaltene (more than 15%), the viscosity reduction is not obvious.

INTRODUCTION

Waxy crude oil has poor flowability at normal temperature during pipeline transportation which poses great threats to flow assurance, such as high energy consumption, restart failure after extended shutdown, etc. To improve the flowability of waxy crude oil is the fundamental solution to flow assurance problems. Electric field treatment is an emerging approach to improve the cold flowability of waxy crude oils with high efficiency and low consumption, whose basic physical principle is the negative electrorheological effect of crude oil. It has found that the electrorheological effect of different crude oil is very different, for instance, for some crude oils, significant electrorheological effect with highest viscosity reduction rate up to 70%~80% can be detected [1, 2], while for some crude oils, almost no electrorheological effect can be observed [2]. The difference of electrorheological effect of different oils may be attributed to the difference of crude oil composition. In this work, the electrorheological effect of 8 waxy crude oils is investigated.

EXPERIMENTAL SECTION

In this work, a stress-controlled rheometer HAAKE MARS III (Thermo Fisher Scientific, Inc., Germany) with a fitted electrorheological module was used to explore the electrorheological

behaviours of waxy crude oil in situ. The main physical properties of 8 studied waxy crude oils are listed in **Table 1**.

Table 1: Physical properties of studied waxy crude oils.

Oil No.	WAT (°C)	Gel Point (°C)	Wax Content (wt%)	Resin Content (wt%)	Asphaltene Content (wt%)	Density @ 20°C (kg/m^3)
1#	26.1	14	10.5	3.8	0.7	797.4
2#	21.6	12	9.8	2.9	1.6	791.4
3#	26.6	12	8.4	3.8	0.2	805.6
4#	32.0	16	12.3	5.6	2.4	836.8
5#	36.8	22	15.4	10.7	1.0	825.5
6#	23.0	16	9.6	19.2	0.4	884.0
7#	65.0	41	23.4	14.6	0.9	895.6
8#	58.0	37	16.3	22.0	0.9	892.9

RESULTS AND DISCUSSIONS

To investigate the electrorheological behaviours of the above 8 waxy crude oils, an electric field of 3 kV/mm was applied for 90 s. The experimental results show that the viscosity reduction rate of oil 1#, 2# and 3# induced by electric field increased first and then decreased with the decrease of temperature, and viscosity reduction rate reached its peak near their gel points, whereas, the viscosity reduction rate of oil 4# and 5# increases monotonically with the decrease of temperature, see **Fig. 1.** For oil 6#, 7# and 8#, no obvious viscosity reduction can be observed, see **Table 2**.

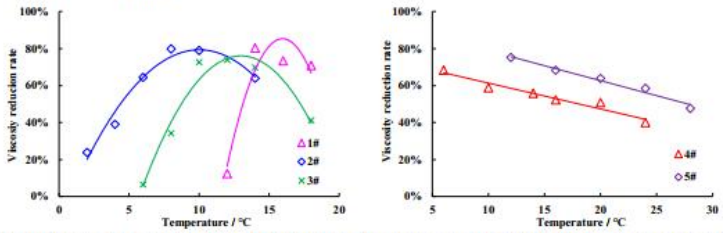

Figure 1: The viscosity reduction of different oil samples under 3 kV/mm at various temperature.

Table 2: Viscosities of oil 6#, 7#, and 8# oil with and without electric field.

Oil No.	Temperature (°C)	Viscosity @ $10s^{-1}$ (mPa·s) 0 kV/mm	3 kV/mm
6#	14	2093	2082
	16	1161	1156
	18	896	897
	20	595	596
7#	40	7669	7471
	43	2309	2104
	46	700	680
	49	400	396
8#	35	2796	2747
	37	1649	1649
	41	553	577
	44	444	426

According to the interface polarization mechanism of the electrorheological effect of crude oil, i.e., charged particles accumulation on the wax particle surface [3], the existence of wax crystal particles is the premise of electrorheological effect, while charged particles, i.e. resin and asphaltene, play an important role, and the electric field provides conditions for charged particles (resin and asphaltene) migrating to wax particles.

Temperature is only a superficial term, different temperatures mean to varied precipitated wax amount, which is the direct factor affecting electrorheological effect of crude oil. For oil 1#, 2# and 3#, the content of resin and asphaltene is less than 5%, when temperature is high, the precipitated wax amount is low, the amount resin and asphaltene is enough to cover the surface of wax particles, thus weakening the interaction force between wax particles and reducing the viscosity of crude oil. When temperature is cooled down and the precipitated wax amount increased to a certain extent, the amount of resin and asphaltene is not enough to cover the surface of wax particles, the viscosity reduction effect began to decrease. For oil 4# and 5#, resin and asphaltene content is medium, and the viscosity reduction increases monotonically with the decrease of temperature, which means the electrorheological effect enhanced with the increase of the precipitated wax amount, this is because with the increase of the precipitated wax amount, more wax particles are affected by resin and asphaltene, so the electrorheological effect is enhanced. For oil 6#, 7# and 8#, resin and asphaltene content is somewhat high. It has been reported that resin and asphaltene in oil will self-associate and form aggregates since insufficient solvent when the content of resin and asphaltene is high [4]. Because of self-association of resin and asphaltene, the aggregates of resin and asphaltene cannot migrate to and then accumulate on the wax particle surface under the electric field, thus, no obvious electrorheological effect can be observed.

ACKNOWLEDGEMENTS

The authors gratefully acknowledge the National Natural Science Foundation of China (No. 52174066) for providing financial support.

REFERENCES

1. Tang, H.; Huang, K.; Tao, R. J. Electrorheology improves transportation of crude oil. *Journal of Intelligent Material Systems and Structures*, 2011, **22(15)**: 1673-1676. https://doi.org/10.1142/9789814340236_0006.
2. Ma, C. B.; Lu, Y. D.; Chen, C. H. Feng, K.; Li, Z. X.; Wang, X. Y.; Zhang, J. J. Electrical treatment of waxy crude oil to improve its cold flowability. *Industrial & Engineering Chemistry Research*, 2017,**56(38)**:10920-10928. https://doi.org/10.1021/acs.iecr.7b02140.
3. Chen, C. H.; Zhang, J. J.; Xie, Y. W.; Huang, Q.; Ding, Y. F.; Zhuang, Y.; Xu, M. M.; Han, S. P.; Li, Z. X.; Li, H. Y. An investigation to the mechanism of the electrorheological behaviors of waxy oils. *Chem. Eng. Sci*, **239**, 116646, 2021. https://doi.org/10.1016/j.ces.2021.116646.
4. Li, T.; Xu, J.; Zou, R; Feng, H; Li, L.; Wang, J. Resin from Liaohe heavy oil: molecular structure, aggregation behavior, and effect on oil viscosity. *Energy & Fuels*, 2017, **32(1)**: 306-313. https://doi.org/10.1021/acs.energyfuels.7b03279.

SIGNIFICANCE OF VOLUME SHRINKAGE ON YIELDING CHARACTERISTICS OF WAXY OIL

Sachin Balasaheb Shinde[1] and Lalit Kumar[1]

[1]Department of Energy Science and Engineering, IIT Bombay, Market Gate Road, IIT Area, Powai, Mumbai, Maharashtra 400076

ABSTRACT

The production and transportation of waxy crude oil in the subsea environment are challenging due to the formation of gel inside the pipeline during shutdown conditions, which disturbs steady-state production. The waxy crude exhibits the complex non-Newtonian behavior below the gelation temperature. It loses its flow characteristics and behaves like a yield stress fluid. The measurement of accurate yield stress is always crucial for understanding and forecasting the flow behavior of such complex fluids. In the literature, several rheological methods were used to measure the yield stress; most of them neglect the effect of volume contraction due to thermal shrinkage during the gelation process[1-2]. Hence, the prime objective of the present study is to measure the accurate yield stress of waxy crude oil by considering the effect of thermal shrinkage. The compensation for thermal shrinkage is achieved with zero normal force and variable gap setting with a stress-controlled rheometer. However, an earlier reported study by Abedi et al. utilizes the fixed gap reduction protocol, which overlooks variation thermal shrinkage with temperature and waxy oil composition, which fails to ensure the removal of complete void formation during the gelation process[3]. Whereas the normal force gap compensation protocol is according to the thermal shrinkage of the gel network, which eliminates the chance of voids formation. Moreover, the yield stress is measured under constant gap conditions and compared with variable gap conditions in order to examine the effect of thermal shrinkage on the yielding characteristic of waxy oil. In addition, the effect of final gel temperature and wax concentration on the yielding behavior of waxy crude oil was investigated experimentally under constant shear rate conditions.

The results shown in **Fig.** 1. depict that the coefficient of variation for yield stress measurement is lower for variable gap conditions compared to constant gap conditions, which shows that the yield stress measurement is more consistent and repeatable at zero normal force and variable gap conditions when compared with constant gap conditions. The variable gap condition minimizes the chances of the formation of voids during cooling, which results in the homogeneous formation of gel in the shear cell. However, the constant gap condition does not compensate for the thermal shrinkage during cooling and leads to the void formation in the shear cell[4]. These locally formed voids create discontinuity in the gel network, which results in an increase in the variation in the yield strength measurement. Moreover, accuracy in the yield

stress measurement also decreases with an increase in wax concentration and decreases in final gel temperature due to increased discontinuity due to shrinkage. Furthermore, the induced voids decrease the contact area of the gel network with a shear cell, which increases the chances of waxy gel adhesive failure. In contrast, the variable gap method reduces the adhesive failure **(slippage)** of the gel, which gives a more repeatable and correct measurement of yield stress. The authors believe that results can help in developing a fundamental understanding yielding behavior of waxy oil which can be utilized for various flow assurance issues during pipeline transportation of waxy crude oil.

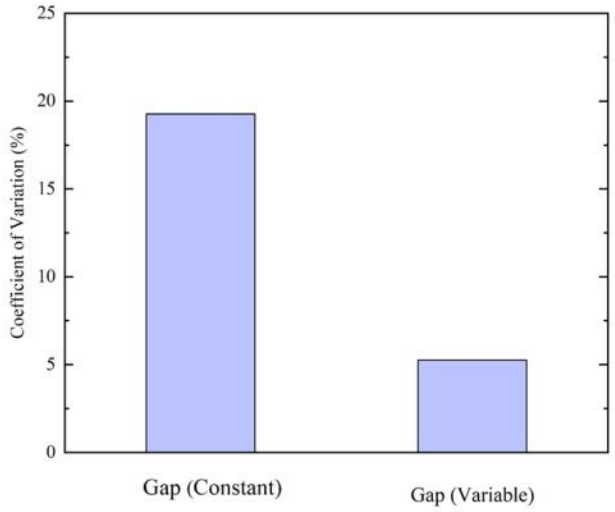

Figure 1: Coefficient of variation for yield stress measurement of 10 wt. % model waxy oil sample at 4 °C with constant gap condition and variable gap (Constant normal force) condition.

ACKNOWLEDGEMENTS

The authors are grateful to the Industrial Research and Consultancy Centre-Indian Institute of Technology Bombay for financial support (RD/0516-IRCCSH0-034).

REFERENCES

1. Chang, C.; Boger, D. V.; Nguyen, Q. D. The Yielding of Waxy Crude Oils *Ind. Eng. Chem. Res.*, **37**, 1551– 1559., 1998. https://doi.org/10.1021/ie970588r.
2. Mendes, R.; Vinay, G.; Coussot, P. On the yield stress and minimum pressure for simulating the flow

restart of a waxy crude oil pipeline. *Energy Fuels*, **31(1)**, 395−407., 2017. https://doi.org/10.1021/acs.energyfuels.6b02576.

3. Abedi, B.; Peres Miguel, M. J.; de Souza Mendes, P. R.; Mendes, R. Startup Flow of Gelled Waxy Crude Oils in Pipelines: The Role of Volume Shrinkage. *Fuel*, **288**, 119726., 2021. https://doi.org/10.1016/j.fuel.2020.119726.

4. Shinde, S. B.; Kumar, L. New Method for Gelation Temperature Measurement without Disturbing the Crystal Network. *Ind. Eng. Chem. Res.*, **60**, 8565– 8578., 2021. https://doi.org/10.1021/acs.iecr.1c00944.

WALL-SLIP EFFECTS ON FLOW RESTART IN A PLUGGED WAXY CRUDE OIL PIPELINE

Aniruddha Sanyal[1,2], Sachin B. Shinde[2] and Lalit Kumar[2]

[1]Department of Chemical Engineering, National Institute of Technology Calicut, Kozhikode 673601, Kerala, India
[2]Department of Energy Science and Engineering, Indian Institute of Technology Bombay, Mumbai 400076, Maharashtra, India

ABSTRACT

The gel degradation mechanism during flow restart operation in a waxy crude oil pipeline can be favorably explained through "indirect structural degradation-based rheological model"[1]. The waxy crude oil at subsea condition undergo gel degradation following irreversible thixotropy when a pressurized fluid is induced at the inlet of the pipeline. The sequence of gel degradation involves initial elastic deformation followed by creep, shear stress localization, strain consolidation, gel failure at wall-fluid interface (for homogeneous type pristine gel), gel compression and viscosity reduction. The waxy crude oil at subsea is a structured elasto-viscoplastic fluid, and at fully deformed condition it becomes Newtonian[2]. In several cases, the flow restart shows wall-slip as a major cause of gel failure at the wall-fluid interface[3]. Our experiments and numerical simulations suggest that the gel deformation is high for a wall-slip induced scenario (Fig. 1). This is opposite to the intuition that wall-slip creates lesser gel deformation in respect to no-slip scenario. Thus, there is an improved accuracy in the estimate for pressure requirements in flow restart operation. The no-slip and wall-slip scenario are mimicked through rough and smooth plates in rheometric experiments. Numerical simulations are done using in-house FORTRAN-based code following finite-volume-methodology[2]. The bulk flow is explained by elasto-viscoplastic rheology[4] and the complexities at the wall-fluid interface is defined by a static-based slip model where the slip-velocity follows a power-law of shearing stress at the wall[5]. It is to be noted that the fluid in this study is considered as weakly compressible.

The simulations in our study can capture the flow intricacies even at the smallest timescale where one can see initial compressive pressure wave propagation, gel degradation, and steady-state flow. The results from the simulations reveal the significance of wall-slip at the initial pressure propagation stage (Fig. 2). Once a sustained flow starts occurring at the outlet, the pronounced effect of wall-slip alleviates in competition to the deformation caused through bulk flow. This is furthermore ascertained by the analysis of transient flow, deformation and shear stress variations at locations in the vicinity of the wall of the pipeline. The article captures the slip-stick mechanism for the scenario where the wall-slip possessing yielding behavior (i.e. the scenario where the wall-slip occurs at a stress (τ) higher than the critical stress for wall-slip (τ_c)at the wall-fluid interface). A series of numerical comparisons are done to distinguish the

gel degradation mechanism for no-slip and wall-slip scenario for various cases of aspect ratio α, and gel degradation constant k.

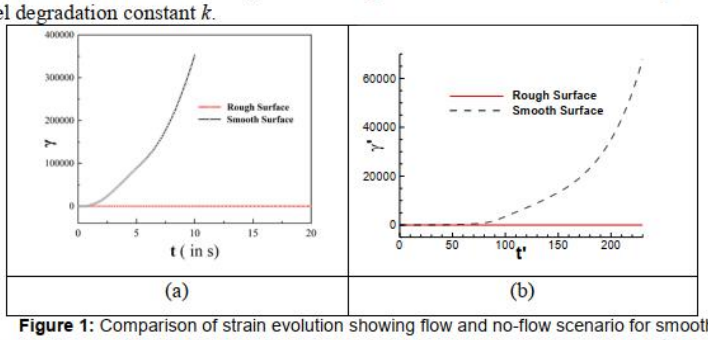

Figure 1: Comparison of strain evolution showing flow and no-flow scenario for smooth surfaces (signifying wall-slip) and rough surfaces (signifying no-slip) using (a) experimental (for parallel plate configuration in Anton Paar MCR 301 rheometer) and (b) numerical simulations (at a location near the inner wall of a pipeline).

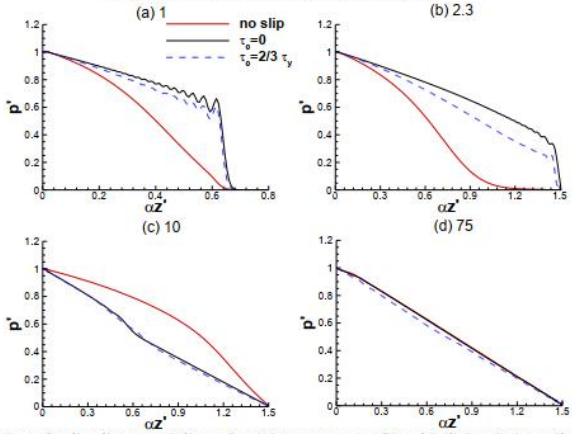

Figure 2: Comparison for the time evolution of axial pressure profile at initial gel viscosity of 100 Pa s, induced pressure P = 40 kPa with the cases for no-slip, shear-thinning slip (τ_c = 0) and conditional slip scenario (τ_c = 2/3 τ_y) at time instants t' = (a) 1, (b) 2.3, (c) 5, and (d) 75.

REFERENCES

1. Mujumder, A.; Beris, A. N.; Metzner, A. B. Transient phenomena in thixotropic systems. *J. Non-Newtonian Fluid Mech.*, **102**, 157–178., 2002. https://doi.org/10.1016/S0377-0257(01)00176-8.
2. Sanyal, A.; Tikariha, L.; Kumar, L. The effects of partial preheating on pressure propagation and Flow-Restart phenomena in a clogged pipeline with a weakly compressible gel. *Phys. Fluids*, **33**, 043101, 2021. doi: 10.1063/5.0046676.

3. Marinho, T.O.; Marchesini, F. H.; de Oliveira, C. K.; Nele, M. Apparent wall slip effects on rheometric measurements of waxy gels. *J. Rheol.*, **65**, 257, 2021.

4. Tikariha, L.; Kumar, L. Pressure propagation and flow restart in a pipeline filled with a gas pocket separated rheomalaxis elasto-viscoplastic waxy gel. *J. Non-Newtonian Fluid Mech.,* **294**, 104582, 2021. https://doi.org/10.1016/j.jnnfm.2021.104582.

5. Graham, W. D. Wall slip and the nonlinear dynamics of large amplitude oscillatory shear flows. *J. Rheol.* **39**, 697-712, 1995. https://doi.org/10.1122/1.550652.

FLOW RESTART MECHANISM IN A MULTIPHASE GELLED PIPELINE

Lomesh Tikariha[1], Aniruddha Sanyal[1], Lalit Kumar[1]

[1] Department of Energy Science and Engineering, IIT Bombay, Mumbai, India

ABSTRACT

A two-phase oil-gas flow in a pipeline exhibits complex flow scenarios severely affecting its transportation and confronts many flow assurance challenges. For Instance, flow restart issues caused by waxy crude gel formation in a pipeline necessitate pressure differential-induced multiphase gel shear degradation. The application of restart pressure encounters the high compressibility of gas voids engendered during gel formation. Relatively higher deformation of gas voids embedded in a gelled oil provides extra free spaces for degraded gel movement. A comprehensive understanding of the gas voids embedded waxy gel degradation during initial pressure propagation is essential to delineate the trade off against the restart pressure requirement. A multiphase-based mathematical model is developed to solve mass and momentum conservation equations together with the volume of fluid (VOF) method. The shear-thinning and elasto-viscoplastic-based gel rheology that governs deformation-dependent structural decay have been considered for low strain rate restart operation[1]. The analysis of initial pressure propagation in a gas void embedded gel pipeline clearly illustrates the delay in the intensity of pressure gradient propagating downstream. The delay in pressure development in a pipeline is due to the difference in compressibility of the two phases[2]. During this delay, the deformation of the gas voids caused extensive gel degradation in the upstream region of the gelled pipeline[3]. The gel movement in these low resistive spaces leads to higher gel deformation, enhancing the flow restart operation. A detailed examination of the gas void's motion and corresponding higher shear strain localized in the vicinity of the gel-gas interface illustrated the vital role of gas voids. The fundamental understanding of the momentum exchanges at the gel-gas interface during the restart pressure and gas void interaction has many other industrial applications[4] that could be utilized to analyse more complex multiphase situations.

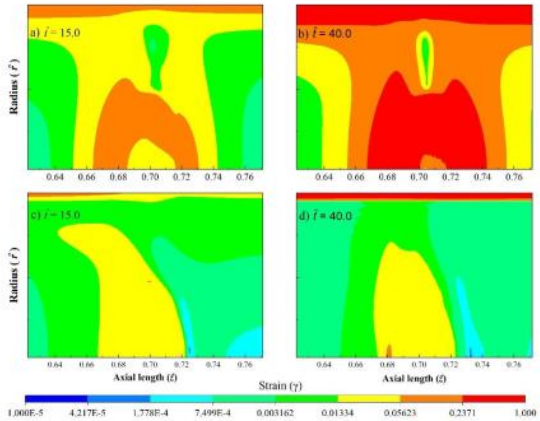

Figure 1: Comparison of strain contours for the bubble embedded filled gelled pipeline (a & b) shear modulus $G_o = 10^4$ and (c & d) shear modulus $G_o = 10^5$, for the gel parameter, compressibility number $\delta = 8 \times 10^{-5}$, relative viscosity $\mu_r = 20$, and steady-state Reynolds number $Re_s = 900$.

REFERENCES

(1) Kumar, L.; Skjæraasen, O.; Hald, K.; Paso, K.; Sjöblom, J. Nonlinear Rheology and Pressure Wave Propagation in a Thixotropic Elasto-Viscoplastic Fluids, in the Context of Flow Restart. *Journal of Non-Newtonian Fluid Mechanics* **2016**, *231*, 11–25. https://doi.org/10.1016/j.jnnfm.2016.01.013

(2) Tikariha, L.; Kumar, L. Pressure Propagation and Flow Restart in the Multi-Plug Gelled Pipeline. *Journal of Fluid Mechanics* **2021**, *911*. https://doi.org/10.1017/jfm.2020.1066

(3) Tikariha, L.; Kumar, L. Pressure Propagation and Flow Restart in a Pipeline Filled with a Gas Pocket Separated Rheomalaxis Elasto-Viscoplastic Waxy Gel. *Journal of Non-Newtonian Fluid Mechanics* **2021**, 104582. https://doi.org/10.1016/j.jnnfm.2021.104582

(4) De Corato, M.; Saint-Michel, B.; Makrigiorgos, G.; Dimakopoulos, Y.; Tsamopoulos, J.; Garbin, V. Oscillations of Small Bubbles and Medium Yielding in Elastoviscoplastic Fluids. *Physical Review Fluids* **2019**, *4* (7), 073301. https://doi.org/10.1103/PhysRevFluids.4.073301

8TH PACIFIC RIM CONFERENCE ON RHEOLOGY, May 15-19, 2023

The Role of Rolling Resistance in the Rheology of Wizarding Quidditch Ball Suspensions

Enzo d'Ambrosio1, Donald L. Koch 1
Sarah Hormozi 1

[1] Robert Frederick Smith School of Chemical and Biomolecular Engineering,
Cornell University, NY 14853, USA

ABSTRACT

To elucidate the effect of particle shape on the rheology of a dense, viscous suspension of frictional, non-Brownian particles, experimental measurements are presented for suspensions of polystyrene particles with different shapes in the same solvent. The first suspension is made of spheres while the particles which compose the second suspension are globular but with flattened faces. We present results from steady shear and shear-reversal rheological experiments for the two suspensions over a wide range of stresses in the viscous regime. Notably, we show that the rheology of the two suspensions is characterized by a shear-thinning behavior, which is stronger in the case of the suspension of globular particles. Since the shear-reversal experiments indicate an absence of adhesive particle interactions, we attribute the shear thinning to a sliding friction coefficient which varies with stress as has been observed previously for systems similar to the first suspension. We observe that the viscosity of the two suspensions is similar at high shear stress where small sliding friction facilitates particle relative motion due to sliding. At lower shear stress, however, the sliding friction is expected to increase and the particle relative motion would be associated with rolling. The globular particles attain a higher viscosity at low shear stress than the spherical particles. We attribute this difference to a shape-induced resistance to particle rolling that is enhanced by the flattened faces. Image analysis is employed to identify features of the particle geometry that contribute to the resistance to rolling. It is shown that the apparent rolling friction coefficients inferred from the rheology are intermediate between the apparent dynamic and static rolling friction coefficients predicted on the basis of the image analysis. All three rolling resistance estimates are larger for the globular particles with flat faces than for the spherical particles and we argue that this difference yields the stronger shear thinning of the globular particle suspension.

ACKNOWLEDGEMENTS

We thank Yahya Al-Majali and Yasaman Madraki for their assistance with crushing the particles, and we thank F. Peters and A. Singh for fruitful discussions. We acknowledge A. Singh for sharing his data from [1]. This work was supported by National Science Foundation (NSF) (Grant No. CBET-1554044-CAREER & CBET-2210322). The authors report no conflict of interest.

REFERENCES

1. Singh, Abhinendra, Ness, Christopher, Seto, Ryohei, de Pablo, Juan J & Jaeger, Heinrich M 2020 Shear thickening and jamming of dense suspensions: the “roll” of friction. Physical Review Letters 124 (24), 248005.

Adjuvanted silica suspensions: from particles contact properties to rheology

Antoine Aubel[1], Francesco Bonacci[1], Xavier Chateau[2], Eric M. Furst[2], Julie Goyon[2] and Anael Lemaitre[2]

[1]PMMH Laboratory, ESPCI Paris, Université PSL, Sorbonne Université, Paris, France
[2]Navier - Univ Gustave Eiffel - ENPC - CNRS, Marne-la-Vallée, France
[3]Department of Chemical and Biomolecular Engineering, University of Delaware, Newark, DE, United States

ABSTRACT

The behavior of dense aqueous silica suspensions is investigated through a comprehensive experimental approach that considers the material's properties at different length scales, from the contact level up to the overall properties.The first part of the study explores the ageing behavior of these suspensions and identifies a contact-controlled ageing process that governs both the shear modulus and yield strength ageing. Subsequently, the effect of a non-ionic surfactant on the yield stress and shear modulus of the same model suspension is studied. Results show that the addition of the surfactant significantly alters the interparticle contact properties, leading to modifications in the suspension's storage modulus and overall yield stress. Importantly, we establish a relationship between the interparticle contact properties and the overall properties of the suspension for both systems.

Ageing in silica suspension

While the ageing behavior of dense suspensions or pastes at rest is almost exclusively attributed to structural dynamics, a set of experiments conducted on dense aqueous silica suspensions allowed us to identify another ageing process: contact-controlled ageing. To do so we have investigated the origin of shear modulus and yield strength ageing in dense aqueous silica suspensions at moderate ionic forces. We first showed by combining rheometry and confocal microscopy that the elastic modulus and yield stress of these suspensions at rest grow logarithmically with time while their structural evolution is rapidly arrested by the formation of thermally irreversible roll-resistant interparticle contacts. So these suspensions age in the absence of structural rearrangement. Then by performing three-point optical tweezer (OT) bending tests on particle rods, we showed that particle contacts resist rolling and yield by overcoming a rolling threshold. We also observed that both the rolling stiffness and rolling threshold grow logarithmically in time. By comparing the results of the measurements on the particle contact properties with the results of the rheometry tests, we were able to show that ageing of interparticle contacts governs both shear modulus ageing and yield stress ageing of these dense aqueous silica suspensions. We also identified simple constitutive relationships between contact-scale bending stiffness and rolling threshold, which transfer to macroscopic scale. This allowed us to propose a constitutive relationship between the macroscopic shear modulus and the yield strength of these silica suspensions that should be generic for an array of colloidal systems.

Effect of an ionic surfactant

Dispersing agents are widely used to formulate high-solids pastes that remain fluid enough to be easily transported and placed. In the cement industry, superplasticizers are used to control the workability of fresh cement pastes containing high volume fractions of solid particles enabling the formulation of concretes with higher mechanical strength, better durability and also lower carbon impacts by substituting cement particles with mineral additions (fly ashes, slag, silica fumes...). Although dispersing agents are commonly used, the mechanism by which they impact the interaction between particles, and thus the paste rheology, remains obscure so that process optimization relies almost essentially on empirical or trial-and-error processes. In order to improve our understanding of these systems, we experimentally investigate the influence of a non-ionic surfactant that mimics superplasticizers on the yield stress and storage modulus of model suspensions containing silica beads suspended in an ionic solution. By combining rheometry, Total Organic Carbon, zeta potential, confocal microscopy and laser tweezers experiments, we show that adding non-ionic surfactant to the suspension strongly alters both the interparticle contact mechanical properties (stiffness and strength) and the overall suspension rheology (yield stress and storage modulus). Change of the contact rigidity is ascribed to the adsorption of the surfactant on beads, which induces a shift from an adhesive rolling resisting contact to a non-adhesive contact due to steric hindrance. As demonstrated by the perfect agreement between rheometry and 3-point bending tests, drop of the suspensions storage modulus originates from a particle contact shift. Same relationship is observed between the flexural contact resistance and overall suspension yield stress or the ageing of the material.

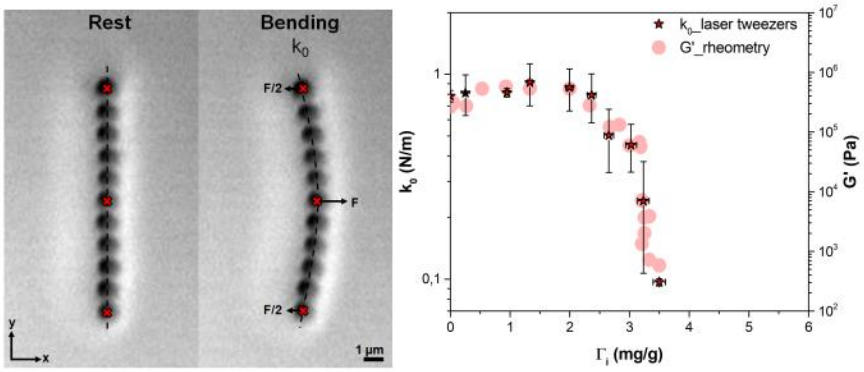

Figure 1: (Left: 3-point bending test on a particle rod using laser tweezers to probe the contact rigidity (k0). Red crosses represent optical traps used to move the beads and to measure the applied forces. Right: Contact stiffness measured through 3-point bending tests and shear elastic modulus (G') of the suspension (solid volume fraction: 45 % ; ionic strenght: 0.15 M) as a function of the mass of surfactant added per unit of bead mass (Γ_i)

REFERENCES

1. Fusier J., Goyon J., Chateau X., Toussaint F., Rheology signature of flocculated silica suspensions, *J. Rheol.*, **62**, 753, 2018.
2. Bonacci F., Chateau X., Furst E. M., Fusier J., Goyon J., Lemaître A., Contact and macroscopic ageing in colloidal suspensions, *Nat. Mater.*, **19**, 775, 2020.
3. Bonacci F., Chateau X., Furst E. M., Goyon J., Lemaître A., Yield stress aging in attractive colloidal suspensions, *Phys. Rev. Lett.*, **128**, 018003, 2022.

Rheology of High Performace Cement-Based Materials For Use in Additive Manufacturing

Nicos S. Martys[1], William L. George[2], Jeffrey W. Bullard[3]

[1]Matls Struc. Sys. Div., NIST, 100 Bureau Drive, Gaithersburg, MD 20899, USA
[2]Appl. Comp. Math Div., NIST, 100 Bureau Drive, Gaithersburg MD 20899, USA
[3]Dept. Matls. Sci. and Engr., Texas A&M, College Station, TX 77843, USA

ABSTRACT

In this presentation I will discuss preliminary results concerning the rheology of certain ultra high performance cement-based materials. Both experiment and computer simulation will be utilized to predict the rheological behaviour. We will take a multiscale approach treating the cement paste as a continuous medium with fibers and sand added to make a mortar. Experimental data of the rheological behavior of the matrix cement paste will be used as input into a smooth-particle-hydrodynamics (SPH) based simulation of suspensions. The SPH simulation will model the effect of fiber and sand that are added to the cement paste. The fiber material properties (e.g. elastic and flexible vs. stiff) and sand volume fraction will be varied for a given sand size distribution based on a standard Ottawa sand. The sand will be modelled as spherical inclusions. Simulation results will be compared to available experiment data. Based on the simulations we will comment on the suitability of such materials for use in additive manufacturing and discuss challenges of using such materials.

ACKNOWLEDGEMENTS

Acknowledgement: This work is suppored by the Engineering Research and Development Center (ERDC) - Construction Engineering Research Laboratory (CERL) under Contract No. W9132T22C0021

8TH PACIFIC RIM CONFERENCE ON RHEOLOGY, May 15-19, 2023

EXPLORING THE INTERPLAY BETWEEN INTERPARTICLE FORCES, RHEOLOGY, AND TRIBOLOGY IN NANOCLAY-BASED NANOLUBRICANTS

Leonardo Martin-Alarcon[1], Vinay Saini[2], Jackson Uhryn[2], Philip Egberts[2], and Milana Trifkovic[1]

[1]Chemical and Petroleum Engineering, University of Calgary, Calgary, Canada
[2]Mechanical and Manufacturing Engineering, University of Calgary, Calgary, Canada

ABSTRACT

Nanoclay additives are an eco-friendly solution for improving the friction and wear properties of grease lubricants. These additives' performance is determined by interparticle forces that impact both tribology at the contact interface and the microstructure's dynamic build-up and breakdown during shear. This study aims to explore the impact of concentration and interparticle interaction on nanoclay lubricants' rheology and tribology. Using polyalphaolefin oil, we prepared yield stress fluid suspensions by thickening it with nano-montmorillonite Cloisite 20A (C20A) or oleic-acid functionalized Cloisite 20A (C20A-OA) at varying concentrations. The suspensions were then examined using a modular rotational rheometer under steady and dynamic shear flows, while a frictional steel ball-on-three-steel plates setup was used to analyze their tribology. Atomic force microscopy and a profilometer were used to examine the interaction forces and wear scars. Our findings reveal that increasing the C20A concentration led to greater nanoparticle crowding and agglomeration, increasing lubricant stiffness and reducing the boundary friction at the tribocontact. However, C20A functionalization with OA increased nanoparticle dispersion and affected stiffness and aging dynamics. Microstructural investigation and time-dependent rheology uncovered that these changes are driven by increased repulsive forces, decreased inter-particle friction between C20-OA nanoparticles, and faster reorganization of the C20-OA nanoparticle network under shear. Greater interparticle repulsion enabled C20-OA nanoclays to align in the direction of shear, reducing overall viscosity. Furthermore, the presence of OA on nanoclays decreased inter-particle friction and particle-steel surface friction. These results provide insight into the interplay between nanoclay network evolution and the resulting rheological and lubricating properties of the derived nanolubricants, offering a platform for the development of novel, high-performing nanolubricants.

8TH PACIFIC RIM CONFERENCE ON RHEOLOGY, May 15-19, 2023

REVERSAL MOTION OF E-COLI BACTERIA IN NEMATIC LIQUID CRYSTALS

M. Goral[1,2], E. Clement[1], T. Lopez-Leon[2] and A. Lindner[1]

[1]Laboratoire de Physique et Mécanique des Milieux Hétérogènes (PMMH), ESPCI-PSL Paris, France
[2] Laboratoire Gulliver, ESPCI-PSL Paris, France

ABSTRACT

In many situations bacteria move in complex environments associated with non-Newtonian rheology. In this context, we seek to understand how these active fluids adapt and deal with geometrical frustration induced by the environment. Interesting spatio-temporal patterns have recently been observed in nematic liquid crystals, where the motion of bacteria is directed by the orientational molecular order of the liquid crystal or director field [1]. In this work, we study the swimming reorientation of a single bacterium, *E. coli*, constrained to move along the director field of a lyotropic chromonic liquid crystal (LCLC) that is confined to a planar cell. In such an environment, the spontaneous run and tumble motion of the bacterium gets frustrated: the elasticity of the liquid crystal prevents flagella from unbundling. Interestingly, in order to change direction, bacteria execute a reversal motion along the director field, shown in the **Fig. 1**, driven by the relocation of a single flagellum to the other side of the bacterial body, coined as a frustrated tumble. We present a detailed experimental characterization of this phenomenon, exploiting exceptional spatial and temporal resolution of bacteria and flagella dynamics during swimming, obtained using a two color Lagrangian tracking technique. We suggest a possible mechanism behind the frustrated run and tumble motion, accounting for these observations.

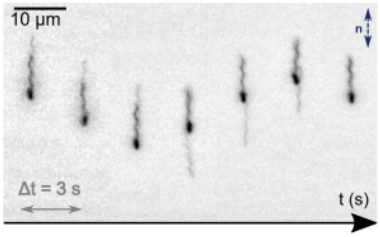

Figure 1: Snapshots of a bacterium swimming and changing direction in the liquid crystal. The nematic director is along the vertical direction, as well as the bacterium alignment.

ACKNOWLEDGEMENTS

This work was funded by the Agence Nationale de la Recherche (ANR) grant ANR-13-JS08-0006-01 and the European Research Council (ERC) Consolidator Grant 'PaDyFlow', Grant Agreement no. 682367.

REFERENCES

1. Zhou S., Sokolov A., Lavrentovich O.D., Aranson I.S. Living liquid crystals, *Proc. Natl. Acad. Sci.*, **111 (4)**, 1265-1270, 2014.

DIFFUSION OF LIPID NANOPARTICLES THROUGH AIRWAY MUCUS

Mohammad-Reza Rokhforouz [1,*], Belal Tafech[2,*], Jerry Leung[3], Pieter Cullis[3], Don D Sin[4,5], and Sarah Hedtrich[2,6,7], James J Feng[1,8]

[1] Department of Chemical and Biological Engineering, University of British Columbia, Vancouver, British Columbia, Canada

[2] Faculty of Pharmaceutical Sciences, University of British Columbia, Vancouver, British Columbia, Canada

[3] Department of Biochemistry and Molecular Biology, University of British Columbia, Vancouver, British Columbia, Canada

[4] Centre for Heart Lung Innovation, University of British Columbia, Vancouver, British Columbia, Canada

[5] Faculty of Medicine, University of British Columbia, Vancouver, British Columbia, Canada

[6] Department of Infectious Diseases and Respiratory Medicine, Charité – Universitätsmedizin Berlin, Corporate member of Freie Universität Berlin and Humboldt Universität zu Berlin, Germany

[7] Center of Biological Design, Berlin Institute of Health at Charité – Universitätsmedizin Berlin, Germany

[8] Department of Mathematics, University of British Columbia, Vancouver, British Columbia, Canada

ABSTRACT

Successful transmucosal delivery promises great therapeutic opportunities for the treatment of various diseases such as cystic fibrosis and chronic obstructive pulmonary disease (COPD). Despite promising results in preclinical studies, nanoparticle (NP) for drug delivery still remains insufficiently explored, thereby limiting effective clinical translation. Using Brownian dynamics (BD) simulations, we investigated lipid nanoparticle (LNP)-mucus interactions under the influences of steric, electrostatic, and hydrogen bond interactions. The mucus is modeled as a cubic periodic box comprised of straight, rigid, infinitely long rods. To obtain statistically reliable diffusion coefficients, we considered one thousand non-interacting spherical particles over at least 10^6 steps. The results revealed that removal of mucin's sialic acid results in higher diffusivity. However, LNP exhibit a non-monotonic behaviour as a function of mucus pH. Besides, both the electrostatic repulsion and the hydrogen-bonding, if acting alone, will hinder diffusivity. But one factor can mitigate the effect of the other to raise the diffusivity. The simulation results are compared with experimental measurements where possible, and the two generally agree. Our results may provide new insights into rational design for mucus-penetrating nanoparticles.

Brownian dynamics simulations

To simulate NP diffusion through mucus, we model the cross-linked mucin chains as rigid edges of a periodic cubic lattice, with the lattice size corresponding to the average mesh size of the mucus [1]. The Brownian diffusion of NPs can thus be tracked within a unit cell with periodic boundary conditions imposed on its faces. For each spherical particle, a Langevin equation is written out that includes a Brownian force, a drag force, and a pairwise interaction potential between the particle and the mucins:

$$m\frac{d\mathbf{v}}{dt} = F^B - \varsigma\mathbf{v} - \nabla U \quad (1)$$

where $m = \frac{\pi}{6}\rho_p d_p^3$ is the mass of particle of density ρ_p and diameter d_p, $\mathbf{v}$ is its velocity, t is the time, F^B is the Brownian force, ς is the drag coefficient, μ_f is the viscosity of the solvent, ∇ the spatial derivative, and U is the total pairwise interaction potential.

Charges on mucin: sialic acid cleavage

Sialic acid (SA) is responsible for most of the negative charge of the mucins [2]. To modify the charges on mucin chains, we have used an enzyme neuraminidase (NA) to cleave some of the negatively charged sialic acid side chains from the mucin backbone. We treated the mucus with NA for 10 min or 4 hours to remove different amounts of SA; the resulting mucus samples are called "semi-cleaved" and "cleaved" for short, with 23% and 56% of SA cleaved, respectively. As a control, an untreated mucus sample was also included. LNP was added separately to each of the three mucus samples, and nanoparticle tracking analysis was performed. As shown in **Fig. 1A**, the median diffusion coefficient (D) of LNP tends to increase as SA is removed by NA, but the data show a large amount of scatter. To model this in BD simulations, we use the untreated mucus as a baseline to determine the Debye length k and the electrostatic potential U_e. From this baseline, we estimate U_e for the semi-cleaved and cleaved mucus in proportion to the amount of charges left on the mucin polymer chains. Thus, we obtain the numerical diffusivity shown by the blue dots in Fig. 1A, in reasonable agreement with the experimental data.

Effect of pH

To understand the impact of pH on NP diffusion through the mucus, we decreased pH from 7 to 5, and 3. A change in pH results in a change in the surface charge density of both the mucin polymer chains and the LNP [3] (See **Table 1**). The measured zeta potential values indicate that by pH reduction from 7 to 3, a transition from electrostatic repulsion to attraction would occur. **Fig. 1B** depicts the diffusion coefficient D at different pH levels. Notably, the variation is non-monotonic, with the highest D value for the intermediate pH=5. This trend is also captured by our BD simulations, which offer an explanation for this behavior. As pH decreases from 7 to 5, D increases because the electrostatic repulsion is weakened. Further reduction to pH = 3 incurs electrostatic attraction, which in our case tends to trap the LNPs near the corners of the lattice and suppress their diffusion greatly.

Effect of hydrogen-bond attraction

Using BD simulations, we studied the interaction between electrostatic repulsion and H-bond attraction. Given the shorter-ranged nature of H-bond interaction, we deliberately chose weak electrostatic repulsions where particles can be influenced by H-bond attractions. As expected,

in the absence of H-bonds, increasing the strength of electrostatic interaction leads to lower diffusivities, as the particles tend to remain in the center of the simulation box. When we have two competing factors, one factor would reduce the effects of the other one, so that a nonmonotonic U_e dependence trend is observed (See **Fig. 1C**). For stronger electrostatic repulsions, the diffusivity will eventually fall again because of too much repulsive forces.

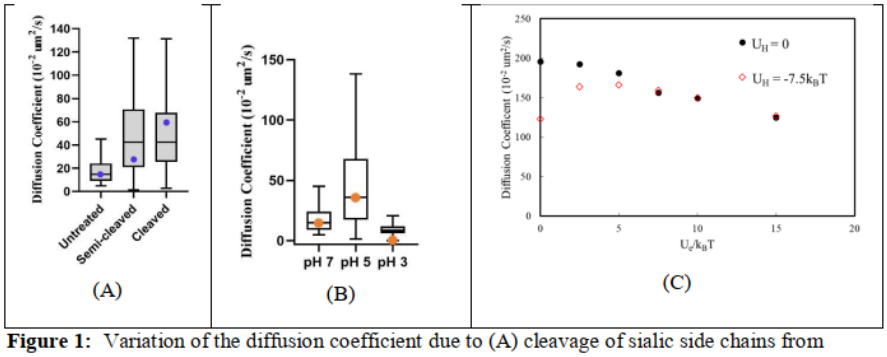

Figure 1: Variation of the diffusion coefficient due to (A) cleavage of sialic side chains from mucin; (B) change in medium pH; (C) hydrogen-bonding mitigating electrostatic repulsion.

Table 1: Zeta potential of mucin and LNP-mRNA at different pH values

	Zeta potential (pH=7)	Zeta potential (pH=5)	Zeta potential (pH= 3)
Mucin[4]	-7.7 mV	-4.8 mV	-2.2 mV
LNP-mRNA	- 6.21 mV	- 7.24 mV	+ 13.0 mV
U_e / k_eT	-76.3	-55.4	+45.6
Type of interaction	Strong repulsion	Weak repulsion	Weak attraction

REFERENCES

1. Hansing J, Ciemer C, Kim WK, Zhang X, DeRouchey JE, Netz RR. Nanoparticle filtering in charged hydrogels: Effects of particle size, charge asymmetry and salt concentration. *The European Physical Journal E*. 2016;39(5):1-13.
2. Lamblin G, Degroote S, Perini J-M, et al. Human airway mucin glycosylation: a combinatory of carbohydrate determinants which vary in cystic fibrosis. *Glycoconjugate journal*. 2001;18(9):661-684.
3. Mitchell MJ, Billingsley MM, Haley RM, Wechsler ME, Peppas NA, Langer R. Engineering precision nanoparticles for drug delivery. *Nature Reviews Drug Discovery*. 2021;20(2):101-124.
4. Yakubov GE, Papagiannopoulos A, Rat E, Waigh TA. Charge and interfacial behavior of short side-chain heavily glycosylated porcine stomach mucin. *Biomacromolecules*. 2007;8(12):3791-3799.

Oscillatory microfluidic thromboelastograph (micro-TEG) analysis of whole blood coagulation and fibrinolysis

Jigang Wang[1] and S. Shin [1,2]

[1]Department of Mechanical Engineering, Korea University, Seoul, Korea
[2]Engineeering Research Center for Biofluid Biopsy, Korea University, Seoul, Korea

ABSTRACT

Understanding of blood coagulation and fibrinolysis is critical for the management of patients who suffer from coagulopathies and need anticoagulation therapy. Conventional thromboelastograph (μ-TEG) analysis provided direct information including R-time, K-time, angle, MA and L30, which can help identify the hypercoagulable, hemorrhagic or fibrinoltic characteristic of blood samples. However, the shear environments of TEG assays are somewhat different from in-vivo hemodynamic shear flow.

We introduce an innovative approach, microfluidic thromboelastography (μ-TEG) that measures the viscoelastic properties of coagulating blood in a linear tube. When periodic oscillatory pressure is applied, anticoagulant blood periodically travels back and forth a certain distance. The variation of reciprocating distance (amplitude) is monitored with a video or pressure sensor and analyzed. The period of a cycle is 10 seconds (0.1 Hz), tube diameter is 1.5 mm, the blood sample volume ranges 5 – 50 μL depending on tube diameter and length. A typical length of blood filled in a tube is 20 mm.

When the blood is mixed with CaCl2 and kaolin, the reciprocating amplitude gradually decreased, showed a minimum value, and then slightly increased again. The obtained results using the newly developed μ-TEG system were analyzed and TEG variables including R-time, K-time, angle, MA and L30 within 10 min. We found that the μ-TEG system can observe the fibrinolysis phenomenon faster and more reliably compared to the existing TEG equipment, thereby reducing the experimental time innovatively.

The results of the present study suggest that μ-TEG would be a useful tool in blood clotting research, being capable of providing a global hemostasis profile in addition to detecting the instant of incipient clot formation. Additionally, due to the rapid assessment of a patient's coagulation status, the μ-TEG highlights the potential for point-of-care use.

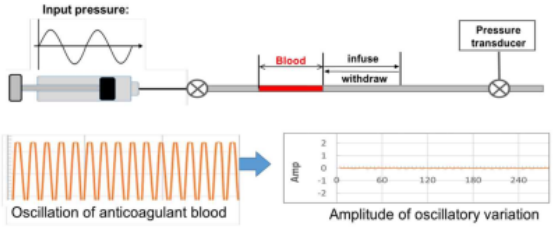

8TH PACIFIC RIM CONFERENCE ON RHEOLOGY, May 15-19, 2023

SCALE-DEPENDENT RHEOLOGY OF SYNOVIAL FLUID LUBRICATING MACROMOLECULES

Leonardo Martin-Alarcon[1,2], Aleksandra Govedarica[2], Randy H. Ewoldt[3], Steven L. Bryant[2], Gregory D. Jay[4], Tannin A. Schmidt[5], and Milana Trifkovic[2]

[1]Biomedical Engineering Graduate Program, University of Calgary, Calgary, Canada
[2]Chemical and Petroleum Engineering, University of Calgary, Calgary, Canada
[3]Mechanical Science and Engineering, University of Illinois at Urbana-Champaign, Urbana, USA
[4]Emergency Medicine, Brown University, Providence, USA
[5]Biomedical Engineering, University of Connecticut Health Center, Farmington, USA

ABSTRACT

The proper function of free joint motion in the body relies on the biomechanical properties of articular cartilage and synovial fluid (SF), which is a remarkable viscoelastic lubricant. The two major lubricant macromolecules in SF, hyaluronic acid (HA) and proteoglycan 4 (PRG4), synergistically interact to lower cartilage friction during boundary lubrication, but how these physical interactions affect SF rheology is still being debated. In this study, we used laser scanning confocal microscopy, rotational shear rheometry, and optical tweezer microrheology to examine the microstructure and rheological properties of physiologically relevant formulations of HA and recombinant human PRG4 (rhPRG4). Our findings suggest that rhPRG4 forms clusters of stiff, gel-like aggregates that do not interact with the surrounding continuous phase of HA polymers. Although the bulk rheology of HA solutions increased in a dose-dependent manner with the addition of rhPRG4, there was no evidence of a favorable physical interaction between the two that could alter the macroscopic rheology of the solutions. Additionally, we found that the interpretation of macrorheological data was significantly impacted by the interfacial adsorption of rhPRG4 molecules at the air-water interface of the rotational rheometer. Clinically relevant non-ionic surfactants used in the stabilization of rhPRG4 formulations were shown to both suppress the interfacial adsorption of rhPRG4 in rotational rheometers and disrupt the aggregation behavior of rhPRG4 in the bulk. Our results suggest that the macrorheology of this system is not governed by a single length scale, but instead responds as a disordered, hierarchical network with solid-like rhPRG4 aggregates distributed throughout the continuous HA phase. These findings provide important insights into the mechanical functionality of HA and PRG4 during cartilage lubrication and may aid in the development of HA-based viscosupplementation therapies for patients with joint diseases, such as osteoarthritis.

RHEOLOGY OF CORN STOVER SLURRIES UNDERGOING DILUTE-ACID PRETREATMENT

Joseph R. Samaniuk[1], Jessica Troxler[1], Jonathan J. Stickel[2], Mike E. Himmel[3], Yudong Li[3]

[1]Colorado School of Mines, Golden, CO 80401, USA
[2]Carbon America, Arvada, CO 80002, USA
[3]National Renewable Energy Laboratory, Golden, CO 80401, USA

ABSTRACT

Converting biomass into renewable resources such as biofuel has continued interest due to the desire to find alternatives to petroleum-derived products. Lignocellulosic biomass is a feedstock that does not compete as strongly with food resources as grain feedstocks, and it can be sourced from a variety of plants and plant components. Corn stover is a popular source of lignocellulosic biomass in North America due to widespread maize cultivation. One route to producing biofuels from lignocellulosic biomass is via an enzymatic hydrolysis reaction that utilizes enzymes to break down cellulose and hemicellulose into simple sugars. This process typically requires an upstream pretreatment step to make the cellulose and hemicellulose more accessible to enzymes. Pretreatment with a dilute acid solution is often used for this purpose The elucidation of the rheological properties of lignocellulose as it is processed during pretreatment is an important aspect of predicting energy requirements for pumping and mixing the resulting slurries; as well as for designing reactor components. In this work, we seek to characterize the rheological changes that take place in a corn stover feedstock undergoing dilute acid pretreatment. Slurries were prepared and pretreated at the National Renewable Energy Laboratory and rheological properties were tested at the Colorado School of Mines. A custom rheometer geometry was fabricated with stereolithography 3D printing to mitigate sample slip and measurements were made of yield stress and plastic viscosity as a function of the extent of pretreatment. The presentation will include a discussion of the rheological behavior observed during shear stress ramps, the result of fitting the Herschel-Bulkley and the Bingham model to the data sets to obtain reaction-time dependent model parameters. An outlook for generalizing this analysis to other lignocellulosic feedstocks will also be given.

8TH PACIFIC RIM CONFERENCE ON RHEOLOGY, May 15-19, 2023

RHEOLOGY OF BIOCOMPOSITES

Anne Shayenne Campos de Bomfim [1], Denis Rodrigue [2]

[1]UENSP, Guaratingueta, Brazil
[2]Université Laval, Quebec, Canada

ABSTRACT

The development of biocomposites has received a great deal of attention recently due to the concepts of sustainable development and circular economy. This is why biobased materials are more interesting to reduce their carbon footprint, especially when all the materials (matrix and reinforcements) are from a "natural" origin.

In this work, polylactic acid (PLA) was selected as the matrix because of its biodegradability and biocompatibility. But this biopolymer is seldom used alone and its properties can be improved by adding different plasticizers and fillers. In particular, spent coffee ground (SCG) is a valuable resource but still considered as a residue going to landfill. Due to its high amount generated every day, it would be interesting to valorize this material by introduction into a biopolymer and determine its effect in terms of mechanical and thermal properties.

So the main objective of this study was to determine the effect of SCG concentration (0, 10, 20 and 30 wt.%) on the properties of PLA-based biocomposites. As a first step, no other additive was added to limit the interaction and the raw materials cost, while producing a 100% biobased material.

The samples were first dried and compounded via twin-screw extrusion and pelletized before being molded by compression. From the sample produced, several characterizations were performed in terms of density, crystallinity and thermal properties to get a general overview of the main properties of the biocomposites produced. Then, a more specific analysis is performed on the rheological properties in the melt state (strain sweeps and frequency sweeps) at different temperature (180, 190 and 200 ºC) to relate the processing conditions with the formulation of the samples. To complete the analysis, rheological measurements in the solid state (strain sweeps, frequency sweeps and temperature sweeps) are also performed to determine the overall behavior under different conditions.

The results obtained showed that the biocomposites have a very complex behavior as their behavior represents a balance between the reinforcing effect of the solid SCG particles and the plasticizing effect of residual extractives inside these particles coming from the coffee making

process. Overall, it was found that 20 wt.% SCG provided the best balanced between all the properties investigated.

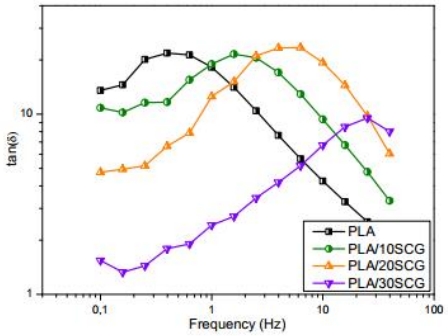

Figure 1: Loss tangent as a function of frequency for PLA biocomposites with different SCG content at 200 °C

HOW MORPHOLOGICAL AND RHEOLOGICAL PROPERTIES OF PLA/MWCNT NANOCOMPOSITES ARE AFFECTED BY MOLECULAR WEIGHT, STEREO CONFIGURATION OF PLA, AND PROCESSING

Mojtaba Mohammadi[1], Marie-Claude Heuzey[1], Pierre Carreau[1]

[1] Center for High Performance and Composite systems (CREPEC), Department of Chemical Engineering, Polytechnique Montreal, Montreal, Quebec, H3T 1J4, Canada

ABSTRACT

The effects of molecular weight, stereo configurations of polylactide (PLA) and processing on morphological and rheological properties of PLA/multiwalled carbon nanotubes (MWCNTs) have been investigated. A co-rotating twin-screw extruder (TSE) was used to disperse the MWCNTs in high (h)- and low (l)-molecular-weight amorphous and semicrystalline PLAs (aPLA and scPLA, respectively). Scanning electron microscopy (SEM) and small amplitude oscillatory (SAOS) and transient shear flow rheometry in the molten state were used to examine the effectiveness of the MWCNT dispersion in the various PLA matrices. Also, the rebuild-up of the destroyed structure due to shearing was investigated through SAOS time sweep experiments following a stress growth experiment. The SEM micrographs showed a better dispersion for the low molecular weight PLA and when processed at a higher temperature (190 °C). The normalized complex viscosity was increased drastically for the nanocomposites based on the low molecular weight amorphous PLA (aPLA), by more than 3 decades for aPLA containing 3 wt% MWCNTs compared to the neat matrix. What is more, at a low applied shear rate of 5 s-1 in stress growth experiments, the neat aPLAs did not exhibit any overshoot, but the transient viscosity (η^+) displayed overshoots at the beginning of the tests that were more significant as the MWCNT concentration was increased. Also, following the stress growth experiments no structural recovery was observed for the neat PLAs whereas a significant structure rebuild-up was detected for all aPLA-MWCNT nanocomposites, especially at larger MWCNT contents.

COMPATIBILIZED POLYLACTIDE/POLYAMIDE 11 (PLA/PA11) BLENDS CONTAINING MULTIWALL CARBON NANOTUBES: MORPHOLOGY, RHEOLOGY, ELECTRICAL AND MECHANICAL PROPERTIES

Zeinab Mousavi, Marie-Claude Heuzey, Pierre J. Carreau

Centre for High performance Polymer and Composite Systems (CREPEC), Chemical Engineering Department, Polytechnique Montreal, Montreal, Quebec H3T 1J4, Canada

ABSTRACT

The effect of adding multiwall carbon nanotubes (CNTs) on the morphology and properties of reactively compatibilized polylactide/polyamide 11 (PLA/PA11) blends with a 75/25 wt% composition was evaluated. PLA/PA11 blends were compatibilized using an epoxy-based chain extender, Joncryl® ADR 4468. Blends and blend nanocomposites were prepared using an internal mixer. The effects of chain extender concentration, mixing strategy, PLA molecular weight and CNT concentration on the morphology was evaluated in light of rheological characterization as well as electrical and mechanical characterization. Changes in the blend morphology upon adding CNTs (pre-mixing with PLA) was observed in which the dispersed phase changed to connected non-spherical, non-coalescing (or partially coalescing) PA11 domains bridged by CNTs at the interface. A network-like structure was formed in the blend nanocomposites containing 2-3 wt.% of nanoparticles characterized by a transition from liquid- to solid-like behavior. The blend nanocomposites based on the lower molecular weight PLA exhibited more significant enhancements of the rheological properties relative to the neat blend. Despite the observed transition in the rheological behavior, the electrical conductivity remained in the insulating range, showing a 6 decade increase compared to the neat blend, largely due to inadequate interconnectivity of PA11-CNT domains. Also the blend nanocomposites based on the lower molecular weight PLA displayed larger relative increase of the Young modulus, compared to the neat blend, indicative of a better CNT dispersion and formation of a more interconnected PA11-CNT network. The blend nanocomposites based on the higher molecular weight PLA retained 80% of the elongation at break of the neat blend up to 2 wt.% CNTs while the blends based on the lower molecular weight PLA retained only 25% of the elongation at break.

WHY IS THE PYANE EFFECT MISSING HIGHER HARMONICS?

Xiaorong Wang[1,2]

[1]School of Chemical Science and Engineering, [2]Institute for Advanced Study,
Tongji University, Shanghai 200092, China. (Email: xrwang@tongji.edu.cn)

ABSTRACT

Rubbers filled with a large amount of nanosized particles, such as carbon black (CB) or silica, often display a very unusual nonlinear behaviour under large-amplitude oscillatory shear (LAOS), where the amplitude stress strongly deviates from the linear dependence of strain while the time dependence of stress remains sinusoid. This unusual sinusoidal responses of filled rubbers, however, should not be confused with the fact that the rubbers are highly nonlinear viscoelastic materials as seen in typical stress-strain curves. In our recent studies, we have referred to this phenomenon as the "linear-nonlinear dichotomy" [1-7] of the Payne effect of filled rubbers. In order to understand the molecular details regarding this unusual behaviour, we chose a system with only three basic ingredients: polymer, filler, and oil. By changing the filler content and particle size, and by studying the matrix of various polymer concentrations and molecular weights, we have observed the impacts of the filler particle size, the filler loading, and the matrix composition on this very unusual rheological behaviour. A summary of our research activities on this subject in Tongji will be presented.

LINEAR-NONLINEAR DICHOTOMY RHEOLOGY

What we mean by this terminology is that the unusual nonlinear behaviour of filled rubber under oscillatory shear consists of two seemingly contradictory parts. The dynamic behaviour is nonlinear in the sense that the storage and loss moduli depend strongly on the strain amplitude, while the stress response appears to be linear because that at each of the strain amplitudes it is simply a sinusoidal offset from the oscillatory strain input (or vice versa). Mathematically, this "dichotomy" nonlinear phenomenon can be described by the following expression:

$$\sigma(t,\gamma_0) = \gamma_0 [G'(\gamma_0,\omega) \sin(\omega t) + G''(\gamma_0,\omega) \cos(\omega t)] \qquad (1)$$

where the input strain γ varies as $\gamma = \gamma_0 \sin(\omega t)$, γ_0 is the strain amplitude and ω is the angular frequency. Equation (1) exhibits the "linear-nonlinear dichotomy" characteristics. It is a linear viscoelastic equation that predicts perfect sinusoidal waves when γ_0 is constant, otherwise it is a nonlinear viscoelastic equation if γ_0 is a variable. Of course, equation (1) simplifies the actual situation of the nonlinear responses of real materials because it is a first-order approximation of the Fourier series. This simplification occurs in many physics. One such example is the ideal gas law as the first approximation that helps us model and predict the behaviour of real gases.

Therefore, the concept of "linear-nonlinear dichotomy" represents an ideal state in the rheological sense. There is no material that behaves exactly ideally, but there are plenty of filled rubber compounds that behave so closely that the concept of an ideal "dichotomy" state is an extremely useful approximation for many situations.[3,4] Fourier transform analysis shows that in many investigations of filled rubbers [1-7] higher-order harmonics of a filled rubber can sometimes be detected by a sensitive rheometer, but they are usually very small and negligible. The ratio of the third to the first harmonic responses (I_3/I_1) in the range when G'' passes through its maximum is typically less than 3%, and sometimes even less than 1%.[2]

As a result, the storage and loss moduli of a filled rubber in the nonlinear regime are still well defined by the first-order harmonic response functions. The standard deconvolution of experimental torque and phase offset in terms of the first harmonics G' and G'' is still appropriate at each strain amplitude in the nonlinear regime. The relationships between the dynamic moduli and the average energies stored and dissipated per cycle per unit volume and their physical meaning are still applicable in the nonlinear regime of a filled rubber due to what we call this ''the linear–nonlinear dichotomy'' of these materials. This unique feature of filled rubbers has been widely used by engineers and compounders in compound designs, characterizations and applications in rubber industries. Tires provide quiet and comfortable driving, due in part to the quasi-sinusoidal responses of tread rubbers to cyclic deformations. Despite the technological significance of the linear–nonlinear dichotomy phenomenon, the root cause for this peculiar "dichotomy" behaviour of filled rubbers has been a long-term puzzle.

THE LASTEST DISCOVERIES

Recently, it was found that particle-filled polymer melts of widely varied molecular weights exhibit a rheological transition [5] as the molecular weight of the matrix, M_n, increases and passes through a characteristic molecular weight M_c^*. Below M_c^*, the system shows typically the classic nonlinearity, where the storage modulus G' decreases as the strain amplitude γ_0 increases and the resulting stress waveforms are distorted from sinusoidal waves. Above M_c^*, the system displays a new nonlinearity, where the stress responses at any given strain amplitude remain surprisingly sinusoidal regardless the drop of modulus G'. The critical point M_c^* is found to be a few times of the entanglement molecular weight M_e.

In addition, it was also observed that particle-filled polymer solutions with wide changes in their compositions display a similar rheological transition [6] as the matrix polymer concentration ϕ approaches and passes through a critical value ϕ_c. Below ϕ_c, the system shows the classic viscoelastic nonlinearity, where the storage modulus G' decreases as strain amplitude γ_0 increases and the deviation of the stress signal from a sinusoidal wave is significant. Above ϕ_c, however, the system displays an anomalous nonlinearity, where the ratio of the third to the first harmonic responses I_3/I_1 of the stress signal is negligibly small and essentially independent of the drop in modulus G', and the system actually shows the quasi-sinusoidal responses in the nonlinear regime. The transition to linear-nonlinear dichotomy takes place in the concentrated polymer solutions where the polymer chains are highly entangled.

Furthermore, it was discovered [7] that this transition is insensitive to the strain amplitude, G'/G'_0, and filler loading but is very sensitive to the filler particle size d. Increasing the filler particle

size significantly decreases the critical ϕ. However, increasing the filler loading basically has no effect on the transition to linear-nonlinear dichotomy. This transition is detectable under either fixed strain amplitudes or fixed G'/G'_0 conditions, and happens when the mesh size ξ of the entangled polymer network in the matrix becomes smaller than the primary filler particle size d.

CONCLUSIONS

The degree of entanglements in polymer chains seems to play a key role in the linear-nonlinear dichotomy rheology. The time scale for topological rearrangements of entangled polymer chains that affect particle motion in the matrix is the crucial factor, and depends on polymer molecular weight, concentration and temperature. As the polymer concentration ϕ approaches and passes through ϕ_e, the filler particles may experience a sudden local blockage of their movements due to the topological hindrance of the entangled polymer chains. The sinusoidal stress response of the material in the nonlinear region is due to a sudden blockage of the filler particle movement when the polymer chains are entangled, and the entanglement mesh size ξ decreases to below the filler particle size d.

IMPLICATIONS

This "linear-nonlinear dichotomy" feature in the nonlinear rheological responses of filled rubbers can directly lead to a much general perspective, i.e., the frequency-deformation separability principle.[3] Thus, the measured dynamical properties can be separated into a linear viscoelastic frequency-dependent part and a nonlinear strain-dependent part, which can directly lead to other superposed behaviours for measured properties. In addition, when the higher order harmonics are negligible, the damping function in static relaxation is equivalent to the Payne effect in oscillatory shear.[4] This equivalence can phenomenologically link the linear and nonlinear properties of filled rubbers and has important implementations.

REFERENCES

1. Robertson, C. G.; Wang, X. Spectral hole burning to probe the nature of unjamming (Payne effect) in particle-filled elastomers. Europhys. Lett. **76(2)**, 278-284, 2006.
2. Randall, A. M.; Robertson, C. G. Linear-nonlinear dichotomy of the rheological response of particle-filled polymers. J. Appl. Polym. Sci. **131(19)**, 41818, 2014.
3. Li, S.; Mi, Y.; Wang, X. Superposed nonlinear rheological behavior in filled elastomers," J. Rheol. **61(3)**, 409-425, 2017.
4. Wang, L.; Xiong, W.; Wang, X. Filled Rubbers Manifesting Superposed Nonlinear Viscoelasticity. Ann. Trans. Nordic Rheol. Soc. **25**, 277-282, 2017.
5. Xiong, W.; Wang, X. Linear-nonlinear dichotomy of rheological responses in particle-filled polymer melts. J. Rheol. **62(1)**, 171-181, 2018.
6. Zou J.; Wang, X. Rheological responses of particle-filled polymer solutions: The transition to linear-nonlinear dichotomy. J. Rheol. **65(1)**, 1-12, 2021.
7. Wu, K.; Zou J.; Wang, X. Impacts of filler loading and particle size on the transition to linear-nonlinear dichotomy in the rheological responses of particle-filled polymer solutions. J. Rheol. **66(3)**, 605–618, 2022.

EFFECT OF INORGANIC FILLER ON RHEOLOGICAL PROPERTIES AND MORPHOLOGY OF POLYLACTIC ACID(PLA)/LOW-DENSITY POLYETHYLENE(LDPE) BLENDS

Min Chan Kim[1] and Kyu Hyun[1]

[1]Pusan National University, Busan, Republic of Korea

ABSTRACT

Among the biodegradable polymers, polylactic acid (PLA) is considered a promising material to solve the environmental pollution caused by plastic waste. However, PLA has weak mechanical properties such as brittleness and poor processability. For this reason, some researchers have tried polymer blend with materials that can compensate for the weaknesses of PLA[1]. In this study, low density polyethylene (LDPE), which shows strain hardening behavior in elongational viscosity, was used as the dispersed phase to overcome the disadvantage of PLA. To improve compatibility between PLA and LDPE, we added three different inorganic fillers, hydrophilic fumed silica, hydrophobic fumed silica and hydrophilic organoclay as compatibilizer. To evaluate the compatibilizer effect of various fillers, linear viscoelastic properties from small amplitude oscillatory shear (SAOS) test and nonlinear viscoelastic properties from elongational test are measured. In addition, we investigated morphology obtained by transmission electron microscopy (TEM) and scanning electron microscope (SEM) to check the location of filler and droplet size of dispersed phase. And we have studied the relation between rheological properties and morphology in PLA/LDPE blend systems.

REFERENCES

1. Lee, S.K., Kim, M.G., Song, H. Y., Hyun, K. Characterization of the effect of clay on morphological evaluations of PLA/biodegradable polymer blends by FT-rheology. *Macromolecules*, **52**, 7904-7919., 2019. https://doi.org/10.1021/acs.macromol.9b00800.

8TH PACIFIC RIM CONFERENCE ON RHEOLOGY, May 15-19, 2023

NORMAL STRESSES AT THE YIELDING POINT

Tatiana N. Rochinha[1,2], Priscilla R. Varges[1,3], and Paulo R. de Souza Mendes[1,4]

[1]Pontifícia Universidade Católica-RJ, Rio de Janeiro, Brazil
[2]tatianarochinha@icloud.com
[3]prvarges@puc-rio.br
[4]pmendes@puc-rio.br

ABSTRACT

Normal stresses are found in most complex fluids, and yield strength materials are ubiquitous in nature and industries. These facts are the motivation of the present research, which aims to study normal stresses developed in shear flow for different yield strength materials, namely a Carbopol dispersion, a commercial hair gel, and a highly concentrated emulsion. The goal is to analyze the stress state required to cause yielding in yield strength materials when a shear load is imposed. A simple but efficient experimental protocol is introduced, using a commercial strain-controlled rheometer to measure the normal stresses while the fluid undergoes steady and transient shear rheological tests. Furthermore, the validity of the Von Mises criterion is checked for the materials tested in this study. The results of this study allow, for shear flow, the determination of the yield strength tensor, that is the stress tensor at the yielding point. It was observed that the initial state plays an important role in the normal stresses. Residual stresses were found to be responsible for the difficulty in reaching repetitive measurements. At low shear rates, values of normal stresses substantially higher than the shear yield strength are observed, for all yield strength materials investigated. In addition, for one of these materials, the measured normal stresses go from positive to negative values as the shear stress is varied from above to below the yield strength. The normal stress values for the Carpobol dispersion tested remained constant at low shear rates. Among other findings, it is observed that the time needed to reach a steady state is much longer for normal stresses than for the shear stress, as already stablished in the literature for polymeric liquids.

Continuous Monitoring of Yield Stress and Solid Fraction of a Solid Suspension Using a Microfluidic Yield Rheometer

Durgesh Kavishvar[1], Arun Ramachandran[1]

[1]Department of Chemical Engineering and Applied Chemistry,
University of Toronto, Toronto, ON-M5T 3E5, Canada.

ABSTRACT

Solid suspensions are widely encountered in oil and gas industry as well as mining industry: from extracting oil from oil sands to discarding solid waste to the tailing ponds. In various applications, the quality of the suspensions is often assessed through the measurement of rheology of the suspensions. Yield stress, τ_y, which is one of the commonly used rheological parameters in industry, denotes the ability of a fluid to prevent the flow under the applied shear stress. τ_y is associated with the network of solid particles in the suspending fluid, emerging due to an attractive or a repulsive force of interaction among particles. τ_y is a function of the weight fraction of the particles ($X\%$), as it governs the structural strength of the particle network[1-3]. For example, a dilute suspension or a weaker network leads to a small τ_y. Thus, the measurement of τ_y enables determination of $X\%$, provided a prescribed relationship between τ_y and $X\%$ can be formulated.

In Canada, bitumen is extracted from Athabasca's oil sands using Clark's hot water extraction process. In this process, a mixture of bitumen, hot water, clay, and sand particles is sent to an extractor. Majority of bitumen oil is recovered through froth flotation, and solids are subject to gravity settling. Settling clay and sand particles split into two sections within the extractor, middlings and tailings, based on the size of the particles. It was demonstrated that both middlings and tailings exhibit a yielding behaviour[4-6] with τ_y varying between 10^{-4} and 10 Pa[4,5]. τ_y influences the transport of the trace amount of bitumen present in the middlings to the top in the flotation section of the extractor. A higher τ_y of middlings may lead to a lower total recovery of bitumen[7]. Further, both τ_y and $X\%$ of tailings determine the transportability and packing efficiency of tailings to the tailing pond. Thus, a continuous or in-line monitoring of τ_y and $X\%$ of middlings and tailings will enable feedback on the extraction process to enhance oil recovery from middlings as well as improve the transportation of tailings to the tailing ponds. Commercially available rheometers are unlikely to measure τ_y as low as 10^{-4} to 1 Pa, except for the ones which are prohibitively expensive. Further, they cannot be employed

for continuous or in-line measurement of τ_y. We propose using a microfluidic platform for the continuous monitoring of low τ_y, and determining X% through the measurement of τ_y.

We employ a microfluidic extensional flow device (MEFD), which is an extension to four-roll mills[8] and has been used in our group for studying properties of emulsions such as interfacial tension[9] and solubility[10]. The MEFD exhibits a characteristic shear stress distribution such that the material exhibits unyielded, solid region where the shear stress is lower than τ_y. On the other hand, in other regions where shear stress is higher than τ_y, the material yields and flows. We measure the size of the unyielded or solid region for a range of flow rates by tracking the flow using a camera. We have developed a scaling theory to determine τ_y of the material flowing in the MEFD through the measurement of the size of the unyielded region, the experimental parameters such as flow rate and device geometry. Since the MEFD enables both the flow of the yielded material through it as well as solid, non-moving regions to exist simultaneously, we are able to measure a τ_y in-line or continuously.

We characterized the MEFD platform using carbopol gel, a model yield stress fluid, of various concentrations ranging between 0.025 and 0.3% by weight, and measured τ_y between 60 mPa and 1.4 Pa. We compared τ_y measured using the MEFD with the rheometer measurements, and we found a fair agreement between the two. We also corroborated the experimental results with the simulation results using COMSOL Multiphysics®. The smallest τ_y we have measured is 4 mPa of wastewater filtrate, and our scaling analysis suggests that the MEFD should be able to measure a τ_y of the order of 0.1 mPa with the current version of the device, as required for middlings. We are working towards measuring a τ_y of the order of 10^{-4} Pa of dilute carbopol solutions. Further, we demonstrated the application of the MEFD to measure τ_y of solid suspensions. We used a suspension of cloisite clay and water as a model for middlings and tailings. We measured τ_y ranged from 65 mPa to 5.9 Pa of cloisite-water suspension of X% ranging between 3 to 6%. τ_y and X% was fitted to a cubic polynomial, and this relationship between the two was used to determine X% through the measurement of τ_y. We also performed in-line measurement of τ_y of a cloisite suspension sample at four different flow rates. τ_y was measured continuously for 15 min at an interval of 15 s, and X% was estimated accurately through $\tau_y - X$% relationship. We are in the process of measuring τ_y of kaolinite suspension of X% between 5 to 30%, which is more representative of middlings and tailings. We have planned to use the samples of middlings and tailings from oil industry in the future to substantiate the application of the MEFD technique.

ACKNOWLEDGEMENTS

We acknowledge our funding sources, which are as follows:

1. Centre for Research and Applications in Fluidic Technologies (CRAFT), University of Toronto, Canada.
2. NSERC CREATE - Training Program in Organ-on-a-Chip Engineering and Entrepreneurship, University of Toronto, Canada.
3. Canada Research Chairs

REFERENCES

(1) Kelessidis, V. C.; Maglione, R. Yield Stress of Water–Bentonite Dispersions. *Colloids Surfaces A Physicochem. Eng. Asp.* **2008**, *318* (1), 217–226. https://doi.org/https://doi.org/10.1016/j.colsurfa.2007.12.050.

(2) King, H. E.; Milner, S. T.; Lin, M. Y.; Singh, J. P.; Mason, T. G. Structure and Rheology of Organoclay Suspensions. *Phys. Rev. E* **2007**, *75* (2), 21403. https://doi.org/10.1103/PhysRevE.75.021403.

(3) Pashias, N.; Boger, D. V; Summers, J.; Glenister, D. J. A Fifty Cent Rheometer for Yield Stress Measurement. *J. Rheol. (N. Y. N. Y).* **1996**, *40* (6), 1179–1189. https://doi.org/10.1122/1.550780.

(4) Adeyinka, O. B.; Samiei, S.; Xu, Z.; Masliyah, J. H. Effect of Particle Size on the Rheology of Athabasca Clay Suspensions. *Can. J. Chem. Eng.* **2009**, *87* (3), 422–434. https://doi.org/https://doi.org/10.1002/cjce.20168.

(5) Piette, J.; Moud, A. A.; Poisson, J.; Derakhshandeh, B.; Hudson, Z. M.; Hatzikiriakos, S. G. Rheology of Mature Fine Tailings. *Phys. Fluids* **2022**, *34* (6), 63104. https://doi.org/10.1063/5.0091505.

(6) Lin, F.; Xu, Y. Impact of a Novel Bitumen Extraction Process on Mined Oil Sands Tailings Behavior. *AIChE J.* **2019**, *65* (1), 250–258. https://doi.org/https://doi.org/10.1002/aic.16424.

(7) Schramm, L. L. The Influence Of Suspension Viscosity On Bitumen Rise Velocity And Potential Recovery In The Hot Water Flotation Process For Oil Sands. *J. Can. Pet. Technol.* **1989**, *28* (03). https://doi.org/10.2118/89-03-07.

(8) Taylor, G. I. The Formation of Emulsions in Definable Fields of Flow. *Proc. R. Soc. London. Ser. A, Contain. Pap. a Math. Phys. Character* **1997**, *146* (858), 501–523. https://doi.org/10.1098/rspa.1934.0169.

(9) Goel, S.; Joshi, N.; Uddin, M. S.; Ng, S.; Acosta, E.; Ramachandran, A. Interfacial Tension of the Water-Diluted Bitumen Interface at High Bitumen Concentrations Measured Using a Microfluidic Technique. *Langmuir* **2019**, *35* (48), 15710–15722. https://doi.org/10.1021/acs.langmuir.9b02253.

(10) Motagamwala, A. H. A Microfluidic , Extensional Flow Device for Manipulating Soft Particles, MASc Thesis, University of Toronto, Toronto, Canada, 2013.

Hercshel-Bulkley parameter evaluation of oil-based drilling fluids

A. Saasen[1], and J.D. Ytrehus[2]

[1]University of Stavanger, Stavanger, Norway
[2]SINTEF, Trondheim, Norway

ABSTRACT

The behaviour of the Herschel-Bulkley parameters as function of temperature is shown for an oil-based drilling fluid. It is shown how these parameters vary if a dimensionless shear rate is used. These parameters are easily tabulated. It is also shown a lesser degree of usability of the consistency index, k, for tabulation purposes.

HERSCHEL-BULKLEY PARAMETERS

A controversy exists around the yield stress term. It is a question how it should be defined, how it should be measured (directly or indirectly), and even whether the yield stress really exists. This problem was discussed in a play enacted by Niall Young and Mads Larsson as Sherlock Holmes and Dr. Watson discussing the yield stress myth in the Nordic Rheology Conference on the Faroe Islands in 2003. Their review article seemingly written by Watson[1], summarised the controversy. For the analysis of drilling fluid properties it is assumed that the time scale of the flow is sufficiently rapid for the yield stress concept to be applicable. The yield stress is currently described in oil-well standards using the method described by Zamora and Power[2]. This method uses a linear extrapolation of the two lowest shear rate measurements to zero shear rate. Since the yield stress is treated as a material property, it shall be determined prior to determination of other properties.

The most common viscosity model for drilling fluids with a reasonable accuracy for a wide span of shear rates is the Herschel-Bulkley model[3]. Herschel-Bulkley fluids combine a Power-law behaviour with a yield stress. Traditionally, the Herschel-Bulkley model is defined as shown in Equation 1,

$$\tau = \tau_y + k(\dot{\gamma})^n \tag{1}$$

where k is the consistency index, n is the flow behaviour index or alternatively the curvature index, and τ_y is the yield stress. As Nelson and Ewoldt[4] discovered, the parameters used in this equation is often difficult to apply in selection of material compositions because the dimension of the consistency index, k, is dependent on the flow index, n: $k=k(n)$. Thus, there is no direct relation between k and viscosity unless n is equal to unity or at least equal in the compared fluids. Nelson and Ewoldt[4] studied fluids with a significant yield stress value. Based on application of yield stresses they modelled a critical shear rate where the shear stress is twice the yield stress. This approach is perfect for high yield stress fluids, but is not practical for drilling fluid description. Drilling fluids normally have smaller yield stresses, or sometimes do

not have any measurable yield stress at all. Therefore, inspired by Nelson and Ewoldt[4], Saasen and Ytrehus[5,6] described the Herschel-Bulkley model using dimensionless shear rates as shown in Equation 2,

$$\tau = \tau_y + \tau_s \left(\frac{\dot{\gamma}}{\dot{\gamma}_s}\right)^n \tag{2}$$

where the term τ_s is the additional shear stress, $\tau_s = \tau - \tau_y$ at a characteristic shear rate of the flow, $\dot{\gamma}_s$. The characteristic shear rate must be selected in accordance with the application. This means that the same drilling fluid's properties should be described with different characteristics when modelled for flow in drill pipe and in different annular sections. Using this type of presentation of the Herschel-Bulkley model, three independent parameters for the fluids can be tabulated: the yield stress, τ_y, the surplus stress, τ_s, at a characteristic shear rate, $\dot{\gamma}_s$, and finally the flow index, n. Of course, in tabulation the entire shear stress at the characteristic shear rate can be tabulate.

An example of application of the parameters of Herschel-Bulkley model with dimensionless shear rates is shown in Figure 1. Here it is shown how the Herschel-Bulkley parameters vary with temperature. The characteristic shear rate is $102 s^{-1}$ which is relevant for annular flow when drilling an 8 ½" section. All curves show a nearly monotonous change with temperature. If using the expression shown in Equation 1, the value k, show a complex connection with temperature since the dimension of k varies with temperature. Hence, as shown in Figure 2, the data do not show a monotonous behaviour and do not help increasing the understanding of fluid properties as function of temperature.

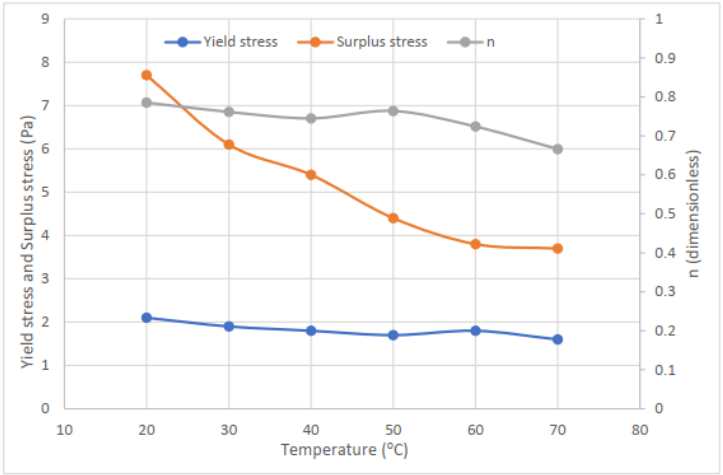

Figure 1: The effect of temperature on Herschel-Bulkley parameters τ_y, τ_s at 102 s^{-1} shear rate and n for a 1.59 s.g. oil-based drilling fluid. (Data from Halvorsen et al.[7])

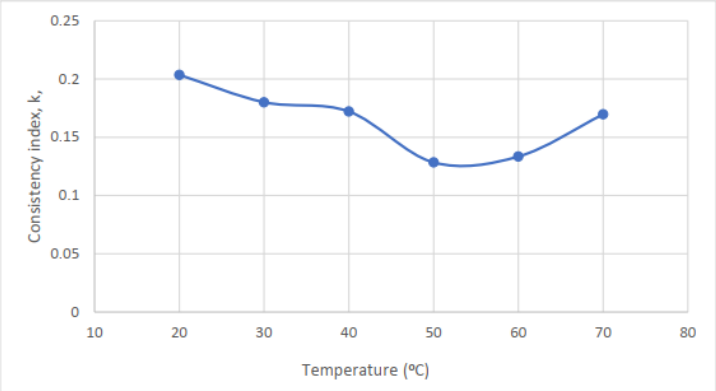

Figure 2: The consistency index, *k*, as function of temperature. (Data from Halvorsen et al.[7])

CONCLUSION

The applicability of Herschel-Bulkley parameters for creating drilling fluid tables is shown. Parameters developed for expressing properties as function of dimensionless shear rates are found more convenient for describing changes in physical properties and, thus, for tabulation of fluid properties.

ACKNOWLEDGEMENTS

The authors would like to thank the Research Council of Norway (grant number 294688), Equinor and OMV for their generous financing of the work presented here.

REFERENCES

1. Watson, J. H. The Diabolical Case of the Recurring Yield Stress. *Annu. Trans. Nord. Rheol. Soc.*, **11**, 73–79, 2003. (reissued in *Appl. Rheol.*, **14 (1)**, 40–45, 2017. https://doi.org/http://doi.org/10.3933/ApplRheol-14-40).
2. Zamora M. and Power D., Making a case for AADE hydraulics and the unified rheological model, paper AADE-02-DFWM-HO-13, the AADE 2002 Technology Conference, Houston, Texas, 2002.
3. Herschel WH, Bulkley R, "Konsistenz-messungen von Gummibenzöllösungen", *Kolloid Z.* **39**, 291-300, 1926.
4. Nelson AZ, Ewoldt RH, 2017, Design of yield stress fluids: A rheology-to-structure inverse problem, *Soft Matter*, **13**, 7578-7594
5. Saasen, A. and Ytrehus, J.D., "Rheological Properties of Drilling Fluids – Use of Dimensionless Shear Rates in Herschel-Bulkley Models and Power-Law Models", *Appl. Rheol.*, **28 (5)**, 54515, 2018. https://doi.org/10.3933/ApplRheol-28-54515
6. Saasen, A., and Ytrehus, J.D., Viscosity Models for Drilling Fluids – Herschel-Bulkley Parameters and Their Use, *Energies*, **13 (20)**, 5271, 2020. https://doi.org/10.3390/en13205271.
7. Halvorsen, H., Blikra, H.J., Grelland, S.S., Saasen, A. and Khalifeh, M., Viscosity of Oil-Based Drilling Fluids, *Annu. Trans. Nord. Rheol. Soc.*, **27**, 77-85, 2019.

An algebraic thixotropic elasto-viscoplastic model for describing pre-yielding and post-yielding behaviour

Lalit Kumar

Department of Energy Science and Engineering, IIT Bombay
, Powai, Mumbai, Maharashtra 400076

ABSTRACT

Formulating an appropriate thixotropic elasto-viscoplastic constitutive equation is challenging, especially for a model describing pre-yielding material behaviour and post-yielding fluid behaviour. Very few models try to explain both behaviour simultaneously[1–3]. Oldroyd's 1946[1] formulation was one of the first models explaining it, however, assumptions of a simple linear elastic and quasi-static deformation before yielding made his model idealistic. At the same time, the quasi-static preyielding deformation assumption allows the possibility for the consideration of preyielding viscous and plastic deformation when quasi-static conditions are not fulfilled. Saramito[2] added a frictional element in Oldroyd's viscoelastic model[1] to avoid a jump in stress at the critical strain, however, his model is unable to predict initial plastic and viscous effect as pointed out by Coussot and rogers[4]. De Souza Mendes and Thompson[3] model is unable to predict true yield stress and no flow behaviour for a finite value of the parameter. Apart from the shortcomings mentioned above, their models consist of complex differential form creating difficulty for practical application. Here, we discuss the structural parameters based thixotropic elasto-viscoplastic (TEVP) constitutive model valid for both reversible (finite thixotropic time scale) and irreversible (infinite thixotropic time scale) thixotropic materials. An extensional of our earlier model[5], which is used to predict flow restart in the pipeline filled with irreversible TEVP materials. Early model was restricted to irreversible TEVP materials, only considered for predicting flow restart without discussing other aspects of the rheological behaviour of TEVP materials. Our present model, despite being a simple algebraic equation, explains both the viscosity plateau at low shear rates and the diverging zero shear rate viscosity appropriately using the same parameters but different shear histories. Furthermore, our model predicts stress overshoot during shear rate startup flow, hysteresis in shear-rate ramps, viscosity bifurcation during creeping flow, delayed yielding, sudden stepdown shear stress test results and shear banding phenomena effectively. Depending on shear histories, our model at the steady state reduces to either Bingham, Herschel Bulkley type, or Newtonian fluids model. The current framework also provides a possible physical interpretation of the Bingham model, which has been elusive despite its enormous use. Our model predicts either a no-flow start or a simple flow start for different thixotropic time scales while keeping other conditions the same, and it can also predict a delayed flow start for an appropriate structure degradation kinetic.

The results in Figure 1 show some of the important TEVP bahviour predicted by our model. Figure 1a shows stress overshoot during a constant shear rate startup flow. Figure 1b shows stress hysteresis during shear-rate up and down calculation. Whearas, figure 1c shows the stress

response of the material, when a material undergoes a high shear rate for a certain period and suddenly shear rate brought to a considerably low value. These results qualitatively predict recent experimental observations of TEVP fluids.

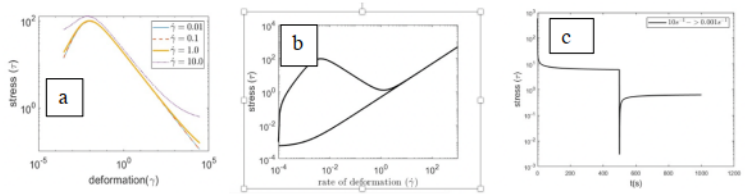

Figure 1 : . (a) shows stress overshoot during a constant shear rate startup flow, (b) shows stress hysteresis during shear up and down calculation and (c) shows the stress response during sudden shear rate down after a certain period of time.

[1] J. G. Oldroyd, n Mathematical Proceedings of the Cambridge Philosophical Society **43**, 100 (1947).
[2] P. Saramito, J. Non-Newton. Fluid Mech. **145**, 1 (2007).
[3] P.R. de Souza Mendes and R.L. Thompson, J. Non-Newton. Fluid Mech. **187–188**, 8 (2012).
[4] P. Coussot and S.A. Rogers, J. Non-Newton. Fluid Mech. **295**, 104604 (2021).
[5] L. Kumar, O. Skjæraasen, K. Hald, K. Paso, and J. Sjöblom, J. Non-Newton. Fluid Mech. **231**, 11 (2016).

8TH PACIFIC RIM CONFERENCE ON RHEOLOGY, May 15-19, 2023

Rheology of active colloids: motility-induced shear-thickening

Hartmut Löwen[1], A. Gülce Bayram[2], Fabian J. Schwarzendahl[1] and Luca Biancofiore[2]

[1]Heinrich-Heine Universität Düsseldorf, Düsseldorf, Germany
[2]Bilkent University, Ankara, Turkey

ABSTRACT

Phase transitions and collective dynamics of active colloidal suspensions are fascinating topics in soft matter physics[1], particularly for out-of-equilibrium systems, which can lead to rich rheological behaviour in presence of steady shear flow. Here the role of self-propulsion in the rheological response of a dense colloidal suspension is investigated by using particle-resolved simulations. Increasing the self-propulsion of the colloids induces a transition from a shear-thinning to a shear-thickening behaviour, which we attribute to clustering in the suspensions induced by motility, a general phenomenon which occurs close to motility-induced phase separation (MIPS)[2]. This novel behaviour of motility-induced shear thickening (MIST) can be used to tailor the rheological response of colloidal suspensions.

ACKNOWLEDGEMENTS

We thank Jürgen Horbach for helpful discussions. The work of A.G.B. was supported within the EU MSCA-ITN ActiveMatter (Proposal No. 812780).

REFERENCES

1. Bechinger, C.; di Leonardo, R.; Löwen, H.; Reichhardt, C.; Volpe, G.; Volpe, G.; Active particles in complex and crowded environments, *Reviews of Modern Physics* **88**, 045006 (1-50) (2016).
2. Buttinoni, I; Bialké, J.; Kümmel, F.; Löwen, H.; Bechinger, C.; Speck, T.; Dynamical clustering and phase separation in suspensions of self-propelled colloidal particles, *Physical Review Letters* **110**, 238301 (1-5) (2013).

DENSITAXIS OF SWIMMING MICROORGANISMS

Vaseem A. Shaik[1] and Gwynn J. Elfring[1]

[1]Department of Mechanical Engineering, Institute of Applied Mathematics,
University of British Columbia, Vancouver, BC, Canada V6T 1Z4

ABSTRACT

Organisms often move through inhomogeneous environments like the gradients in heat, light, nutrients, fluid viscosity or density. They respond to these inhomogeneities by reorienting and changing speed, often exhibiting directed motion termed *taxis*. For instance, *E. coli* reorients to swim up nutrient gradients but swims down light or viscosity gradients. Here we present theoretical evidence of taxis in density gradients, which we call *densitaxis*. This taxis is sensitive to whether the organisms generate thrust in-front (so-called pullers) or back (pushers). Pullers, like *Chlamydomonas reinhardtii* for instance, reorient to swim up or down the gradients depending on their initial orientation. But pushers like *E. coli* rotate to swim normal to the gradients. This taxis could help explain the motion of marine organisms in the ocean where density gradients are prevalent or be leveraged to sort or organize a suspension of organisms.

Hydrodynamic interactions of active matter near boundaries

S. Arman Abtahi[1], Gwynn J. Elfring[1]

[1]Institute of Applied Mathematics, University of British Columbia, Vancouver, Canada

ABSTRACT

Microorganisms and synthetic active particles frequently present in large numbers near boundaries, such as in a petri dish of suspended bacteria or experiments with Quincke rollers near a substrate. Active matter systems have the ability to self-organize into complex dynamic structures when they reach a certain density. These structures are driven by particle-particle and particle-fluid interactions, such as hydrodynamic or electrostatic forces. Confinement can affect self-organization in active suspensions, leading to the formation of vortex-like structures and unidirectional pumping motions. These complex dynamics are distinct from those observed in bulk, such as bacteria forming race-tracks and Quincke rollers spinning[1,2,3,4]. This study highlights the importance of understanding the role of boundaries in driving the collective behavior of bacteria and other active matter systems. When suspensions of particles are dense, many-body hydrodynamic interactions take place and far-field approximations can become ineffective. The Stokesian Dynamics method[5] has been extended to simulate dense suspensions of active particles near boundaries using the squirming model[6]. We then use the active SD[7,8] method to demonstrate various examples of interesting dynamics due to hydrodynamic interactions of active particles near a wall[9].

REFERENCES

1. Wioland H., Lushi E., Goldstein R.E. Directed collective motion of bacteria under channel confinement, *New J. Phys.*, **18**, 075002, 2016.

2. Lushi E., Wioland H., Goldstein R.E. Fluid flows created by swimming bacteria drive self-organization in confined suspensions, *PNAS*, **111**, 9733–9738, 2014.

3. Theillard M., Alonso-Matilla R., Saintillan D. Geometric control of active collective motion, *Soft Matter*, **13**, 363, 2017.

4. Bricard A., Caussin J.B., Das D., Savoie C., Chikkadi V., Shitara K., Chepizhko O., Peruani F., Saintillan D., Bartolo D. Emergent vortices in populations of colloidal rollers, *Nat. Commun.*, **6**, 7470, 2015.

5. Swan J.W., Brady J.F., Moore R.S. Modeling hydrodynamic selfpropulsion with Stokesian dynamics. or teaching Stokesian dynamics to swim, *Phys. Fluids*, **23**, 071901, 2011.

6. Lighthill M.J. On the squirming motion of nearly spherical deformable bodies through liquids at very small Reynolds numbers, *Commun. Pure Appl. Math.*, **5**, 109–118, 1952.

7. Elfring G.J., Brady J.F. Active Stokesian dynamics, *J. Fluid Mech.*, **952**, 2022.

8. Ishikawa T., Simmonds M.P., Pedley T.J. Hydrodynamic interaction of two swimming model micro-organisms, *J. Fluid Mech.*, **568**, 119–160, 2006.

9. Abtahi S.A. Hydrodynamic interactions: microswimmers near boundaries (T), *UBC*, 2022.

DYNAMICS OF 2D COLLOIDAL CRYSTALS IN THE PRESENCE OF LOCALIZED INTERNAL STRESSES CREATED BY ACTIVE PARTICLES

Jacob John and Giovanniantonio Natale

Department of Chemical and Petroleum Engineering, Schulich School of Engineering, University of Calgary, Canada

Structured interfaces such as 2D colloidal crystals are model systems to study the mechanics of various natural and engineered systems. Active colloidal particles exhibit self-propelling motion by exploiting chemical, temperature, or force gradients around individual particles. The presence of active particles as impurities in 2D colloidal crystals can be considered as simplified models to understand the motion of bacterial cells in biofilms[1], stability of Pickering emulsion microreactors[2], human crowd behavior[3] and the motion of molecular motors at cell membranes[4]. In this work, we report the dynamics and rheology of 2D colloidal crystals formed using spherical polystyrene (PS) particles at oil-water interfaces in the presence of active PS-Platinum Janus particles. The particle dynamics is studied using video microscopy and image analysis. The rheological behavior of the interface is investigated using interfacial shear rheology and microrheology. At high surface coverage of the particles and low ionic strength, the passive particles form a two-dimensional crystal with a hexagonal lattice structure due to dipole-dipole repulsive interactions. These interfaces exhibit a viscoelastic solid-like behavior in linear regimes and reversible structural rearrangements at large strains. However, with an increase in the number of active particles, the crystal loses its orientational and spatial order and forms multiple domains of crystals separated by grain boundaries, even in the absence of activity. In the presence of activity, the overall crystal becomes more dynamic and heterogeneous and loses its hexagonal order. Particle tracking microrheology and interfacial shear rheology quantify the transition to the liquid-like nature of the interface due to the presence of active impurities. We show how local perturbations can have long-range effects on the dynamics of particles in 2D colloidal crystals and their overall viscoelasticity. We identify the electrostatic repulsion between particles and the propagation of internal stress as two competing forces that exist in the crystal in the presence of activity. This work provides insights into the motion of bacterial cells in crowded biofilms, how stress relaxation occurs in crystals with defects and internal stresses and how particle arrangements at interfaces of Pickering emulsion microreactors are affected by interfacial chemical reactions.

REFERENCES

1. Boyang Q., Chenyi F., Andrew A. B., Ameya A. M., Howard A. S.,Ned S. W., Bonnie L. B., Cell position fates and collective fountain flow in bacterial biofilms revealed by light-sheet microscopy, *Science*, **369**, 71-77, 2020.

2. Chun Y. X., Shi X. M., Long H. X., Rui X. B., Xin Y., Yaolei W., Zhong P. Q., Bernard P.

B., Ting G., and Tao M., Light and Magnetic Dual-Responsive Pickering Emulsion Micro-Reactors, *Langmuir*, **33**, 14139-14148, 2017.

3. Shreetam B., Debi P. D., Malay B., Partha P. R., Understanding Crowd Flow Patterns Using Active-Langevin Model, *Pattern Recognition*, **119**, 1-12, 2021.

4. Víctor G. L., Fang C., Lizanne G. N., Guillaume D., Amir A., Anatoly B. K., Jacob T. R., Gufeng W., Robert P. and James M. T., Molecular machines open cell membranes, *Nature*, **548**, 567-572, 2017.

Poster Session: Welcome Reception & Poster Session - Sage Bistro (7:00 PM - 10:00 PM)

8TH PACIFIC RIM CONFERENCE ON RHEOLOGY, May 15-19, 2023

ADVANCES IN CONE-PLATE RHEOMETERS FOR BUSY LABS

David J. Moonay[1]

[1]Brookfield AMETEK, Middleboro, Massachusetts, USA

ABSTRACT

Numerous laboratories in myriad industries have time, materiel and personnel constraints. Pharmaceutical, medical or biomedical labs, in particular, may also have to deal with 21 CFR Part 11 and/or good [automated] manufacturing practices compliance. Cone-Plate geometry has been and is used because of (1) the small sample size required and (2) easy portion loading and cleaning or "presentation". This paper presents data for a variety of products, covering a range of viscosities. E.g.: aqueous solutions, lotions and creams, among others. Simple tests may involve one speed, for quick QC/QA checks. Rotational, multi-shear rate data, on the other hand, provide more information concerning shear-thinning or thixotropic behavior. Furthermore, simple math models, such as Bingham, Casson [variants] or Herschel-Bulkley, may be used to calculate practical yield stresses. Rheometry is important because it helps quantify product behavior and, therefore, assists product formulation and end-use tailoring. Convenient upgrades, to aid and ease the work burdens of practitioners, include, for example: (1) magnetic couplings for quick cone removal and reattachment, (2) barcode scanning capability to help automate sample logging, and (3) 21 CFR Part 11 compliance in both standalone mode and with optional software for instrument control and data acquisition. Relevant equipment advances will be discussed.

Active Particles Crossing Sharp Viscosity Gradients

Jiahao Gong[1], Vaseem A. Shaik[1] and Gwynn J. Elfring[1]

[1]University of British Columbia, Vancouver, Canada

ABSTRACT

Swimming microorganisms and other active particles often navigate through complex and inhomogeneous environments by exhibiting taxis, where they reorient themselves to move up or down gradients in chemical or material properties of their surroundings. Recent experiments conducted on the alga Chlamydomonas reinhardtii have revealed complex refraction and scattering behavior when encountering sharp viscosity gradients. Inspired by these findings, we developed a simple hydrodynamic model of active particles swimming near and across similar sharp changes in the viscosity of the suspending fluid. The algae are modelled as spherical squirmers and we have found the reorientation process of pushers, pullers and neutral swimmers is qualitatively similar. Our theory is consistent with the experimental observations as the scattering phenomenon occurs only when the initial orientation of the particle relative to the interface normal is large and it is crossing from low to high viscosity. Otherwise, the particle crosses the interface by undergoing some reorientation. The law we derived governing the reorientation of neutral swimmers is analogous to Snell's law of ray optics as previously shown for gliders on a frictional substrate.

EFFECT OF THE TEMPERATURE ON THE RHEOLOGICAL BEHAVIORS OF LITHIUM-ION BATTERIES ANODE SLURRY

Yeseul Kim and Jun Dong Park*

Department of Chemical and Biological Engineering, Sookmyung Women's University, Seoul, Republic of Korea

ABSTRACT

It is important to design and control the rheological behavior of lithium-ion battery slurry since it has a substantial impact on the productivity and performance of the electrode. While there are numerous alternatives for controlling the rheology of slurry, most are related to LIB slurry components such as concentration of components, type of active material, and polymeric binder molecular weight. In this work, we demonstrate that the rheological behavior of LIB anode slurry is temperature-dependent and that temperature, a process variable, might be a beneficial alternative to modify the rheological behavior of anode slurry. It was discovered that at lower temperatures, the values of G' and G" of the slurry gradually decreased with increasing temperature. We attribute the observed temperature dependency to changes in the segmental motion of the CMC polymer binder. At low temperatures, an increase in temperature leads to a rise in the segmental motion of the CMC polymer binder. This results in a reduction of entanglement between the concentrated CMC polymer and graphite surfaces, leading to a decrease in the values of G' and G". Beyond a specific temperature threshold, the rheological properties of the slurry exhibit a rapid increase, which is attributed to the change in entropy-driven hydrophobic interaction. Water molecules form a clathrate cage structure around graphite particles, reducing the slurry system's total entropy due to its oriented and structured state. Consequently, graphite particles tend to aggregate stronger, minimizing the interface between graphite and water and increasing the system's entropy[1,2]. The increase in both G' and G" values beyond a specific temperature threshold, where the entropy plays an important role, is related to the intensification of the hydrophobic interaction due to the temperature increase. It's worth noting that the increase in G' and G" is only observed in the small strain amplitude region of the strain amplitude sweep test, while G' and G" continuously decrease at larger strain amplitudes. This observation supports our interpretation, as previous studies have shown that yielding at small strain amplitudes is correlated with graphite-graphite attraction, whereas yielding at large strain amplitudes is correlated with polymeric binder interaction[3].

REFERENCES

1. Head-Gordon, T. Is water structure around hydrophobic groups clathrate-like?. *Proceedings of the National Academy of Sciences*, *92*(18), 8308-8312, 1995. https://doi.org/10.1073/pnas.92.18.8308
2. Yangshuai, Q., Yongfu, Y., Lingyan, Z., Weijun, P., & Yupeng, Q. Dispersion and agglomeration mechanism of flaky graphite particles in aqueous solution. *Journal of Dispersion Science and Technology*, *38*(6), 796-800, 2017. https://doi.org/10.1080/01932691.2016.1198703
3. Kim, Y., Kim, S., Kim, B. S., Park, J. H., Ahn, K. H., & Park, J. D. (2022). Yielding behavior of concentrated lithium-ion battery anode slurry. *Physics of Fluids*, *34*(12), 123112, 2022. https://doi.org/10.1063/5.0128872

RHEOLOGICAL DIFFERENCES IN ANODE SLURRIES CAUSED BY SHAPE DIFFERENCE BETWEEN NATURAL AND SYNTHETIC GRAPHITE

Yeeun Kim[1], Jun Dong Park[1]

[1]Department of Chemical and Biological Engineering, Sookmyung Women's University

ABSTRACT

Rechargeable lithium-ion batteries (LIBs) play an important role in today's industry because of their excellent charge capacity and high energy density[1]. The performance of LIBs is heavily dependent on the quality of the electrode, which must be well-constructed using active materials, binders, and additives. In particular, graphite is one of the most significant components serving as the active material in the anode electrode. Depending on the production method, graphite is classified as either natural or synthetic. It's application to small electronic devices or electric vehicles should take into account the unique advantages and disadvantages of each type. Natural graphite is known for its high capacity and affordability, making it a popular choice for small lithium batteries and general electronic products[2]. In contrast, synthetic graphite boasts excellent cycle performance and high charge/discharge efficiency, making it a preferred choice for batteries in automobiles and high-end electronic products[3]. To successfully manufacture the electrode, it is important to consider not only economic feasibility and electrical properties but also rheological properties. The rheological properties of the slurry are greatly influenced by the particle shape and composition of graphite, which can result in various slurry characteristics[4]. By analyzing the rheological behavior, it is possible to predict the microstructure of the slurry and develop solutions to prevent defects during the coating and drying process.

The aim of this study is to investigate changes in rheological properties based on the particle shape of graphite. To achieve this, slurries were prepared using natural graphite with a spherical shape and synthetic graphite with a flake shape, and different volume fractions of graphite were used while keeping the ratios of graphite, carbon black, and CMC fixed. Rheological tests such as oscillatory strain amplitude sweep tests were conducted to estimate the microstructure of the anode slurry. Additional experiments such as tap density measurement tests and sedimentation experiments were also conducted to support the results. The findings of this study will aid in controlling the rheological characteristics of battery slurry and designing optimal slurry constituents for the industry.

REFERENCES

1. Wu, F.; Maier, J.; Yu, Y. Guidelines and Trends for Next-Generation Rechargeable Lithium and Lithium-Ion Batteries. *Chem. Soc. Rev.* 2020, ***49*** **(5)**, 1569–1614. https://doi.org/10.1039/C7CS00863E.
2. Shi, M.; Song, C.; Tai, Z.; Zou, K.; Duan, Y.; Dai, X.; Sun, J.; Chen, Y.; Liu, Y. Coal-Derived Synthetic Graphite with High Specific Capacity and Excellent Cyclic Stability as Anode Material for Lithium-Ion Batteries. *Fuel* 2021, *292*, 120250. https://doi.org/10.1016/j.fuel.2021.120250.
3. Wissler, M. Graphite and Carbon Powders for Electrochemical Applications. *Journal of Power Sources* 2006, ***156*** **(2)**, 142–150. https://doi.org/10.1016/j.jpowsour.2006.02.064.
4. Heine, D. R.; Petersen, M. K.; Grest, G. S. Effect of Particle Shape and Charge on Bulk Rheology of Nanoparticle Suspensions. *The Journal of Chemical Physics* 2010, ***132*** **(18)**, 184509. https://doi.org/10.1063/1.3419071.

TWO-STEP YIELDING BEHAVIOR OF CONCENTRATED LITHIUM-ION BATTERY ANODE SLURRY

Yeseul Kim[1], Jeong Hoon Park[2], Kyung Hyun Ahn[2] and Jun Dong Park[1]

[1]Sookmyung Women's University, Seoul, South Korea
[2] Seoul National University, Seoul, South Korea

ABSTRACT

The nonlinear rheology of a concentrated lithium-ion battery anode slurry was investigated under large amplitude oscillatory shear and interpreted using sequence physical process (SPP) analysis. A complex interaction between three anode slurry components—graphite (Gr) as an active material, carbon black (CB) as a conductive additive, and carboxymethyl cellulose (CMC) as a binder—results in a two-step yielding behavior, which is represented by the secondary plateau in dynamic strain and stress sweep tests. Through the examination of intra-cycle rheological transition under oscillatory shear flow, we demonstrate that a two-step yielding behavior is represented by double deltoids in SPP analysis. Two-step yielding is observed in Gr-CMC slurries but not in CB-CMC slurries, indicating that Gr and CMC are the principal causes of two-step yielding in an anode slurry. A sedimentation test performed on a dilute Gr-CMC solution resulted in phase separation between graphite particles, with CMC adsorbed on their surface and graphite particles aggregated by hydrophobic attraction. This suggests that there are two different forms of interactions in a concentrated slurry: a hydrophobic interaction between graphite particles and a physicochemical interaction resulting from CMC adsorption on graphite particles. The initial yielding stage is associated with the hydrophobic interaction between graphite particles, resulting in a network structure that is expected to be brittle and break under a small strain. The second yielding stage is attributable to the interaction between concentrated CMC, as evidenced by the overlap between the secondary deltoid of the anode slurry and the single deltoid of the concentrated CMC solution in SPP analysis.

REFERENCES

1. Kim, Y., Kim, S., Kim, B. S., Park, J. H., Ahn, K. H., & Park, J. D. (2022). Yielding behavior of concentrated lithium-ion battery anode slurry. *Physics of Fluids*, *34*(12), 123112, 2022. https://doi.org/10.1063/5.0128872

8TH PACIFIC RIM CONFERENCE ON RHEOLOGY, May 15-19, 2023

JAMMING MECHANISMS OF DILUTE FIBRE SUSPENSIONS UNDER DEAD-END AND CROSS-FLOW CONDITIONS

Miguel E. Villalba[1,2], Masoud Daneshi[1,3], D. Mark Martinez[1,2]

[1]University of British Columbia, Vancouver, Canada
[2]Department of Chemical and Biological Engineering, 2360 E Mall, Vancouver, BC V6T 1Z3
[3]Department of Mathematics, 1984 Mathematics Rd, Vancouver, BC V6T 1Z2

ABSTRACT

The jamming of particles in small constrictions is a critical problem encountered across different systems such as in the dry granular flows and the filtration of colloidal suspensions. While the jamming of suspensions consisting of isotropic particles is well-investigated, we find that the jamming of anisotropic particles such as fibres is less understood. Motivated by the pressure screening process in the pulp and paper industry, we study the fundamental jamming mechanisms of dilute nylon fibre suspensions in a single constriction under dead-end and cross-flow filtration conditions.

We identify three distinct jamming mechanisms for both flow configurations: single fibre bridging, in-situ floc formation (IFF) and upstream floc formation (UFF). The bridging mechanism is a function of fibre to constriction width ratio l/w, position and orientation. With the help of visualization tools and a numerical model, we estimate the range of critical positions and orientations for bridging, which were subject to the flow field as it dictates the trajectories of the fibres. We demonstrate that the number of fibres between bridging events follows an exponential probability distribution and is mostly concentration independent as bridging depends on the probabilities of individual fibres coming from impermissible regions.

The flocculation mechanisms are both functions of l/w and concentration. The IFF mechanism showed a dynamic of intermittent fibre aggregation and shedding over time, which likely arises from the interplay between the hydrodynamic forces and the fibre-fibre and fibre-wall interactions. We show that time intervals between flocculation events follow an exponential probability distribution which is concentration dependent. Moreover, the average time interval between flocculation events is inversely proportional to the square-root of the suspension concentration. Flocculation mechanisms are more likely to result in permanent plugging when the average time interval between events is about half of the total flocculation residence time. Finally, we demonstrate that, unlike isotropic particles, fibres display a wider range of jamming mechanisms with different dynamics that warrant further investigation.

DIAGNOSING THE STATE OF THE BATTERY SLURRIES USING A MACHINE LEARNING TECHNIQUE

Seunghoon Kang, Howon Jin, Chan Hyeok Ahn and Kyung Hyun Ahn

Seoul National University, Seoul, Republic of Korea

ABSTRACT

Battery slurries have attracted intensive attention as the battery industry has grown rapidly due to the increasing demand in transportation, and energy storage systems. Rheologists have been trying to characterize these slurries because battery performance (capacity, efficiency), safety and lifespan depend not only on the slurry composition but also on its microstructure. However, the characterization is difficult as the internal structure constantly changes during the manufacturing process such as mixing, storage, transport, coating, and drying. Therefore, periodic sampling and measuring rheological properties are required through the whole processes to successfully control the battery production, which can be time-consuming and labor-intensive.

In this study, we propose a new method to classify different battery slurries using machine learning techniques rather than fully characterizing the slurries. We first built a closed pipe system and circulated a graphite based anode slurry in the system. Pressure and flow rate signals were collected from the sensors. Classification was carried out for each of the two groups. One group was established by circulating a single slurry sample for 7 days. The other was established by changing the content of carboxylmethyl cellulose (CMC), which acts as the binder and dispersant in the slurry. We used a machine learning technique called echo state network (ESN) to train the fluctuating patterns of different classes of sensor signals. We found that the slurries can be classified with these signals and the proposed method is expected to be used to optimize battery production. We proved the applicability of this method with battery slurries. However, this method is expected to be further applicable for other fluids, such as polymer melts, suspensions, emulsions, etc.

Rheology and Drag Reduction and Engineering Applications of Novel Oil-phase Suspended Polyacrylamide Slicker water Fracturing Fluids

LU Yongjun[1], LiYang[1], FANG Bo[2], XU Ke[1], GAO Hang[2],TIAN Zhenrui[2], YU Luyao[2],Li Kejing[2]

1.China petroleum exploration and development research institute, Beijing, 100083, China;

2. Shanghai Key Laboratory of Multiphase Materials Chemical Engineering, Lab of Chemical Engineering Rheology, East China University of Science and Technology, Shanghai, 200237, China.

Oil and gas are important strategic resources, industrial "blood" and energy chemical materials of national economy. Fracturing of deep oil and gas reservoirs is an important industrial measure and technological means to increase oil and gas storage and production. In this paper, a new oil-phase suspended polymeric drag reducing agent with high solid content (50wt% HPAM) for shale oil and gas fracturing has been developed. The optimal preparation conditions were determined as follows: 50-55wt% polyacrylamide powder + 30-40wt% mineral oil + 2-3wt% organic bentonite + 3-4wt% AEO_3 and OP compounding emulsifier + 3-5wt% D18dispersant.

The rheology and drag reduction performance of the optimized oil-phase suspended polymer solution were evaluated. The results showed that, in the experimental concentration range (0.01-0.08wt%), the viscosity could be regulated in the range of 1.8-6.8mPa.s,which could meet different fracturing construction requirements. The flow curves could be described by Power's law as shown in Fig.1. The drag reduction rate increased with the decreases of solution concentration, and the maximum drag reduction rate was 72%, with good drag reduction effect, as shown in Fig.2.

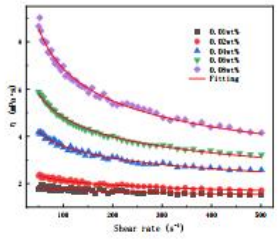

Fig.1 Power-law model fitting curves of suspension system slick-water of different concentrations

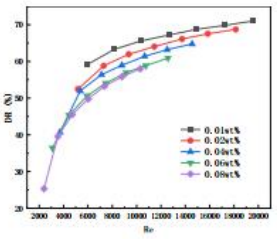

Fig.2 Drag reduction percentage of suspension slick-water of different concentrations vary with generalized Reynolds number

The intrinsic correlation between rheology and drag reduction performance was also

investigated, and the equation of frictional resistance coefficient of oil-phase suspension polymer solution and the novel empirical relationship between frictional resistance coefficient and generalized Reynolds number (Re) were established as Eq.1 to facilitate the field application of this system.

$$f^{-0.5} = \left(\frac{4}{n^{0.75}} + \xi_1\right)\lg\left(Ref^{1-\frac{n}{2}}\right) - \frac{0.4}{n^{1.2}} - \xi_2 \qquad \text{Eq.1}$$

Where, f is Fanning friction coefficient, Re is Generalized Reynolds number, n is the parameter for Power's Law model, ξ_1 and ξ_2 are modified parameters related to concentration of polymer slick waters.

The Linear fits of suspension slick-water of different concentrations of $f^{-0.5}$ versus $\lg\left(Ref^{1-\frac{n}{2}}\right)$ and parameters of ξ_1 and ξ_2 were shown in Fig.3 and Table 1 respectively. The linear relationship coefficient is near 1.0.

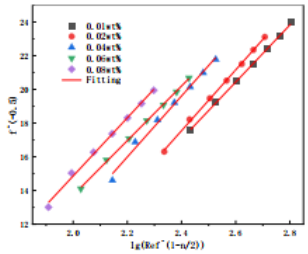

Fig. 3 Linear fits of suspension slick-water of different concentrations of $f^{-0.5}$ versus $\lg\left(Ref^{1-\frac{n}{2}}\right)$

Table 1 Parameters linear fits of suspension slick-water of different concentrations of $f^{-0.5}$ versus $\lg\left(Ref^{1-\frac{n}{2}}\right)$

Concentration (wt%)	K (mPa·s^n)	n	$\frac{4}{n^{0.75}} + \xi_1$	ξ_1	$\frac{0.4}{n^{1.2}} + \xi_2$	ξ_2	R
0.01	2.348	0.9224	16.94	12.69	23.61	23.17	0.9987
0.02	4.013	0.8628	18.05	13.58	25.78	25.30	0.9991
0.04	10.04	0.7768	18.08	13.25	23.79	23.25	0.9908
0.06	16.78	0.7288	16.20	11.13	18.69	18.11	0.9992
0.08	29.90	0.6806	17.27	11.93	19.69	19.06	0.9951

Optimized the new oil-phase suspension polymer drag reducing agent's medium process successfully completed the production in scale. The fracturing fluid has excellent rheological

properties, and has been successfully applied in the fracturing scale of shale oil Wells in Xinjiang and shale gas in Sichuan oilfield, with low friction, good drag reduction effect and good sand carrying capacity. The average fluid volume per well exceeding 35,000 m^3, fracturing pump rate reaching 18m^3/min, proppant concentration exceeding 200Kg/m^3, and fracturing stimulation period exceeding 230 days. The cumulative oil production per shale oil well exceeded 2,070 tons, and the cumulative production per shale gas well exceeded 25 million cubic meters.

Keywords : Novel Oil-phase suspended polymer fracturing fluid, Drag reduction, Modified relationship between Fanning friction coefficient and generalized Reynolds number, Rheology, Shale oil and gas fracturing.

Funding information:

This work was financially supported by the National Science and Technology Major Project of China(No. 2017ZX05023003), "Synthesis and Characterization of Thickener for High Temperature Clean Fracturing Fluid", and the Advanced Research Program of Research Institute of Exploration and Development, CNPC (No. 2020B-4120) "Research on Ultra-high Temperature Cleaning Fracturing Fluid and Adhesive Functional Slick Water".

Rheology and Self-Assembly of Carboxylated Cellulose Nanocrystals

Madeleine Hallman[1], Behzad Zakani[1,2], Dana Grecov[2], Emily Cranston[1,3,4]

[1]Department of Chemical and Biological Engineering, University of British Columbia, Vancouver, British Columbia
[2]Department of Mechanical Engineering, University of British Columbia, Vancouver, British Columbia
[3]Department of Wood Science, University of British Columbia, Vancouver, British Columbia
[4]UBC Bioproducts Institute, 2385 East Mall, Vancouver, British Columbia

ABSTRACT

The demand for biobased materials is ever increasing and one such material are cellulose nanocrystals (CNCs). CNCs are the crystalline regions of cellulose polymers which have had the amorphous regions chemically cleaved, some methods include acid hydrolysis or oxidation. The remaining nanoparticles have charged acid groups on the surface which allow them to remain suspended in water. They are useful in a variety of applications as emulsifiers, flow modifiers, etc. To understand the extent in which CNCs can be used, a thorough understanding of self-assembly and flow behaviour is required. The acid hydrolysis of cellulose using high concentration sulfuric acid is a common way to produce sulfated CNCs, the rheological properties of which have been well explored in published works[1,2,3]. However, the carboxylated cellulose nano crystals utilized in this study are produced commercially by Anomera, through oxidation using hydrogen peroxide. The only by-product of this process is water, this procedure is has much fewer harmful by products than the more common acid hydrolysis. However, the rheological properties of carboxylated CNCs have not been explored. In this work the viscosity and viscoelastic properties of carboxylated cellulose nanocrystals are examined to determine if there are major behavioural differences caused by the acid group on the surface. In suspension carboxylated CNCs exhibit self-assembly behaviour above a critical concentration where they orient themselves into chiral nematic structures called tactoids. As the concentration continues to increase the tactoids grow and begin to coalesce until they separate to form a liquid crystalline phase. The critical concentration is determined through the examination of phase separation at increasing concentrations. The onset of tactoid formation and tactoid evolution in reference to concentration is examined using polarized optical microscopy. A visible progression of tactoid size and coalescence is observed starting just above the determined critical concentration. This self-assembly also has an impact on rheology. At low concentrations the viscosity profile demonstrates shear thinning flow. As the concentration increases the overall viscosity of the suspensions increases and shear thinning behaviour intensifies. Once a significant amount of the suspension has phase separated the suspensions start to demonstrate “three-region” flow behaviour. Three-region flow is characterized by three distinct flow behaviours along a range of shear rates. Region one is at low shear rates where flow is shear thinning. Region two occurs as shear rate increases and the interactions between particles in the liquid crystalline phase

break apart causing a hitch in the viscosity profile where the flow behaviour becomes more Newtonian. Region three occurs once interactions between particles have completely broken and the particles have aligned in the direction of shear, the flow behaviour returns to shear thinning at high shear rates. Interestingly, the onset of three-region flow behaviour does not correspond perfectly with the critical concentration so the presence of a few tactoids is not enough to alter the flow behaviour and a larger portion needs phase separated for the behaviour to change. This behaviour is in line with the literature focused on sulfated CNCs, where three-region flow is also visible in concentrations where phase separation occurs[1,2,3]. At even high concentrations kinetic arrest occurs which results in the CNCs showing purely shear thinning behaviour. Self-assembly is largely dependent on the surface charge of the CNCs. This work demonstrates that an increasing surface charge decreases interactions between particles which is evident in the overall lower viscosity at the same concentrations and the onset of phase separation, and by extension three-region flow behaviour, occurring at higher concentrations.

ACKNOWLEDGEMENTS

I would like to acknowledge the continued support of Anomera through providing material and insights. I would also like to acknowledge Behzad Zakani and Dana Grecov for their guidance in my work.

REFERENCES

1. Shafeiei-Sabet, Sadaf, Wadood Y. Hamad, and Savvas G. Hatzikiriakos. "Influence of degree of sulfation on the rheology of cellulose nanocrystal suspensions." Rheologica Acta 52 (2013): 741-751.
2. Shafiei-Sabet, Sadaf, Wadood Y. Hamad, and Savvas G. Hatzikiriakos. "Rheology of nanocrystalline cellulose aqueous suspensions." Langmuir 28.49 (2012): 17124-17133.
3. Wu, Qiang, et al. "Rheological behavior of cellulose nanocrystal suspension: Influence of concentration and aspect ratio." Journal of Applied Polymer Science 131.15 (2014).

IMPACT OF EXTENT OF DIGESTION ON THE SHEAR RHEOLOGICAL BEHAVIOUR OF ANAEROBIC DIGESTED SLUDGE

Tanmoy Das[1], Shane P. Usher[2], Damien J. Batstone[3], Maazuza Othman[1], Anthony D. Stickland[2], Nicky Eshtiaghi[1]

[1]RMIT University, Melbourne, Victoria, Australia
[2]The University of Melbourne, Melbourne, Victoria, Australia
[3]The University of Queensland, St. Lucia, Queensland, Australia

ABSTRACT

Anaerobic digestion of sewage sludge is widely used in wastewater treatment facilities to produce biogas and reduce solids disposal[1,2]. Although well-mixed digester configuration is the most common, technologies such as covered anaerobic lagoons (CALs), biofilm or plug flow reactors are also used[2]. To maintain design hydraulic retention time (HRT) and consistent temperatures, microbes and solids distribution, effective mixing of the digester content is necessary during anaerobic digestion[3]. Mixing is energy intensive and dependent on the shear rheological properties especially viscosity[4,5], which is non-Newtonian for anaerobic digested sludge[6,7]. Hence, the shear rheological behaviour of the digested sludge is critical for effective heat and mass transfer during anaerobic digestion. The evolution of sludge rheology has been studied widely and it has been observed that the shear yield stress and viscosity decrease (improves) through the anaerobic digestion process[8,9]. This can be attributed to the simultaneous impact of the reduction in solids concentration due to the degradation of organic matter and changes to the microstructure due to digestion. The degree of degradation is expressed as the volatile solids destruction (VSD). There is a need for systematic and comprehensive characterization of shear rheological properties across a wide range of solids volume fractions and VSD to quantitatively differentiate the impacts of digestion and solids concentration, which is currently unavailable in existing literature. The evolution of shear rheological properties in anaerobic digestion reflects the complex changes in the sludge microstructure as organic matter is degraded and microbial colonies exude extracellular polymeric substances (EPS)[10,11]. These EPS networks have been reported as responsible for higher viscosity of the digested sludge[10], indicating the presence of a strong correlation for the shear rheological properties of anaerobic digested sludge as a function of VSD, which has not yet been rigorously developed. In addition, most of the existing studies on the shear rheological behaviour have been conducted in the mesophilic temperature range (37°C)[9,12]. Efficient digestion of organic matter is influenced by the operating temperature[13,14]. Some anaerobic digestion processes such as anaerobic lagoons are unheated systems where there is a significant seasonal variation in operating temperature typically in the psychrophilic temperature range

(15-25°C) which has lower VSD than mesophilic digestion[15,16]. Hence, understanding the shear rheological behaviour in these psychrophilic conditions can have potential application in the modelling and optimization of unheated anaerobic digestion systems.

In this study, the simultaneous impact of VSD and solids concentration on the shear rheological behaviour of anaerobic digested sludge was investigated in the psychrophilic temperature range. To obtain a wide range of VSD (42% to 70%), two continuous digesters were operated at different combinations of digestion temperatures (15°C and 25°C) and HRT (16, 24 and 32-d). Shear rheological measurements (generating experimental rheograms) were conducted for digested sludge samples collected at each set of operating condition and corresponding VSD at varying solids concentrations. The Herschel-Bulkley (HB) model parameters, shear yield stress and consistency, for sludge samples at different VSDs were fitted as continuous functions of the solids volume fraction using power law and exponential correlations. The impact of key physicochemical and operational factors (volatile solids fraction, temperature, HRT and VSD) was analysed on each fitting parameter of the power and exponential correlations via linear modelling. In general, VSD had a strong impact on all parameters and no other operating parameters had significant impact compared to VSD. This implied that the proportion of volatile solids that had been consumed plays significant role on shear rheology rather than the total amount of volatile solids of sludge. This observation further supports the hypothesis that the EPS which is a product of digestion drive rheological changes. The power law and exponential fitting parameters for shear yield stress and consistency and flow behaviour index were correlated as continuous functions of VSD. The correlations for shear rheological properties as functions of solids volume fraction and VSD can be used to predict the viscosity of digested sludge for any given combination(s) of solids volume fraction and VSD. This facilitates designing the mixing systems of the digesters as non-Newtonian viscosity model for digester content is a critical input for mixing systems design.

To demonstrate the impact of VSD on shear rheology independent of the solids volume fraction, the viscosities of digested sludge samples were calculated at four different solids volume fractions using developed models at a shear rate of 10 s^{-1}, which approximates the average shear rate of 6.8 s^{-1} in industrial digesters[17]. The viscosity of the digested sludge increased with the increase of VSD at the same solids concentration, which might reflect the microstructural changes in the EPS network.

Analysis of a hypothetical digester was conducted to understand the combined impact of solids volume fraction and VSD on the viscosity. The digester was fed with a sludge with 80% volatile solids and the feed solids concentration was varied 5%, 6% and 7%. Outlet concentrations were determined for these feed concentrations at different VSD values (40%-90%). The viscosity of digested sludge at shear rate of 10 s^{-1} were calculated to determine the optimum viscosity level where the increase in viscosity caused by VSD is balanced by the decrease in viscosity caused by lower solids concentration due to digestion. There was an asymmetric shallow optimum generally in the 65%-80% VSD range depending on feed concentration. In general, it is better to achieve a higher VSD to achieve optimal viscosities, with the increase in viscosity caused by more EPS than compensated for by the decreased effluent solids except at very high VSDs.

ACKNOWLEDGEMENTS

Tanmoy Das acknowledges the receipt of research scholarship from RMIT University and ARC linkage project (LP170100257) funded by Australian Government through Australian Research Council.

REFERENCES

(1) Mata-Alvarez, J.; Macé, S.; Llabrés, P. Anaerobic digestion of organic solid wastes. An overview of research achievements and perspectives. *Bioresource Technology* **2000**, *74* (1), 3-16. DOI: https://doi.org/10.1016/S0960-8524(00)00023-7.

(2) Mao, C.; Feng, Y.; Wang, X.; Ren, G. Review on research achievements of biogas from anaerobic digestion. *Renewable and Sustainable Energy Reviews* **2015**, *45*, 540-555. DOI: https://doi.org/10.1016/j.rser.2015.02.032.

(3) McLeod, J.; Othman, M.; Parthasarathy, R. Process Intensification Of Anaerobic Digestion: Influence On Mixing And Process Performance. *Bioresource Technology* **2019**, *274*, 533-540. DOI: 10.1016/j.biortech.2018.12.011.

(4) Singh, B.; Szamosi, Z.; Siménfalvi, Z. State of the art on mixing in an anaerobic digester: A review. *Renewable Energy* **2019**, *141*, 922-936. DOI: https://doi.org/10.1016/j.renene.2019.04.072.

(5) Battista, F.; Fino, D.; Mancini, G.; Ruggeri, B. Mixing in digesters used to treat high viscosity substrates: The case of olive oil production wastes. *Journal of Environmental Chemical Engineering* **2016**, *4* (1), 915-923. DOI: https://doi.org/10.1016/j.jece.2015.12.032.

(6) Sadino-Riquelme, C.; Hayes, R. E.; Jeison, D.; Donoso-Bravo, A. Computational fluid dynamic (CFD) modelling in anaerobic digestion: General application and recent advances. *Critical Reviews in Environmental Science and Technology* **2018**, *48* (1), 39-76. DOI: 10.1080/10643389.2018.1440853.

(7) Wei, P.; Tan, Q.; Uijttewaal, W.; van Lier, J. B.; de Kreuk, M. Experimental and mathematical characterisation of the rheological instability of concentrated waste activated sludge subject to anaerobic digestion. *Chemical Engineering Journal* **2018**, *349*, 318-326. DOI: https://doi.org/10.1016/j.cej.2018.04.108.

(8) Miryahyaei, S.; Olinga, K.; Ayub, M. S.; Jayaratna, S. S.; Othman, M.; Eshtiaghi, N. Rheological measurements as indicators for hydrolysis rate, organic matter removal, and dewaterability of digestate in anaerobic digesters. *Journal of Environmental Chemical Engineering* **2020**, *8* (4), 103970. DOI: https://doi.org/10.1016/j.jece.2020.103970.

(9) Miryahyaei, S.; Olinga, K.; Abdul Muthalib, F. A.; Das, T.; Ab Aziz, M. S.; Othman, M.; Baudez, J. C.; Batstone, D.; Eshtiaghi, N. Impact of rheological properties of substrate on anaerobic digestion and digestate dewaterability: New insights through rheological and physico-chemical interaction. *Water Res* **2019**, *150*, 56-67. DOI: 10.1016/j.watres.2018.11.049.

(10) Li, X. Y.; Yang, S. F. Influence of loosely bound extracellular polymeric substances (EPS) on the flocculation, sedimentation and dewaterability of activated sludge. *Water Res* **2007**, *41* (5), 1022-1030. DOI: 10.1016/j.watres.2006.06.037.

(11) Wu, B.; Dai, X.; Chai, X. Critical review on dewatering of sewage sludge: Influential mechanism, conditioning technologies and implications to sludge re-utilizations. *Water Research* **2020**, *180*. DOI: 10.1016/j.watres.2020.115912.

(12) Cao, X.; Jiang, Z.; Cui, W.; Wang, Y.; Yang, P. Rheological Properties of Municipal Sewage Sludge: Dependency on Solid Concentration and Temperature. *Procedia Environmental Sciences* **2016**, *31*, 113-121. DOI: https://doi.org/10.1016/j.proenv.2016.02.016.

(13) Vanwonterghem, I.; Jensen, P. D.; Rabaey, K.; Tyson, G. W. Temperature and solids retention time control microbial population dynamics and volatile fatty acid production in replicated anaerobic digesters. *Scientific Reports* **2015**, *5* (1), 8496. DOI: 10.1038/srep08496.

(14) De Vrieze, J.; Saunders, A. M.; He, Y.; Fang, J.; Nielsen, P. H.; Verstraete, W.; Boon, N. Ammonia and temperature determine potential clustering in the anaerobic digestion microbiome. *Water Res* **2015**, *75*, 312-323. DOI: 10.1016/j.watres.2015.02.025 From NLM.

(15) Bowen, E. J.; Dolfing, J.; Davenport, R. J.; Read, F. L.; Curtis, T. P. Low-temperature limitation of bioreactor sludge in anaerobic treatment of domestic wastewater. *Water Science and Technology* **2013**, *69* (5), 1004-1013. DOI: 10.2166/wst.2013.821 (accessed 7/5/2022).

(16) Lin, Q.; He, G.; Rui, J.; Fang, X.; Tao, Y.; Li, J.; Li, X. Microorganism-regulated mechanisms of temperature effects on the performance of anaerobic digestion. *Microb Cell Fact* **2016**, *15*, 96. DOI: 10.1186/s12934-016-0491-x From NLM.
(17) Singh, B.; Szamosi, Z.; Siménfalvi, Z. Impact of mixing intensity and duration on biogas production in an anaerobic digester: a review. *Critical Reviews in Biotechnology* **2020**, *40* (4), 508-521. DOI: 10.1080/07388551.2020.1731413.

MEASURING TRANSIENT EXTENSIONAL VISCOSITY USING FILAMENT STRETCHING ON AN ARES G2 RHEOMETER

Tianhong (Terri) Chen [1]; Chris W Macosko [2]

[1] TA Instruments – Waters LLC, 159 Lukens Drive, New Castle, DE 19720
[2] Department of Chemical Engineering and Materials Science, University of Minnesota, Minneapolis, MN 55455

ABSTRACT

Many polymer processing flows involve extensional flow, which makes the extensional viscosity measurement a valuable testing method. Currently, the most commonly used extensional viscosity measurement technique on rotational rheometers is using the counter-rotating drums (CRD), which is available via SER, EVA or EVF fixtures. In a CRD test, the sample is placed horizontally and attached to the surface of 2 drums with metal clips, then stretched by rotation of the drums which creates a constant Hencky strain rate. This type of measurement requires solid-like samples for loading and a relatively high viscosity after melting to prevent sagging during the course of testing. In this work, we program the axial motion of the ARES G2 to increase exponentially. Samples are confined between parallel plates and a filament is formed by the exponential stretching. The normal force transducer measures the transient extensional behavior of selected materials. In addition to higher viscosity molten polymers, this method allows extensional viscosity measurements on lower viscosity polymer melts and polymer solutions. By selecting the appropriate filament aspect ratio, we show that the measurements obtained by this method are in good agreement with the measurements from CRD test methods.

Deformational Vorticity in Constitutive Equations: The Co-Rigid Rotational Maxwell Model

Cody Wade Mischel

University of Illinois - Chicago, Chicago, USA

ABSTRACT

The presented work incorporates an objective vorticity (kinematic variable) into a novel constitutive equation - the co-*rigid rotational Maxwell model*. This model is applied to large amplitude oscillatory shear test conditions and compared to experimental data where it showed to have an improvement over the corotational Maxwell model. Finally, this research establishes a foundation for further evaluation, analysis, and development of constitutive equations that use this objective vorticity for better characterization of non-Newtonian fluids.

INTRODUCTION

The vorticity tensor is widely known to capture a fluid's rotational properties and is thought to hold valuable kinematic information about the fluid. However, this information has largely gone unused in constitutive equations due to the vorticity tensor's failure to adhere to the material objectivity requirements. Attempts have been made to incorporate vorticity into constitutive equations. [1–3, 5–8, 11, 12] In prior work proposed by Wedgewood [9, 10], a vorticity decomposition was introduced that was able to separate the vorticity tensor $\boldsymbol{\omega}$ into a rigid-body rotational, non-objective part $\boldsymbol{\omega}_R$ and a deformational, objective part $\boldsymbol{\omega}_D$. However, their decomposition was not utilized within constitutive equations. In this paper, we build upon that work and present a mathematical formalism for incorporating the objective, deformational vorticity into a proposed constitutive equation model for large amplitude oscillatory shear (LAOS) flow.

METHODOLOGY

In this work, the fluid is assumed to be incompressible and homogeneous with unsteady, homogeneous shear flow fluid kinematics characterized as $v_x = \dot{\gamma}(t)y$, $v_y = 0$, and $v_z = 0$. The focus of this research is specifically on the *LAOS* experimental design and conditions.

Taking inspiration from the corotational Maxwell model (Eq. 1), which includes a Jaumann derivative that removes all the vorticity through a corotating reference frame, the co-rigid rotational Maxwell model is proposed as seen in Eq. 2.

$$\boldsymbol{\tau} + \lambda \frac{\mathscr{D}\boldsymbol{\tau}}{\mathscr{D}t} = -\eta_0 \dot{\boldsymbol{\gamma}} \tag{1}$$

$$\boldsymbol{\tau} + \lambda \left[\frac{D}{Dt}\boldsymbol{\tau} + \frac{1}{2}\{\boldsymbol{\omega}_R \cdot \boldsymbol{\tau} - \boldsymbol{\tau} \cdot \boldsymbol{\omega}_R\} + \frac{1}{2}\{\hat{\boldsymbol{\omega}}_D \cdot \boldsymbol{\tau} - \boldsymbol{\tau} \cdot \hat{\boldsymbol{\omega}}_D\} \right] = -\eta_0 \dot{\boldsymbol{\gamma}} \tag{2}$$

This model, however, removes only the *rigid-body vorticity* and allows the fluid particle to rotate with a portion of the deformational vorticity—the fluid's *observed deformational vorticity*—described as shown in Eq. 3, where a is the observed amplitude (magnitude) and b is the "lag" time (phase shift) response of the fluid particle. The range for a is from zero to one, where the particle rotates with none or all of the deformational vorticity, respectively. Parameter b ranges from zero to $\frac{\pi}{2}$, where it is in-phase or out-of-phase, respectively, of the shearing rate of strain. The corotational Maxwell model can be recovered when $a = 1$ and $b = 0$.

$$\hat{\omega}_D(t) = a\,\dot{\gamma}^0 \cos(t\,\omega - b) \tag{3}$$

An analytical solution was obtained using a perturbation method where the shear stress, the first normal stress, and the second normal stress are expanded as a power series in terms of strain-rate amplitude. Additionally, a numerical simulation of the LAOS co-rigid rotational Maxwell model was conducted using MATLAB R2022a. The dimensionless numbers used for the simulation were $De = 1.0$ and $We = 0.486$.

RESULTS AND DISCUSSION

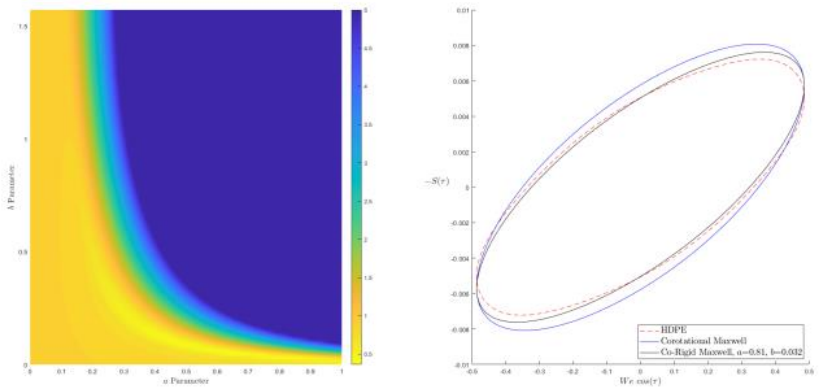

(a) (b)

Figure 1: (a) Average error between co-rigid rotational Maxwell model and HDPE data. (b) LAOS result comparison for co-rigid rotational Maxwell model (black), corotational Maxwell model (blue), and HDPE data (red).

The numerical MATLAB results for the co-rigid rotational Maxwell model were compared to experimental data for HDPE at 160 °C obtained by Giacomin [4]. **Fig. 1a** is a heatmap of the error between simulated and experimental results that span the entire range of a and b. The yellow color depicts the areas of lowest error, to which a global minimum is found to be located at $a = 0.81$ and

$b = 0.032$. A Lissajous curve, shown in **Fig. 1b**, compares the HDPE data, corotational Maxwell model, and the proposed co-rigid rotational Maxwell model at the optimum a and b values.

CONCLUSION

The co-rigid rotational Maxwell model is a simple quasi-linear differential model. As expected, it was not able to capture the HDPE data perfectly; however, it did improve the accuracy of the predicted shear stress. More notably, this research acts as a stepping stone and illustrates a working methodology to incorporate an objective vorticity into constitutive equations, as well as lays the foundation to analyze and evaluate future models against experimental data.

References

[1] ASTARITA, G. Objective and generally applicable criteria for flow classification. *Journal of Non-Newtonian Fluid Mechanics 6*, 1 (1979), 69–76.

[2] DROUOT, R., AND LUCIUS, M. Second-order approximation of the behavior law of fluids simple. Classical laws deduced from the introduction of a new tensor purpose. *Archives of Mechanics*, 2176 (1976), 189–198.

[3] GAO, Y., AND LIU, C. Rortex based velocity gradient tensor decomposition. *Physics of Fluids 31*, 1 (2019), 011704.

[4] GIACOMIN, A., BIRD, R., JOHNSON, L., AND MIX, A. Large-amplitude oscillatory shear flow from the corotational maxwell model. *Journal of Non-Newtonian Fluid Mechanics 166*, 19-20 (2011), 1081–1099.

[5] HUILGOL, R. R. On the Concept of the Deborah Number. *Transactions of the Society of Rheology 19*, 2 (1975), 297–306.

[6] LIU, J., GAO, Y., AND LIU, C. An objective version of the Rortex vector for vortex identification. *Physics of Fluids 31*, 6 (2019).

[7] SCHUNK, P. R., AND SCRIVEN, L. E. Constitutive equation for modeling mixed extension and shear in polymer solution processing. *Journal of Rheology 34*, 7 (1990), 1085–1119.

[8] SOUZA MENDES, P. R., PADMANABHAN, M., SCRIVEN, L. E., AND MACOSKO, C. W. Inelastic constitutive equations for complex flows. *Rheologica Acta 34*, 2 (1995), 209–214.

[9] WEDGEWOOD, L. E. An objective rotation tensor applied to non-Newtonian fluid mechanics. *Rheologica Acta 38*, 2 (1999), 91–99.

[10] WEDGEWOOD, L. E., AND GEURTS, K. R. A non-affine network model for polymer melts. *Rheologica Acta 34*, 2 (1995), 196–208.

[11] YAO, D. A non-Newtonian fluid model with an objective vorticity. *Journal of Non-Newtonian Fluid Mechanics 218* (2015), 99–105.

[12] ZHU, J.-Z. Vorticity and helicity decompositions and dynamics with real schur form of the velocity gradient. *Physics of Fluids 30*, 3 (2018), 031703.

DEVELOPMENT OF EXTENSIONAL RHEOMETER USING PARALLEL DISK RING

Yukihiro Mineyama[1], Manabu Kato[2] and Tsutomu Takahashi[3]

[1]National Institute of Technology, Tsuyama College, Advanced Mechanical and Control System Engineering Course, Tsuyama, Okayama, Japan
[2]National Institute of Technology, Tsuyama College, Tsuyama, Okayama, Japan
[3]Nagaoka University of Technology, Niigata, Japan

ABSTRACT

We developed an extensional rheometer to measure the planar elongational viscosity of low-viscous fluids. The rheometer uses two parallel disk rings to create a cylindrical film of the sample fluid, which is subjected to a planar elongational deformation. The position and thickness of the sample and the forces acting on the rings were measured during elongation. Elongation rate and elongation stress were evaluated from the experimental results. From these results, the planar elongational viscosity was calculated and it shows reasonable results.

BACKGROUND

Elongational viscosity affects formability in molding processes such as film molding and blow molding[1]. Therefore, understanding the rheology of polymeric materials is essential for improving the functionality and manufacturing efficiency of end products. Rotational rheometers are used to measure the rheology of complex fluids, including polymeric fluids. However, the rheological properties obtained in shear flow cannot be applied to extensional flow due to the uncertainty of the constitutive equations in complex fluids. Therefore, to accurately understand the flow field used in polymer forming, it is necessary to conduct rheological measurements in extensional flow. RFX (Rheometric Scientific) and CaBER (Thermo Scientific HAAKE) were the only available extensional rheometers capable of handling highly fluidized fluids and measuring uniaxial elongation viscosity. While both instruments are no longer available for sale, they still provide valuable data on the rheological properties of materials under elongation deformation. This study proposes a method for measuring the properties of planar elongational flow that uses parallel disk rings as a simple and direct extensional rheometer for highly flowing fluids.

EXPERIMENTAL APPARATUS AND TEST FLUIDS

Two-disc rings were used in the experiment. They have an inner diameter of 30 mm and an outer diameter of 40 mm. The ring was made of ABS resin and fabricated by a 3D printer.

CTAB/NaSal surfactant solution was used in the experiment, consisting of a viscoelastic fluid CTAB solution (0.10 mol/l) and NaSal (0.30 mol/l).

Fig. 1 shows a schematic diagram of the elongation force measurement. The upper disc ring is attached to the balance and the lower disc ring to the moving stage. A load cell (UL-2GR, rated capacity 19.61 mN, Minebea) is placed under the right end of the balance. **Fig 2** shows a schematic diagram of film thickness measurement. A sample is filled between two parallel disk-shaped rings to form a cylindrical film. A film thickness measuring instrument (CL-P015, standard measuring range ±1.3 mm, manufactured by Keyence) is set up to measure the thickness of this film.

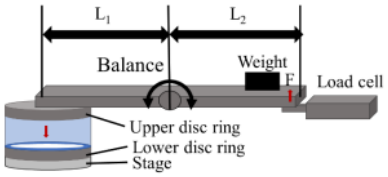

Figure 1: Schematic diagram of elongation force measurement

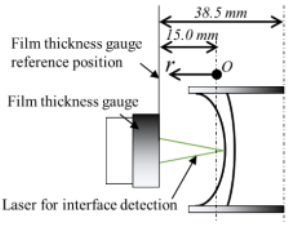

Figure 2: Schematic diagram of film thickness measurement

EXPERIMENTAL METHODS

As shown in **Fig. 1**, the test fluid is filled between the two disk rings at the left end of the balance; the initial gap between the two disk rings is 2.0 mm. The balance is balanced by placing a weight on the right arm of the balance. A cylindrical film is formed between the two rings by manually adjusting the balance and the stage up and down until the film thickness enters the measurement range. Subsequently, the film thickness is measured to ensure that it falls within the desired range, and the measurement process is halted upon confirmation. The measurement of film thickness and elongation force resumes concurrently, and the stage is incrementally lowered by approximately 1.00 mm every 10 seconds. The experiments were carried out at four distinct stage movement speeds:0.25, 0.50, 0.75 and 1.00 mm/s. Prior to stage movement, the balance in **Fig. 1** is tilted clockwise and a downward force (negative) is applied to the load cell. As the stage is subsequently lowered, an upward (positive) force acts on the load cell.

EXPERIMENTAL RESULTS

Fig. 3 shows the measurement results of elongation force F and film thickness. The stage was moved 9 times with a stage movement speed of 0.25 mm/s and a stage movement distance of 1.00 mm. Relaxation is observed when the stage is stopped. When the stage stops moving, the change in film thickness becomes small. The peak value of the elongation force and the film thickness both decrease with each repetition of the movement.

The elongation force, denoted as Fs, can be determined by calculating the difference between the force acting on the stage before movement and the force acting at the peak elongation. As shown in **Fig. 2**, the film thickness sensor measures the distance r between the position of the

film interface and the reference position. To determine the film thickness and outer diameter, the method involves measuring the position of the interface between the sample and the air (i.e., top surface of the film) relative to a reference point using a thickness gauge. Specifically, the film thickness is obtained by calculating the difference in position between the interface and the reference point, while the outer diameter is obtained from the position of the thickness sensor and the film interface. When calculating the cross-sectional area of the sample, the film thickness Δr is the average of the film thickness Δr_1 at the beginning of the stage movement and the film thickness Δr_2 at the point where the movement stopped. The sample cross-sectional area A is calculated using Eq. 1. The elongation speed $\dot{\varepsilon}$ is obtained from Eq. 2. Let Δr be the film thickness at a certain point during stage movement.

Fig. 4 shows $\Delta r/\Delta r_1$ as a function of time. To evaluate the elongation rate, we compared the experimental results with Eq. 2 and performed a curve fitting process. By fitting the experimental data to Eq. 2, we determined the constant in the equation as the elongation rate.

$$A = 2\pi * r_o * \Delta r \tag{1}$$

$$\frac{\Delta r}{\Delta r_1} = e^{-\dot{\varepsilon}t} \tag{2}$$

The elongational viscosity was determined by analyzing the data on film thickness and elongation force obtained during the first stage movement. The planar elongational viscosity was found to be in the range of 200 to 700 Pa·s, while the shear viscosity of the sample was approximately 200 Pa·s. Although CTAB/NaSal is a non-Newtonian fluid and therefore cannot be directly compared, the planar extensional viscosity measured here falls within a reasonable range of values reported in the literature. To further validate the proposed rheometer, additional measurements using different samples and molar concentration ratios are recommended.

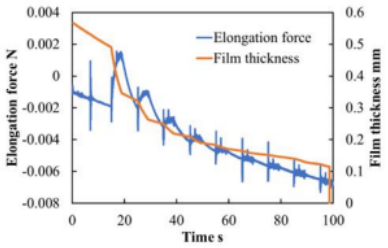

Figure 3: Measurement results of elongation force and film thickness

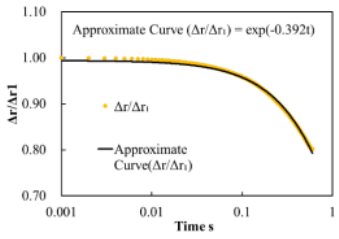

Figure 4: Determination of elongation rate

REFERENCES

1. Masubuchi Y. Polymer Elongation and Polymer Processing, Journal of Chemical Engineering of Japan, **82(4)**, 2018
2. Masuda T.; Takahashi M.; Ohno H.; Li L. A New Extensional Rheometer for Polymer Melts, Journal of the Society of Rheology Japan, **16(3)**, 111~116, 1988,

OPTIMIZATION OF THE DRAG-REDUCING EFFECT BY CONTROLLING THE PREPARATION CONDITIONS OF ADDITIVES

Takashi Saeki[1], Aya Kaide[1] and Shigetoshi Nagasaka[2]

[1]Yamaguchi University, Ube, Japan

[2]Shin Nippon Air Technologies Co., Ltd., Nagano, Japan

ABSTRACT

The drag-reducing (DR) effect by cationic surfactants has been applied to the water circulation system of general building air conditioning equipment as an energy-saving technology for fluid transportation. Water pipes are usually designed for average flow velocities of 1 to 1.5 m/s, and some cationic surfactants have a DR effect within this range. In recent years, the authors have been examining the application of the DR effect in geothermal heat utilization systems. In such systems, due to the heat extraction from the ground and the operating conditions of the heat pump, the average flow velocity in the heat extraction tube is approximately 0.5 m/s, so there is the problem that a sufficient DR effect cannot be obtained. Aqueous surfactant solutions that induce DR effects are known to exhibit a shear-induced state (SIS). However, the viscosity increase due to the SIS contributes to lowering the DR effect in the low flow velocity region (low Re number region). Furthermore, Zhang et al. state that a SIS is not a necessary element for the DR effect.[1] The purpose of this study was to obtain basic data for developing a DR agent that suppresses the expression of the SIS and can be used in a geothermal heat utilization system.

EXPERIMENTAL PROCEDURE

A mixture of cationic surfactant, oleyl-bishydroxyethyl-methyl-ammonium chloride ($C_{18}H_{35}N^{+}(CH_3)(C_2H_4OH)_2Cl^{-}$, Lipothoquad O/12 produced by Lion Corporation, Japan) and sodium salicylate (NaSal., $HOC_6H_4COO^{-}Na^{+}$) was used as the drag-reducing (DR) agent. The optimal mixing ratio of both is 1:1.5 by molar ratio from the viewpoint of achieving the high DR effect reported by Chou et al.,[2] and the present research was also based on this rate. The experimental apparatus used for evaluating drag reduction was a recirculation system (Fig 1). Different concentrations of the DR additive were mixed in a tank to prepare solutions. The fluid temperature was kept constant at 15℃ in consideration of the actual value of circulating water in ground thermal energy systems. The flow rate and pressure difference in a straight pipe 1.6 m long were measured with an electromagnetic flow meter and an electric differential

manometer, respectively. The Reynolds number was calculated using the properties of water. The friction factor, f, was calculated by the Funning equation. For convenient comparison of the drag reduction results between the water and test solutions, the DR rate, $DR\%$, was defined as

$$DR\% = \frac{f_W - f_{DR}}{f_W} \times 100, \qquad (1)$$

where f_w and f_{DR} are the friction factor of water and that of the solution, respectively; f_w was obtained using the Blasius equation.

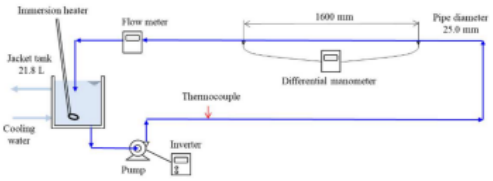

Figure 1: Experimental apparatus

RESULTS AND DISCUSSION

Figure 2 shows the relationship between $DR\%$ and the average flow velocity u. When the surfactant concentration was 500 mg/L (▲, the set concentration in a normal water pipe), the $DR\%$ at 0.5 m/s was only 7%. While the concentration was 200 mg/L (○), the DR% at the same u was 30%. When the concentration of surfactant was set at 500 mg/L, which is the set value for a normal building air-conditioning circulation system, the $DR\%$ was only 7% at u=0.5 m/s. When the concentration was increased to 200 mg/L, the $DR\%$ increased to 30%, but it is expected that it will not show a stable DR effect for a long period of time because it is so diluted.

Since it is necessary to add a corrosion inhibitor to the circulating water in actual fluid transportation, two corrosion inhibitors, A and B (c.i.-A and c.i.-B) were tested in the present study with a surfactant concentration of 500 mg/L. The addition of either corrosion inhibitor did not adversely affect DR; on the contrary, c.i.-B greatly increased DR% in the low-velocity region. C.i.-A is of the type that dissociates in water to form ions, while c.i.-B forms a complex.

Figure 3 shows the equilibrium flow properties when adding different concentrations of c.i.-B to the DR agent (a mixed aqueous solution of 500 mg/L Lipothoquad O/12 and 300 mg/L sodium salicylate). The higher the amount of c.i.-B added, the lower the viscosity of the aqueous solution, and the shear-induced state was exhibited only slightly in the high shear rate region. The addition of c.i.-B had some effect on the rod-like micelle structure formed by the surfactant and the counterion.

ACKNOWLEDGEMENTS

This work was supported by JST A-STEP Grant Number JPMJTM22E1.

REFERENCES

1. Zhang, H.; Wang, D.; Chen, H. Experimental study on the effects of shear induced structure in a drag-reducing surfactant solution flow. *Archive of Applied Mechanics*, **79**, 773-778, 2019. https://doi.org/10.1122/1.4826543.
2. Chou, L.-C.; Christensen, R. N.; Zakin, J. L. The influence of chemical composition of quaternary ammonium salt cationic surfactants on their drag reducing effectiveness, in Drag Reduction in Fluid Flows, Sellin, R. H. J., and Moses, J. T., Eds., Ellis Horwood, Chichester, UK, 141-148, 1989.

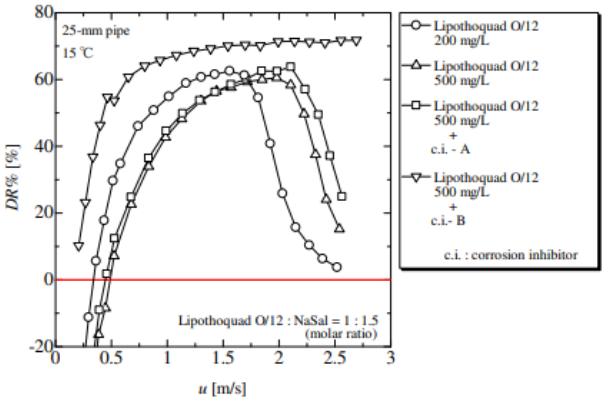

Figure 2: Effect of the addition conditions of the DR agent and corrosion inhibitors on the DR effect

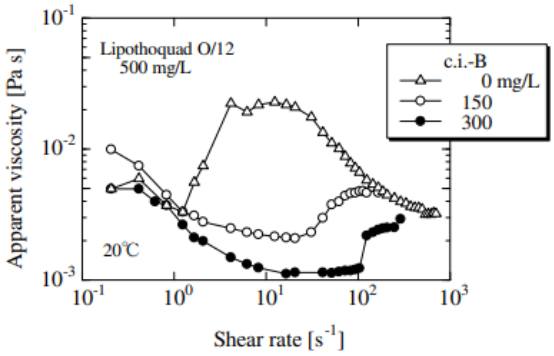

Figure 3: Equilibrium flow properties of the DR additive with different concentrations of c.i.-B measured by a cone-plate rheometer (IR-200).

EFFECTS OF RELAXATION TIME OF POLYMER SOLUTIONS ON THE SPATIO-TEMPORAL FLUCTUATION IN A TWO-DIMENSIONAL FLOW

Kengo Fukushima[1], Ruri Hidema[1] and Hiroshi Suzuki[1]

[1]Kobe University, Kobe, Japan

ABSTRACT

Addition of a small amount of polymer or micelle-forming surfactants to a fluid reduces frictional drag and delays the transition to turbulent flow. Main feature of this phenomena is that the extensional flow induces extension of polymers, and the extended polymers affect coherent structure of the fluids such as vortices in the flow. Therefore, we have been working on flowing soap films as a two-dimensional (2D) turbulent flow where the extensional stress mainly affects the flow to observe the effects of extensional rheological properties of the fluids on the vortex shedding in the 2D flow[1,2]. We have found the deformation of vortices, and the modification of energy transfer in polymer doped 2D flow[1]. Furthermore, the deformation of vortices may be caused as a result of elastic instability in the flow. In this study, we calculated spatio-temporal correlation of velocity fluctuations and the turbulent energy in 2D turbulent flow. The addition of polymers makes differences between the temporal correlation and the spatial correlation converted by the mean local velocities in the streamwise direction. The delay between the temporal correlation function and the spatial correlation function seemed to be affected by the relaxation time of the solution.

ACKNOWLEDGEMENTS

This study was supported in part by the Japan Science and Technology Agency (JST) FOREST Program (Grant Number JPMJFR203O, Japan).

REFERENCES

1. Hidema, R.; Fukushima, K.; Yoshida, R.; Suzuki, H. Vortex deformation and turbulent energy of polymer solution in a two-dimensional turbulent flow. *Journal of Non-Newtonian Fluid Mechanics*, **285**, 104385, 2020.
2. Fukushima, K.; Kishi, H.; Suzuki, H.; Hidema, R. Modification of turbulence caused by cationic surfactant wormlike micellar structures in two-dimensional turbulent flow. *Journal of Fluid Mechanics*, **933**, A9, 2022.

RHEOLOGICAL METHOD TO INVESTIGATE PSEUDOLAYER COMPRESSION ELASTIC CONSTANT AND THE DYNAMICS OF THE TWIST-BEND NEMATIC LIQUID CRYSTAL

Praveen Kumar M.[1], Karcz. J.[2] , Kula. P.[2] and Dhara. S.[1]

[1]School of Physics, University of Hyderabad, Telangana, India
[2] Institute of Chemistry, Military University of Technology, Warsaw, Poland

ABSTRACT

Liquid crystals are intermediate state of matter between completely ordered crystals and amorphous liquids. They exhibit both the liquid like and the solid like properties. The common liquid crystal phases are nematic (N), smectic-A (SmA) and cholesteric (N*) etc. Recently, some new nematic LCs with a nano and micro scale modulation of director such as twist-bend nematic (NTB) and splay nematic (NS) have been discovered. We study the flow behaviour of a twist-bend nematic (NTB) liquid crystal. It shows three distinct shear stress (σ) responses in a certain range of temperatures and shear rates ($\dot{\gamma}$). In Region-I, $\sigma \sim \sqrt{\dot{\gamma}}$ [1], in region-II, the stress shows a plateau, characterised by a power law, $\sigma \sim \dot{\gamma}^{\alpha}$, where $\alpha \sim 0.1$- 0.4 and in region-III, , $\sigma \sim \dot{\gamma}$. With increasing shear rate, σ changes continuously from region-I to II, whereas it changes discontinuously with a hysteresis from region-II to III. In the plateau (region-II), we observe a dynamic stress fluctuations, exhibiting regular, periodic and quasiperiodic oscillations under the application of steady shear. The observed spatiotemporal dynamics in our experiments are close to those were predicted theoretically in sheared nematogenic fluids [2].

We study the rheological properties of NTB phase and compare the results with those of an ordinary SmA phase**.** Our results show that the structural rheology of NTB phase is strikingly similar to that of the ordinary smectic LCs. Analysing the shear response and adapting a simplied physical model for rheology of defect mediated lamellar systems we measure the pseudolayer compression elastic constant (B_{eff}) of NTB phase from the measurements of dynamic modulus G*(ω) [3, 4] **Fig(1(b)).** We find that B_{eff} of the NTB phase increases with decreasing temperature as shown in **(Fig.1(c)),** and it follows a temperature dependence, $B_{eff} \sim (T_{TB} - T)^2$ as predicted by the recent coarse-grained elastic theory [5]. Thus our results provide a valuable test of the validity of the proposed theoretical models.This experiment also

offer new perspectives on NTB LCs and open unexplored aspects of the rheology of nematic LCs with nanoscale modulation of director.

.

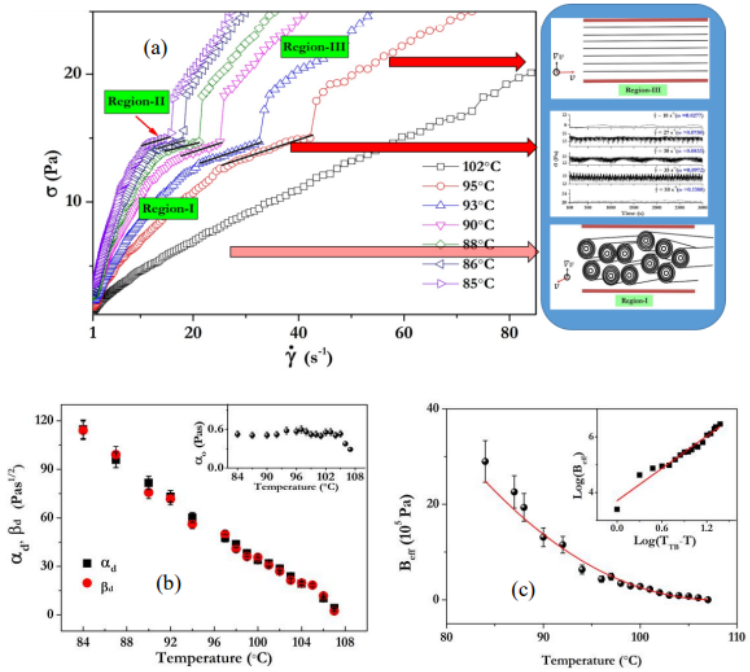

Figure 1: (a)The flow curve of NTB phase shows three distant regions (Region-1, Region-II, and region-III) and their corresponding schematic picture of layer alignment and dynamics (b) frequency dependent shear modulus is fitted to a simple theoretical model where the fitting parameters (α_d and β_d) with temperature inset α_0 represents viscosity with respect to temperature (c) Temperature dependence of B_{eff} inset the linear fit of of temperature dependence which agrees well with the coarse grain model of Dozov and Mayer [5] .

ACKNOWLEDGEMENTS

S.D. acknowledges financial support from SERB (Ref. No. CRG/2019/000425) and DST-FIST-II, School of Physics. P.K. acknowledges financial support from MUT UGB 22-760. P.K. acknowledges UGC-CSIR for a fellowship

REFERENCES

1. *Panizza. P, Archambault. P and Roux. D, Effects of Shear on the Smectic A Phase of Thermotropic Liquid Crystals, J. Phys. II France, **5**, 303(1995).*
2. *Chakrabarthi. B, Das. M, Dasgupta. C, Ramaswamy. S and Sood. A. K., Phys. Rev. Lett., 92, 055501 (2004)..*
3. *Kawasaki. K and Anuki, A Dynamics and rheology of diblock copolymers quenched into microphase-separated states Phys. Rev. A 42, 3664 (1990).*
4. *Ramos L, Zapotocky M, Lubensky T. C and Weitz D. A, Rheology of defect networks in cholesteric liquid crystals, Phys. Rev. E 66, 031711-1 (2002).*
5. *Meyer C and Dozov I, Local distortion energy and coarse-grained elasticity of the twist-bend nematic phase Soft Matter 12, 574 (2016)*

PREDICTICTING THE RATE OF CEMENT PLUG FAILURE

Scott Charabin[1], Ian Frigarrd [1,2]

[1] Department of Mechanical Engineering, University of British Columbia, Vancouver, BC, Canada
scott.charabin@ubc.ca
[2] Department of Mathematics, University of British Columbia, Vancouver, BC, Canada

ABSTRACT

Plugging is an essential part of decommissioning wells. Often cement plugs are set at various depths to isolate critical zones of interest. These zones can include production zones, aquifers and surfaces, ensuring the wellbore is isolated correctly. The cement slurry is either pumped on top of a mechanical support (retainer, bridge plug), or is placed directly over the wellbore fluid. The cement plug should hydrate and form an impenetrable barrier between the subsurface and the surface. Since the cement slurry (with a yield stress) is typically denser than the fluid below, there is a tendency to destabilize mechanically. Proper selection of cement properties, namely the yield stress, is therefore essential to the success of the abandonment process. If the cement does not set correctly, the well integrity is compromised and another cement plug will need to be placed.

The success of the cement placement is governed by the interface between the cement and lighter (usually Newtonian) fluid. Over the initial setting time, the interface can become unstable allowing light fluid to propagate upwards into the denser fluid. Experimental studies conducted with water under a denser yield stress fluid show that the interface usually takes the form of a long finger moving centrally upwards. If this finger can reach a critical height in the cement plug before it sets sufficiently, the plug will lose its integrity and fail. Therefore, being able to predict the velocity of the finger is of critical importance. Here the viscous finger is modelled using a lubrication approximation of the momentum equations. We can then derive an analytical expression for the flow rate and mean velocity of both the viscous finger and the dense fluid flowing down. Experiments show that the model accurately predicts the velocity of the finger for a range of rheological properties and densities. The speed of the finger is governed by the yield stress, the density contrast between the two fluids and the ratio of effective viscosities.

MICRORHEOLOGY OF POLYELECTROLYTE SOLUTIONS IN THE SEMIDILUTE ENTANGLED REGIME

Atsushi Matsumoto[1], Chi Zhang[2], Frank Scheffold[2], and Amy Q. Shen[3]

[1]Graduate School of Engineering, University of Fukui, 3-9-1 Bunkyo, Fukui-shi, Fukui 910-8507, Japan
[2]Department of Physics, University of Fribourg, Chemin du Musée 3, 1700, Fribourg, Switzerland
[3]Micro/Bio/Nanofluidics Unit, Okinawa Institute of Science and Technology Graduate University, 1919-1 Tancha, Onna-son, Kunigami-gun, Okinawa 904-0495, Japan

ABSTRACT

Entanglements and their effects on the polymer dynamics for polyelectrolyte solutions have been a long-standing debate over the past 30 years since many experimental studies reported conflicting information on their viscoelastic properties when compared with those predicted based on the tube model developed for electrically neutral polymers. These existing rheological studies of polyelectrolyte systems with low-viscosity solvents are limited by the accessible frequency range (≦100 rad s^{-1}) provided by conventional shear rheometers. To overcome this issue, we employed diffusing wave spectroscopy (DWS) based microrheological technique to investigate the linear viscoelastic response of aqueous polyelectrolyte solutions containing poly(sodium styrene sulfonate) (NaPSS) at different degrees of polymerization N. We found that the entanglement monomer concentration c_e, determined by the presence of the plateau regime in the complex modulus spectra, followed the scaling of $c_e \propto N^{-0.77}$ for $N < 7000$, in good agreement with the predicted scaling law of c_e for electrically neutral polymers. However, the estimated scaling exponent changed to -2 when $N > 7000$, the value agreeing well with the predicted value for salt-free polyelectrolyte solutions. We also found the critical monomer concentration at which the charge effects are fully screened by polyelectrolyte itself to be 0.03 M for NaPSS in water. These results indicate that NaPSS can behave as both neutral polymer and polyelectrolyte chains in the entangled regime, depending on the degree of polymerization. We confirmed the observed transition of the NaPSS chain behavior through the scaling analysis of the reptation time τ_{rep} and the Rouse time of an entanglement strand τ_e with respect to the molar concentration of NaPSS monomers c_p, showing $\tau_{rep}/\tau_e \propto c_p^{1.2}$ for $N > 7000$ and $\tau_{rep}/\tau_e \propto c_p^{3.3}$ for $N < 7000$, both of which agree well with the predicted scaling law of τ_{rep}/τ_e for salt-free polyelectrolyte and neutral polymer solutions in the semidilute entangled regime, respectively. Our results demonstrate that the observation of the charge effects on the entanglement properties of polyelectrolytes requires the use of high molecular weight polyelectrolytes having c_e much smaller than the polymer concentration where the self-screening of charge effects occurs. Moreover, we show that the scaling theory proposed by Dobrynin et al. [1] can capture the entanglement dynamics of polyelectrolytes.

[1] Dobrynin et al., *Macromolecules*, 1995, 28, 1859-1871

Gelatinization of Individual Starch Granules

Lanxin Mo[1], James Cheon[2] and John M. Frostad[1,2]

[1]Food Science, University of British Columbia, Vancouver, Canada
[2]Department of Chemical and Biological Engineering, Vancouver, Canada

ABSTRACT

Starch gelatinization is key to starch's ability to affect the rheology of a large number of consumer products and food in particular. During gelatinization, starch granules swell as the intermolecular bonds within the granules are disrupted, resulting in the release of amylose and amylopectin which increase the solution viscosity. Because starch originates as granules formed in plants, we employ a Particle Cohort Study (or ParCS) to track individual granules and provide useful insight into the gelatinization process. In this work, we study the swelling of individual pulse-starch granules and define new parameters to characterize the swelling. We also present a new algorithm to for analyzing a common rheological test used industrially called starch pasting. The results are compared with dynamic scanning calorimetry to validate our results.

EFFECT OF ASPHALTENE ON THE RHEOLOGICAL PROPERTIES OF BITUMEN

Ruiying Xiong[1,2], **Jourdain H. Piette**[1], Ziyue Zhang[1] , Jixiang Guo[2] ,and Savvas G. Hatzikiriakos[1]

[1]Department of Chemical and Biological Engineering, The University of British Columbia, Vancouver, Canada
[2]Unconventional Petroleum Research Institute, China University of Petroleum, Beijing, China

ABSTRACT

The rheological behaviour of bitumen as a function of asphaltene concentration has been studied. Several bitumen samples having distinctly different amounts of asphaltene were prepared and characterized using differential scanning calorimetry and rheological measurements. The glass transition temperature of bitumen increases with an increase of the asphaltene concentration. This correlation can be used to estimate the asphaltene concentration of bitumen samples using DSC measurements. Small-amplitude oscillatory shear data for the bitumen-derived samples were fit by the generalized Maxwell model with good agreement. A constitutive model is proposed, where the zero-shear complex viscosity of the bitumen sample is a strong function of the asphaltene concentration, and it can be used to predict the asphaltene concentration.

EVALUATION OF THE LIQUID HOLDUP IN A STRATIFIED GAS-LIQUID INCLINED PIPELINE ACCORDING TO THE HERSCHEL–BULKLEY FLUID MODEL

Lintong Hou[1,2] and Jingyu Xu[1,2]

[1]School of Engineering Sciences, University of Chinese Academy of Sciences, Beijing 100049, China
[2]Institute of Mechanics, Chinese Academy of Sciences, Beijing, 100190, China

ABSTRACT

The theoretical models of gas-liquid flow based on Newtonian fluid, power-rate fluid and Bingham fluid cannot be accurately applied to the unconventional petroleum field. To this end, based on the Herschel-Berkeley fluid constitutive, with the help of the two-fluid theory and flow control equations, a prediction model of liquid holdup in a two-phase stratified pipe flow is derived. The effects of non-Newtonian fluid rheological parameters, flow conditions and pipe angle on the gas-liquid stratified flow of the Herschel-Berkeley fluid are comprehensively considered. The results show that non-Newtonian rheological characteristics (such as power law index and yield stress) have a significant effect on the liquid holdup in two-phase flow. The specific performance is that the enhancement of liquid yield and shear thinning characteristics will lead to an increase in liquid holdup. Comparing the experimental data, the liquid holdup calculation model shows a good prediction effect. The main feature of this prediction model is that even if the liquid has complex rheology or contains solid particles, it can also describe the two-phase stratified flow through the gas/non-Newtonian fluid behaviour. This model provides new insights into the gas-liquid flow characteristics of complex fluids in inclined pipes.

Key words: Herschel-Bulkley fluid; Gas-liquid stratified flow; Liquid holdup; Prediction model

EFFECT OF CARBON NANOTUBES (CNTs) DISPERSITY IN AG/POLYDIMETHYLSILOXAN (PDMS) COMPOSITE CONDUCTORS

Eun Hui Jeong[1,2], Jun Dong Park[1*], Byoung Soo Kim[2*]

[1]Department of Chemical and Biological Engineering, Sookmyung Women's University, Seoul 04310, Republic of Korea
[2] Bio-Convergence R&D Division, Korea Institute of Ceramic Engineering and Technology (KICET), Chungbuk 28160, Republic of Korea

ABSTRACT

Incorporating electrically conductive fillers into a polydimethylsiloxane (PDMS) matrix has emerged as the most common strategy for developing highly stretchable composite conductors.[1] It is well known that the uniform distribution of conductive fillers in viscous PDMS oligomers during fabrication substantially affects the electrical conductivity, processability, and reliability of the resulting composite conductors. However, systematic studies on enhancing the dispersion stability of the conductive fillers in viscous and oily PDMS matrices are still lacking. Here, we propose a novel rational design of Ag/PDMS composite conductors combined with surface-functionalized carbon nanotubes (CNTs) and methyl group-terminated PDMS.[2,3,4] First, we investigated the relationship between the different types of CNTs and polar solvents that affect the dispersity of CNTs in the resulting conductive composites. Next, we examined the role of methyl group-terminated PDMS as a mediator between Ag, CNT, and PDMS, resulting in homogenously hybridized Ag/CNT fillers within the PDMS matrix. The resulting Ag/CNT/PDMS composite exhibited a metal-like initial electrical resistance of 1.0 ohm/sq and maintained its electrical resistance over 3,000 stretching cycles. This work provides new chemical insights and guidelines for preparing conductive composites.

REFERENCES

1. Larmagnac, A.; Eggenberger, S.; Janossy, H.; Vörös, J. Stretchable electronics based on Ag-PDMS composites. *Scientific reports* **2014**, *4*, 1-7.

2. Deborah, M.; Jawahar, A.; Mathavan, T.; Dhas, M. K.; Benial, A. M. F. Spectroscopic studies on sidewall carboxylic acid functionalization of multi-walled carbon nanotubes with valine. *Spectrochimica Acta Part A: Molecular and Biomolecular Spectroscopy* **2015**, *139*, 138-144.

3. Kim, J. H.; Hwang, J.; Hwang, H. R.; Kim, H. S.; Lee, J. H.; Seo, J.; Shin, U. S.; Lee, S. Simple and cost-effective method of highly conductive and elastic carbon nanotube/polydimethylsiloxane composite for wearable electronics. *Scientific reports* **2018**, *8*, 1375.

4. Zhang, J.; Gao, L. Dispersion of multiwall carbon nanotubes by sodium dodecyl sulfate for preparation of modified electrodes toward detecting hydrogen peroxide. *Mater Lett* **2007**, *61*, 3571-3574.

INFLUENCE OF VISCOSITY HIERARCHY ON DENSITY-UNSTABLE FLUID-FLUID DISPLACEMENT IN VERTICAL CONCENTRIC ANNULI

Maryam Ghorbani[1,2], Hans Joakim Skadsem[1,3]

[1] Department of Energy and Petroleum Technology, University of Stavanger, Norway
[2]PhD student, maryam.ghorbani@uis.no
[3]Accosiate professor, hans.j.skadsem@uis.no

ABSTRACT

Primary cementing of a casing string involves removing drilling fluid from the annular space behind the casing string and replacing it with a cement slurry. The annular cement sheath should provide zonal isolation along the well and prevent leakage of formation fluids to the environment. In the conventional cementing operation, the cementing fluids are pumped down the well inside the casing and up toward the surface within the annulus to be cemented. In reverse circulation cementing operations, the cementing fluids are instead injected directly to the annulus from the surface, and the drilling fluids is displaced downward from the surface. Since reverse cementing requires less circulation pressure, it may be preferrable to use the reverse circulation method when cementing across weak formations. However, it may also lead to an increased risk of fluid contamination during mud displacement since the denser cementing fluids are now displacing the drilling fluid downward in a density-unstable configuration. We present an experimental study of reverse circulation displacement of a vertical concentric annulus. Our focus is on the effect of the viscosity hierarchy of fluids on the displacement. Our results show that there is a strong tendency for backflow and transverse flow during density-unstable displacements. When considering displacements involving fluid pairs with a fixed mean viscosity, we find a stabilization of the displacement when the displacing fluid is the more viscous of the two. When the less viscous Newtonian fluid is displacing the more viscous shear thinning fluid, the displacing fluid elongates more along the annulus. Investigation of iso-dense fluid pairs shows that there is a clearer interface between two fluids when the displaced fluid is more viscous than the displaced fluid, but the shape of the interface between two fluids is not steady.

DYNAMIC VISCOELASTICITY AND SPINNING BEHAVIOR OF AN ORGANOGELATOR, PMDA-R, DISSOLVED IN VARIOUS OILS

Aya Kaide[1,2] and Takashi Saeki[1,2]

[1]Yamaguchi University, Ube, Yamaguchi, Japan
[2]Graduate School of Sciences and Technology for Innovation, 2-16-1 Tokiwadai, Ube City, Yamaguchi 755-8611, Japan

ABSTRACT

We synthesized a low-molecular-mass organogelator, pyromellitamides (PMDA-R),[1] which is composed of four amide groups with two kinds of side chains (R and R'). We evaluated the effects of compounds with one side chain on 2-ethylhexyl or oleyl and those of the other side chain systematically modified on the rheological properties of compounds dissolved in paraffin oil and three kinds of ester oils as solvents. For the application of such additives in cosmetics, paints, etc., it is necessary to obtain not only the viscosity and viscoelasticity data, but also spinning characteristics such as thread pulling and thread breakage. We used a prototyped spinnability measuring device[2] to classify the threading patterns of the samples and organize them in relation to the viscoelasticity of the fluid. We also observed transmission electron microscopy (TEM) images that may be related to the degree of crystallinity of compounds.

RESULTS AND DISCUSSION

Figure 1 shows the results of different concentrations of PMDA-C_6/oleyl in isododecane. Figure 1(a) shows the steady-state flow characteristics. Although not shown in the figure, the viscosity of isododecane remained constant at 1.4 mPa·s independent of the shear rate. Open shapes in the figure indicate viscosity, and closed shapes indicate the first normal stress difference. The addition of 1 wt% caused a viscosity increase by one order, showing an almost constant value in the low-shear-rate range (up to $\gamma = 14.7\ s^{-1}$), which is considered to correspond to a plateau region. At shear rates above 14.7 s^{-1}, the viscosity gradually increased with decreasing shear rate, down to 2.9 mPa·s at 1000 s^{-1}. At 0.3 wt%, the viscosity value increased by approximately two orders of magnitude compared to the solvent, up to a shear rate of 1.47 s^{-1}, and the viscosity gradually decreased at higher shear rates. The increasing viscosity effect in the low-shear-rate range became more pronounced with increasing additive concentration, and a tendency to exhibit shear thinning was apparent in the low-shear-rate range as the concentration increased. Here, the value of the first normal stress difference was negative for all regions measured at 0.1 wt%, but at 0.3 wt%, two-order values were observed at high shear

rates, and three-digit values were observed thereafter. Figure 1(b) shows the dynamic viscoelastic moduli. At the low concentrations of 0.1 and 0.3 wt%, G' and G'' were proportional to the square and first power of ω, respectively, and their positional relationship was reversed as ω increased. At 0.5 wt% or more, a similar phenomenon was observed at low frequencies, and with increasing concentration. Both G' and G'' increased with increasing concentration while the intersection hardly changed position.

On the other hand, the reciprocal of ω at the intersection point is the relaxation time of the sample, and this result indicates that the relaxation times of the samples are almost the same regardless of the concentration.

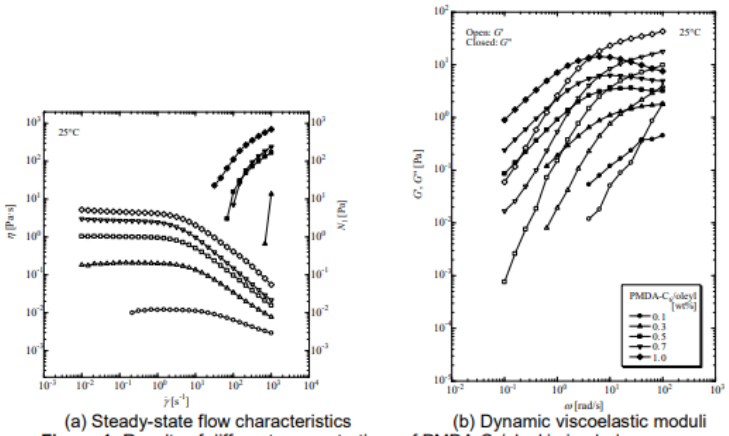

(a) Steady-state flow characteristics (b) Dynamic viscoelastic moduli

Figure 1: Results of different concentrations of PMDA-C_6/oleyl in isododecane

Figure 2(a) shows the results of the stringiness test. Spinnability was observed from a sample with an added concentration of 0.5 wt% in the device used in this experiment. The rod in contact with the liquid surface of the sample rises as if pulling the sample, increasing the stress. Then, after the stress reaches maximum value, it takes on a thread-like shape, and the thread gradually becomes thinner until it finally breaks. Since the thread remained present even when stress was below 0, we used the data up to the length at which the thread broke, which we measured from video footage. According to the figure, if the lifting speed is the same, the gradient corresponding to the part where the liquid surface rises is almost the same, so we can consider that the lifting force of the sample is almost the same at an addition concentration of 0.5 wt% or more. At 0.5 wt%, the maximum stress was 0.67 N and the string length was 4 mm. At 0.7 wt%, there is a portion where the gradient changes until the thread breaks, and the inflection point is approximately 6 mm. This trend was also seen at 1.0 wt%. The maximum stresses at 0.7 and 1.0 wt% were 1.2 and 2.2 mN, respectively, and the spinning lengths were 9.7 and 19.3 mm. This is simply the result that, when the concentration of the additive increases and the viscosity and viscoelasticity of the sample increase, spinning becomes apparent and the maximum spinning stress and length increase.

For this reason, the maximum value of the spinning stress is standardized to 1 and the maximum spinning length is 1. The results are shown in Fig. 2(b). Focusing on the upward

convex part, the shape is almost line-symmetrical around the maximum stress value at any concentration, but at 0.7 and 1.0 wt%, the tail spreads until the thread breaks and there is also a distortion in the symmetry. The process from the emergence of spinning to breakage is expressed after the maximum stress, and it can be clearly seen that the higher the concentration of the additive, the longer the period after the stress drops below 0.

In addition, we plan to report on the effects of changing the side chain.

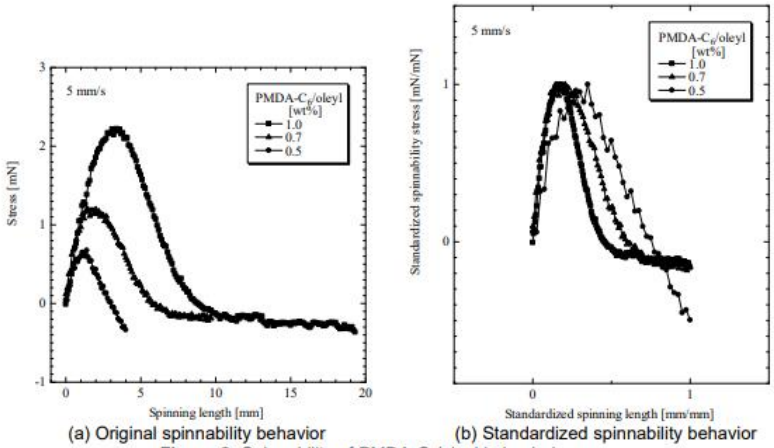

(a) Original spinnability behavior (b) Standardized spinnability behavior

Figure 2: Spinnability of PMDA-C6/oleyl in isododecane

ACKNOWLEDGEMENTS

The authors wish to thank Dr. Y. Sakanishi (Taiyo Kagaku Co., Ltd.) for the synthesized PMDA-R compounds. This research was supported by JSPS KAKENHI, Grant-in-Aid for Young Scientists, 2020-2022 (JP20K15076, Aya Kaide) and Grant-in-Aid for Scientific Research (C), 2022-2025 (JP22K04805, Aya Kaide).

REFERENCES

1. Sakanishi Y.; Narusaka Y.; Itoh M.; Arita T.; Saeki T. Development of New Series of Organogelators: N,N',N'',N'''-1,2,4,5-Tetra Alkyl/Alkenyl Pyromellitamides. *Nihon Reoroji Gakkaishi (J Soc Rheol Jpn)*, **43**, 1, 1-9, 2015. https://doi.org/10.1678/rheology.43.1.

2. Kaide A.; Saeki T. Synthesis of Organogelators: Pyromellitamides (PMDA-R) and Their Rheological Properties during Commercial Scale-Up. *Nihon Reoroji Gakkaishi (J Soc Rheol Jpn)*, **49**, 5, 319-328, 2021. https://doi.org/10.1678/rheology.49.319

CAPILLARY IMBIBITION IN A DIVERGING FLEXIBLE CHANNEL

Mouad Boudina, Gwynn J. Elfring

Department of Mechanical Engineering
University of British Columbia, Vancouver, Canada

ABSTRACT

We study the imbibition of a wetting liquid between flexible sheets that are fixed on both ends. Assuming a narrow gap between the sheets, we solve the lubrication equation coupled with slender body deformation. When the sheets are parallel, we find that the deformation speeds up the flow, as shown in previous studies, but only up to the middle of the channel. The channel then contracts, increases the hydrodynamic resistance and slows down the filling process. Below a threshold stiffness, the sheets collapse and imbibition stops. We propose a scaling of the filling duration near this threshold. Next we show that if the sheets are initially tilted with a minimal angle, the channel avoids collapse. The liquid front pulls the diverging sheets and spreads in nearly parallel portions, which maintains the capillary propulsion and enhances the wicking. Therefore, while it is established that diverging rigid plates imbibe liquids slower than parallel ones, we show that elasticity reverses this principle: diverging flexible sheets imbibe liquids faster than parallel ones. We find an optimal tilt angle that gives the shortest filling time.

Wednesday, May 17, 2023

Plenary Presentation - GEOG 100 (9:00 AM - 10:00 AM)

8TH PACIFIC RIM CONFERENCE ON RHEOLOGY, May 15-19, 2023

COMPARISON OF VISCOELASTIC AND DIELECTRIC PROPERTIES OF TYPE-A CHAIN:

EXPERIMENTAL ATTEMPT FOR DEEPER UNDERSTANDING OF POLYMER RHEOLOGY

Hiroshi Watanabe[1,2]

[1]Institute for Chemical Research, Kyoto University, Uji, Kyoto, JAPAN
[2]Chagchun Institute of Applied Chemistry, Chinese Academy of Sciences, Changchun, CHINA

ABSTRACT

Viscoelastic and dielectric properties of type-A chains differently average the same chain dynamics, so that comparison of those properties resolves some details of this dynamics in a purely experimental way. Some examples of this comparison are presented in the talk.

INTRODUCTION

Molecular understanding of polymer rheology has been one of the central targets in the community of rheology, and extensive studies have been made from both experimental and theoretical aspects.[1,2] Comparing viscoelastic and dielectric properties of so-called *type-A chains* in long time scales, we may find some details of the molecular dynamics underlying the rheological behavior of those polymers, as explained below.

The type-A chain has the electrical dipoles **p** parallel along the chain backbone (cf. **Fig.1**) and its viscoelastic and dielectric properties in long time scales commonly reflect the large-scale chain motion over the end-to-end distance R. Nevertheless, this motion is differently averaged in the viscoelastic and dielectric properties. For example, the relaxation modulus $G(t)$ under a step strain γ and the dielectric relaxation function $F(t)$ under a step electric field E are expressed in terms of the bond vector of n-th subchain (or coarse-grained segment) at time t, $\mathbf{u}(n,t)$, as[3-5]

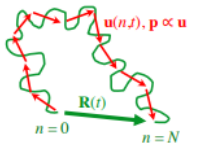

Fig.1. Schematic illustration of type-A chain without dipole inversion.

$$G(t) = \frac{\nu k_B T}{\gamma} \int_0^N \left\{ 3 / \left\langle \mathbf{u}^2 \right\rangle_{eq} \right\} \left\langle u_x(n,t) u_y(n,t) \right\rangle_\gamma \mathrm{d}n \tag{1}$$

$$F(t) = \frac{\nu}{E} \int_0^N m_d \left\{ \left\langle u_E(n,\infty) \right\rangle_E - \left\langle u_E(n,t) \right\rangle_E \right\} \mathrm{d}n \tag{2}$$

Here, ν is the number density of the chain, $k_B T$ is the thermal energy, $\langle \mathbf{u}^2 \rangle_{eq}$ is the mean-square end-to-end distance of the subchain at equilibrium, and m_d is the dipole moment per unit length of the backbone of the type-A chain (with no dipole-inversion being considered in Eq.2). In Eq.1, u_x and u_y stand for the components of $\mathbf{u}(n,t)$ in the shear (x) and shear gradient (y) directions, respectively, and $\langle \cdots \rangle_\gamma$ denotes the ensemble average under the step strain. In Eq.2, u_E is a component of $\mathbf{u}(n,t)$ in the direction of the electric field, and $\langle \cdots \rangle_E$ indicates the ensemble

average under the step electric field E. For sufficiently small γ and E (in the linear response regime), the chain dynamics determining $\langle u_x u_y \rangle_\gamma$ and $\langle u_E \rangle_E$ coincides with the equilibrium dynamics. However, $G(t)$ and $F(t)$ are determined by the second- and first moment averages of $\mathbf{u}(n,t)$, respectively. Namely, the same dynamics is differently averaged in the viscoelastic $G(t)$ and dielectric $F(t)$. This difference enables us to experimentally resolve some details of the chain dynamics through comparison of viscoelastic and dielectric properties of type-A chains. Some examples of this comparison are presented below.

TEST OF TUBE DILATION PICTURE FOR ENTANGLED POLYMERS

For entangled chains, tube models consider that the chain relaxes through several different mechanisms, reptation (for linear chains) and/or arm retraction (for star chains), contour length fluctuation (CLF), and constraint release (CR).[1,2] Among these mechanisms, the CR mechanism considers the relaxation of a given chain (probe) activated by the motion of surrounding chains, thereby introducing a flavor of multiple chain dynamics into the tube model. Some models further assume that the relaxed portion of chains serves as a solvent for the probe chain to *fully* dilate the tube (to a level in the corresponding solution), thereby successfully describing $G(t)$ of linear and star chains.[4,5] However, comparison of dielectric and viscoelastic data of a typical type-A polymer, high-*cis* polyisoprene (PI), resolved a limitation of this *full-DTD* molecular picture, as explained below.[4,5]

For this comparison, it is convenient to rewrite Eq.2 with the aid of the Green-Kubo theorem (valid at equilibrium) as[4,5]

$$\Phi(t) \equiv \frac{F(t)}{F(0)} = \frac{1}{N}\int_0^N \mathrm{d}n \int_0^N \mathrm{d}n'\ C(n,t;n') \quad \text{with } C(n,t;n') = \left\langle \mathbf{u}^2 \right\rangle_{\mathrm{eq}}^{-1} \left\langle \mathbf{u}(n,t) \cdot \mathbf{u}(n',0) \right\rangle_{\mathrm{eq}} \qquad (3)$$

A conformational analysis shows that $\Phi(t)$ is essentially identical to the survival fraction $\varphi'(t)$ of the dilated tube.[4,5] Thus, the $\Phi(t)$ data (obtained from dielectric experiments for PI) allow us to formulate the reduced relaxation modulus $\mu(t) = G(t)/G(0)$. Specifically, the full-DTD molecular picture assumes that the relaxed portion of the chains always behaves as a solvent to dilate the tube diameter to $a_{\text{f-DTD}}(t) = a_{\text{eq}} \{\varphi'(t)\}^{-d/2}$, with a_{eq} = equilibrium tube diameter and $d \cong 1.3$ (tube dilation exponent). This full-DTD assumption leads to a relationship, $\mu_{\text{f-DTD}}(t) = \{a_{\text{eq}}/a_{\text{f-DTD}}(t)\}^2 \varphi'(t) = \{\varphi'(t)\}^{1+d}$.

For binary blends of linear PI with molecular weights M_2 = 308k and M_1 = 21k, $\mu_{\text{f-DTD}}(t)$ thus obtained dielectrically (green curves) is compared with the viscoelastically measured $\mu(t)$ data (black circles) in **Fig.2**. At t = 0.5-500 ms where the low-M chain has fully relaxed but the high-M chain has not, $\mu_{\text{f-DTD}}(t)$ is smaller than the $\mu(t)$ data of the blends having a small fraction of the high-M chain, $\upsilon_2 = 0.2$ and 0.1. This failure of the full-DTD picture results from the assumption that the relaxed portion of the chain (the whole backbone of the low-M chain at those t) always behaves as the solvent to fully dilute the tube for the high-M chain. In reality, the high-M chain moving through the CR motion cannot always explore the whole part of this diluted tube and thus the effective tube diameter for that chain $a^*(t)$ is smaller than $a_{\text{f-DTD}}(t)$ at those t. This problem of the full-DTD picture can be removed if we evaluate the maximum possible lateral displacement $a_{\text{CR}}(t)$ allowed by the CR motion and express the reduced relaxation modulus as $\mu_{\text{f-DTD}}(t) = \{a_{\text{eq}}/a^*(t)\}^2 \varphi'(t)$ with $a^*(t) = \min\{a_{\text{CR}}(t),\ a_{\text{f-DTD}}(t)\}$.

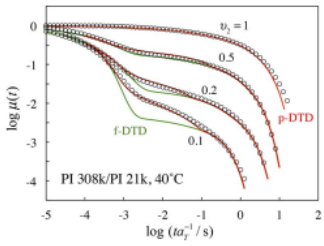

Fig.2. Comparison of $\mu_{\text{f-DTD}}(t)$ and $\mu_{\text{p-DTD}}(t)$ deduced within the tube model with $\mu(t)$ data of PI/PI blends with various υ_2.

Viscoelastic measurements for reference binary blends (containing *self-unentangled* high-M components) allow us to evaluate $a_{CR}(t)$ and thus $\mu_{f\text{-}DTD}(t)$ for the partial-DTD picture.[4,5] This $\mu_{f\text{-}DTD}(t)$, shown with the red curve in Fig.2, is in excellent agreement with the $\mu(t)$ data in the entire ranges of t and v_2. This result in turn demonstrates an importance of the comparison between dielectric and viscoelastic data.

EIGENFUNCTION OF LOCAL CORRELATION FUNCTION

Chemical coupling of living anionic PI chains of different M allows us to prepare homo-PI chains with inversion of type-A dipoles at a given (n^*-th) segment. For those dipole-inverted PI, the dielectric relaxation function is expressed in terms of C defined in Eq.3 as[4]

$$\Phi(t;n^*)=\frac{1}{N}\left\{\int_0^{n^*}\mathrm{d}n-\int_{n^*}^{N}\mathrm{d}n\right\}\left\{\int_0^{n^*}\mathrm{d}n'-\int_{n^*}^{N}\mathrm{d}n'\right\}C(n,t;n') \qquad (4)$$

The local correlation function C can be expanded with respect to its eigenfunctions $f_p(n)$ as $C(n,t;n')=\Sigma_p f_p(n)f_p(n')\exp(-t/\tau_p)$ (with τ_p being p-th relaxation time). Thus, the dielectric data of a series of dipole inverted PI having the same M but different n^* allow us to experimentally resolve $f_p(n)$ for a few low-order modes. An example is shown in **Fig.3** for PI being entangled with polybutadiene and exhibiting CR relaxation.[4] The standard tube model assumes the Rouse-type CR associated with sinusoidal $f_p^{[R]}(n)=\sin(p\pi n/N)$ (black curves). However, experimental $f_p(n)$ moderately deviate from $f_p^{[R]}(n)$. From mathematical coincidence of the Rouse eigenfunction equation and the Schrödinger equation for a quantum particle in a well potential, this deviation can be related to an extra relaxation enhanced at around the chain end[4] (where the motional constraint is weaker compared to the middle of the chain).

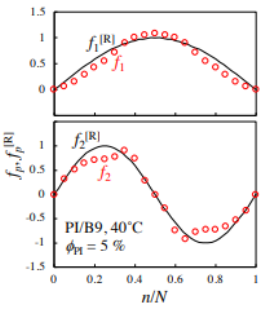

Fig.3. Eigenfunction of PI relaxing through CR mechanism.

If the chain moves coherently along its backbone (as in the case of reptation), the eigenfunction is common for $C(n,t;n')$ and the orientation function governing the viscoelastic relaxation, $S(n,t)=\{3/\langle\mathbf{u}^2\rangle_{eq}\}\langle u_x(n,t)u_y(n,t)\rangle_\gamma$ shown in Eq.1. In contrast, if the chain motion is incoherent, $f_p(n)^2$ determines $S(n,t)$. Thus, comparison of dielectrically determined $f_p(n)$ and viscoelastic data allows us to test this motional coherence. It turned out that the chains in unentangled solutions exhibit the incoherent motion whereas some magnitude of coherence emerges for entangled chains in concentrated solutions/bulk.[4] An importance of the comparison between dielectric and viscoelastic data is demonstrated also from this experimental finding.

REFERENCES

1. Watanabe, H. Viscoelasticity and dynamics of entangled polymers. *Prog. Polym. Sci.* **24 (9)**, 1253-1403, 1999. https://doi.org/10.1016/S0079-6700(99)00029-5
2. McLeish, T.C.B. Tube theory of entangled polymer dynamics. *Adv. Phys.* **51 (6)**, 1379-1527, 2002. https://doi.org/10.1080/00018730210153216
3. Watanabe, H. Dielectric Relaxation of Type-A Polymers in Melts and Solutions. *Macromol. Rapid Commun.* **22 (3)**, 127-175, 2001. https://doi.org/10.1002/1521-3927(200102)22:3<127::AID-MARC127>3.0.CO;2-S
4. Watanabe, H. Slow Dynamics in Homopolymer Liquids, *Polym. J.*, **41 (11)**, 929-950, 2009. https://doi.org/10.1295/polymj.PJ2009148
5. Matsumiya, Y.; Watanabe, H. Entanglement-Loosening Dynamics Resolved Through Comparison of Dielectric and Viscoelastic Data of Type-A Polymers: A Review. Rubber Che, Technol. **93 (1)**, 22-62, 2020. https://doi.org/10.5254/rct.19.80388

8TH PACIFIC RIM CONFERENCE ON RHEOLOGY, May 15-19, 2023

Role of network compressibility on the complex conductivity of structured polyelectrolyte hydrogels

Reghan J Hill[1],

[1]McGill University, Montreal, Canada

ABSTRACT

Electrical conductivity, as measured by DC conductivity and its dynamic counterpart, impedance spectroscopy, are sensitive indicators of electrical charge and ionic charge mobility. Impedance spectra, widely reported in biomedical and advanced materials literature, are customarily interpreted using circuit models for which it can be challenging to draw clear connections between the circuit elements and the physical micro/nanostructure. In this work, a physical model is developed for ion transport in polyelectrolyte hydrogels under the oscillatory perturbations applied in impedance spectroscopy. The model couples electro-migration, diffusion and advection, in the framework of nonlinear Poisson-Boltzmann thermodynamics and continuum transport phenomena, which together control micro-scale electrical polarization. Here, focus will be on the role of the network compressibility (p-wave modulus) in shaping the complex conductivity and dielectric permittivity spectra of polyelectrolyte hydrogels with cavities or having spatial modulations in the charge and polymer segment density (e.g., layered polyelectrolytes). The guiding physical principle is that, on nano- and micro-scales, the draining time is short, thus giving rise to fixed-charge-density fluctuations that may affect the complex conductivity in the frequency range of impedance spectroscopy.

ACKNOWLEDGEMENTS

Funding for this work from an NSERC Discovery Grant is gratefully acknowledged.

ULTRASOUND EFFECT ON DISPERSION AND DISTRIBUTION OF GRAPHITIC MATERIALS INSIDE DIFFERENT PDMS

Manon Favre[1], Emna Helal[1,2], Tatiana Kaydanova[2], Giovanna Gutierrez[2], Nima Moghimian[2], Éric David[2], and Nicole R. Demarquette[1]

[1]École de Technologie Supérieure, Department of Mechanical Engineering, Montréal, Canada
[2]NanoXplore Inc., Montréal, Canada

ABSTRACT

For decades, the creation of new materials by mixing nanoparticles with polymeric matrices continues to attract the attention of industrialists and academics. Indeed, adding nanoparticles with better electrical or mechanical properties, such as graphitic materials, to polymers, allows obtaining enhanced materials for multiple applications including automotive, energy storage, aerospace, biomedical and more. Nevertheless, performance improvement is highly dependent on the achievement of good distribution and dispersion of the nanoparticles inside the host polymer matrix. In this context, it has been shown, in the literature, that sonication can be an effective method to obtain an efficient dispersion of fillers such as clay and carbon nanotubes inside solvents. However, few studies have investigated sonication for dispersing nanoparticles inside highly viscous mediums such as molten polymers. Moreover, the propagation of the ultrasonic waves within the molten polymers and nanocomposites is still not clearly understood. In this work, the effect of ultrasonic vibration on graphitic materials distribution and dispersion in polydimethylsiloxane, PDMS, was investigated. PDMS grades of different viscosities (3, 30, and 300 Pa.s) were hand-mixed with 0.5 wt% graphitic materials of three different sizes distribution (D90* = 33, 40, or 128 µm), then an ultrasound treatment was applied for 3 minutes with different amplitudes (20, 50 and 90%) and pulses (10, 50, 100%). The continuous ultrasound treatments (i.e. the 100% pulse) were filmed using a high-speed camera in order to observe the mixing pattern. Furthermore, an optical microscope has been used to evaluate the distribution and dispersion of the samples (employing a Python program). The results revealed that the ultrasound treatment effect is dependent on the particle size and the fluid viscosity.
*D90 means 90% of the particles have a size below it.

FLUID COMPOSITES AS ALTERNATIVES TO SOLID ELECTRICAL COMPONENTS

Dominik S. Schmidt[1], Sergio Lago-Garrido[1], Srishti Arora[1], and Lola Gonzalez-Garcia[1,2]

[1]INM-Leibniz Institute for New Materials, Campus D2 2, 66123 – Saarbrücken, Germany
[2]Department of Materials Science and Engineering, Saarland University, Campus D2 2, 66123 – Saarbrücken, Germany

ABSTRACT

Today, most electronics and robots are composed of solid metals and semiconductors and composites based on them. As alternative, we propose "Electrofluids", that exhibit electrical conductivity while flowing. We create highly concentrated suspensions of conductive particles -carbon black (CB) and carbon nanotubes (CNTs)- in solvents with different polarity and viscosity. The idea is to create 3D networks of the solid fillers that allow for electron transport like in solid composites, but here, the contacts between the particles are transient. The particles can move in the liquid and rearrange under mechanical deformations.

We studied the electrical properties of different mixtures as a function of the filler content and found that the amount of it required to achieve electrical conductivity in the material (percolation threshold) strongly depends on a) the polarity of the solvent matrix, b) its viscosity, and c) the shape of the particles.

Using carbon black (CB) as conductive filler, we observed a decrease in the percolation threshold from 8.34 wt%, when dispersed in PDMS to 0.55 wt%, when glycerol was used. Both pure solvents have a comparable viscosity (on the order of 10^3 mPa·s), but whereas glycerol is a polar molecule, PDMS is composed of hydrophobic polymer chains. The percolation threshold can be further reduced to 0.26 wt%, by using ethylene glycol (a polar solvent with a lower viscosity, on the order of 10 mPa·s). When using CNTs as filler, the percolation threshold for the glycerol mixture is lowered to 0.05 wt%. This reduction can be attributed to the high aspect ratio (around 150) of the CNTs.

The electrical properties of these materials are dominated by the 3D network formed by the filler. To understand the network's structure and its dynamics, we performed rheological and rheoelectrical studies. All the samples at concentrations above percolation presented a shear thinning behaviour. Amplitude sweeps experiments revealed a clear correlation between the changes in the electrical properties and the shape of the storage and loss moduli, G' and G''.

We exploited this behaviour and created soft strain sensors. The Electrofluids were then encapsulated in elastomeric tubes and underwent uniaxial deformations. We performed cyclic and stress relaxation tests and found large differences in the mechanoelectrical performance (sensitivity and time dependency) of the mixtures. We will discuss their applicability in truly soft electrical devices.

THE RHEOLOGICAL PROPERTIES OF HOT MELT ADHESIVES DOPED WITH CARBON NANOTUBES

Paulina Latko-Durałek[1,2]
[1]Faculty of Materials Science and Engineering, Warsaw University of Technology, Wołoska 141, 02-507 Warsaw, Poland
[2]Technology Partners Foundation, Adolfa Pawińskiego 5A, 02-106 Warsaw, Poland
e-mail: paulina.latko@pw.edu.pl; paulina.latko@technologypartners.pl

Electrically conductive adhesives (ECAs) are an innovative group of engineering materials used to replace the traditional Pb-Sn solders or as a bonding medium of thermoplastic or thermosetting matrix composite for the aviation and automotive sectors. The main component of ECAs are thermoset resins such as silicone, epoxy, or acrylate, and conductive fillers the most popular of which is micro silver[1,2]. However, achieving the necessary level of electrical conductivity requires loading a high amount of metal particles, which has a negative effects on their processing and mechanical properties. To avoid this, lightweight carbon-based fillers such as carbon nanotubes, graphene, carbon black or graphite are extensively studied as the conductive fillers for ECAs. Owing to their high surface area, a percolated network is formed at much lower concentrations than in the case of metal fillers. Unfortunately, even at small concentrations, the carbon-based fillers - especially those of nano size - strongly affect the rheological properties[3].

This research focuses on a novel type of ECAs consisting of thermoplastic hot melt adhesive and multi-walled carbon nanotubes. Using the oscillatory rheometer, it was possible to determine the rheological percolation threshold, changes in the viscosity, in storage and loss modulus for various types of the hot melt adhesives. For all of the composites, the rheological percolation threshold lies below 2wt% of carbon nanotubes, the materials behave more like elastic than viscous liquids, and for some of them, increasing the test temperature does not decrease the viscosity. The rheological properties of ECAs was discussed in the context of the carbon nanotubes dispersion and further processing of ECAs.

ACKNOWLEDGEMENTS

The research leading to these results has received funding from the Norway Grants 2014-2021 via the National Centre for Research and Development. Grant number: NOR/SGS/3DforCOMP/0171/2020-00.

REFERENCES

1. Aradhana, R.; Mohanty, S.; Nayak, S. K.: A review on epoxy-based electrically conductive adhesives. Int J *Adhes Adhes*, **99**, 102596 (2020). http://doi:10.1016/j.ijadhadh.2020.102596.
2. Nele, L.; Palmieri, B.: Electromagnetic heating for adhesive melting in CFRTP joining: study, analysis, and testing. *Int. J. Adv. Manuf. Technol*, **106**, 5317–5331 (2020). http://doi:10.1007/s00170-019-04910-9
3. Latko-Durałek, P.; Kozera, R.; Macutkievic, J.; Dydek, K.; Boczkowska, A. Relationship between viscosity, microstructure and electrical conductivity in copolyamide hot melt adhesives containing carbon nanotubes. *Materials*. Vol. 13, 4469 https://doi.org/10.3390/ma13204469 (2020)

8TH PACIFIC RIM CONFERENCE ON RHEOLOGY, May 15-19, 2023

RESPONSE OF BLOCK COPOLYMER ELECTROLYTES TO IONIC CURRENT

Nitash P. Balsara[1,2]

[1]Department of Chemical and Biomolecular Engineering, University of California, Berkeley, California 94720, USA
[2]Materials Sciences Division, Lawrence Berkeley National Laboratory, Berkeley, California 94720, USA

ABSTRACT

Lithium-salt-doped block copolymers have the potential to serve as solid electrolytes in rechargeable batteries with lithium metal anodes. In this work, we use small angle X-ray scattering (SAXS) to study the structure of polystyrene-block-poly(ethylene oxide) doped with bis-(trifluoromethylsulfonyl)amine lithium salt (LiTFSI) during dc polarization experiments in lithium-lithium symmetric cells. The block copolymer studied is nearly symmetric in composition, has a total molecular weight of 39 kg mol^{-1}, and it exhibits a lamellar morphology at all studied salt concentrations. When ionic current is passed through the electrolyte, a salt concentration gradient forms which induces a spatial gradient in the domain spacing, d. The dependence of d on distance from the positive electrode, x, was determined experimentally by scanning the incident X-ray beam from one lithium electrode to the other. By studying the 2D SAXS patterns as a function of azimuthal scattering angle, we find that lamellae with PS-PEO interfaces oriented perpendicular to the flow of ionic current swell and contract to a greater degree than those with interfaces oriented parallel to the current direction. While domains with the perpendicular lamellae do not provide direct conducting pathways between the electrodes, our analysis suggests they play an important role in establishing the salt concentration gradient necessary for sustaining large ionic current through greater expansion and contraction.

RESULTS AND DISCUSSION

There is considerable interest in the possible use of block copolymers in lithium batteries.[1-4] We studied a block copolymer which we call SEO(19-20) with added LiTFSI, the molar ratio of lithium ions to ether oxygens in the electrolyte was 0.16 [1]. This electrolyte was inserted in a custom electrochemical cell to allow simultaneous SAXS measurements. This cell is shown schematically in **Fig. 1a**. The lithium electrodes are in the y-z plane such that the nominal direction of ionic current is parallel to the x-axis. The length of the sample in the x-direction, L, was 0.14 cm. In **Fig. 1b**, we show an example of a SAXS pattern obtained from SEO(19-20) where the incident beam is oriented in the z-direction. By scanning the beam along the x-axis, the 2D scattering patterns contain information about the structure of lamellae with normal vectors in the x-y plane along the axis which the salt concentration gradient forms in a dc

polarization experiment. We define the azimuthal angle, χ, in Fig. 1b and denote $\chi = 0°$ along the y-axis, pointing upwards and increasing counterclockwise. By analyzing data at $\chi = 0$ and 180° (as defined in Fig. 3b) we obtain information about grains with PS-PEO interfaces oriented parallel to the flow of ionic current (we call these lamellae $LAM_{||}$, and note that their normal vectors are parallel to the y-axis). For $\chi = 90$ and 270°, we obtain information about grains with PS-PEO interfaces oriented perpendicular to the flow of ionic current (we call these lamellae $LAM_{\perp}$, and note that their normal vectors are perpendicular to the y-axis).

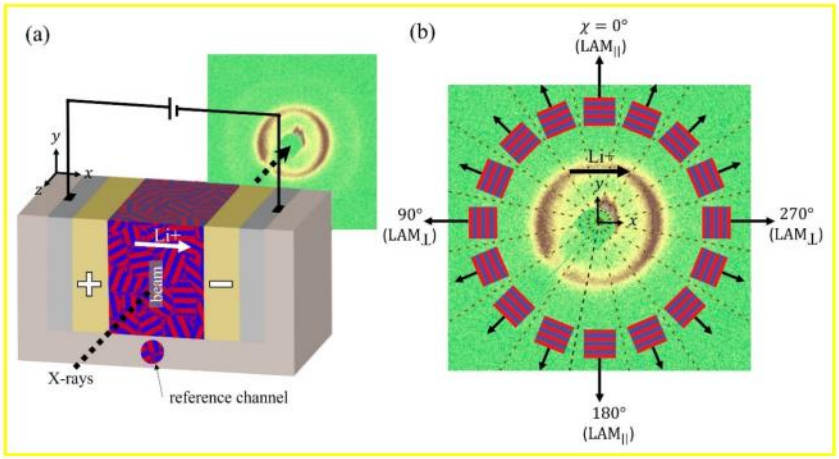

Figure 1: (a) Schematic representation of the simultaneous polarization and SAXS experiment. An SEO/LiTFSI electrolyte with randomly oriented grains is sandwiched between two lithium electrodes with current passing parallel to the x-axis. X-rays pass parallel to the z-axis, perpendicular to the current and the shaded gray box shows the beam footprint on the sample. Scanning the beam along the x-axis allows for spatial resolution between the electrodes. A reference channel filled with electrolyte was placed next to the electrochemical cell. (b) Characteristic 2D SAXS pattern obtained from experiments. The pattern is divided into 16 sectors defined by the azimuthal angle, χ. Scattering data in each sector corresponds to lamellae oriented with the angle between the vector normal to the PEO-PS interfaces and the positive y-axis equal to χ. The cartoons in each sector show the lamellar orientation with their respective normal vectors.

The SAXS data were used to determine the domain spacing, d, at three different current densities, i. We present data as a function of the normalized current density iL. Before polarization, we find that $d(\chi)$ was exactly not constant. To account for this, we redefine the quantity Δd for a fixed position x/L in Eqn. 16:

$$\Delta d(\chi, t) = d(\chi, t) - d(\chi, t = 0) \quad (1)$$

In **Figs. 2a-c**, we plot Δd as a function of χ for each position in the cell for the cells polarized at (a) $iL = 1.96$ μA cm^{-1} (b) $iL = 3.74$ μA cm^{-1}, and (c) $iL = 11.1$ μA cm^{-1}. The results presented in these figures show that grains with PS-PEO interfaces perpendicular to the flow of ionic

current ($LAM_{\boxplus}$) undergo greater expansion (near the positive electrode) or contraction (near the negative electrode) when compared to those with PS-PEO interfaces oriented parallel to the flow of ionic current ($LAM_{||}$). To highlight this point, we plot the difference in lamella spacing between $LAM_{\boxplus}$ and $LAM_{||}$, $d_{LAM_{\boxplus}} - d_{LAM_{||}}$, in **Fig. 1d.** As the concentration gradient builds up, the $LAM_{\boxplus}$ near the positive electrode are swollen between 0.6 and 1.2 nm larger than $LAM_{||}$. Near the negative electrode, the $LAM_{\boxplus}$ are between 0.2 and 1.2 nm smaller than the $LAM_{||}$.

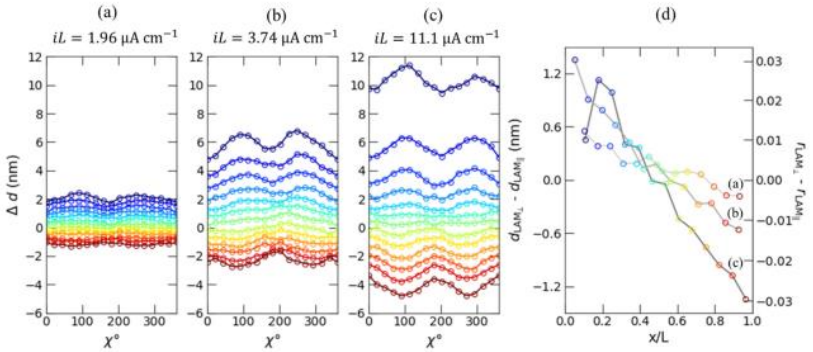

Figure 2: Orientation dependence of lamellar distortion. The change in domain spacing, Δd, defined by Eqn. 1 as a function of azimuthal angle, χ, is plotted for each cell position for the cell polarized at (a) iL = 1.96 μA cm^{-1} at t = 46.7 h, (b) iL = 3.74 μA cm^{-1} at t = 46.7 h, and (c) iL = 11.1 μA cm^{-1} at t = 60.7 h. Each data set is based on the last scan taken at the end of each polarization. (d) Difference in domain spacing between $LAM_\perp$ and $LAM_{||}$ as a function of normalized position, x/L, for the three data sets in (a), (b), and (c). The right axis is the difference in molar salt concentration, r, based on Eqn. 2. The color of each data set in (a), (b), and (c) correspond to the x/L position plotted in (d).

CONCLUSIONS

The SAXS experiments show that that there was a net increase in the domain spacing of the block copolymer as the salt concentration gradient develops. We observed that grains with PS-PEO interfaces oriented perpendicular to the flow of ionic current ($LAM_\perp$) swell and contract to a greater extent compared to those with PS-PEO interfaces oriented parallel to the flow of ionic current ($LAM_{||}$). It is obvious that $LAM_{||}$ play an important role in ion transport as the conducting domains in these grains are parallel to the direction of macroscopic ion transport. Our work indicates that $LAM_\perp$ also play an important role. The formation of a salt concentration gradient that must arise due to ion transport across macroscopic length scales relies on the ability of the lamellae to swell and contract. These distortions occur to a greater extent in

$LAM_{\perp}$. Both $LAM_{||}$ and $LAM_{\perp}$ appear to be necessary to accommodate large ionic currents in block copolymer electrolytes.

ACKNOWLEDGEMENTS

This work was supported by the Assistant Secretary for Energy Efficiency and Renewable Energy, Vehicle Technologies Office, under the Advanced Battery Materials Research (BMR) Program, of the U.S. Department of Energy under Contract No. DE-AC02-05CH11231.

REFERENCES

1. Tu, Z.; Nath, P.; Lu, Y.; Tikekar, M. D.; Archer, L. A. Nanostructured Electrolytes for Stable Lithium Electrodeposition in Secondary Batteries. *Acc. Chem. Res.* **2015**, 48 (*11*), 2947–2956.
2. Newman, J.; Balsara, N. P. *Electrochemical Systems*, 4th ed.; Wiley, **2021**.
3. Cheng, X.-B.; Zhang, R.; Zhao, C.-Z.; Zhang, Q. Toward Safe Lithium Metal Anode in Rechargeable Batteries: A Review. *Chem. Rev.* **2017**, 117 (*15*), 10403–10473.Caenn, R.; Darley, H. C. H.; Gray, G. R. *Composition and Properties of Drilling and Completion Fluids*, 5th ed.; Gulf Publ Co, 1988.
4. Singh, M.; Odusanya, O.; Wilmes, G. M.; Eitouni, H. B.; Gomez, E. D.; Patel, A. J.; Chen, V. L.; Park, M. J.; Fragouli, P.; Iatrou, H.; Hadjichristidis, N.; Cookson, D.; Balsara, N. P. Effect of Molecular Weight on the Mechanical and Electrical Properties of Block Copolymer Electrolytes. *Macromolecules* **2007**, 40 (*13*), 4578-4585.

GLASS TRANSITION AND ENTANGLEMENT IN SEMIFLEXIBLE CONJUGATED POLYMER MELTS

Abigail M. Fenton,[1] Renxuan Xie[1], Daniele Parisi[2], Enrique D. Gomez[1,3] and Ralph H. Colby[2,3]

[1]Department of Chemical Engineering, The Pennsylvania State University, University Park, PA 16802, USA

[2]Department of Materials Science and Engineering, The Pennsylvania State University, University Park, PA 16802, USA

[3]The Materials Research Institute, The Pennsylvania State University, University Park, PA 16802, USA

Correspondence to: rhc@plmsc.psu.edu

ABSTRACT

Polymers with conjugated backbones and flexible side chains are semiflexible and exhibit two glass transitions, one for the conjugated backbone and a lower T_g for the side chains. Both glass transitions are broadened, since the side chains are covalently attached to the backbones, and are challenging to detect by standard calorimetry methods (i.e., DSC). By compression molding in a glove box, it is possible to measure the linear viscoelastic response (LVE) of conjugated polymers from the lower T_g up to roughly 300 °C. The two glass transitions are detected in LVE temperature sweeps at 1 rad/s as local maxima in the loss modulus G" and the width of these transitions is reflected in how much higher in temperature tanδ = G"/G' exhibits a local maximum.[1] A simple model is presented to predict the backbone glass transition from volume fraction of backbone and molecular characteristics of the backbone,[2] enabling molecular design of conjugated polymers for flexible electronics with T_g below ambient.

Many of the conjugated polymers with more rigid backbones exhibit liquid crystalline phases above their melting temperature. The ones with a nematic phase are very easy to detect in the LVE temperature sweeps, as the nematic → isotropic transition is easily seen as a roughly 10 K window where viscosity actually *increases* as temperature is raised[3,4] (which is the biphase) whereas this weakly first order transition is virtually undetectable by DSC. In the isotropic phase at high temperature, the plateau modulus is measured by constructing an LVE master curve and with the molecular weight distribution this is fit to a molecular LVE model based on reptation dynamics, originally developed for more flexible polymers. The Kuhn length is determined either by small-angle neutron scattering in solution or by calculation using the bond angles and lengths via the freely rotating chain model.[4] For semiflexible conjugated polymers, these two methods agree nicely and the plateau modulus G_N^0 is correlated with backbone stiffness, allowing prediction of

G_N^0 just by estimating the Kuhn length.[4] That is very powerful, since the plateau modulus (number density of entanglements) is vital for understanding the semicrystalline modulus of conjugated polymers that have T_g below room temperature, needed for flexible electronics.[5]

The liquid crystalline phases, including ones that form in shear flow, can be detected by quantifying the shear rate dependence of birefringence.[6,7] We present some preliminary rheo-optical results using shear-induced polarized light imaging[8] (SIPLI) on an Anton Paar MCR-502 controlled stress rotational rheometer with a transparent bottom plate and a mirror-finish top plate. A polarized white light source comes from below the transparent bottom plate, reflects off the mirror-finish top plate and is collected by a CCD camera below the bottom plate, after passing through a crossed polarizer. This method facilitates identification of the nematic phase (at rest) and the critical shear rate for any flow-induced nematic alignment of polymers that have isotropic phases at rest.

REFERENCES

1. R. Xie, Y. Lee, M. P. Aplan, N. J. Caggiano, C. Müller, R. H. Colby and E. D. Gomez, Glass Transition Temperature of Conjugated Polymers by Oscillatory Shear Rheometry, *Macromolecules* **50**, 5146 (2017).
2. R. Xie, A. R. Weisen, Y. Lee, M. A. Aplan, A. M. Fenton, A. E. Masucci, F. Kempe, M. Sommer, C. W. Pester, R. H. Colby and E. D. Gomez, Glass Transition Temperature from the Chemical Structure of Conjugated Polymers, *Nat. Comm.* **11**, 893 (2020).
3. R. Xie, M. P. Aplan, N. J. Caggiano, A. R. Weisen, T. Su, C. Müller, M. Segad, R. H. Colby and E. D. Gomez, Local Chain Alignment via Nematic Ordering Reduces Chain Entanglement in Conjugated Polymers, *Macromolecules* **51**, 10271 (2018).
4. A. M. Fenton, R. Xie, M. P. Aplan, Y. Lee, M. G. Gill, R. Fair, F. Kempe, M. Sommer, C. R. Snyder, E. D. Gomez and R. H. Colby, Predicting the plateau modulus from molecular parameters of conjugated polymers, *ACS Central Science* **8**, 268 (2022).
5. R. Xie, R. H. Colby and E. D. Gomez, Connecting the Mechanical and Conductive Properties of Conjugated Polymers, *Advanced Electronic Materials*, 1700356 (2017).
6. D. Parisi, J. Seo, B. Nazari, R. P. Schaake, A. M. Rhoades and R. H. Colby, Shear-Induced Isotropic−Nematic Transition in Poly(ether ether ketone) Melts, *ACS Macro. Lett.* **9**, 950 (2020).
7. D. Parisi, J. Seo, R. P. Schaake, A. M. Rhoades and R. H. Colby, Shear-Induced Nematic Phase in Entangled Rod-Like PEEK Melts, *Prog. Polym. Sci.* **112**, 101323 (2021).
8. O. O. Mykhaylyk, N. J. Warren, A. J. Parnell, G. Pfeifer, J. Laeuger, Applications of Shear-Induced Polarized Light Imaging (SIPLI) Technique for Mechano-Optical Rheology of Polymers and Soft Matter Materials, *J. Polym. Sci., Polym. Phys.* **54**, 2151 (2016).

Nano Rheology of Glassy Materials using Dielectric Molecular Probe

Osamu Urakawa[1], Syogo Nobukawa[2], and Tadashi Inoue[1]

[1]Osaka University, Toyonaka, Japan
[2]Nagoya Institute of Technology, Nagoya, Japan

ABSTRACT

We consider viscoelastic effects of the matrix polymer on molecular dynamics of dielectric molecular probes using the generalized Langevin equation[1], which was derived to include the retardation effect of viscous force. By solving the equation, we successfully obtained a universal relationship between the complex relaxation modulus, $G^*_{eff}(\omega)$, and the dielectric constant of the probe, $\varepsilon^*_P(\omega)$. In the case of a viscous matrix, $\varepsilon^*_P(\omega)$ is described with the Debye function. If the matric is supposed to have a power-law type relaxation spectrum, $\varepsilon^*_P(\omega)$ is found to be the empirical Cole-Cole function, which is often observed for glassy materials. If the power law type G^*_{eff} has a cutoff time, $\varepsilon^*_P(\omega)$ can be represented with the Davison-Cole function. The proposed method was applied to a previous study[2] on a low-mass probe in a polystyrene matrix around the glass transition zone. By measuring $\varepsilon^*_P(\omega)$ of 5CB and 5CT used as dielectric probs, we successfully estimated the effective complex modulus, G^*_{eff} for the probes. The G^*_{eff} depends on the probe size and is not agreed with the bulk complex modulus of medium, $G^*(\omega)$, reflecting the local molecular dynamics. Thus, the dielectric molecular probe can be utilised to examine the viscoelastic properties in molecular level.[3]

ACKNOWLEDGEMENTS

We applicate professor Hiroshi Watanabe for his guidance and valuable comments.

REFERENCES

1. Mori H. Transport, Collective Motion, and Brownian Motion. *Prog. Theor. Physs. Acta*, **33 (3)**, 423–282., 1965. https://doi.org/10.1007/s00397-017-0999-y.
2. Nobukawa S.; Urakawa O.; Shikata T.: Inoue T. Cooperative Dynamics in Polystyrene and Low-Mass Molecule Mixtures, *Macromolecules*, **46**, 2206, 2013.
3. Urakawa O.; Nobukawa S.; Inoue T. Viscoelastic Effects on Molecular Dynamics of Dielectric Probes in Polymer Matrices, Nihon Reoroji Gakkaishi, in press.

8TH PACIFIC RIM CONFERENCE ON RHEOLOGY, May 15-19, 2023

DRIFT FLUX MODELING OF GAS RELEASE IN OIL SAND TAILING PONDS

O. Hajieghrary[1], M. Daneshi[2], I. Frigaard[1,2]

[1.] Department of Mechanical Engineering, University of British Columbia, (omid.eghrary@ubc.ca)
[2.] Department of Mathematics, University of British Columbia,

ABSTRACT

Gas bubbles trapped in liquids occur in natural and industrial processes such as tailing ponds, swamps, food processing, drilling fluids, etc. The bubbles are either introduced as part of the process (foamed cement, aerated chocolate, etc), or are generated in situ via chemical or biodegradation. These examples demonstrate a similar phenomenon of gas storage due to the slurry/paste-like properties of the materials. The trapping happens since the materials involved often show yield stress properties. Unless the bubble's buoyancy is large enough to overcome the yield stress, it will stay trapped in the material. For example, bubbles in a yield stress fluid are found in Canadian oil sands tailings, which consist of a mix of clay, bitumen residue, and various organic solvents. Both the Mature Fine Tailing (MFT) and Fluid Fine Tailing (FFT) strata of the tailing ponds show thixotropic yield stress properties. These layers provide a suitable environment for anaerobic bacteria to digest organic compounds and produce Carbon Dioxide (CO_2) and Methane (CH_4). The produced gasses will stay in FFT/MFT until the bubbles grow large enough to overcome yield stress and can rise to the surface. Methane release can be either continuous or transient. The latter scenario is that explored here.

In this study, we are interested in modeling the bubble growth and release in the tailing ponds and relating bacterial activities to the gas release rate. We are developing a 1D drift flux model to estimate the total bubble storage capacity of the pond as well as stability criteria for the pond. Using this model, we may estimate the gas release rate as a function of lake conditions: atmospheric pressure, temperature, and rheological properties. A set of experiments have also been conducted to study bubble cloud release in a test material (Carbopol). The drift flux velocity of bubbles in a model yield stress fluid can be estimated from these experiments and other sources.

Acknowledgement *This research was made possible by funding from NSERC and COSIA/IOSI (project numbers CRDPJ 537806-18 and IOSI Project #2018-10).*

RHEOLOGY OF FRESH CEMENT PASTE AS AFFECTED BY CELLULOSE NANOFIBRES AND SUPERPLASTICIZER

Jose R.A. Goncalves, Yaman Boluk, Mounir El Bakkari and Vivek Bindiganavile

University of Alberta, Edmonton, Canada

ABSTRACT

Cellulose nanofibres (CNFs) have high water-retention capacity, which can potentially affect the rheology of fresh cement paste. This study examines the effect of 0-1.2 vol.% fraction of dry CNFs, prepared with high-carboxyl content, upon the rheology of two series of cement pastes. One series was without any superplasticizer and the other was cast with a polycarboxylate-based superplasticizer, that was adjusted in dosage to keep the workability equal to that of the reference paste. Controlled shear-rate experiments were performed using a rotational rheometer with vane spindles, to obtain the flow data that was used to calculate the yield stress and viscosity. In addition, the direct method provided the static yield stress. The results reveal that adding CNFs greatly increased the yield stress and to a lesser extent, also the viscosity. As expected, the superplasticizer reversed this action.

BACKGROUND

Satisfactory workability in oil-well cementing is vital to its transport, placement, consolidation and finishing. It also ensures both strength and durability in the hardened composite. Fresh cement-based systems behave as per the Bingham model[1], whereby, once the shear stress exceeds a yield value, it increases linearly with the growth of the shear rate. However, other fluid models have been proposed including, the Herschel-Bulkley model, the Casson model and the Power Law model[2,3]. In all cases, two flow parameters are defined namely, (i) the yield stress and (ii) the plastic viscosity. In cement-based systems, the flow is governed by inter-particle contact, flocculation of fine particles, hydration kinetics of cement, the aqueous phase content, and the particle sedimentation, geometry, and size distribution. High range water-reducing admixtures, also called superplasticizers (SP) are often used to aid the flow of fresh cementitious composites. Cellulose nanofibres (CNFs) are a novel, renewable and bio-based fibrous derivatives of cellulose[4]. In comparison with other nanofibres, they are inexpensive and abundant in nature[5]. CNF is obtained as an aqueous suspension from chemically-assisted nano-

fibrillation after the biomass undergoes mechanical grinding[6]. One of the more common chemical agents is TEMPO (2,2,6,6-tetramethylpiperidine-1-oxyl radical)-mediated oxidation[7]. TEMPO breaks the hydrogen bonds of cellulose fibres and introduces several anionic carboxyl and hydroxyl groups on the nanofibrils' surface[8]. The surface-active groups render the cellulose nanofibre with strong charges to repel the nanofibrils away from one another, and impart high chemical reactivity, colloidal stability, tunability and, above all, exceptional hydrophilicity[9]. The CNF suspensions mostly behave as shear thinning fluids, although they are reported also to demonstrate thixotropic behaviour. To the authors' knowledge, there is no information for cement paste containing the CNF alongwith a superplasticizer. Hence, the focus of this study is to examine the rheological parameters of plastic cement pastes loaded with CNFs and combinations of CNF and SPs. The rheological parameters of two distinct series of CNF-reinforced pastes were examined. The first series had an increasing amount of the CNF gel, while the other incorporated judicious dosages of a polycarboxylate SP in addition to the CNF, with a view to keeping the flow within the range of the plain reference paste.

PRINCIPAL FINDINGS

The paste samples were examined first in accordance with the controlled-shear-rate protocol and later, with the direct-static-yield-stress method. The flow parameters were estimated based on curve fitting along the Herschel-Bulkley model, the Casson model and the Power Law model. The following conclusions may be drawn:

- Adding increments of CNF to the reference plain paste increases all the stress parameters and also the viscosity. The rise was more accentuated in the yield stress than in the viscosity. Consequently, the CNF decreases the workability of fresh cement paste.
- Adding the polycarboxylate-based SP to the CNF-reinforced cement paste universally lowers the viscosity and to a lesser extent, also the yield stress.
- All the mixtures that were reinforced with CNF demonstrate a shear thinning fluid behaviour. On the other hand, the mixtures having the largest dosage of both CNF and the superplasticizer behaved as a shear thickening fluid.
- The cellulose nanofibres bridge the cement particles and create a fibrous network. This uniformly raised the rheological parameters of CNF-reinforced cement paste. The polycarboxylate superplasticizer mitigates the above by lubricating the surface of the cement particles, facilitating ease of flow. This mechanism is illustrated in Figure 1.

ACKNOWLEDGEMENTS

This study was funded by the Natural Sciences and Engineering Research Council (NSERC) Canada as a Collaborative Research and Development grant, in partnership with Lehigh Hanson Canada, Millar-Western Forestry Industries and Alberta Innovates Bio-Solutions.

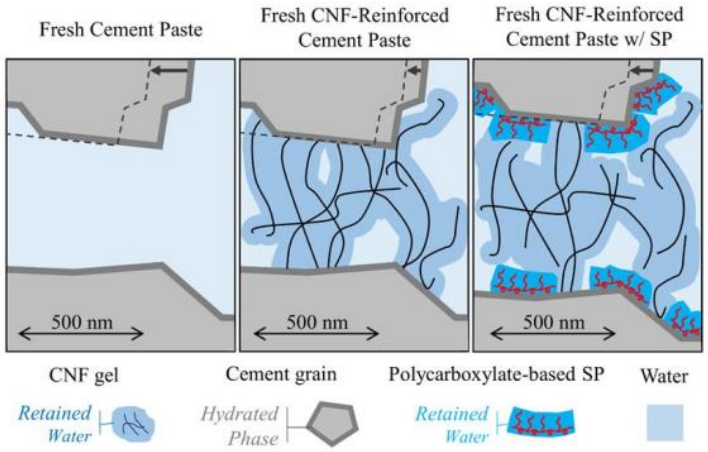

Figure 1: • CNFs restrain the solid particle displacement whereas SP mitigates this effect

REFERENCES

[1] G. H. Tattersall, Workability and Quality Control of Concrete, 14th Edition. Taylor & Francis, New York, US, 1991.

[2] A. Papo, Rheological models for cement pastes, Materials and Structures. 21(1) (1988) 1-41. https://doi.org/10.1007/BF02472527.

[3] G. Sant, C. F. Ferraris, J. Weiss, Rheological properties of cement pastes: A discussion of structure formation and mechanical property development, Cement Concrete Research. 38(11) (2008) 1286–1296. https://doi.org/10.1016/j.cemconres.2008.06.008.

[4] H. A. Barnes, J. O. Carnali, The vane-in-cup as a novel rheometer geometry for shear-thinning and thixotropic materials, Journal of Rheology. 34 (1991) 841-866. https://doi.org/10.1122/1.550103.

[5] O. Onuaguluchi, D. K. Panesar, M. Sain, Properties of nanofibre reinforced cement composites, Construction and Building Materials. 63 (2014) 119-124. https://doi.org/10.1016/j.conbuildmat.2014.04.072.

[6] X. Sun, Q. Wu, S. Lee, Y. Qing, Y. Wu, Cellulose nanofibres as a modifier for rheology, curing and mechanical performance of oil well cement, Scientific Reports. 6 (2016) 31654. https://doi.org/10.1038/srep31654.

[7] T. Saito, S. Kimura, Y. Nishiyama, A. Isogai, Cellulose nanofibres prepared by TEMPO-mediated oxidation of native cellulose, Biomacromolecules. 8(8) (2007) 2485-2491. https://doi.org/10.1021/bm0703970.

[8] M. El-Bakkari, V. Bindiganavile, J. Goncalves, Y. Boluk, Preparation of cellulose nanofibres by TEMPO-oxidation of bleached chemi-thermomechanical pulp for cement applications, Carbohydrate polymers. 203 (2019) 238-245. https://doi.org/10.1016/j.carbpol.2018.09.036.

[9] Z. Tang, W. Li, X. Lin, H. Xiao, Q. Miao, L. Huang, L. Chen, H. Wu, TEMPO-Oxidized cellulose with high degree of oxidation, Polymers (Basel). 9 (2017) 3-4. https://doi.org/10.3390/polym9090421.

DEFYING GRAVITY: THE FLUID MECHANICS OF OFF-BOTTOM PLUG PLACEMENT

I. Karimfazli[1], A. Ghazal[1]

[1]Department of Mechanical, Industrial and Aerospace Engineering, Concordia University
1515 St. Catherine W., Montreal, QC, H3G 2W1, Canada

ABSTRACT

The abandonment protocols of oil and gas wells may vary among regions and countries. Most commonly, however, two or more cement plugs are placed along the well for this purpose. The plugs above the lowermost plug are often referred to as off-bottom. Balanced-plug is a common technique to place off-bottom plugs. The placement process involves: (i) identifying the plug location, (ii) placing the injector at the target position and pumping the cement slurry, and (iii) pulling the injector out of the well once the cement slurry is levelled in the injector and the annulus. In Western Canada, it is common to use the balanced-plug method to place off-bottom plugs without using a barrier; i.e., to inject the cement slurry directly in wellbores that are otherwise filled with water.[2] A successful placement is achieved when the injected cement slurry (a yield stress fluid) accumulates at the target position, over the lighter wellbore fluids.

While displacement flows in primary cementing have been studied extensively, the hydrodynamics of the balanced-plug method, in the absence of a barrier, remain largely unexplored. Considering the hydrodynamics of the placement process, four primary phases may be presumed: (i) *the onset of injection*, (ii) *the quasi-steady injection*, (iii) *pulling out of the hole*, and (iv) *the final steady-state*. Each flow development phase is a complex two-fluid problem that may reveal diverse flow dynamics and different modes of instability. We develop hydrodynamic models of the process in a representative two-dimensional domain and explore the effect of fluid properties and the flow domain. Our findings provide a mechanistic perspective of the processes that may prevent the buoyancy-driven failure of the placement process and the role of the rheology of the fluid.

References

[1] M. Achang, L. Yanyao, and M. Radonjic. A Review of Past, Present, and Future Technologies for Permanent Plugging and Abandonment of Wellbores and Restoration of Subsurface Geologic Barriers. *Environmental Engineering Science*, 37(6):395–408, 2020.

[2] E. Trudel, M. Bizhani, M. Zare, and I. A. Frigaard. Plug and abandonment practices and trends: A british columbia perspective. *Journal of Petroleum Science and Engineering*, 183:106417, 2019.

[3] R. Govindarajan and K. C. Sahu. Instabilities in viscosity-stratified flow. *Annual review of fluid mechanics*, 46:331–353, 2014.

RHEOLOGICAL BEHAVIOR OF MATURE FINE TAILINGS

Amir Malmir, Jourdain H. Piette and Savvas G. Hatzikiriakos
Chemical and Biological Engineering Department
The University of British Columbia, Vancouver, BC, CANADA

ABSTRACT

The rheological behavior of mature fine tailings (MFTs) is investigated using transient and steady shear flow fields. First, the structure breakdown of intact MFT samples is examined by startup flow experiment at various shear rates. The yield stress of MFTs is estimated by the steady shear stress values at low shear rates. MFT samples exhibit thixotropy and positive hysteresis loop at short shearing time intervals in increasing and decreasing step-wise shear rate tests. The observed hysteresis loops and thixotropy disappear by increasing the shearing time intervals, as the systems reaches its equilibrium steady state structure. The time-dependent rheological behavior of MFTs is quantified by a structural kinetics model through dimensionless structure parameter, λ.(Toorman, Rheologica Acta, 36, 56-65 (1997)). The kinetic parameters are estimated based on steady-state stresses, elucidating the relative effects of shear rate and Brownian motion on build-up and breakdown of the structure. The flow behavior of MFTs predicted by structural kinetics model is nearly in agreement with the experimental data.

INVESTIGATIONS ON METHANE HYDRATE FORMATION, DISSOCIATION, AND VISCOSITY IN GAS-WATER-SAND SYSTEM

Shangfei Song[1], Shunkang Fu[2], Qingyun Liao[1], Bohui Shi[1], Hongju Chen[1,3] and Jing Gong[1]

[1] National Engineering Research Center of Oil and Gas Pipeline Transportation Safety / MOE Key Laboratory of Petroleum Engineering/ Beijing Key Laboratory of Urban Oil and Gas Distribution Technology, China University of Petroleum-Beijing, Beijing, China,
[2] PipeChina West East Pipeline Company, Shanghai, China
[3] Key Lab of Deepwater Engineering, CNOOC Research Institute, Beijing, China

ABSTRACT

Understanding the kinetics and viscosity of hydrate slurry in gas-water-sand system is of great significance for the high-efficiency and high-safety development of natural gas hydrates. The effect of micron-sized sands with various concentrations and particle sizes on the hydrate formation, dissociation, and viscosity in gas-water-sand system are investigated in this work. The experimental results show that the hydrate induction time in the sandy system is slightly prolonged compared to the pure gas-water system, and the inhibition effect first strengthens and then weakens as the sand concentration increases from 0 wt% to 5 wt%. Besides, the difference of hydrate formation amount in various cases is not obvious. The concentration and particle size of sand have little effect on the kinetics of hydrate formation. Both promoting and inhibiting effects on hydrate formation have been found in the sandy multiphase fluid. For the viscosity characteristics, there are three variations of hydrate slurry viscosity during the formation process: Steep drop type, S-type and Fluctuation type. Moreover, appropriate sand size is helpful to reduce the randomness of slurry viscosity change. Meanwhile, even at the same hydrate volume fraction, the slurry viscosity in the formation process is significantly higher than that in dissociation process, which needs further research. This work provides further insights of hydrate formation, dissociation, and viscosity in gas-water-sand system, which is of great significance for safe and economic development of natural gas hydrates.

ACKNOWLEDGEMENTS

This work is supported by the National Natural Science Foundation of China [Grand numbers: 52104069, 51874323, U20B6005]; Science Foundation of China University of Petroleum, Beijing [Grand number: 2462020YXZZ045], all of which are gratefully acknowledged.

Plenary Presentation - MATH 100 (12:50 PM - 1:50 PM)

COATING PROCESS FOR BATTERY ELECTRODE

Jaewook Nam
Department of Chemical & Biological Engineering, Institute of Chemical Processes, Seoul National University, South Korea

For next-generation electronics systems and devices, such as flexible displays and energy harvesting (or storage) devices, high performance, versatility, and flexibility are frequently necessary. A film, which is often a polymer or soft substrate with numerous layers of electrically conductive, semiconducting, and insulating materials superimposed on it, is a key component of these devices. These layers can be created using a variety of coating techniques. The continuous liquid coating technique, a kind of roll-to-roll process, is one of them and is widely acknowledged as an appealing way to generate affordable, high-throughput, and large-area coated layers. The coating liquid may exhibit complex rheological characteristics if it contains a variety of particles, additives (such a binder), and solvents. The main challenges in this process are how to regulate flows inside large manufacturing equipment to regulate microscopic properties, such as thickness homogeneity, particle microstructures inside coated layers, etc. Such problems require an understanding of the physical or chemical phenomena underlying them from a fundamental engineering perspective. Such knowledge might be beneficial for the process' analysis and design. For instance, while analyzing complex film formation flow in various types of applicators, such as slot die, roll, and spray, the rheological characteristics of a coating liquid must be taken into consideration. To help with the design of the drying machine, a microstructures index or indication must also be created. In this talk, various research initiatives to address these coating difficulties, including flows inside pipe systems and coating machines, will be shown. Some elements of these coating issues will also be highlighted.

8TH PACIFIC RIM CONFERENCE ON RHEOLOGY, May 15-19, 2023

VISCOELASTIC PROPERTIES OF BIDISPERSE LINEAR POLYMERS UNDER ELONGATIONAL FLOW

Evelyne van Ruymbeke[1], Alexis André[1,2] and Céline Hannecart[1,2]

[1]Bio and Soft Matter, IMCN, UCLouvain, Louvain-La-Neuve, Belgium
[2]Department of Chemical Engineering, KU Leuven, Celestijnenlaan 200F, 3001 Leuven, Belgium

ABSTRACT

The Doi−Edwards tube model, coupled with relaxation mechanisms, such as reptation, contour length fluctuation, and constraint release, allows us to quantitatively predict the linear viscoelastic properties of entangled polymers. However, for nonlinear elongational flows, large discrepancies between theoretical predictions based on the tube model and experimental results still persist. This is, for example, the case for the experimentally observed strong qualitative differences in extensional flow of entangled polystyrene (PS) melts and solutions, characterized by the same number of entanglements and exhibiting the same linear viscoelastic behaviour.[1] The cause of this non-universality is usually attributed either to a monomeric friction reduction or to an interchain pressure effect.

In this work, we investigate the extensional flow behaviour of binary blends of linear polymers, in order to further understand the role of the molecular environment on the stretch state of a probe chain. For this purpose, we measured the nonlinear extensional responses of different polystyrene (PS) chains, both in the monodisperse and bidisperse state, and systematically vary the concentration and the molar mass of the chains, to obtain different interactions between the long chains and their molecular environment. This allows us to highlight scaling relationships for describing the steady-state elongational viscosity.[2,3,4]

Our data confirm that the linear evolution of the steady-state extensional viscosity with the molar mass, that was first observed by Bach et al.[5] for melts, can be extended to polymeric solutions. The results also show that the steady-state extensional viscosity of bidisperse systems follow a simple mixing rule only if both components are stretching.[3]

While in a previous work, we found that all polystyrene long chains diluted in a short, non-stretching short chain matrix (with molar mass higher than 9 kg/mol) exhibit different transient strain hardening properties but the same apparent steady-state elongational viscosity; i.e., the long chains reach the same final stretch state,[5] we explore here the behaviour of these long

chains diluted in even shorter matrices, as it is expected that too short chains enhance the strain hardening of the long component.[6] By varying the composition of our solutions, we further quantify this effect.

REFERENCES

1. Huang, Q.; Mednova, O.; Rasmussen, H. K.; Alvarez, N. J.; Skov, A. L.; Almdal, K.; Hassager, O. Concentrated polymer solutions are different from melts: Role of entanglement molecular weight. *Macromol.* **46**, 5026−5035., 2013. https://doi.org/10.1021/ma4008434.
2. Hannecart, C.; Shahid, T., Vlassopoulos, D.; Oosterlinck, F.; Clasen, C.; van Ruymbeke, E. Decoding the steady elongational viscosity of monodisperse linear polymers using tube-based modeling, *J. Rheol* **66,** 197., 2022. https://doi.org/10.1122/8.0000182
3. André, A.; Shahid, T.; Oosterlinck, F.; Clasen, C.; van Ruymbeke, E., Investigating the transition between polymer melts and solutions in nonlinear elongational flow, Macromol. **54** (6), 2797-2810., 2021. https://doi.org/10.1021/acs.macromol.0c02542
4. Shahid, T.; Clasen, C.; Oosterlinck, F.; van Ruymbeke, E. Diluting Entangled Polymers Affects Transient Hardening but Not Their Steady Elongational Viscosity. *Macromol.* **52**, 2521−2530., 2019. https://doi.org/10.1021/acs.macromol.8b02701
5. Bach, A.; Almdal, K.; Rasmussen, H. K.; Hassager, O. Elongational viscosity of narrow molar mass distribution polystyrene. *Macromol*. **36**, 5174−5179., 2003. https://doi.org/10.1021/ma034279q
6. Huang, Q.; Alvarez, N. J.; Matsumiya, Y.; Rasmussen, H. K.; Watanabe, H.; Hassager, O. Extensional Rheology of Entangled Polystyrene Solutions Suggests Importance of Nemtic Interactions, *ACS Macro Lett*. **2**, 8, 741-744.; 2013. https://doi.org/10.1021/mz400319v

DUAL SLIP-LINK SIMULATION STUDY ON STRETCH-ORIENTATION-INDUCED REDUCTION OF FRICTION IN BI-DISPERSE BLENDS

Souta Miyamoto[1] Takeshi Sato[2] and Takashi Taniguchi[1]

[1] Graduate School of Engineering, Kyoto University, Kyoto 615-8510, Japan
[2] Institute for Chemical Research, Kyoto University, Kyoto 611-0011, Japan

ABSTRACT

We investigated the rheological properties of bi-disperse entangled-polymer blends under high-deformation-rate flows by slip-link simulations with a friction reduction mechanism. The friction reduction mechanism induced by the stretch and orientation (SORF) is important to predict the viscoelasticity in highly nonlinear regime under uniaxial elongational flows. To examine the applicability of this mechanism for bi-disperse systems, we incorporated an expression of friction reduction (Yaoita et al. Macromolecules 45:2773–2782 2012) into the Doi-Takimoto slip-link model (DT model). For six experimental bi-disperse systems, i.e., four polystyrene blends and two polyisoprene blends, the extended DT model where the order parameter of the friction reduction mechanism is evaluated through the component averages succeeds in reproducing the data under uniaxial elongation and shear. This success is due to the suppression of the stretch of the longer chains using the statistical average over each component. Through this study, the SORF expression improves the rheological prediction for bi-disperse entangled polymer melts under uniaxial elongational flows with strain rates comparable to or larger than the inverse of the Rouse relaxation time of the longer chains. Additionally, the predictions with the SORF using the component average for the stretches reproduce the steady viscosities because under elongational flows, the states of the components with different molecular weights clearly differ from each other depending on their Rouse relaxation time. The finding means that for chain dynamics, the friction coefficient is determined by the state of the surrounding polymer chains and the state of the chain[1].

ACKNOWLEDGEMENTS

We acknowledge the "Joint Usage/Research Center for Interdisciplinary Large-scale Information Infrastructures" and "High Performance Computing Infrastructure" in Japan (jh21001-MDH and jh220054) for supporting and providing computational resources Wisteria/BDEC-01 at the Information Technology Center, University of Tokyo.

REFERENCES

1. Miyamoto, S; Sato, T; Taniguch T, Stretch-orientation-induced reduction of friction in well-entangled bidisperse blends: a dual slip-link simulation study. Rheologica Acta **62**, 57-70, 2023.

ELONGATIONAL VISOCOSITY OF A POLY(STYRENE-B-2-VINYLPYRIDINE) BLOCK COPOLYMER FORMING SPHERICAL MICROPHASE-SEPARATED STRUCTURE

Yuya Doi,[1] Shumpei Yamakami,[1] Takato Ishida,[1] Takashi Uneyama[1] and Yuichi Masubuchi[1]

[1]Nagoya University, Nagoya 4648603, Japan

Block copolymers generally form microphase-separated structures, and thus exhibit characteristic linear and nonlinear rheological properties that reflect their structures, which is essentially different from homopolymers. Polystyrene (PS) and poly(2-vinylpyridine) (P2VP) have the same Kuhn segment size, the same glass transition temperature, and nearly identical melt viscoelastic properties, and hence poly(styrene-*block*-2-vinylpyridiene) (PS-*b*-P2VP) is a model block copolymer suitable for various linear and nonlinear rheological investigations. In fact, Takahashi et al. have experimentally examined the linear rheology and viscosity under shear flow of PS-*b*-P2VP melts with various molecular weights and compositions.[1,2] Over the past two decades, with the development of measurement instruments, the elongational viscosity of polymer melts and solutions has been extensively examined and their molecular picture is becoming better understood.[3] However, there are still limited reports on the elongational viscosity of block copolymers, and the full picture has not yet been clarified. In this study, we experimentally investigated the elongational viscosity of a PS-*b*-P2VP sample that forms a spherical microphase-separated structure. The PS-*b*-P2VP sample used in this study (purchased from Polymer Source) has a weight average molecular weight M_w = 101 kg/mol and volume fraction of P2VP Φ_{P2VP} = 0.092. This sample is hereafter denoted by SP009, reflecting Φ_{P2VP}. Disk-shaped samples of SP009 were prepared by hot pressing and annealing, and their elongational viscosity was measured by a filament stretch rheometer VADER1000 (Rheo Filament) at various strain rates $\dot{\varepsilon}$ (= 0.001~0.1 s^{-1}) at 200 °C. The terminal relaxation time τ_d of SP009, which originates from the relaxation of the spherical phase-separated interface determined by linear viscoelastic (LVE) measurements, is approximately 10^3 s at 200 °C, and hence the Weissenberg number Wi (= $\dot{\varepsilon}\tau_d$) corresponds to ca. 1~100. SP009 exhibits a steady-state elongational viscosity $\eta_E(\dot{\varepsilon})$ that is almost two order of magnitude lower than that expected from LVE even at Wi = 1, and $\eta_E(\dot{\varepsilon})$ decreases with increasing Wi, indicating the strain softening. Moreover, Wi dependence of $\eta_E(\dot{\varepsilon})$ itself is similar to that found in homopolymer melts.[3] In the presentation, we will discuss the origin of the strain softening observed in SP009.

1. Fang, L.; Takahashi, Y.; Takano, A.; Matsushita, Y. Molecular Weight Dependence of Viscoelastic Properties for Symmetric Poly(styrene-*b*-2-vinylpyridine)s in the Nanophase Separated Molten States. *Macromolecules*, **46 (17)**, 7097–7105, 2013. https://doi.org/10.1021/ma400957p
2. Takahashi, Y.; Fang, L.; Takano, A.; Torikai, N.; Matsushita, Y. Viscoelastic Properties of Low Molecular Weight Symmetric Poly(styrene-*b*-2-vinylpyridine)s in the Ordered and Disordered States under Steady Shear Flow. *Nihon Reoroji Gakk.*, **41 (2)**, 83–91, 2013. https://doi.org/10.1678/rheology.41.83
3. Bach, A.; Henrik, A.; Rasmussen, H. K.; Hassager, O. Elongational Viscosity of Narrow Molar Mass Distribution Polystyrene. *Macromolecules*, **36 (14)**, 5174-5179, 2003. https://doi.org/10.1021/ma034279q

PRIMITIVE CHAIN NETWORK SIMULATIONS FOR NON-LINEAR RHEOLOGY OF MONODISPERSE POLYSTYRENE MELTS WITH FRICTION CHANGE AND VIOLATION OF THE FLUCTUATION-DISSIPATION THEOREM

Yuichi Masubuchi[1], Giovanni Ianniruberto[2], Manfred Wagner[3] and Giuseppe Marrucci[2]

[1]Nagoya University, Nagoya, Japan
[2] Federico II University, Napoli, Italy
[3] Berlin Institute of Technology, Berlin, Germany

To describe the elongational viscosity of concentrated polymers, the change in monomeric friction has been proposed and implemented in molecular models[1]. In these theories, the validity of the fluctuation-dissipation theorem (FDT) is implicitly assumed. However, FDT requires local equilibrium, which is inconsistent with the mechanism of friction change induced by a disturbed monomeric environment. Indeed, a recent analysis of data on Rouse melts by Watanabe et al.[2] demonstrates that FDT is violated under fast flow; the Brownian force intensity is almost independent of the flow rate, even though drag friction drastically decreases. In this study, Brownian simulations using a multi-chain slip-link model[3] were conducted for two monodisperse entangled polystyrene melts, for which non-linear shear and elongational rheology data are available in the literature. Two different friction reduction models[4,5] were examined, and the effect of switching FDT on and off was tested. The results demonstrate that irrespective of FDT, the two friction models examined can reasonably well reproduce the rheology, even with the same model parameters. This finding supports the use of molecular theories assuming the validity of FDT since the violation of FDT does not significantly affect the prediction of on-linear rheology.

(1) Ianniruberto, G.; Marrucci, G.; Masubuchi, Y. Melts of Linear Polymers in Fast Flows. *Macromolecules* **2020**, *53* (13), 5023–5033. https://doi.org/10.1021/acs.macromol.0c00693.

(2) Watanabe, H.; Matsumiya, Y.; Sato, T. Revisiting Nonlinear Flow Behavior of Rouse Chain: Roles of FENE, Friction-Reduction, and Brownian Force Intensity Variation. *Macromolecules* **2021**, *54* (8), 3700–3715. https://doi.org/10.1021/acs.macromol.1c00013.

(3) Masubuchi, Y.; Takimoto, J.-I.; Koyama, K.; Ianniruberto, G.; Marrucci, G.; Greco, F. Brownian Simulations of a Network of Reptating Primitive Chains. *J. Chem. Phys.* **2001**, *115* (9), 4387–4394. https://doi.org/10.1063/1.1389858.

(4) Yaoita, T.; Isaki, T.; Masubuchi, Y.; Watanabe, H.; Ianniruberto, G.; Marrucci, G. Primitive Chain Network Simulation of Elongational Flows of Entangled Linear Chains: Stretch/Orientation-Induced Reduction of Monomeric Friction. *Macromolecules* **2012**, *45* (6), 2773–2782. https://doi.org/10.1021/ma202525v.

(5) Wagner, M. H.; Narimissa, E. A New Perspective on Monomeric Friction Reduction in Fast Elongational Flows of Polystyrene Melts and Solutions. *J. Rheol.* **2021**, *65* (6), 1413–1421. https://doi.org/10.1122/8.0000345.

UNIVERSALITY OF POLYMER MELTS

Chen-Yang Liu[1]

[1]Institute of Chemistry, the Chinese Academy of Sciences, Beijing, China

ABSTRACT

The packing length p, measured as the ratio of the occupied volume over the cross-sectional area R_0^2 of a polymer coil, is introduced as a renormalized length scale that defines the invariant degree of polymerization $\bar{N}$ and so provides a universal blob-based description of the *single-chain* size ($R_0^2 = \bar{N}p^2$). Different polymer melts with chains represented by the same number of blobs $\bar{N}$ will have identical conformational statistics and *many-chain* packing structures in the renormalized space, which is the origin of the universal dynamics in entangled and unentangled polymer melts.

8TH PACIFIC RIM CONFERENCE ON RHEOLOGY, May 15-19, 2023

COMPUTATIONAL ROD CLIMBING AND DIPPING DEPENDENT UPON NORMAL STRESSES

Youngdon Kwon[1]

[1]School of Chemical Engineering, Sungkyunkwan University, 2066 Seobu-ro, Jangan-gu, Suwon, Gyeonggi-do 16419 Korea

ABSTRACT

With recent advancement in accurately measuring the second normal stress difference, the rheology community becomes interested in the Weissenberg effect, i.e., rod climbing[1], which is caused and regulated by the second (N_2) as well as the first normal stress difference (N_1). In this study, computational description of the rod climbing is carried out with the Leonov viscoelastic model implemented. First, we adjust the relative magnitude of the first and the second normal stress differences in simple shear flow in terms of constitutive modification of the equations within appropriateness for mathematical well-posedness. Applying the finite element analysis combined with the level set method, we observe that the climbing height of the liquid decreases as the relative strength of the second normal stress increases and eventually the rod climbing transforms into the rod dipping. This transition is proven to occur when the absolute value of the second normal stress difference is a quarter of the first one, which coincides with the classical result derived under the assumption of the second order fluid[2]. Furthermore, it is also shown to incur reversal of rotational direction in secondary flow.

RESULTS AND DISCUSSION

To numerically express the rod climbing of the viscoelastic liquid, we employ the Leonov viscoelastic constitutive equation. Following is the mathematical representation of rheological field equations applied in this study:

$$\overset{\nabla}{\mathbf{c}} + \frac{1}{\theta}\left[b_1\left(\mathbf{c}^2 - \frac{I_1 + I_2}{3}\mathbf{c} + \boldsymbol{\delta}\right) + \frac{I_2}{3}\mathbf{c} - \boldsymbol{\delta}\right] = \mathbf{0},$$

$$\text{Mooney potential: } U = \frac{G}{2}[(1-\beta)I_1 + \beta I_2 - 3],$$

$$\boldsymbol{\tau} = 2(1-s)\left(\frac{\partial U}{\partial I_1}\mathbf{c} - \frac{\partial U}{\partial I_2}\mathbf{c}^{-1}\right) + 2s\eta\mathbf{e} = (1-s)G[(1-\beta)\mathbf{c} - \beta\mathbf{c}^{-1}] + 2s\eta\mathbf{e}. \qquad (1)$$

Here $\mathbf{c}$ is the conformation tensor expressing the recoverable strain, $\mathbf{v}$ is velocity, G is the modulus, θ is the relaxation time, $\eta = G\theta$ is the zero shear viscosity, the invariants of $\mathbf{c}$ are defined as $I_1 = \mathrm{tr}\,\mathbf{c}$ and $I_2 = \frac{1}{2}\left({I_1}^2 - \mathrm{tr}\,\mathbf{c^2}\right)$, and $\overset{\nabla}{\mathbf{c}} \equiv \frac{d\mathbf{c}}{dt} - \nabla\mathbf{v}^T \cdot \mathbf{c} - \mathbf{c} \cdot \nabla\mathbf{v}$ is its upper convected time derivative. $\boldsymbol{\tau}$ is the stress, s is the retardation parameter and $\mathbf{e} = 1/2\,(\nabla\mathbf{v} + \nabla\mathbf{v}^T)$. b_1 and β are fitting parameters for proper description of liquid, they as well control the magnitude of the normal stress differences in shear flow and their admissible range lie between 0 and 1. Since the steady shear flow curve (shear rate vs. shear stress) shows non-monotonic behaviour in the case of $1/2 < b_1 \leq 1$, its specification in $0 \leq b_1 \leq 1/2$ is appropriate for physical consistency as well as mathematical stability.

Simple analysis shows that the relation $-N_2/N_1 = b_1/2$ in simple shear flow holds in the asymptotic limit of vanishing shear rate when $\beta = 0$. Also, we can prove that the effect of normal stresses in the Weissenberg effect disappears when $-N_2/N_1 = 1/4$ and the rod climbing (precisely dipping) is solely determined by the centrifugal force, which exactly coincides with the classical analysis obtained for the second order fluid[2].

Rod climbing is a viscoelastic phenomenon expressed by the combination of normal stresses, centrifugal force and surface tension. Adjusting values of β as well as b_1 and thus modulating the relative amount of the first and second normal stress differences in the flow, we obtain the result of **Fig. 1** which shows simulated interfaces of rotating viscoelastic liquid according to the ratio of normal stresses on the rod surface. One can distinctly observe that the height of liquid surface near the rod decreases and eventually the climbing transforms to the dipping as the relative amount of N_2 increases.

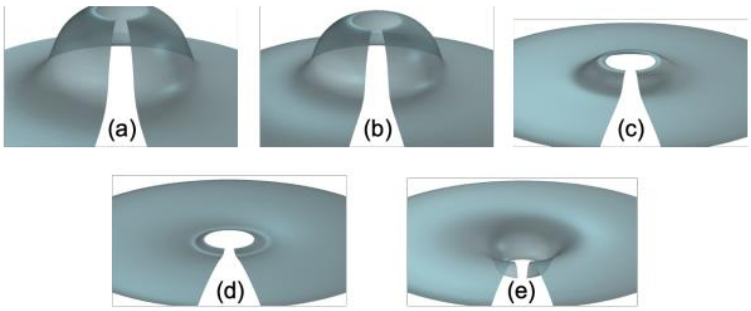

Figure 1: Shapes of gas-liquid interface at the Deborah number $De = 0.298$ for $-N_2/N_1$ equal to (a) 0; (b) 0.092; (c) 0.187; (d) 0.236; (e) 0.286

Indeed, the surface profile is shown to be determined mainly by the weak secondary flows, and at the transition of rod climbing into dipping the reversal of rotational direction in secondary flow is found to occur. The present work suggests that the rod climbing experiment cooperated with computational modelling may be utilized at least as a tool supporting the rheometry measuring normal stresses in simple shear flow.

ACKNOWLEDGEMENTS

This research was supported by Basic Science Research Program through the National Research Foundation of Korea (NRF) funded by the Ministry of Education (NRF-2021R1F1A1046417).

REFERENCES

1. Maklad, O.; Poole, R.J. A review of the second normal-stress difference; its importance in various flows, measurement techniques, results for various complex fluids and theoretical predictions , *J. Non-Newton. Fluid Mech.* **292**, 104522, 2021.
2. Beavers, G. S.; Joseph, D. D. The rotating rod viscometer, *J. Fluid Mech.* **69 (3)**, 475–511, 1975.

ALIGNMENT OF WORMLIKE MICELLES UNDER SHEAR FLOW: COMPARISON WITH POLYMERS

Yusuke Koide and Susumu Goto

Osaka University, Osaka, Japan

ABSTRACT

We investigate the effect of scission on the alignment of wormlike micelles under shear flow. For this purpose, we conduct dissipative particle dynamics simulations of nonionic surfactant and polymer solutions. To compare the alignment of wormlike micelles and polymers, we introduce the Weissenberg number defined as the product of the shear rate and the longest relaxation time. Comparing their mean orientation angles demonstrates that wormlike micelles align less in the flow direction than polymers when the Weissenberg number is larger than a threshold value. By evaluating the average lifetime of wormlike micelles, we show that flow-induced scission causes the suppression of micellar alignments.

INTRODUCTION

It is well known that polymers under shear flow align more in the flow direction as the shear rate increases. Similarly to polymers, rodlike and wormlike micelles also align in the flow direction. However, unlike polymers, micelles constantly exhibit scission and recombination. Moreover, as the shear rate increases, scission occurs more frequently due to flow-induced scission[1]. Recent experimental results suggest that scission kinetics affects micellar alignment for high shear rates[2]. However, little is known about the effect of scission on micellar alignment because it is difficult to experimentally measure the scission frequency and observe the structures and dynamics of individual micelles in flowing solutions. In the present study, we investigate both the alignment and scission kinetics of wormlike micelles under shear flow using the dissipative particle dynamics (DPD) simulations. Specifically, to reveal the scission effect on micellar alignment, we compare the alignment of wormlike micelles and polymers (i.e., chains without scission kinetics) and evaluate the average lifetime of micelles under shear flow.

SIMULATION METHOD

The model of a nonionic surfactant molecule contains a hydrophilic head particle and two hydrophobic tail particles, which are connected by harmonic springs. The interaction parameters between particles are the same as in our previous study[1]. For DPD simulations of polymer solutions, we use

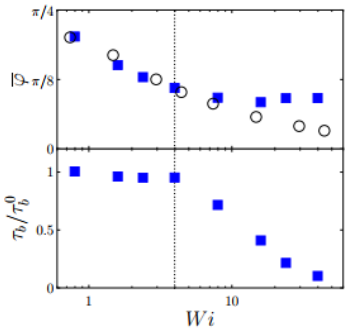

Figure 1: Weissenberg-number Wi dependence of mean orientation angle $\overline{\varphi}$ (top panel) for polymer chains (○) and micelles with $N_{\rm ag} = 400$ (■) and average lifetime τ_b (bottom panel) normalized by the value τ_b^0 at equilibrium. The black dotted line indicates the threshold Weissenberg number Wi_c for flow-induced scission.

the fully flexible polymer model used in the previous study[3]. To generate a uniform shear flow, we use the Lees-Edwards boundary condition and the SLLOD equations.

RESULTS

To investigate the effect of scission kinetics on micellar alignment, we compare the alignment of wormlike micelles and polymers (i.e., chains without scission kinetics). Since wormlike micelles and polymers have different timescales, we introduce the Weissenberg number $Wi = \tau\dot{\gamma}$ defined as the product of the longest relaxation time τ and the shear rate $\dot{\gamma}$. We estimate τ of polymers by fitting the autocorrelation function $C(t)$ of the end-to-end vector with an exponential function $C_0 \exp(-t/\tau)^3$. For wormlike micelles, we employ the method proposed in our previous study[1]. This method considers the scission effect on micellar relaxation. We define the direction of micelles and polymers as the eigenvector $\boldsymbol{e}^{(1)}$ of the gyration tensor with the largest eigenvalue. To evaluate the alignment in the flow direction, we focus on the angle φ defined by $\tan\varphi = e_y^{(1)}/e_x^{(1)}$. Here, x and y indicate the flow and gradient directions, respectively. In the following, we characterize Wi dependence of alignment with a mean orientation angle defined as $\overline{\varphi} = \langle e^{2i\varphi}\rangle/2$ [4]. The top panel of Fig. 1 shows $\overline{\varphi}$ of micelles with the aggregation number $N_{\rm ag} = 400$ and polymers as a function of Wi. When Wi is smaller than the threshold Weissenberg number $Wi_c(\simeq 4)$, $\overline{\varphi}$ of micelles and polymers collapse on a single function of Wi, indicating the similar alignment behavior of wormlike micelles and polymers. In contrast, wormlike micelles have larger values of $\overline{\varphi}$ than polymers for $Wi \gtrsim Wi_c$. This deviation demonstrates the suppression of micellar alignments in stronger shear flow.

To explore the origin of the alignment suppression, we evaluate the average lifetime τ_b of wormlike micelles under shear flow. The definition of micellar scission and the method to evaluate τ_b are the same as in our previous study[1]. The bottom panel of Fig. 1 shows τ_b normalized by the value τ_b^0

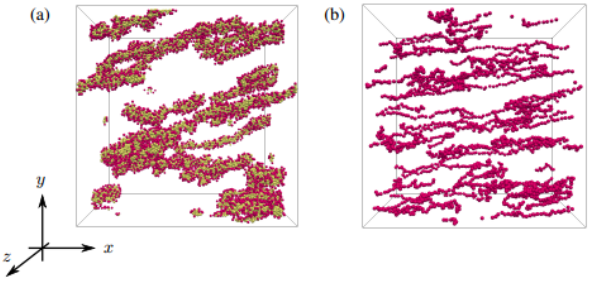

Figure 2: Visualization of (a) micelles with $200 \leq N_{\mathrm{ag}} \leq 600$ for $Wi = 48$ and (b) polymers for $Wi = 44$. In panel (a), hydrophilic and hydrophobic particles are indicated in red and yellow, respectively. In panel (b), some of the polymers in the system are shown for clarity.

at equilibrium as a function of Wi. Interestingly, $\tau_b/{\tau_b}^0 \simeq 1$ for $Wi \lesssim Wi_c$, whereas $\tau_b/{\tau_b}^0 \lesssim 1$ for $Wi \gtrsim Wi_c$. Therefore, we conclude that flow-induced scission occurs for $Wi \gtrsim Wi_c$ and it suppresses micellar alignments. Although one may think that the suppression is intuitively obvious considering the increase in the number of smaller micelles, we emphasize that we have evaluated the micellar alignment for fixed N_{ag}.

We also confirm the suppression of micellar alignments through visualization of wormlike micelles and polymers for a given Wi. Figure 2 (a) shows micelles with $200 \leq N_{\mathrm{ag}} \leq 600$ for $Wi = 48$, and Fig. 2 (b) shows some polymers which are randomly chosen for $Wi = 44$. In Fig. 2 (b), polymers significantly align in the flow direction, whereas wormlike micelles slightly tilt from the flow direction in Fig. 2 (a). This observation is consistent with the quantitative results shown in Fig. 1. In the conference, we will also demonstrate the mechanism of the alignment suppression due to flow-induced scission through the effective longest relaxation time under shear flow.

REFERENCES

1. Koide, Y., Goto, S. Flow-induced scission of wormlike micelles in nonionic surfactant solutions under shear flow. *J. Chem. Phys.* **157**, 084903, 2022.
2. Arenas-Gómez, B., Garza, C., Liu, Y., Castillo, R. Alignment of worm-like micelles at intermediate and high shear rates. *J. Colloid Interface Sci.* **560**, 618-625, 2020.
3. Jiang, W., Huang, J., Wang, Y., Laradji, M. Hydrodynamic interaction in polymer solutions simulated with dissipative particle dynamics. *J. Chem. Phys.* **126**, 044901, 2007.
4. Fisher, N. I. *Statistical Analysis of Circular Data*; Cambridge University Press, 1993.

MOLECULAR DYNAMICS SIMULATION OF THE BEHAVIOR OF THIN LUBRICATION FILM

Dongjie Liu, Fei Chen*, Jinjia Wei

School of Chemical Engineering and Technology, Xi'an Jiaotong University,
No. 28, Xianning West Road, Xi'an, Shaanxi 710049, P. R. China

ABSTRACT

Lubrication system is an essential component for spacecrafts, and lubrication failure has become one of the challenges in developing advanced space technology. However, the process and mechanism of lubrication in space is still unclear due to a complex environment in both physicochemical and mechanical aspects. Molecular dynamics simulations provide new insights to understand the lubrication behavior, especially at the thin film lubrication state. In this work, we study the lubricant conformation changes and energy transfer of confined thin lubricant films by molecular dynamics simulations. It can be concluded that the thickness of film has a power exponential relationship with the pressure loads and the film presents a stratification phenomenon. By introducing the moving slab, the film velocity will redistribute under the entanglement among polymer chains and the friction of the adjacent layers, during which the polymer conformation will change through a "one-step" or "two-step" adjustment. Under low pressure loads, the film behaves like the Couette flow and the temperature profile is parabolic as well as symmetrical, with the maximum temperature appearing at the center of the lubrication film, which may cause the film's viscosity to diminish and ultimately result in lubrication failure. Under high pressure load, the boundary slip phenomenon occurs and the temperature jump exists. From our simulations, it can be noted that the increase in pressure load can lead to a boundary slip phenomenon, where the load-carrying capacity decreases due to the slip and lubrication failure may occur. This work provides new guidance in understanding the lubrication behavior in space.

EFFECT OF VISCOSITY CONTRAST IN STRUCTURE -RHEOLOGY RELATIONSHIP IN SHEARED LAMELLAR MESOPHASE IN 3-D

Arkaprava Pal[1], V Kumaran[2]

[1,2]IISc Banaglore, Bengaluru 560012, India

The structure-rheology relation in a sheared lamellar mesophase is studied by varying Ericksen number Er (viscous/elastic stress), Schmidt number Sc_o (momentum/mass diffusivity) and difference in viscosity between hydrophilic and hydrophobic phase(μ_1) using a mesoscale model. It is observed that the coarsening process is not altered by viscosity contrast for any Er or Sc, because the dominant mechanism is diffusion at early times, but the scaled effective viscosity evolution (scaled by well aligned span wise configuration viscosity) is different for systems with contrast at both before and after segregation . After layer formation, the scaled effective viscosity decreases slowly for systems with high viscosity contrast, because the process is affected by momentum transfer. The effect of viscosity contrast is prominent at a moderately high value of $Er = 0.03$, where the stiffness of the layers leads to a steady state defect density in layers aligned in the span-wise direction (shown in Fig.**??**) at low Sc_o which is otherwise perfectly aligned state for no contrast. However, viscosity contrast reduces defect density at higher Sc_o but still the effective viscosity is enhanced.

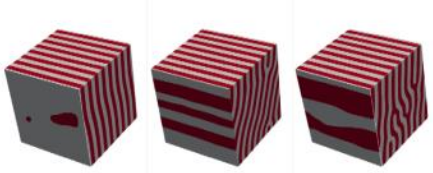

(a) (b) (c)

Figure 1: steady state configuration at $Sc_o = 0.33$, $Er = 0.03$ (a) $\mu_1 = 0.0$ (b) $\mu_1 = 1.0$ (c) $\mu_1 = 2.0$

This significant change in long time layer arrangement and effective viscosity due to introduction of viscosity contrast is not present at higher $Er = 0.3$. The dominant contribution of shear stress is from viscous effects for lesser stiff layers and presence of partially formed layers in velocity gradient direction brings the viscosity below 1. When Er is decreased further ($Er = 0.003$) at low $Sc_o = 0.33$, the alignment direction changes from span-wise to wall normal direction with tilted layers, though the viscosity decease's scaling with time after coarsening is same as that at moderately high Er. Despite having a direction change of alignment being seen on introduction of contrast, long time limit viscosity is hardly altered though transient effective viscosity is seen to be much higher as usual due to having stiff layers in low Er limit.The change in layer arrangement at steady state could be because the flow of stiff layers through low viscosity regions results in the layer tilt and alignment in wall normal direction whose signature is much slower decrease of effective viscosity after segregation.However this change in steady state layer normal direction is missing for higher Sc_o in this regime again signifies the importance of higher momentum transfer rate in alignment process.

8TH PACIFIC RIM CONFERENCE ON RHEOLOGY, May 15-19, 2023

SIMULATION OF COMPETITION BETWEEN REACTION AND RELAXATION IN GELATION KINETICS

Takashi Uneyama[1]

[1]Nagoya University, Nagoya, Japan

ABSTRACT

Recently, a new type of network formation process in a dilute tetra-functional polymer solution was reported[1]. The percolation process during the gelation in a dilute solution induces large scale phase-separated structures, and the resulting gel becomes turbid. One interpretation for the formation of such phase-separated structures is that the polymer-rich regions which are much larger than precursor polymers are formed during the gelation process. Since the geleation process in essentially nonequilibrium, such a structural formation should be controlled by the kinetics of gelation. In this work, we propose a simple lattice model which can handle the competition between the reaction and the relaxation of polymers. We show that the phase-separation like structures can be reproduced by our simple model when the reaction process is much slower than the relaxation process.

MODEL

To study the gelation process at the long time scale, coarse-grained models are useful. In the previous work[1], a coarse-grained molecular model in which a tetra-functional polymer is expressed only with five points was utilized. Even with such a coarse-grained model, it is not easy to perform very long time simulations with a very low reaction rate.

To overcome the difficulty, we propose more coarse-grained and simplified model. We model a tetra-functional polymer by just one point, and put them on a two-dimensional square lattice with the lattice constant b. Initially, polymers (particles) are randomly dispersed on the lattice, and each polymer has four unreacted arms. Two polymers can react and form a covalent bond between them, if they have unreacted sites and the distance between them is short. After the reaction, the number of unreacted sites decreased. A polymer can randomly jump on the lattice. If a polymer is not reacted at all, this random motion can be interpreted as the diffusion. If a polymer is reacted, then it is a part of a cluster or a network. Then the random motion can be interpreted as the relaxation of a cluster or a network.

Both the reaction and jump are stochastic. If we ignore collective motion, we can utilize the Monte Carlo model. We employ the following rules for the Monte Carlo model. At one Monte Carlo trial, a reaction or a jump is randomly attempted. The probability to For the reaction, we

select a polymer randomly, and then select a neighboring site randomly. The nearest neighbor and next near-lest neighbor sites are candidates for the neighboring site. If there is a polymer on the neighboring site, and if two polymers have unreacted arms, the reaction occurs by the following probability:

$$P_{\text{react}} = \min(1, \exp(-E_{\text{bond}}/k_BT)). \tag{1}$$

Here, E_{bond} is the elastic energy of a newly created bond and k_BT is the thermal energy. We employ the elastic energy $E_{\text{bond}} = k(\Delta r^2 - b^2)/2$, with k being the spring constant and Δr being the distance between two polymers.

For the jump, we select a polymer randomly and then select a neighboring site. If the neighboring site is not occupied by a polymer, then the polymer jumps to the neighboring site by the following probability:

$$P_{\text{jump}} = \min(1, \exp(-\Delta E/k_BT)). \tag{2}$$

ΔE is the difference of the total bond energy before and after the jump. We express the number of reacted arms of the target polymer as n, and the distance between this polymer and the j-th polymer connected to this polymer before and after the jump as Δr_j and $\Delta r'_j$. Then we have

$$\Delta E = \sum_{j=1}^{n} \frac{k}{2}(\Delta r_j'^2 - \Delta r_j^2). \tag{3}$$

RESULTS

We perform lattice Monte Carlo simulations with some different parameter sets. We set the lattice constant $b = 1$, the spring constant $k = 1$, and the thermal energy $k_BT = 1$. The nubmer of lattice sites is 128^2. We change the probability to attempt the reaction event f and the occupied fraction of polymers ϕ. By tuning f, we can control the competition between the reaction and relaxation processes. **Fig. 1** shows the structural evolution in a simulation with $f = 10^{-3}$ and $\phi = 0.5$. After 500 Monte Carlo steps (MCS), most of arms are reacted and percolated network structure is formed. We observe that the density fluctuation grows as the simulation proceeds. Finally we observe a pattern which is similar to those observed in the phase separation process[2]. Unlike the normal phase separation process, however, the spatial scale of the density fluctuation does not grow after the reaction is completed. This means that the pattern observed in our model is essentially frozen (or arrested). Although our model is highly simplified, we consider that it can qualitatively capture the kinetics of the gelation-induced structural formation.

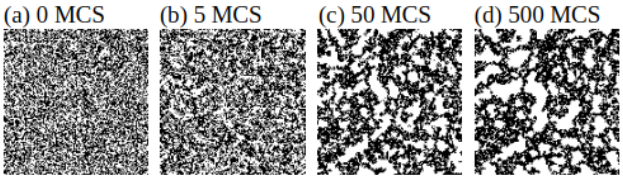

Figure 1: Snapshots of a simulation with $f = 10^{-3}$ and $\phi = 0.5$. (a) The initial state, and (b) 5 Monte Carlo steps (MCS), (c) 50 MCS, and (d) 500 MCS. Polymers are visualized as black dots.

Fig. 2 shows the snapshots at 500 MCS with different values of f and ϕ. In **Fig. 2**(a) and (b), we fix the reaction probability f and change the polymer fraction ϕ. If ϕ is small (the dilute condition), we observe a clear phase-separation like pattern. But if ϕ is large, the density fluctuation is suppressed and the patter seems to be close to homogeneous. In **Fig. 2**(c) and (d), we fix the polymer fraction ϕ and change the reaction probability f. If f is small (the reaction is slow compared with the structural relaxation), we observe a large phase-separation like pattern. On the other hand, if f is large, the characteristic length scale of the phase-separation pattern is small. From these simulation results, we consider that the gelation-induced pattern is controlled by the competition between the reaction and structural relaxation. If the polymer fraction is small and/or the reaction probability is low, clusters and networks can easily relax into compact forms before the reaction proceeds. Then we observe dense polymer-rich regions. If the polymer fraction is large and/or the reaction probability is high, reaction occurs before clusters and networks relax. In this case, the formation of polymer-rich regions is suppressed, and we observe rather homogeneous structure.

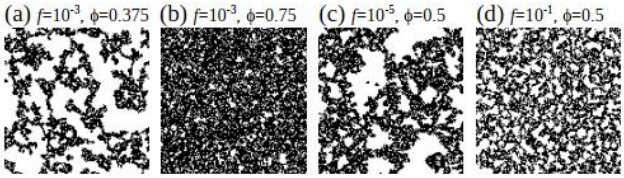

Figure 2: Snapshots of a simulation with different reaction probabilities and polymer fractions after 500 Monte Carlo steps. The same reaction rate ($f = 10^{-3}$) with the different fraction: (a) $\phi = 0.375$ and (b) $\phi = 0.75$. ($\phi = 0.5$ corresponds to **Fig. 1**(d).) The same polymer fraction ($\phi = 0.5$) with the different reaction probability: (c) $f = 10^{-5}$ and (d) $f = 10^{-1}$. ($f = 10^{-3}$ corresponds to **Fig. 1**(d).)

ACKNOWLEDGMENTS

This work was supported by JST, PRESTO Grant Number JPMJPR1992.

REFERENCES

1. Ishikawa S. et al Percolation induced gel–gel phase separation in a dilute polymer network, arXiv:2202.09754 (2022).
2. Onuki A. *Phase Transition Dynamics*, Cambridge University Press, 2002.

Quantifying the Enhancement Effect of Strain Induced Crystallization on Tearing Energy by Edge Crack Test Method

Katsuhiko Tsunoda[1], Kenji Urayama[2]

[1]Suntainable and Advanced Materials Division, Bridgestone Corporation, Tokyo, Japan
[2]Department of Material Chemistry, Graduate School of Engineering, Kyoto University, Kyoto, Japan

ABSTRACT

Fracture toughness in elastomer can be described utilizing fracture mechanics based on the tearing energy concept. Tearing energy, G, is significantly influenced by the visco-elastic properties arising from mechanical hysteresis, resulting G increases with increasing strain rate and/or decreasing ambient temperature as viscoelastic energy dissipation increases.

However, this influence of viscoelastic energy dissipation becomes less marked for strain induced crystallizing elastomer, like natural rubber (NR). If the sufficient strain induced crystallization (SIC) can be generated ahead of advancing crack tip, catastrophic crack growth process is postponed and fracture process is governed by SIC originated strength, G_{SIC}, which is considerably higher than viscoelastic energy dissipation effect. Hence SIC elastomer can be regarded as self-assemble elastomer. However, this self-assemble capability has threshold condition as crystal has melting temperature and SIC is kinetic phenomena. In another word, fracture toughness in SIC elastomer shows transition between governed by SIC and merely by viscoelastic energy dissipation at certain temperature and strain rate. It is clearly important to fully understand this threshold condition for engineering appreciation but was not fully investigated and elucidated.

It has been shown that the failure of elastomer is initiated from flaws or stress raisers present in elastomer. For a strain-crystallizing elastomer, an abrupt drop in fracture toughness as a function of initial flaw size is observed. The mechanism of this abrupt fall is thought to be the change in fracture process from a cyclic crack growth process to catastrophic tearing. We focused on this failure mechanism transition to determine the threshold condition for generating G_{SIC} and extended conventional theoretical studies.

In this presentation, newly extended theoretical understanding for fracture toughness transition as a function of initial crack length, quantitative determination of G_{SIC} and its threshold condition linking to nano-micro-macro polymer structure will be reported.

REVEALING THE CORRELATION BETWEEN STRAIN-INDUCED CRYSTALLIZATION AND LOCAL STRAIN FIELD AROUND THE CRACK-TIP OF NATURAL RUBBER

Thanh-Tam Mai[1], Tomohiro Yasui[2], Ruito Tanaka[2], Hiroyasu Masunaga[3], Taizo Kabe[3], Katsuhiko Tsunoda[4], Shinichi Sakurai[2] and Kenji Urayama[1]

[1]Kyoto University, Kyoto, Japan
[2]Kyoto Institute of Technology, Kyoto, Japan
[3]Spring-8, Hyogo, Japan
[4]Bridgestone Corporation, Tokyo, Japan

ABSTRACT

Natural rubber (NR)[1] exhibits strain-induced crystallization (SIC) which is an important feature setting NR apart from other elastomer types. SIC serves as a self-strengthening mechanism, significantly improving the mechanical strength and fracture toughness of the rubber[2]. Specifically, the crystallization that occurs near the crack-tip increases crack-growth resistance which ultimately determines the lifespan of the elastomers[3]. Indeed, several studies[4-7] revealed the occurrence of SIC near the crack-tip of NR using micro-beam wide-angle X-ray scattering (μ-WAXS). In general, the area near the crack-tip has an inhomogeneous strain distribution as characterized by digital image correlation (DIC) technique[8,9]. However, the correlation between the SIC and strain field near the crack-tip has yet to be fully explored and comprehended[1-3].

In this study, we investigate the correlations between the degree and orientation of SIC, and the local strain field around the crack-tip in NR using a combination of μ-WAXS and μ-DIC techniques. We characterize the boundary of the SIC region and the spatial distributions of the crystallinity index and the c-axis of the SIC crystals. By relating the 2D strain field, we elucidate the strain criteria for the occurrence of SIC, and the relationship between the c-axis of SIC crystals and the principal axis of strain tensor.

ACKNOWLEDGEMENTS

This work was partly supported by JST, CREST (grant number JPMJCR2091), Japan.

REFERENCES

1. Huneau, B. Strain-Induced Crystallization of Natural Rubber: A Review of X-Ray Diffraction Investigations. *Rubber Chem. Technol.*, ***84*** **(3)**, 425–452., 2011. https://doi.org/10.5254/1.3601131.
2. Persson, B. N. J.; Albohr, O.; Heinrich, G.; Ueba, H. Crack Propagation in Rubber-like Materials. *J. Phys. Condens. Matter*, ***17*** **(44)**. 2005. https://doi.org/10.1088/0953-8984/17/44/R01.
3. Creton, C.; Ciccotti, M. Fracture and Adhesion of Soft Materials: A Review. *Reports Prog. Phys.*, ***79*** **(4)**,

046601., 2016. https://doi.org/10.1088/0034-4885/79/4/046601.

4. Trabelsi, S.; Albouy, P. A.; Rault, J. Stress-Induced Crystallization around a Crack Tip in Natural Rubber. *Macromolecules*, ***35*** **(27)**, 10054–10061., 2002. https://doi.org/10.1021/ma021106c.

5. Brüning, K.; Schneider, K.; Roth, S. V.; Heinrich, G. Strain-Induced Crystallization around a Crack Tip in Natural Rubber under Dynamic Load. *Polym. (United Kingdom)*, ***54*** **(22)**, 6200–6205., 2013. https://doi.org/10.1016/j.polymer.2013.08.045.

6. Rublon, P.; Huneau, B.; Verron, E.; Saintier, N.; Beurrot, S.; Leygue, A.; Mocuta, C.; Thiaudière, D.; Berghezan, D. Multiaxial Deformation and Strain-Induced Crystallization around a Fatigue Crack in Natural Rubber. *Eng. Fract. Mech.*, ***123***, 59–69., 2014. https://doi.org/10.1016/j.engfracmech.2014.04.003.

7. Demassieux, Q.; Berghezan, D.; Creton, C. Microfocused Beam SAXS and WAXS Mapping at the Crack Tip and Fatigue Crack Propagation in Natural Rubber. *Adv. Polym. Sci.*, ***286***, 467–491., 2021. https://doi.org/10.1007/12_2020_79.

8. Osumi, R.; Yasui, T.; Tanaka, R.; Mai, T.-T.; Takagi, H.; Shimizu, N.; Tsunoda, K.; Sakurai, S.; Urayama, K. Impact of Strain-Induced Crystallization on Fast Crack Growth in Stretched Cis -1,4-Polyisoprene Rubber . *ACS Macro Lett.,* ***11*** **(6)**, 747–752., 2022. https://doi.org/10.1021/acsmacrolett.2c00241.

9. Schreier, H.; Orteu, J.-J.; Sutton, M. A. *Image Correlation for Shape, Motion and Deformation Measurements*; Springer US: Boston, MA, Vol. **54**, 2009. https://doi.org/10.1007/978-0-387-78747-3.

CLUSTER FORMATIONS OF TERMINAL GROUPS OF POLYISOPRENES IN NATURAL RUBBERS: MOLECULAR DYNAMICS SIMULATION STUDY

Mayank Dixit[1,2] and Takashi Taniguchi[1,2]

[1] Graduate School of Engineering, Kyoto University, Kyoto 615-8510, Japan
[2]Japan Science and Technology, Crest

ABSTRACT

Hevea Natural Rubber (NR) consists of 99%-cis-polyisoprene with dimethyl allyl-(Trans-1,4-isoprene)$_2$ (ω) and alpha terminal groups. These terminal groups provide excellent mechanical and physical properties to NR. Oouchi et al[1]. have elucidated the structures of six types of alpha terminals of NR by using solid state NMR study. We examine seven types of cis-1,4-polyisoprene (PI) melt systems with different combination of dimethyl allyl-(Trans-1,4-isoprene) (ω) and α6 terminal groups i.e., pure PI (no terminal) (PI0), ω-PI-α1 (PII), ω-PI- α2 (PIII), ω-PI- α3 (PIIII), ω-PI- α4 (PIIV), ω-PI-α5 (PIV) and ω-PI-α6(PIVI). From the obtained equilibrated systems, we computed the end-to-end vector autocorrelation function ($C(t)$), average relaxation time (τ), end-to-end distance (R_e), radius of gyration (R_g) of polymer chains and radial distribution functions (RDFs) between terminal residues and survival probability ($P(\tau)$) for terminal groups. The presence of hydrogen bond between α2-α2, α4-α4 and α6-α6 residues makes slower dynamics of polymer chains in ω-PI-α2, ω-PI-α4, and ω-PI-α6 melt systems. From the analyses of RDFs and potentials of mean force ($W(r)$), the associations between α2-α2, α4-α4 and α6-α6 are significantly stronger than α1-α1, α3-α3 and α5-α5 and isoprene-isoprene. We found that in the pure PI (no terminal), ω-PI-α1, ω-PI-α3, and ω-PI-α5 no cluster formation is observed, on the other hand, stable clusters of α2, α4 and α6 terminals with a size s ($2 \leq s \leq 5$) are observed, which supports the formation of multiple cross-links of chains through α2, α4 and α6 terminals of them[2].

ACKNOWLEDGEMENTS

We are grateful to the computing resources provided by the High-Performance Computing Infrastructure of the University of Tokyo (No. hp220128o) and thankful for the computing resources provided by the Tohoku University Computer Center (202112-SCKXX-0017).

REFERENCES

1. Oouchi, M.; Ukawa, J.; Ishii, Y.; Maeda, H. Structural Analysis ofthe Terminal Groups in Commercial Hevea Natural Rubber by 2DNMRwith DOSY Filters and Multiple-WET Methods Using Ultrahigh-Field NMR. Biomacromolecules **20**(3), 1394−1400, 2019.
2. Dixit, M.; Taniguchi, T. Substantial Effect of Terminal Groups in cis-Polyisoprene: A Multiscale Molecular Dynamics Simulation Study. Macromolecules, **55**, 9650−9662, 2022.

DIVERCITY IN STRAIN-INDUCED CRYSTALLIZATION OF NATURAL RUBBER BY BIAXIAL ELONGATION

Ruito Tanaka[1], Tomohiro Yasui[1], Yuji Kitamura[2], Katsuhiko Tsunoda[2], Hideaki Takagi[3], Nobutaka Shimizu[3], Noriyuki Igarashi[3], Kenji Urayama[4] and Shinichi Sakurai[1,*]

[1]Department of Biobased Materials Science, Kyoto Institute of Technology, Kyoto, Japan
[2]Bridgestone, Kodaira, Tokyo, Japan
[3]High Energy Accelerator Research Organization, Tsukuba, Ibaraki, Japan
[4]Department of Material Chemistry, Kyoto University, Kyoto, Japan

INTRODUCTION

Natural rubber (NR) is soft and simultaneously robust to meet requirements for exclusive safety of tires of aircrafts. Namely, they should not be broken when momentary stress is applied. Strain-induced crystallization (SIC) is considered to play an important role for the toughening of NR. To check the significance of SIC behaviors experimentally, we have thoroughly conducted wide-angle X-ray scattering (WAXS) measurements on NR specimens under the biaxially elongated states using some beamlines at Japanese synchrotron radiation facilities such as SPring-8 and Photon Factory of KEK. For this purpose, we have developed the specially-designed apparatus (**Fig. 1**), which enables biaxial elongation of the sheet specimen of vulcanized NR. The studies on SIC of NR by WAXS have an extremely long history since 100 years ago [1], and reliable crystalline lattice parameters have been reported by Nyburg as the orthorhombic lattice with $a = 1.246$, $b = 0.889$, and $c = 0.81$ nm [2]. Then, comparatively recently, have actively reported such studies by using the X-ray scattering technique [3-7]. In this presentation, we will show the diversity of the strain-induced crystallization (SIC) behaviors by conducting biaxial extension of NR in several manners including the planar deformation (equibiaxial and non-equibiaxial, as well as the hysteresis of the crystallization behaviors depending upon the ways of deformation of the specimen).

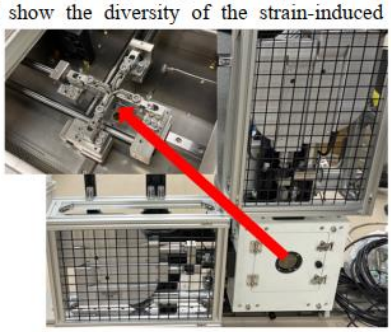

Figure 1: Apparatus for the measurement of the X-ray scattering of the NR sheet specimen subjected to the biaxial deformation. The stress measurement is simultaneously possible. Also, temperature-control up to 130˚C is possible.

EXPERIMENTAL

The elongation apparatus is compact and bears the thermally isolated chamber which enables temperature control of the specimen subjected for the biaxial elongation from room temperature up to about 130˚C (**Fig. 1**). The chamber contains four crossheads to grip the sheet specimen with 90˚ crossed angles. The minimum length between two crossheads is 1 cm, and its maximum stroke is 10 cm, resulting

in the 10-fold elongation ratio at most. Unfortunately for the vulcanized NR sheet specimens, we have encountered the problem of slippage at the gripping jaws. To avoid this unfavorable slippage during elongation, we utilized the cross shape of the NR sheet specimen, taking after the idea by Beurrot et al. [8].

Fig. 2 shows the images of the specially prepared specimen used for the experiment. The specimen is cross-shaped with a cylindrical protrusion at each end to avoid slippage of the specimen sheet out from the jaw during elongation, bearing a round-shaped dimple with thinner thickness in its central portion. This was designed to be more easily deformed under a given strain, as compared to the remained four arm portions (limbs) of the specimen. It was required to calibrate the real strain of the dimpled portion by video-recording the deformation process of the mesh lattice (with 1 mm spacing of the lattice pattern) during the deformation of the specimen. Note that the lattice pattern was stamped on the surface of the dimpled portion in prior to installing the specimen. Then, it was found that the dimpled portion can be elongated up to 4-flod of the elongation ratio for the condition of the apparatus operation with maximum stroke between the two crossheads. The incident X-ray beam was introduced at the center of the dimple of this sheet specimen for the WAXS measurements during the biaxial elongation.

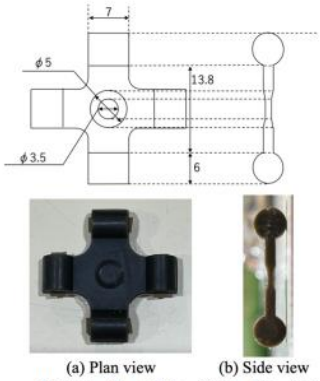

Figure 2: Blue print for the specially prepared NR specimen for the biaxial elongation and (a) images of the real NR specimen (a) the plan view and (b) the side view.

RESULTS AND DISCUSSSION

Fig. 3 compares the 2-dimensional wide-angle X-ray diffraction (2d-WAXD) patterns obtained for the specimens under (a) the uniaxial and (b) the planar extension mode, where in the latter case the specimen was drawn in one direction while its size was kept constant by holding the specimen with the gripping jaws to prevent shrinkage. Although these patterns look similar to each other, closer examination finds the lack of the (120) reflection peaks in the latter case, which appear in the horizontal direction in the former case (as has been already reported by Katz [1]). Our extensive studies ascribed the lack to the planar orientation of the (120) planes parallel to the surface of the sheet specimen [9]. Furthermore, it was revealed that the crystallites melted completely when the drawn specimen was relaxed. However, the strain at the melting of the crystallites was lower than that at the onset of SIC. This clearly indicates that once-formed crystallites by the SIC is stable in the reversing process where the drawn specimen was relaxed. As for the equibiaxial extension, we confirmed SIC at 3.7 strain with the random orientation of the crystal lattice, as has been reported by Beurrot et al. [8], which is very much contrasted

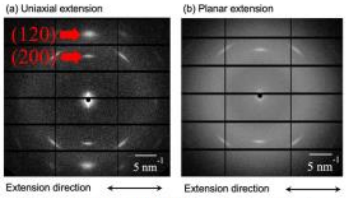

Figure 3: 2d-WAXD patterns for the NR sheet specimens under (a) the uniaxial and (b) the planar extension mode, where in the latter case the specimen was drawn in one direction while its size was kept constant by holding the specimen with the gripping jaws to prevent shrinkage.

to the case of the uniaxial or planar elongation where the *c* axis is parallel to the extension direction (**Fig. 3**).

We also examined the SIC behaviors upon the two-step extension, as the following manner; the specimen was first drawn in one direction (the planar extension) to form crystallites and then the drawn specimen (of which size was fixed at the strain where the 2d-WAXD pattern exhibited the crystalline reflection peaks) was further drawn in the direction perpendicular to the extension direction in the first step of the extension. The 2d-WAXD pattern as shown in **Fig. 3(b)** was obtained in the beginning of the second step of the extension. Then, the arcs of the (200) reflection was diffused with an increase of the strain in the direction perpendicular to the extension direction of the first step, indicating the randomization process of the crystallite orientation. Simultaneously, the reflection became vague, and finally disappeared before reaching the equibiaxial state if the strain of the first step of the extension was much lower than 3.7, which is the onset of SIC for the case of the equibiaxial extension. In case when the strain was closer to 3.7 but even slightly lower than that, the Debye-Scherrer ring of the (200) reflection remained in the 2d-WAXD pattern, suggesting the survival of the crystallites with random orientation. This result indicates that once-formed crystallites by SIC in the first step of the extension is still stable in the final state of the equibiaxial extension, even though the equibiaxial strain is slightly lower than the critical strain value of the onset of SIC for the case of the equibiaxial extension.

As a conclusion, the diversity of the SIC behaviors of NR were found by conducting the biaxial extension, suggesting that the SIC strongly depends upon hysteresis of the applied strain.

ACKNOWLEDGEMENTS

This study was financially supported by JST CREST (Grant No. JPMJCR2091).

REFERENCES

1. Katz, J. R. Ro¨ntgenspektrographische Untersuchungen am gedehnten Kautschuk und ihre mo¨gliche Bedeutung fu¨r das Problem der Dehnungseigenschaften dieser Substanz. *Naturwissenschaften*, **19**, 410-416., 1925.
2. Nyburg, S. C. A statistical structure for crystalline rubber. *Acta Cryst.*, **7**, 385-392., 1954. https://doi.org/10.1107/S0365110X54001193.
3. Toki, S.; Fujimaki, T.; Okuyama, M. Strain-induced crystallization of natural rubber as detected real-time by wide-angle X-ray diffraction technique. *Polymer*, **41** (**14**), 5423-5429., 2000. https://doi.org/10.1016/S0032-3861(99)00724-7.
4. Tosaka, M.; Murakami, S.; Poompradub, S.; Kohjiya, S.; Ikeda, Y.; Toki, S.; Sics, I.; Hsiao, B. S. Orientation and crystallization of natural rubber network as revealed by WAXD using synchrotron radiation. *Macromolecules*, **37** (**9**), 3299-3309., 2004. https://doi.org/10.1021/ma0355608.
5. Huneau, B. Strain-Induced Crystallization of Natural Rubber: A Review of X-Ray Diffraction Investigations. *Rub. Chem. Tech.*, **84** (**3**), 425-452., 2011. https://doi.org/10.5254/1.3601131.
6. Chen, X.; Meng, L.; Zhang, W.; Ye, K.; Xie, C.; Wang, D.; Chen, W.; Nan, M.; Wang, S.; Li, L. Frustrating Strain-Induced Crystallization of Natural Rubber with Biaxial Stretch. *ACS Appl. Mater. Interfaces*, **11** (**50**), 47535-47544., 2019. https://doi.org/10.1021/acsami.9b15865.
7. Osumi, R.; Yasui, T.; Tanaka, R.; Mai, T.-T.; Takagi, H.; Shimizu, N.; Tsunoda, K.; Sakurai, S.; Urayama, K. Impact of Strain-Induced Crystallization on Fast Crack Growth in Stretched cis-1,4-Polyisoprene Rubber. *ACS Macro Lett*, **11** (**6**), 747-752., 2022. https://doi.org/10.1021/acsmacrolett.2c00241.
8. S. Beurrot, B. Huneau, E. Verron, In *Constitutive models for rubber VII: Proceedings of the 7th European conference on constitutive models for rubber, ECCMR, Dublin, Ireland, 20-23 Sept 2011. CRC/Taylor & Francis, Boca Raton*, S. Jerrams, N. Murphy (eds), 23-28, 2011.
9. Tanaka, R.; Yasui, T.; Kitamura, Y.; Tsunoda, K.; Takagi, H.; Shimizu, N.; Igarashi, N.; Urayama, K.; Sakurai, S., to be submitted, 2023.

8TH PACIFIC RIM CONFERENCE ON RHEOLOGY, May 15-19, 2023

FLOW AND SHEAR THICKENNING OF DENSE SUSPENIONS OF RIGID RODS

Mohan Das[1,2], George Petekidis[1,2]

[1]IESL-FORTH, Crete, Greece
[2]Department of Materials Science and Technology, University of Crete, Greece

ABSTRACT

We present the rheological response of dense suspensions and glasses of colloidal rods under nonlinear steady and oscillatory shear, follow their yielding behaviour and critically compare it with that of their spherical hard sphere counterpart. In general dense suspensions of particles often exhibit shear thickening at high shear rates/stresses. While spherical particles have been extensively studied, particle shape anisotropy can be an important factor affecting and tuning shear thickening effects. Here we investigate shear thickening in dense suspensions of silica rigid rods in a refractive index matched medium that promotes interparticle interactions through hydrogen bonding. Using a combination of rheology and confocal microscopy we decipher the role of particle orientation in the continuous and discontinuous shear thickening regime. Our study reveals that both in continuous and discontinuous shear thickening regime there is no change in rod orientation while strong fluctuations and presence of "rheochaos" are not observed contrary to findings in other systems. Therefore, it is possible that frictional contacts between closely packed rods in a flow aligned state can induce discontinuous shear thickening at very high shear stresses without the need for reorientation effects to take place.

ACKNOWLEDGEMENTS

We acknowledge the support from the Marie-Sklodowska Curie Innovative Training Network "DiStruc" (Grant Agreement No. 641839) as well as innovation program "EUSMI" (Grant Agreement No. 731019). We would also like to thank L. Chambon, E. Vasilaki, and M. Vamvakaki, Univ. Crete, for providing the particles.

Flow-induced structural change of cathode slurry during storage and its mechanism

JH. Park[1], KH. Ahn[1*]

[1]School of Chemical and Biological Engineering, Seoul National University, Seoul, 08826, Korea

ABSTRACT

Dispersion state of the electrode slurry is of great interest in industry and academia as it is directly related to the electrode performance as well as the productivity in electrode manufacturing [1, 2]. Electrode slurry is agitated in a storage tank to maintain dispersion quality before entering the subsequent electrode process [3]. Even if the electrode slurry is well prepared, various problems may occur if the slurry dispersion is deteriorated during storage. However, an understanding of the change in the slurry dispersion during storage is still lacking [4]. In this study, we find out how the dispersibility of the cathode slurry changes during storage and which parameter governs the change, along with the mechanism. We observe that the conductive nanoparticles are severely agglomerated under certain low-speed agitation to form large spherical agglomerates of several tens of μm, and accordingly, the elasticity of the slurry decreases sharply. Then, to characterize the main parameters governing the structural change, we simultaneously control the matrix viscosity (η_m) and agitation speed (shear rate, $\dot{\gamma}$). The product of the two variables can be integrated into the hydrodynamic stress ($\tau = \eta_m \dot{\gamma}$) induced by the flow. Finally, we correlate the changes in microstructure of the slurry with hydrodynamic stress during storage. The mechanism is understood by considering the relative affinity between each particle and the hydrodynamic stress induced by flow.

REFERENCES

1. Akuzum, B.; Agartan, L.; Locco, J.; Kumbur, E. Effects of particle dispersion and slurry preparation protocol on electrochemical performance of capacitive flowable electrodes. *Journal of Applied Electrochemistry* **2017**, *47* (3), 369-380.
2. Park, J. H.; Sung, S. H.; Kim, S.; Ahn, K. H. Significant Agglomeration of Conductive Materials and the Dispersion State Change of the Ni-Rich NMC-Based Cathode Slurry during Storage. *Industrial & Engineering Chemistry Research* **2022**, *61* (5), 2100-2109.
3. Kwon, Y. I.; Kim, J. D.; Song, Y. S. Agitation effect on the rheological behavior of lithium-ion battery slurries. *Journal of Electronic Materials* **2015**, *44* (1), 475-481.
4. Wang, Z.; Zhao, T.; Takei, M. Clarification of particle dispersion behaviors based on the dielectric characteristics of cathode slurry in lithium-ion battery (LIB). *Journal of The Electrochemical Society* **2019**, *166* (2), A35.

PRACTICAL RHEOMETRY FOR SUSPENSIONS AND OTHER FUN COMPLEX SYSTEMS

David J. Moonay[1]

[1]Brookfield AMETEK, Middleboro, Massachusetts, USA

ABSTRACT

Industrial operators use various instruments and geometries to analyze the rheology of commercial products. The latter may include suspensions, colloidal dispersions and solutions, for example. Product formulations vary widely, and their rheological behavior is often complicated. Measurement techniques may be relatively simple for quick QC/QA checks, or more sophisticated, for R&D or process engineering, for example. 3-D Printing or Additive Manufacturing allows the creation of complex geometries that extend the utility of existing equipment. This talk presents rotational and oscillatory shear data for a few different materials, illustrating some different techniques, rheometric tools and material behaviors.

YIELD AND FLOW IN AGGREGATED PARTICULATE SUSPSENSIONS IN WATER

Peter J. Scales[1], Shane P. Usher[1], Maria Barmar Larsen[2], Anthony D. Stickland[1], Hui-En Teo[1], Ross G. de Kretser[1] and Richard Buscall[3]

1. ARC Centre of Excellence for Enabling Eco-Efficient Beneficiation of Minerals Department of Chemical Engineering, The University of Melbourne, Parkville, Australia
2. Department of Chemistry and Bioscience, University of Aalborg, Aalborg, Denmark
3. Maritime Court, Exeter, EX2 8GP, UK

ABSTRACT

Understanding the compressive strength or resistance to consolidation of aggregated particulate suspensions is relevant to processes such as filtration, centrifugation and gravity settling, where the compressive strength defines an upper boundary for processing. New data for the compressive strength of consolidating flocculated particulate suspensions in water from our own laboratories, including alumina and calcium carbonate, are compared with earlier data from the literature. The three sets of data for the compressive strength of alumina agree well. Differences are noted for data measured in shear between our own laboratories and others. New data for the shear strength of an alumina are also presented and, although the agreement is not as good, the difference is implied to be due to wall slip associated with a difference in measurement techniques[1].

A simple non-linear poro-elastic model of the compressive strength was applied to the eight sets of compressive strength data and was found to account for most features of the observed behaviour. The agreement strongly supports the mechanistic failure mode in compression for these systems to be one of simple strain hardening. The one feature that it does not account for is the observed irreversibility of consolidation. It is however suspected that wall adhesion might provide such a ratchet in reality, since wall adhesion has been neglected in the analysis of raw compressive strength until recently, notwithstanding the pioneering work of Michaels and Bolger[2]. Overall, the data analysis and fitting indicate a limited data set in both compression and shear, can now be used to predict comprehensive curves for the shear yield stress and compressive yield stress of samples using a simple poro-elastic model.

REFERENCES

1. Stickland, A.D., A. Kumar, T.E. Kusuma, P.J. Scales, A. Tindley, S.R. Biggs, and R. Buscall, *The effect of premature wall yield on creep testing of strongly-flocculated suspensions.* Rheol. Acta, 2015. **54**(5): p. 337-352.
2. Michaels, A.S. and J.C. Bolger, *Plastic flow behavior of flocculated kaolin suspensions.* Industrial & Engineering Chemistry Fundamentals, 1962. **1**(3): p. 153-162.

8TH PACIFIC RIM CONFERENCE ON RHEOLOGY, May 15-19, 2023

RHEO-DIELECTRIC BEHAVIOR OF UNENTANGLED POLY (BUTADIENE OXIDE) UNDER STEADY SHEAR

Yumi Matsumiya[1], Takeshi Sato[1], Quan Chen[2] and Hiroshi Watanabe[1,2]

[1] Kyoto University, Kyoto, Japan
[2] Changchun Institute of Applied Chemistry, Chinese Academy of Sciences, Changchun, China

ABSTRACT

A rheo-dielectric test for a type-A unentangled melt, poly(butylene oxide), was performed to measure η, Ψ_1, and ε_y" in the velocity gradient (y) direction. Analyzing these ε_y", η, and Ψ_1 data, we found that the spring strength κ increases moderately while the off-diagonal components of the friction coefficient tensor $\boldsymbol{\zeta}$ remain negligibly small on an increase of Wi up to 1.2. We also found that the diagonal components ζ_{xx} (with x being the velocity direction) and B_{yy} hardly change while ζ_{yy} decreases moderately. These results, suggesting the onset of the finite extensive nonlinear elasticity and violation of a relationship $B_{yy} \propto \zeta_{yy}$, serve as a starting point for deeper investigation of κ, $\boldsymbol{\zeta}$, and $\mathbf{B}$.

INTRODUCTION

Recently, extensive studies have been made for flow-induced changes in the local properties of polymer chains. In the bead-spring chain model, these changes can be expressed as changes in the spring constant κ, the bead friction ζ, and the mean-square intensity B of the Brownian force acting on the bead. An experimental evaluation of the magnitude of flow-induced changes in these parameters is desired. In this regard, we have recently conducted the Rouse analysis of dielectric and diffusion properties measurable with Lab devices under shear.[1] Based on this analysis, we have performed the rheo-dielectric measurement for a typical type-A polymer, poly(butylene oxide) (PBO), in the unentangled melt.[2]

EXPERIMENTAL

A linear unentangled polybutylene oxide (PBO) ($M_w = 16\times10^3$, $M_w/M_n = 1.30$) was used. Linear viscoelasticity and rheo-dielectric measurements were performed on a rheometer ARES-G2 (TA Instruments) using a parallel plate (5ϕ) and a homemade cone-plate electrode (10ϕ, 0.025 rad), respectively. In the rheo-dielectric measurements, the cone-plate electrode was connected to a dielectric bridge (ModuLab XM MTS; Solartron Analytical) *via* a Hg reservoir, and dielectric frequency sweep tests were performed in the range of $10^4 \geq f/\mathrm{Hz} \geq 1$ under steady shear flow.

RESULTS AND DISCUSSION

The rheo-dielectric measurements of PBO-16k were performed at −20°C and the resulting steady-state viscosity η, first normal stress difference coefficient Ψ_1, and dielectric loss ε_y" in the velocity gradient direction are summarized in **Figs. 1 and 2**. For comparison, complex

viscosity $|\eta^*|$ and elastic factor $2G'/\omega^2$ obtained from the linear viscoelastic measurements are also shown in **Fig. 1**.

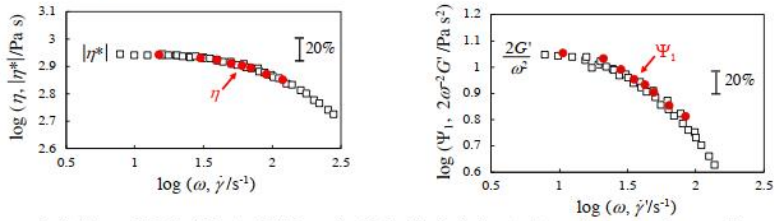

Figure 1: (left) η of PBO-16k at −20˚C against $\dot{\gamma}$ in filled circles. $|\eta^*|$ against ω is shown with open squares. **(right)** Ψ_1 against $\dot{\gamma}' = \dot{\gamma}/1.4$ in filled circles. $2G'/\omega^2$ against ω is shown with open squares.

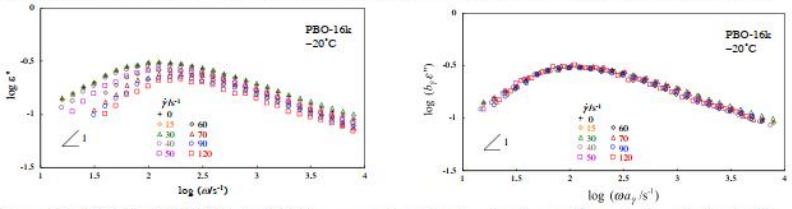

Figure 2: (**left**) ε'' of PBO-16k at −20˚C measured under steady shear at the rate $\dot{\gamma}$ as indicated is plotted against ω.**(right)** Normalized plots of the rheo-dielectric ε'' data.

We have solved the equation of motion of the type-A Rouse chain to express its ε'' analytically in terms of κ and ζ.[1] (The mean-square intensity of the Brownian force **B** vanishes on the averaging of the first order moments, and is not included in this expression.) The key quantities in that expression are the non-equilibrium parameter r defined for κ and ζ:

$$r_\kappa \equiv \kappa_{sf}/\kappa_{eq} \tag{1a}$$

$$r_{\zeta,ij} \equiv \zeta_{ij,sf}/\zeta_{eq} \tag{1b}$$

Here, the subscripts "sf" and "eq" stand for the quantities under steady flow and at equilibrium, respectively. ζ_{ij} is the ij component of the friction coefficient tensor $\boldsymbol{\zeta}$ ($i,j = x$: velocity direction, y: velocity gradient direction, z: vorticity direction). If ζ_{yx} is negligibly small, the dielectric mode distribution is not affected by the shear and ε_y'' is simply related to $\varepsilon_{eq}''(\omega)$ as[1]

$$\varepsilon_y''(\omega) = \frac{1}{r_\kappa}\varepsilon_{eq}''(\omega\{r_{\zeta,yy}/r_\kappa\}) \tag{2}$$

The experimentally observed shear-insensitivity of the dielectric mode distribution (**Fig. 2**) strongly suggests that our PBO-16k sample had negligibly small ζ_{yx} at $\dot{\gamma}$ examined. Then, the intensity factor $b_{\dot{\gamma}}$, used for the vertical shift in **Fig. 2**, coincides with the non-equilibrium parameter r_κ (Eq. 1a), and the frequency shift factor $a_{\dot{\gamma}}$ is identical to the $r_{\zeta,yy}/r_\kappa$ (Eq. 2). These relationships allow us to evaluate $r_{\zeta,yy}$ and r_κ. The results are shown in **Fig. 3**.

As mentioned earlier, dielectric data are independent of **B**. However, the rheological data depend on **B**, so that combination of dielectric and rheological data allows us to obtain the non-equilibrium parameter for **B**:

$$r_{B,ij} \equiv B_{ij,\mathrm{sf}} / B_{\mathrm{eq}} \quad (i,j = x, y, z) \tag{3}$$

By solving the Rouse equation of motion, η and Ψ_1 can be expressed analytically in terms of r_κ, $r_{\zeta,ij}$, $r_{B,ij}$. When $r_{\zeta,yx} \sim 0$ as in the present experiment, r_κ and $r_{\zeta,yy}$ obtained from the dielectric data (**Fig. 2**) and the rheological η/η_0 and $\Psi_1/\Psi_{1,0}$ data give $r_{\zeta,xx}$ and $r_{B,yy}$ as

$$r_{\zeta,xx} = \frac{\left\{\Psi_1/\Psi_{1,0}\right\}}{\left\{\eta/\eta_0\right\}} r_\kappa \tag{4}$$

$$r_{B,yy} = \frac{r_\kappa}{2}\left\{\frac{\eta}{\eta_0}\right\}\left(1 + \frac{r_{\zeta,yy}}{r_\kappa}\frac{\left\{\eta/\eta_0\right\}}{\left\{\Psi_1/\Psi_{1,0}\right\}}\right) \tag{5}$$

The non-equilibrium parameters r_κ, $r_{\zeta,yy}$, $r_{\zeta,xx}$, and $r_{B,yy}$ thus evaluated are summarized as a function of Weissenberg number $Wi = \tau_1^{[G]}\dot{\gamma}$ in **Fig. 3**. ($\tau_1^{[G]}$: the longest linear viscoelastic relaxation time). $r_{\zeta,xx}$ and $r_{B,yy}$ remain close to unity, whereas r_κ and $r_{\zeta,yy}$ increases and decreases, respectively, on an increase of Wi up to 1.2. This nonlinearity of r_κ and $r_{\zeta,yy}$ is just moderate (possibly because Wi is not increased well beyond unity). Nevertheless, the following features are worth noting: the increase of r_κ suggests the *onset* of finite extensible nonlinear elasticity, and the difference between $r_{B,yy}$ and $r_{\zeta,yy}$ suggests a violation of the proportionality, $B_{yy} \propto \zeta_{yy}$, naively expected from the fluctuation-dissipation theorem. In addition, for $Wi \leqq 1.2$, $\eta/\eta_0 \cong 2/\{r_\kappa(1 + r_{\zeta,yy})\}$, $\Psi_1/\Psi_{1,0} \cong 2/\{r_\kappa^2(1 + r_{\zeta,yy})\}$.[2] Namely, the thinning of η and Ψ_1 is determined by a delicate balance between the increase of r_κ and decrease of $r_{\zeta,yy}$. Further rheo-dielectric experiments covering larger Wi are desired for a deeper understanding of these features of η, Ψ_1 and r, and are now being planned with a setup of a CPP shearing fixture/electrode.

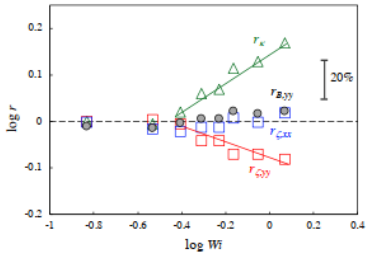

Figure 3: Changes of non-equilibrium parameters *r*'s with the Weissenberg number *Wi*.

REFERENCES

1. Sato, T.; Matsumiya, Y.; Watanabe, H., Rheo-Dielectrics and Diffusion of Type-A Rouse Chain under Fast Shear Flow: Method of Evaluation of Non-Equilibrium Parameters for FENE, Friction-Reduction, and Brownian Force Intensity Variation, *Nihon Reoroji Gakkaishi* (*J. Soc. Rheol. Jpn.*), **50**, 253-268, 2022. https://doi.org/10.1678/rheology.50.253.
2. Matsumiya, Y.;Sato, T.; Chen, Q.; Watanabe, H., Rheo-dielectric Behavior of Unentangled Poly(butylene oxide) under Steady Shear: Non-equilibrium Parameters at the Onset of Nonlinearity, *Nihon Reoroji Gakkaishi* (*J. Soc. Rheol. Jpn.*), **50**, 371-385, 2022. https://doi.org/10.1678/rheology.50.371.

EXPERIMENTAL STUDY ON PHASE SEPARATION DYNAMICS OF UNENTANGLED POLYMER BLEND WITH DYNAMIC ASYMMETRY

Takeshi Sato[1], Yumi Matsumiya[1], and Hiroshi Watanabe[1,2]

[1]Institute for Chemical Research, Kyoto University, Kyoto, Japan
[2]Changchun Institute for Applied Chemistry, Chinese Academy of Science, Changchun, China

ABSTRACT

To design intelligent polymeric materials, we are frequently required to predict phase separation behavior of polymer blends. Thus, it is important to understand the phase separation dynamics since the behavior is tightly related to the dynamics of each component in blends. To evaluate the component dynamics in blends, we focus on a combination of dielectric and viscoelastic measurements. Utilizing this combination of experimental methods, we attempted to obtain the mobility of the component fluxes Λ, which is required to predict the time evolution of the phase separation. We examined blends of dielectrically active polyisoprene (PI) and dielectrically inert poly(4-ethylstyrene) (PC2St) samples, having the molecular weights of $M = 7.5 \times 10^3$ and $M = 4.2 \times 10^3$, respectively. Here, we note that PI has a dipole parallel along the chain backbone and PC2St does not, the large scale molecular motion of PI chains can be exclusively detected by the dielectric measurements. The blend system with the low-M components shows the upper critical solution temperature, and thus exhibits an uniform state at temperatures higher than the phase separation temperature (T_s). For various PI/PC2St blends with different PI weight fractions w_PI, we first conducted dielectric and viscoelastic measurements at several temperatures above T_s to determine the friction coefficient ζ_i (i = PI or PC2St), which is needed to evaluate Λ. We found that the T-dependence of ζ_i is reasonably captured by the Williams–Landel–Ferry (WLF) equation. The WLF results were extrapolated to obtain the composition-dependent friction coefficient ζ_i^* at test temperature T^* below T_s. Then, Λ values were deduced from the incompressible theory[1] that relates Λ with experimental ζ_i^* values. Utilizing Λ values, we numerically solved the time-dependent Ginzburg-Landau (TDGL) equation with the composition-dependent Λ in a 2D system. From the TDGL simulation, we obtained the droplet-like and PI-rich phase, which is consistent with the observation by the optical microscope.[2]

REFERENCES

1. Brochard F., Jouffroy J., and Levinson P. Polymer-polymer diffusion in melts, *Macromolecules*, **16**, 1638 (1983).
2. Sato T., Matsumiya Y., Watanabe H. Experimental study of phase separation in dynamically asymmetric unentangled polymer blend, *J. Chem. Phys.*, **157**, 224908 (2022).

SIMULATION STUDY OF UNENTANGLED POLYMERS UNDER FAST FLOW

Jun-ichi Takimoto, Sathish K. Sukumaran

Yamagata University, Yonezawa, Japan

ABSTRACT

Viscosity η, 1st normal stress coefficient Ψ_1 and the chain dimension R under fast shear flow are calculated by using the Rouse model with excluded volume interaction among monomers of different chains. Simple application of the friction reduction (FR) model can describe the decrease of η and Ψ_1 at high shear rate, but it fails to describe the increase of R. On the other hand, the shear blob model can correctly predict η and R, but it is hard to describe Ψ_1. We are also studying unentangled polymer solutions by using Kremer-Grest model. Behavior of the steady elongational viscosity is qualitatively consistent with FR model, but the shear thinning in solution is rather close to that in melt, suggesting that FR alone can not describe this thinning.

SOFT CORE MODELS

The friction reduction[1,2] (FR) under fast flow is now considered as one of the key concepts for understanding the polymer dynamics. Since FR is believed to be independent of the entanglement, it is preferable to study unentangled polymers since we can avoid complications due to the entanglement. For this purpose, we can use the standard Kremer-Grest (KG) model with small number of monomers N per chain. But with short chains the effect of finite extensibility would start at relatively low strain rates. In order to extend the range of strain rate, we use models that allow long but unentangled chains.

First we tried soft core models such as DPD. In these models monomers can overlap and chains can cross with each other. We have found that these models show only very weak shear thinning. Experimentally[3], however, the steady shear viscosity $\eta(\dot{\gamma})$ of unentangled polymers shows shear thinning described by the following empirical formula:

$$\eta(\dot{\gamma}) = \frac{\eta(0)}{[1 + (\tau\dot{\gamma})^2]^{1/4}} \tag{1}$$

where $\dot{\gamma}$ is the shear rate and τ is the stress relaxation time. We will see that the excluded volume interaction is necessary to reproduce this shear thinning.

ROUSE MODEL WITH HARD CORE REPULSION

Next we use the Rouse model with excluded volume interaction. In this model, each chain is described by the Rouse model, but there is a hard core repulsion among monomers in different chains. This model is equivalent to the KG model in which the bond potential is replaced by a simple spring $U(r) = 3k_BT/\sigma^2$ (σ is the monomer diameter). Although monomers (of different chains) can not overlap, bonds can extend and the chain crossing can take place. We have confirmed that this model does not show entanglement up to $N = 800$. Under steady shear flow, this model shows the shear thinning as Eq.1. Moreover, we have found that the 1st normal stress coefficient $\Psi_1(\dot{\gamma})$ and $\eta(\dot{\gamma})$ satisfy

$$\frac{\Psi_1(\dot{\gamma})}{\Psi_1(0))} = \left(\frac{\eta(\dot{\gamma})}{\eta(0)}\right)^2 \tag{2}$$

According to the generalized Rouse model[4] by Watanabe et al., this relation indicates that the fluctuation-dissipation theorem holds even under shear flow in which the friction coefficient ζ is reduced. We've found, however, that the chain dimension under shear flow $R(\dot{\gamma})$ behaves at high shear rate as

$$\frac{R(\dot{\gamma})^2}{R(0)^2} \propto (\dot{\gamma}\tau)^{1/2} \tag{3}$$

This relation can't be explained by a simple application of the generalized Rouse model. On the other hand, the "shear blob" model by Colby et al.[3] can correctly predict the exponents in both Eq.1 and Eq.3. But we haven't yet succeeded to derive Eq.2 by this model. A kind of unification of the FR and blob models may be required.

POLYMER SOLUTION STUDIED BY KG MODEL

It is widely believed that in polymer solution the reduction of friction between the polymer segment and the surrounding solvent molecules is much weaker than in polymer melts. To see whether this can be reproduced by using coarse-grained model, we are studying polymer solutions by KG model (short chain). Here the solvent molecules is the same as the monomer of the polymer chain (athermal solvent).

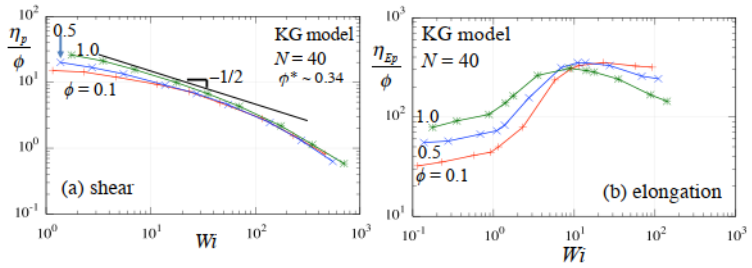

Figure 1: Steady shear (a) and elongational (b) viscosities of polymer solutions (KG model)

Fig. 1 shows the steady shear and elongational viscosities of polymer solutions as functions of the Weissenberg number Wi (elongational viscosity is calculated by the UEF package of LAMMPS). Here, ϕ is the volume fraction of the polymer, and $\eta_p = \eta - \eta_s$ (η and η_s is the viscosities of the solution and solvent). In the case of elongational flow, the hardening ($Wi \sim 1 \sim 10$) is stronger in solution, and the following thinning is weaker. This is at least qualitatively consistent with the FR model. In the case of shear flow, on the other hand, thinning in solution is only slightly weaker than in the melt. This indicates that the solution ($\phi = 0.1$) has similar FR as the melt, or there may be other cause(s) of the *shear* thinning. We also need to consider that KG model, with no angle/torsion potentials and no side chains, may have weaker friction than the real polymers even under no flow.

REFERENCES

1. Yaoita T., Isaki T., Masubuchi Y., Watanabe H., Ianniruberto G, Marrucci G. Primitive Chain Network Simulation of Elongational Flows of Entangled Linear Chains: Stretch/Orientation-induced Reduction of Monomeric Friction, *Macromolecules*, **45**, 2773 − 2782, 2012.

2. Ianniruberto G., Brasiello A., Marrucci G. Simulations of Fast Shear Flows of PS Oligomers Confirm Monomeric Friction Reduction in Fast Elongational Flows of Monodisperse PS Melts As Indicated by Rheooptical Data, *Macromolecules*, **45**, 8058 − 8066, 2012.

3. Colby R. H., Boris D. C., Krause W. E., Dou S., Shear thinning of unentangled flexible polymer liquids, *Rheol. Acta*, **46**, 569-575, 2007.

4. Watanabe H., Matsumiya Y., Sato T., Revisiting Nonlinear Flow Behavior of Rouse Chain: Roles of FENE, Friction-Reduction, and Brownian Force Intensity Variation, *Macromolecules*, **54**, 3700-3715, 2021.

MOLECULAR DYNAMICS SIMULATIONS FOR VISCOSITY GROWTH AND CONFORMATIONS OF UNENTANGLED POLYMERS UNDER SHEAR FLOW

Takashi Uneyama[1], Stephen Sanderson[2], Mingchao Wang[2], and Debra J. Searles[2]

[1]Nagoya University, Nagoya, Japan
[2]The University of Queensland, Brisbane, QLD, Australia

ABSTRACT

Melts and solutions unentangled polymers exhibit shear thinning under fast shear. Colby et al[1] reported that the shear thinning behavior is universal and the flow curve of the steady state viscosity can be fitted to the Carreau model. Recently, Costanzo et al[2] conducted rheological measurements including very high shear rate regions, and reported that dilute unentangled solutions exhibit the shear thickening behavior followed by the shear thinning behavior. Matsumiya et al[3] combined the rheology and dielectric measurements and studied the dynamics of polymer chains under fast shear. These experimental data suggest that an effective friction for segments is modulated under fast shear. In this work, to study the dynamics of unentangled polymers under fast shear in detail, we perform molecular dynamics (MD) simulations. We show that the shear thinning behavior depends on the method to apply the shear flow. We discuss the molecular level mechanism which gives the different shear thinning behaviors.

MODEL

We use the Kremer-Grest model[4], in which a polymer is modeled by connecting repulsive beads by bonds. The repulsive interaction between beads is expressed by the truncated Lennard-Jones potential (the Weeks-Chandler-Andersen potential), and the bond is expressed by the finitely extensible non-linear (FENE) potential.

In the original Kremer-Grest model, the Langevin equation is employed as the dynamic equation for beads. To apply shear flow to the system, we should change the dynamics model. The most widely used method to apply shear is the SLLOD (strictly speaking, the atomic SLLOD) model. In the atomic SLLOD model, the following dynamic equations are utilized:

$$\frac{d\boldsymbol{r}_{i,k}(t)}{dt} = \frac{\boldsymbol{p}_{i,k}(t)}{m} + \boldsymbol{\kappa} \cdot \boldsymbol{r}_{i,k}(t), \tag{1}$$

$$\frac{d\boldsymbol{p}_{i,k}(t)}{dt} = -\frac{\partial \mathcal{U}(\{\boldsymbol{r}_{i,k}(t)\})}{\partial \boldsymbol{r}_{i,k}(t)} - \boldsymbol{\kappa} \cdot \boldsymbol{p}_{i,k}(t) - \alpha(t)\boldsymbol{p}_{i,k}(t). \tag{2}$$

Here, $\boldsymbol{r}_{i,k}$ and $\boldsymbol{p}_{i,k}$ are the position and peculiar momentum of the k-th bead in the i-th chain. m is the mass of a bead, $\boldsymbol{\kappa}$ is the velocity gradient tensor, and $\mathcal{U}(\{\boldsymbol{r}_{i,k}\})$ is the total interaction potential energy. $\alpha(t)$ is the coefficient of the Nosé-Hoover thermostat. The SLLOD dynamic equations (1) and (2) assume the homogeneous shear flow for all beads. Although the atomic SLLOD works well for low shear rates, it is reported that it shows some artificial behaviors for high shear rates[5].

In actual rheology experiments, shear flow is generated by moving fixtures (such as the parallel plates and cone-plate). Also, the temperature of polymers are not directly controlled but indirectly controlled by the heat conduction from fixtures. To mimic such a situation, we introduce walls and control the shear flow and temperature by using walls. We employ the canonical equations as the dynamic equations for beads in polymer chains:

$$\frac{d\boldsymbol{r}_{i,k}(t)}{dt} = \frac{\boldsymbol{p}_{i,k}(t)}{m}, \quad \frac{d\boldsymbol{p}_{i,k}(t)}{dt} = -\frac{\partial \mathcal{U}(\{\boldsymbol{r}_{i,k}(t)\})}{\partial \boldsymbol{r}_{i,k}(t)}. \tag{3}$$

The walls consist of fixed wall particles and graft chains attached to wall particles. The wall particles are moved with a constant velocity to generate a shear flow. The Langevin thermostat is used for the graft chains, and the temperature of the graft chains are controlled. The flow and temperature of polymer chains are controlled only via the interaction potential (in Eq. (3)) between polymer chains and walls (wall particles and graft chains).

In what follows, we use the dimensionless units by setting the Lennard-Jones parameters as $\sigma = 1$ and $\epsilon = 1$, and the mass as $m = 1$. We set the degree of polymerization (number of beads per one chain) as $N = 25$, which is below the entanglement polymerization degree. The thermostat temperature is set to $k_B T = 1$ and the density of beads is $\rho = 0.83$. The viscoelastic Rouse relaxation time determined from the linear viscoelasticity (LVE) data is $\tau_R = 2.4 \times 10^2$. The (apparent) shear rate $\dot{\gamma}$ is changed in the range from 0.0001 to 0.1. (The range of the Weissenberg number $\mathrm{Wi} = \tau_R \dot{\gamma}$ is from 0.024 to 24.) The shear rate for a wall-driven system is determined from the gradient of the velocity field at the steady state.

RESULTS

Fig. 1(a) shows the viscosity growth functions for SLLOD and wall-driven systems with several different shear rates. Both the SLLOD and wall-driven systems show similar viscosity growth curves. If the Weissenberg number is sufficiently low ($\mathrm{Wi} = 0.24$), the viscosity growth functions at the long-time region almost coincide to the LVE envelope. As the Weissenberg number increases ($\mathrm{Wi} = 2.4$), we observe that the viscosity decreases (the shear thinning behavior) in both systems. If the Weissenberg number becomes sufficiently large ($\mathrm{Wi} = 24$), we observe that two systems exhibit qualitatively similar but quantitatively different viscosity growth functions. **Fig. 1**(b) shows the steady state viscosity data for the SLLOD and wall-driven systems. At the low Weissenberg number region, two systems show almost the same viscosity. However, if the Weissenberg number becomes large ($\mathrm{Wi} \gtrsim 10$), the viscosity of the wall-driven system becomes clearly higher than that of the SLLOD system.

We consider that there are several origins which cause the difference in the shear viscosities in the high shear region. One is the viscous heating effect. In the wall-driven system, the temperature is controlled only at the wall region. By applying the shear flow, polymers are heated by the viscous dissipation and the temperature will be inhomogeneous. In fact, we can observe that the temperature of the wall-driven system is clearly inhomogeneous in the high shear region. Such a change of the temperature affects the viscosity. We expect that the viscous heating may not be negligible in some experimental systems.

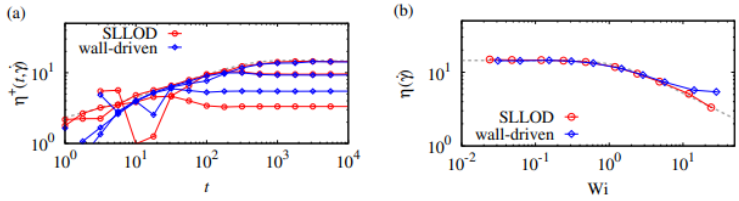

Figure 1: (a) The viscosity growth curves of SLLOD and wall-driven systems for Wi $= 0.24, 2.4$, and 24 (from top to bottom). The dashed gray curve is the LVE envelope. (b) The steady state viscosities. For comparison, fitting to the Carreau model[1] is also shown as the dashed gray curve.

Another is the artifact of the atomic SLLOD model and the thermostat[5]. In the SLLOD model, all beads effectively feel the forces generated by a homogeneous shear field. Also, beads feel the forces exerted by the Nosè-Hoover thermostat. These forces may become artificially strong when the shear rate is high. Then polymers will be driven too strongly and the viscosity will be underestimated. The rotational motion of a polymer chain can be also affected by the artifact in a similar way. In both systems, $\eta(\dot{\gamma})$ can be well correlated to the gyration tensor: $\eta(\dot{\gamma}) \propto S_{yy}^{1.4}$ (S_{yy} is the yy-component of the average gyration tensor at the steady state). S_{yy} can be related to the angular momentum, and thus this result implies that the viscosity is strongly related to the angular momentum and also to the rotational behavior. Careful examination of the SLLOD equations and thermostats will be required to clarify the dynamics of polymer chains under fast shear.

ACKNOWLEDGMENTS

This work was supported by JST, PRESTO Grant Number JPMJPR1992.

REFERENCES

1. Colby R. H., Boris D. C., Krause W. E., Dou S. Shear thinning of unentangled flexible polymer liquids, *Rheol. Acta*, **46**, 569-575, 2007.
2. Costanzo S. et al, Strain Hardening of Unentangled Polystyrene Solutions in Fast Shear Flows, *Macromolecules*, **55**, 9206-9219, 2022.
3. Matsumiya Y., Sato T., Chen Q., Watanabe H. Rheo-Dielectric Behavior of Unentangled Poly-(butylene oxide) under Steady Shear: Preliminary Evaluation of Non-Equilibrium Parameters at the Onset of Nonlinearity, *Nihon Reoroji Gakkaishi*, **50**, 371-385, 2022.
4. Kremer K., Grest G. S. Dynamics of entangled linear polymer melts: A molecular-dynamics simulation, *J. Chem. Phys.*, **92**, 5057-5086 , 1990.
5. Travis K. P., Daivis P. J., Evans D. J. Thermostats for molecular fluids undergoing shear flow: Application to liquid chlorine, *J. Chem. Phys.*, **103**, 10638-10651, 1995.

8TH PACIFIC RIM CONFERENCE ON RHEOLOGY, May 15-19, 2023

PSYCHORHEOLOGY: TOWARD UNDERSTANDING HOW WE EXPERIENCE VISCOUS AND VISCOELASTIC MATERIALS

Jeffrey Martin[1], Matjaz Jogan[2], Eric Burgeson[3], and Simon Rogers[3]

[1]Johnson & Johnson Consumer Inc., Skillman, NJ, USA
[2]Ethicon Endo-Surgery, Cincinnati, OH, USA
[3]University of Illinois at Urbana-Champaign

ABSTRACT

Physical properties of materials with which we interact are perceived by combining information gathered with our senses. Properties like "thickness" (viscosity) and "firmness" (elasticity) can be experienced using different senses, e.g., vision and/or touch. We perceive feedback from different modalities during material deformation, e.g., resistance to force, appearance, shape, and motion; however, it is unclear how these measurable properties map to perceptions while driving our behavior and decision-making.

When discriminating differences in the viscosity of *Newtonian liquids* in a two-alternative forced choice (2AFC) task, the observers' sensitivity to changes in viscosity depends on the modality of perception as well as the magnitude of viscosity itself. Furthermore, we found that fluid transparency and opaqueness influenced the visual judgments of thickness. This appearance bias was reduced when observers were able to combine information from vision and touch, but the bias increased when their performance accuracy was negatively affected by mood. Overall, combining information from vision and touch improved discrimination in certain ranges of viscosity but not others. This behavior was well reproduced by a sensory cue combination model with normalization which weighs information from each modality based on its reliability.

When discriminating differences in firmness of six model *viscoelastic* materials (hand therapy putties) in a 2AFC task where both samples are identical, subjects exhibited a strikingly wide range of probing behavior where 70% of the variance is described by creep time, stress rate, and stress. Furthermore, we observe a bias toward whichever sample was probed for a longer total time. In a 2AFC task where all six samples were compared against each other, subjects were unexpectedly accurate when discriminating samples whose linear viscoelastic and traditionally measured nonlinear (LAOS) moduli and viscosities vary by small amounts that are significantly less than the just noticeable difference thresholds for both elastic solids and viscous liquids. This suggests that the material properties that subjects are using to make their determinations are likely not these traditionally measured properties, but rather transient rheological properties which can be readily measured by transient recovery rheology.

MODELLING DROP MOBILITY ON LUBRICATED SURFACES USING A TERNARY FREE ENERGY LATTICE BOLTZMANN ALGORITHM

Sirio Orozco-Fuentes[1] and Ciro Semprebon[1]

[1]Smart Materials & Surfaces Laboratory, Northumbria University,
Newcastle upon Tyne, United Kingdom, NE1 8ST

ABSTRACT

Slippery Liquid-Infused Porous Surface (SLIPS) and Lubricant-Impregnated Surfaces (LIS) consist of a nano/micro-structured porous material infused with a lubricant fluid whose purpose is to facilitate the removal of material defects and imperfections from the surface. This feature places them at the forefront of many fields including anti-biofouling, anti-icing, anti-corrosion and droplet manipulation[1].

The properties of the infused lubricant layer and its interaction with the substrate and the fouling fluid become an integral part of their success in achieving these features. The viscosity of the lubricant layer of a SLIPS/LIS surface plays a fundamental role in drop mobility[2,3]. For practical applications, a compromise is necessary: lubricants with small viscosity favour large mobility, but easily leak out under shear[4], and lubricants with large viscosity are more stable but reduce drop mobility. The apparent viscosity in non-Newtonian liquids varies due to the local shear rate, thus we hypothesise that SLIPS/LIS made of non-Newtonian lubricants may eliminate this drawback, offering new opportunities to control droplets and their motion. For example, non-Newtonian lubricants could allow for enhanced drop mobility and prevent lubricant leakage.

The gathering or depletion of the lubricant is related to the redistribution by capillary flows. When a droplet sits on a SLIPS/LIS, the lubricant is gathered around its edge forming a meniscus. As the droplet moves, it leaves a wake and the menisci break their symmetry making a distinction between the advancing and receding sections. This plays a key role in the resilience of the SLIPS/LIS to maintain its functionality. An example of this effect can be seen in **Fig. 1**, in which the advancing meniscus grows larger than the receding meniscus leaving a depletion wake. Upon adjusting the rheology of the lubricant, this effect can be reversed so that the lubricant layer can recover its thickness more quickly.

In this work, we use a high-density ratio ternary lattice Boltzmann method[5] to model SLIPS/LIS as a flat surface coated with a lubricant layer. We validate the numerical method for a variety of non-Newtonian fluid models in the shear-thinning or shear-thickening regimes, such as the power-law and Carreau-Yasuda[6]. We study the system behaviour under actuation by external forces by quantifying the dissipative forces and by measuring the response of the apparent contact angle of a droplet when actuated by a body force.

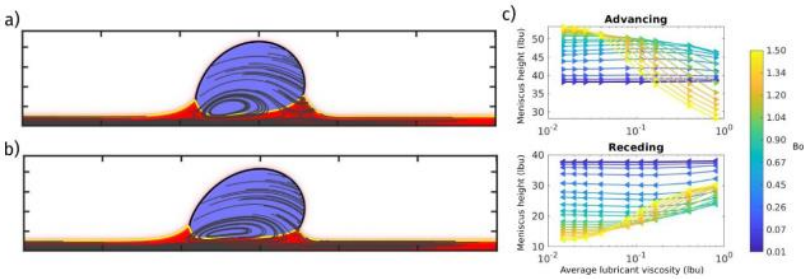

Figure 1: Droplet sliding on a LIS with an average viscosity (a) $\langle \mu_{lub} \rangle = 50\mu_{drop}$ and (b) $\langle \mu_{lub} \rangle = 2\mu_{drop}$ for Bo $= 0.8$. (c) Advancing and receding ridge heights as a function of the average lubricant viscosity under the effect of an external body force actuating on the LIS.

ACKNOWLEDGEMENTS

This project is supported by EPSRC Grant Number: EP/S036857/1.

REFERENCES

1. S. Peppou-Chapman, J.K. Hong, A. Waterhouse, C. Neto. Life and death of liquid-infused surfaces: a review on the choice, analysis and fate of the infused liquid layer.
2. J. D. Smith, R. Dhiman, S. Anand, E. Reza-Garduno, R. E. Cohen, et al. Droplet mobility on lubricant-impregnated surfaces. *Soft Matter*, **6**, 2013.
3. Keiser A., Keiser L., Clanet C., Quéré. Drop friction on liquid-infused materials. *Soft Matter*, **39**, 2017.
4. J. S. Wexler, I. Jacobi and H. A. Stone. Shear-Driven Failure of Liquid-Infused Surfaces. *Phys. Rev. Lett.* **114**, 168301 *Chem. Soc. Rev.*, **49**, 3688, 2020.
5. Sadullah M.S., Semprebon C. and Kusumaatmaja H. Drop Dynamics on Liquid-Infused Surfaces: The Role of the Lubricant Ridge. *Langmuir*, **34**(27):8112-8118, 2018.
6. J. Boyd, J Buick, S. Green. A second-order accurate lattice Boltzmann non-Newtonian flow model. *J. Phys. A: Math. Gen.* **39** (2006), 14241-14247.

ANALYSIS OF PULSATILE FLOWS OF COMPLEX FLUIDS IN TWO-DIMENSIONAL CHANNELS

Nayeon Park[1], Jaewook Nam[1]

[1]School of Chemical and Biological Engineering, Seoul National University, Seoul, Republic of Korea

ABSTRACT

In chemical processes, solutions transported through a series of pipe systems are often exposed to various external disturbances, such as oscillations from flow pumps. The solution transport process is essential when manufacturing high value-added products, where its performance may be significantly affected by changes in the rheological properties or microstructure of complex fluids induced by unpredictable disturbances during transportation. Therefore, it is necessary to understand the flow characteristics of time-dependent complex flows.

There already exists an analytic solution for pulsatile Newtonian flows, and some limiting behaviors of non-Newtonian flows can be anticipated from flow curves. Here, we specifically targeted flow regimes where fluid cannot be simplified to a power-law or Newtonian fluid and where a numerical solution is inevitable, focusing on gaining insights into such flows with the aid of numerical methods. The characteristic viscosity was determined based on steady-state analysis of non-Newtonian flows and was used to form a non-Newtonian Womersley number, which acts as a key model parameter of the system.

Numerical experiments using Carreau fluids with various rheological parameters were conducted to assess the effect of each parameter on flow behavior. Master curves were revealed, exhibiting the amplitude and phase lag dependency on non-dimensional Womersley numbers. Such master curves imply that it is possible to effectively express the competition between viscous and pulsatile time scales by using the proposed non-Newtonian Womersley number. Notably, the shape of the master curve was found to be determined by the degree of shear-thinning. Furthermore, we demonstrate that the flow dynamics can be predicted precisely using precomputed master curves, presenting a novel method for predicting pulsatile flow dynamics of complex fluids without costly transient computations. The proposed approach is expected to be extended to three-dimensional pipe systems to be used in industrial applications[1].

REFERENCES

1. Park, N.; Nam, J. *Physical Review Fluids* **2022**, 7, 123301.

Solving the closure problem for dilute polymer solutions

Shaurya Kaushal[1], Ganesh Subramanian[1], Santosh Ansumali[1]

[1] Engineering Mechanics Unit, Jawaharlal Nehru Centre for Advanced Scientific Research, Bengaluru, India

ABSTRACT

Typically, rheological models for dilute polymer solutions are obtained via approximate representation of the underlying micro-mechanical model of the individual macromolecules[1]. The most simple micro-mechanical model for a dilute polymer solution is the elastic dumbbell model that consists of two beads connected by an entropic spring. The simplistic Hookean spring force approximation yields an **O**ldroyd-B type fluid which suffers from many fallacies when the distribution is far from Gaussian. While, Warner's finitely extensible non-linear elastic spring (FENE) is more realistic and leads to better rheological predictions, it leads to a closure problem at the macroscopic level. The **F**ENE-P approximation to FENE model allows us to formulate a closed form constitutive equation for the conformation tensor. While this is a good model and qualitatively correct, in strong flows and transient flows it leads to erroneous predictions. In complex flows such as flow past a cylinder, FENE-P approximation predicts stresses that are substantially times larger than FENE, even at a moderate Weissenberg number.

We revisit this question of approximate constitutive models for FENE model and focus our attention on the **tensorial structure** of many closure approximations in literature, and their intrinsic inability to capture the second normal stress difference ($N2$) in simple shear flows. We suggest a simple and elegant approach to correct the tensorial structure of the polymeric stress approximation. This understanding is then carried forward to the framework in the second part of the work, where we focus on the selection of relevant macroscopic variables in the system.

We recognize that the non-linearity of the spring is crucial for predicting correct rheological behaviour. Similar to kinetic theory of gases, one needs more variables to represent highly non-linear situations. We show that this new model FENE-NP, drastically improves the steady state and time dynamics results over FENE-P model, even in strong extensional flows. Finally, we discuss possible coupling of this constitutive model with flow solvers such as lattice Boltzmann.

REFERENCES

In-text citations

For references to documents referred to in the reference list, use superscript sequentially[1−6]. Author names may be used together with a superscript number.

[1]RB Bird, RC Armstrong, O Hassager., *Dynamics of polymeric liquids. Vol. 2: Fluid mechanics.* (1987).

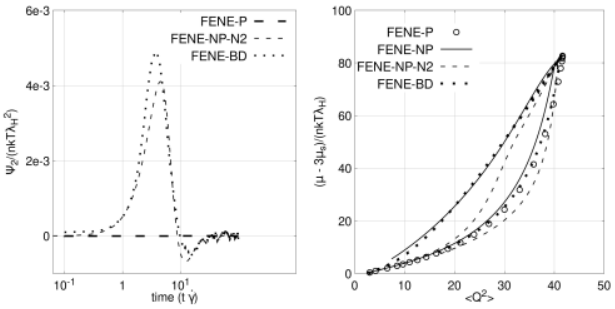

Figure 1: (a)Non-zero N2 for a simple shear flow at Wi=10.
(b)Hysteresis observed in a uniaxial extensional flow.
FENE-P fails to predict a transient non-zero second normal stress difference (**N2**) in simple shear flows and **fails to predict hysteresis** in strong extensional flows. BD : Brownian dynamics

EXAMPLE OF REFERENCE LIST STYLES

1. Robert Byron Bird, Robert Calvin Armstrong, and Ole Hassager. Dynamics of polymeric liquids. vol. 2 Kinetic theory. 1987
2. Hans Christian Ottinger. On the stupendous beauty of closure. Journal of Rheology, 53(6) 1285 1304, 2009
3. Anton Peterlin. Hydrodynamics of macromolecules in a velocity field with longitudinal gradient. Journal of Polymer Science Part B: Polymer Letters, 4(4) 287 291, 1966.
4. Roland Keunings. On the peterlin approximation for finitely extensible dumbbells. Journal of Non-Newtonian Fluid Mechanics, 68(1) 85 100, 1997.

8TH PACIFIC RIM CONFERENCE ON RHEOLOGY, May 15-19, 2023

Relationships between viscoelastic relaxation and network connectivity in transient networks with well-controlled network structures

Takuya Katashima[1], Mitsuru Naito[1], Satoru Nagatoishi[1], Kanjiro Miyata[1], Kouhei Tsumoto[1], Ung-il Chung[1] and Takamasa Sakai[1]

[1]The University of Tokyo, Tokyo, Japan

ABSTRACT

Polymers crosslinked by reversible interactions form transient networks, which show fascinating viscoelasticity due to a finite lifetime of crosslinks. However, the molecular understanding of such viscoelasticity has remained incomplete because of the difficulty of experimentally evaluating bond lifetimes and heterogeneous structures in conventional transient networks. In this study, we developed a model system of transient networks with well-controlled structures (Tetra-PEG slime) to overcome these problems. We demonstrate an experimental comparison of the bond lifetime, estimated using surface plasmon resonance (SPR) and the viscoelastic relaxation time as a function of network connectivity. With decreasing network connectivity, the viscoelastic relaxation time accelerated and became shorter than the bond dissociation time. With increasing polymer concentration, the connectivity at which the viscoelastic relaxation time matched the dissociation time shifted to the high-connectivity region. The dependence of viscoelastic relaxation on connectivity can be adequately explained within the framework of the lifetime of a "backbone." The backbone has numerous breakage points in low-connectivity region nearby the gelation point, resulting in a shorter lifetime than the dissociation time. These findings provide a crucial foundation for the molecular comprehension of transient network materials.

INTRODUCTION

Transient networks formed through reversible crosslinking show fascinating viscoelasticity due to a finite lifetime of crosslinks. Recently, there have been reports that temporary crosslinks play an essential role in polymeric materials' toughness and self-healing ability, making it important to understand the correlation between micro-kinetics and macro-viscoelasticity.[1] However, the molecular understanding of such viscoelasticity has remained incomplete because of the difficulty of evaluating bond lifetimes and heterogeneous structures in conventional experimental systems. Primarily, heterogeneities are comprised of static structures (dangling chains, heterogeneous distribution of network strand length, and branching number), and dynamics (mixture of slow dynamics from network components and fast dynamics from micellar or unimer structures in one system).[2] These heterogeneities are impossible to evaluate quantitatively and prevent molecular understanding the viscoelastic properties of transient networks. In this study, we developed a model system of transient networks consisting of mutually associative star-armed polymers to control the network structures precisely (called Tetra-PEG slime).[3] Using this system, we demonstrate an experimental comparison of the bond lifetime, estimated using surface plasmon resonance (SPR) and the terminal relaxation time for

the Tetra-PEG slime. Here, to control the network connectivity precisely, we mixed the precursors in an imbalanced ratio (Figure 1).[4]

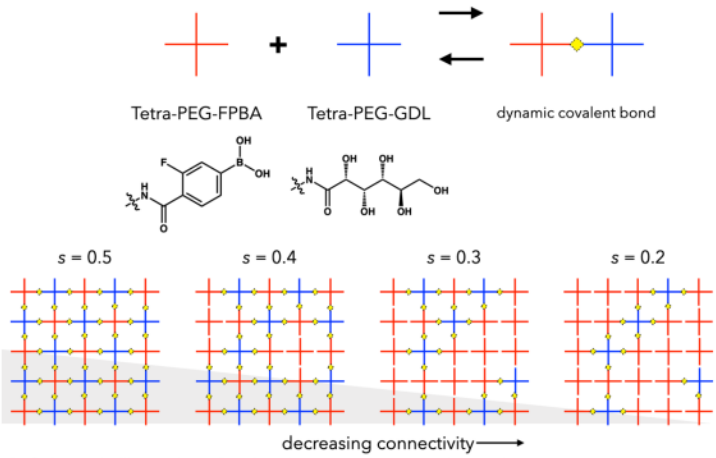

Figure 1: Schematic illustration of tuning the network connectivity, where two precursors are mixed at either a stoichiometric ratio ($s = 0.5$) or an imbalanced ratio ($s \neq 0.5$).

RESULTS AND DISCUSSION

The temperature dependence of the terminal relaxation time (τ) followed the Arrhenius-type equation over a wide range, independent of the detailed network structures. On the other hand, the dissociation time of the end groups estimated from SPR measurements also showed a similar temperature dependence, strongly suggesting that the elementary reaction of the viscoelastic relaxation is the dissociation process.

Figure 2 shows the relationship between τ and p. The termination relaxation time was delayed with increasing p. Furthermore, the degree of delay was more pronounced at lower polymer concentrations. The relaxation time was also delayed by increasing the molecular weight of the precursor. The solid line in the figure indicates the dissociation time obtained from SPR. Interestingly, τ was larger than the dissociation time in the high-p region. On the other hand, as p decreased, τ decreased and became smaller than the dissociation time.

This is well explained by the durability of the "backbone," which essentially supports the stress in the networks. At high connectivity, one dissociation cannot kill the backbone since the other strands support the stress. Meanwhile, at low connectivity near the gelation point, the backbone resembles a linear chain with some breakable points and has a shorter lifetime than the dissociation time. Conventional theoretical models[5] do not predict the concentration dependence, indicating that network formation in the semi-dilute region is far from a random branching process. The reported direct comparison of bond lifetime-viscoelasticity-relaxation times provides essential information for the molecular design of transient network materials.

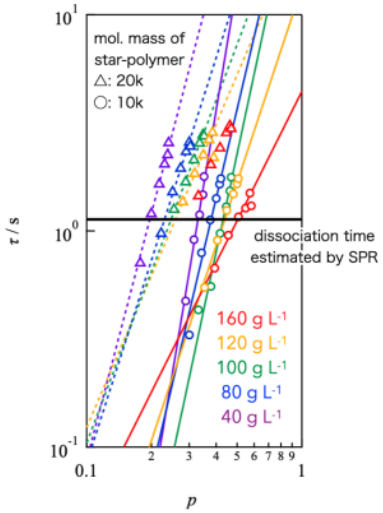

Figure 2: Double logarithmic plot of viscoelastic relaxation time against network connectivity (p). Circles and triangles represent the data of different molar masses of precursors of 10,000 and 20,000 g mol^{-1}, respectively. The solid line represents the bond lifetime estimated by SPR.

ACKNOWLEDGEMENTS

This work was supported by the Japan Society for the Promotion of Science (JSPS) through the Grants-in-Aid for Early-Career Scientists to T.K. (grant No. 20K15338), and the Japan Science and Technology Agency (JST) to T.S. (CREST) (grant No. JPMJCR1992).

REFERENCES

(1) Creton, C. 50th Anniversary Perspective: Networks and Gels: Soft but Dynamic and Tough. *Macromolecules* **2017**, *50* (21), 8297–8316.

(2) Katashima, T. Molecular Understanding of Viscoelasticity in Transient Polymer Networks Based on Multiple Methods. *Nihon Reoroji Gakkaishi* **2022**, *50* (1), 51–56.

(3) Katashima, T.; Kudo, R.; Naito, M.; Nagatoishi, S.; Miyata, K.; Chung, U.-I.; Tsumoto, K.; Sakai, T. Experimental Comparison of Bond Lifetime and Viscoelastic Relaxation in Transient Networks with Well-Controlled Structures. *ACS Macro Lett.* **2022**, *11* (6), 753–759.

(4) Katashima, T.; Kudo, R.; Onishi, R.; Naito, M.; Nagatoishi, S.; Miyata, K.; Tsumoto, K.; Chung, U.-I.; Sakai, T. Effects of Network Connectivity on Viscoelastic Relaxation in Transient Networks Using Experimental Approach. *Front. Soft. Matter* **2022**, *2*. https://doi.org/10.3389/frsfm.2022.1059156.

(5) Rubinstein, M.; Semenov, A. N. Thermoreversible Gelation in Solutions of Associating Polymers. 2. Linear Dynamics. *Macromolecules* **1998**, *31* (4), 1386–1397.

PHANTOM CHAIN SIMULATIONS FOR TETRA AND TRI-BRANCHED NETWORKS

Yuichi Masubuchi[1], Yuya Doi[1], Takato Ishida[1], Naoyuki Sakumichi[2], Takamasa Sakai[2], Koichi Mayumi[3] and Takashi Uneyama[1]

[1] Nagoya University, Nagoya 4648603, Japan
[2] The University of Tokyo, Tokyo 1138654, Japan
[3] The University of Tokyo, Chiba 2778581, Japan

Effects of branch functionality on mechanical properties of polymer networks have not been fully elucidated yet, although multi-functional approaches have been mainly attempted. For instance, Fujiyabu et al.[1] have recently reported that polymer networks made from tri-branch prepolymers exhibit superior mechanical properties to tetra-branch analogs. Although they attribute the difference to stretch-induced crystallization observed in tri-branch poly (ethylene glycol) networks, the mechanism still needs to be clarified. In this study[2], we performed coarse-grained molecular simulations to extract the effect of branch functionality. The prepolymers were replaced by bead-spring phantom chains, and gelation was simulated by a Brownian dynamics scheme[3,4] We subjected the resultant networks to energy minimization and uniaxial stretch by introducing breakage for elongated segments. In the stress-strain relation thus obtained, stress and strain at the break were larger for tri-branch networks than for tetra-branch analogs, consistent with the experiment. The superiority of tri-branch networks is observed in a wide range of the conversion ratio in gelation, molecular weights of prepolymers, and polymer concentrations. The result implies that the mechanical superiority of tri-branch networks to tetra-branch ones is due to a fundamental structural difference generated during gelation.

1. Fujiyabu, T.; Sakumichi, N.; Katashima, T.; Liu, C.; Mayumi, K.; Chung, U.; Sakai, T. Tri-Branched Gels: Rubbery Materials with the Lowest Branching Factor Approach the Ideal Elastic Limit. *Sci Adv* **2022**, *8* (14), abk0010_1-abk0010_10. https://doi.org/10.1126/sciadv.abk0010.
2. Masubuchi, Y.; Doi, Y.; Ishida, T.; Sakumichi, N.; Sakai, T.; Mayumi K.; Uneyama, T. Phantom chain simulations for the fracture of energy-minimized tetra and tri-branched networks. Submitted to *Macromolecules*
3. Masubuchi, Y.; Uneyama, T. Retardation of the Reaction Kinetics of Polymers Due to Entanglement in the Post-Gel Stage in Multi-Chain Slip-Spring Simulations. *Soft Matter* **2019**, *15*, 5109–5115. https://doi.org/10.1039/C9SM00681H.
4. Masubuchi, Y.; Yamazaki, R.; Doi, Y.; Uneyama, T.; Sakumichi, N.; Sakai, T. Brownian Simulations for Tetra-Gel-Type Phantom Networks Composed of Prepolymers with Bidisperse Arm Length. *Soft Matter* **2022**, *18* (25), 4715–4724. https://doi.org/10.1039/d2sm00488g.

Negative energy elasticity in polymer gel elasticity

Takamasa Sakai and Naoyuki Sakumichi

Graduate School of Engineering, The University of Tokyo, Japan

In thermodynamics and statistical mechanics, elasticity of rubber appears as a representative example of "entropic force" arising from the thermal motion of chains. To confirm that "entropic force" dominates the elasticity of real rubber, it is enough to measure the temperature (T) dependence of the shear modulus (G) under constant volume conditions. This is because the relationship equation $G_S = TdG/dT$ derived from the general theory of thermodynamics can be used to separate the elasticity G into entropic elasticity G_S and energy elasticity G_E ($G = G_S + G_E$) originating from changes in entropy and internal energy, respectively. This equation has been experimentally confirmed that the elasticity of natural and synthetic rubber is mostly entropic ($G \approx G_S$) [1,2].

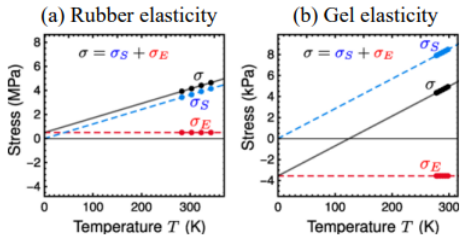

On the other hand, for polymer gels (hereinafter simply referred to as gels), a model of rubber elasticity theory is conventionally used without experimental verification, assuming that its elasticity is entropic [3,4]. Usually, the elastic modulus of gels is predicted based on classical rubber elasticity models (affine network models, phantom network models, etc.) [3,4]. The central assumption of these models is that "elasticity is mostly determined by entropic elasticity."

Recently, we have discovered that the assumption that the elasticity of polymer gels is solely due to entropy changes is incorrect and that the elasticity of polymer gels also includes a large "negative energy elasticity" G_E from the solvent in addition to entropy elasticity G_S [5-7]. The elasticity of the gel can be approximated as a linear function of temperature ($G = aT+b$), with the first term ($G_S = aT$) corresponding to the contribution of entropy and the second term ($G_E = b$) corresponding to the contribution of internal energy. A large negative energy elasticity means that b has a significant negative value. In the first report of negative energy elasticity, the ratio $|G_E|/G$ reached 1.8 at the maximum. When the polymer concentration of the gel is increased, or in other words, when the gel is made closer to rubber by reducing the solvent, the negative energy elasticity b approaches zero. Thus, the conventional understanding that rubber's elasticity is mainly determined by entropy elasticity ($G \approx G_S$) is consistent with this. Conversely,

negative energy elasticity originates from the solvent and gives the fundamental difference between rubber and gel elasticities.

The negative energy elasticity was first discovered in hydrogels with polyethylene glycol (PEG) as the main chain [5], and has since been reported in other gels such as PDMS gels [8]. Although it is not yet clear whether negative energy elasticity is present in all gels, it is expected to be universally present in many gels that have good solvents and low polymer concentrations.

REFERENCES

1. K. H. Meyer and C. Ferri, Helv. Chim. A. **18**, 570 (1935).
2. R. L. Anthony, R. H. Caston, and E. Guth, J. Phys. Chem. **46**, 826 (1942).
3. Y. Osada, K. Dusek, M. Shibayama, K. Urayama, "Gel no Kagaku" Kodansha, 2020.
4. M. Zhong, J. A. Johnson, *et al*., Science 353, 1264 (2016).
5. Y. Yoshikawa, N. Sakumichi, U. Chung, and T. Sakai, Phys. Rev. X **11**, 011045 (2021).
6. N. Sakumichi, Y. Yoshikawa, and T. Sakai, Polymer J. **53**, 1293 (2021).
7. T. Fujiyabu, T. Sakai, R. Kudo, Y.Yoshikawa, N. Sakumichi, *et al*., Phys. Rev. Lett. **127**, 237801 (2021).
8. T. Aaoyama, K. Urayama, Abstract of Gel Symposium 2M06 (2023).

Universal Equation of State of Osmotic Pressure for Polymer Gels

Takashi Yasuda[1], Naoyuki Sakumichi[1], and Takamasa Sakai[1]

[1]Department of Bioengineering, The University of Tokyo, Bunkyo-ku, Japan

ABSTRACT

Polymer gels are soft solids consisting of three-dimensional polymer networks with predominantly liquid content. The polymer networks is dissolved in the solvents and thus have the osmotic pressure while being a viscoelastic solid. Examining the precisely controlled polymer gels with various network structures, we successfully decompose the elastic contribution to the osmotic pressure and experimentally reveal that the osmotic pressure throughout the gelation process is described by the universal osmotic equation of state of polymer solutions. Furthermore, we find that the semidilute scaling law of polymer solutions, including the critical exponent of self-avoiding walks, universally governs polymer gels. Our findings demonstrate that the semidilute scaling law is a fundamental principle for governing the osmotic pressure of polymer gels.

INTRODUCTION

The osmotic pressure is a kind of colligative property that exhibits a law independent of the type of substance. For dilute solutions, it is widely known that the osmotic pressure obeys the van 't Hoff law, which is analogous to the ideal gas law. However, because of the significant excluded volume of polymer chains, the osmotic pressure in polymer gels is not described through the van 't Hoff law[1,2].

On the other hand, for solutions of linear polymer chains, the elaborate studies in the 1970-80s[3,4] have revealed that the osmotic pressure for the dilute to semidilute regime in good solvents is described by the universal equation of state (EOS): $\hat{\Pi} = f_{\Pi}(\hat{c})$. Here, $\hat{\Pi} \equiv \Pi M/(cRT)$ is the reduced osmotic pressure and $\hat{c} \equiv c/c^*$ is the reduced polymer mass concentration c normalized by overlap concentration $c^* \equiv 1/(A_2 M)$, where M is the molar mass, R is the gas constant, T is the absolute temperature, and A_2 is the second virial coefficient. In the dilute regime ($0 \leq \hat{c} < 1$), each molecular chain is isolated to sufficiently describe the universal EOS through virial expansion:

$$\hat{\Pi} = 1 + \hat{c} + \gamma \hat{c}^2 + \cdots, \tag{1}$$

where $\gamma \approx 0.25$ is the dimensionless virial ratio[5]. In the semidilute regime ($\hat{c} > 1$), the molecular chains interpenetrate, and the universal EOS is asymptotic to the semidilute scaling law[6]:

$$\hat{\Pi} = K c^{\frac{1}{3\nu-1}}, \tag{2}$$

where $K \approx 1.1$ is the universal constant and $1/(3\nu - 1) \approx 1.31$ because of the excluded volume parameter $\nu \approx 0.588$ for good solvents[5]. Here, ν is also known as the universal critical exponent of the self-avoiding-walk universality class[7].

In this study, we experimentally reveal that the osmotic pressure throughout the gelation process (i.e., polymer chains in solutions are crosslinked to form the infinite polymer networks) is described by the universal EOS of polymer solutions[1]. Furthermore, we find that the semidilute scaling law of polymer solutions [Eq. 2], including the critical exponent of self-avoiding walks, universally governs polymer gels[1,2].

RESULTS AND ANALYSIS

To investigate the governing law of osmotic pressure in polymer gels, we experimentally measured the osmotic pressure throughout the gelation process via membrane osmometry[1]. Here, we statically reproduced the gelation process to measure the osmotic pressure by using *AB*-type polymerization system[8]. Moreover, we decompose the elastic contribution $\Pi_{\rm el}$ to the measured osmotic pressure Π to evaluate the mixing contribution $\Pi_{\rm mix} = \Pi - \Pi_{\rm el}$ in polymer gels. Here, we measured the shear modulus G_0 of polymer gels at the as-prepared state via dynamic viscoelasticity measurement to evaluate the elastic contribution $\Pi_{\rm el} = -G_0$.

Figure 1(a) shows Π, $\Pi_{\rm el}$ and $\Pi_{\rm mix}$ during the gelation process. Unlike the sol state ($0 \leq p < p_{\rm gel}$, where p is the network connectivity and $p_{\rm gel}$ is the gelation point), the gel state ($p_{\rm gel} < p \geq 1$) has elastic contributions $\Pi_{\rm el}$ to the osmotic pressure Π. As the connectivity p increases at a constant c, Π in the sol state decreases because of the increase of M (blue solid line). After gelation, $\Pi_{\rm mix}$ reaches a constant (blue solid line); polymer gels are always in a semidilute regime with an infinite M. On the other hand, Π decreases (blue dotted line) and $\Pi_{\rm el}$ increases (red solid curve) as p increases in gel state.

We demonstrate that the decrease of Π in the sol state and the constant $\Pi_{\rm mix}$ in gel state in **Fig. 1**(a) is described through the universal EOS of polymer solutions[3,4] and the semidilute scaling law[5] [Eq. 2], respectively. To change the state variable ($c \rightarrow \hat{c}$ and $\Pi \rightarrow \hat{\Pi}$), we evaluate M and c^* for each p in the sol state, using the square root plot[5] $\sqrt{\Pi/c} \simeq \sqrt{RT/M}[1 + c/(2c^*)]$ for small c/c^*. The obtained M and c values are consistent with the scaling prediction of $c^* \sim M^{1-3\nu}$.

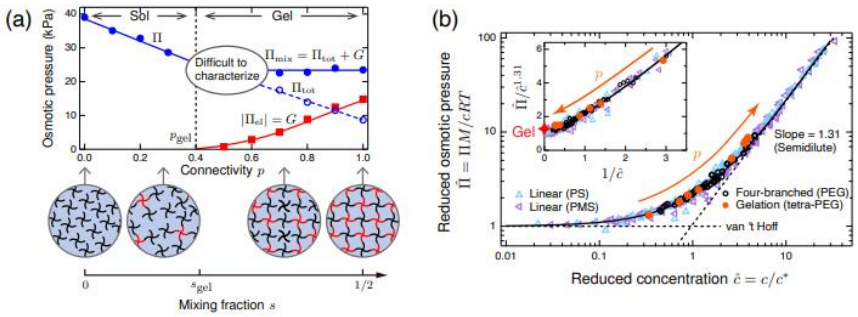

Figure 1: (a) Osmotic pressure and (b) universal equation of state during gelation process[1].

Figure 1(b) shows the universal EOS (black solid curve) in the linear polymer solutions[3,4] (light blue and purple open triangles), in the prepolymer solutions ($p = 0$) (black open circles), and during the gelation process in the sol state (orange filled circles). With the increase of M and decrease of c^* as p increases, the osmotic pressure during gelation process in the sol state is described by the same universal laws as for the polymer solutions.

On the other hand, in the gel state, $\hat{\Pi} \to \infty$ and $\hat{c} \to \infty$ because $M \to \infty$ and $c^* \to 0$. However, we can consider $\hat{\Pi}_{\rm mix}\,\hat{c}^{1/(1-3\nu)}$ for the gel state, using the obtained scaling relation $c^* \sim M^{1-3\nu}$ for the sol state. The inset in **Fig. 1**(b) demonstrate that $\hat{\Pi}\,\hat{c}^{1/(1-3\nu)}$ during the gelation process in the sol state (orange filled circles) and in the gel state (red stars) converge to the universal value $K \approx 1.1$, which is independent of M, c, and p. Thus, $\Pi_{\rm mix}$ of the polymer gels is universally governed by the semidilute scaling law of polymer solutions [Eq. 2]. Therefore, the osmotic pressure throughout the gelation process is described by the universal EOS of polymer solutions.

REFERENCES

1. Yasuda T., Sakumichi N., Chung U., and Sakai T. Universal equation of state describes osmotic pressure throughout gelation process. *Phys. Rev. Lett.* **2020**, 125, 267801.
2. Sakumichi N., Yasuda T., and Sakai T. Semidilute principle for gels. arXiv:2210.15275.
3. Noda I., Kato N., Kitano T., and Nagasawa M. Thermodynamic properties of moderately concentrated solutions of linear polymers. *Macromolecules* **1981**, 14, 668-676.
4. Higo Y., Ueno N., and Noda I. Osmotic pressure of semidilute solutions of branched polymers. *Polym. J.* **1983**, 15, 367-375.
5. Flory P.J. *Principle of Polymer Chemistry* (Cornell University Press, Ithaca, 1953).
6. Des Cloizeaux J. The Lagrangian theory of polymer solutions at intermediate concentrations. *J. Phys. (Paris)* **1975**, 36, 281-291.
7. Pelissetto A., and Vicari E. Critical phenomena and renormalization-group theory. *Phys. Rep.* **2002**, 368, 549-727.
8. Sakai T., Matsunaga Y., Yamamoto Y., Ito C., Yoshida R., Suzuki S., Sasaki N., Shibayama M., and Chung U. Design and fabrication of a high-strength hydrogel with ideally homogeneous network structure from tetrahedron-like macromonomers. *Macromolecules* **2008**, 41, 5379-5384.

8TH PACIFIC RIM CONFERENCE ON RHEOLOGY, May 15-19, 2023

INFLUENCES OF SHAPE OF MOLECULAR WEIGHT DISTRIBUTION ON TENSILE PROPERTIES OF POLYETHYLENE SOLIDS

Takumitsu Kida[1,2], Ryo Tanaka[3], Takeshi Shiono[3],
Masayuki Yamaguchi[1], Katsuhisa Tokumitsu[2]

[1]Japan Advanced Institute of Science and Technology, Ishikawa, Japan
[2]The University of Shiga Prefecture, Shiga, Japan
[3]Hiroshima University, Hiroshima, Japan

The molecular weight distribution (MWD) is one of the most important molecular parameters affecting the rheological and mechanical properties of polymeric materials. For the solid-state polymers, it has been reported that the strength and strain-hardening modulus of samples with broad MWD containing high-molecular-weight chains are significantly high compared with those with narrow MWD.[1] However, the mechanism of the improvement of the strength and strain-hardening modulus by adding the high-molecular-weight component has not been elucidated due to the complex morphology. In this study, we prepared a series of samples with different shapes of MWD to investigate the influences of the MWD on the mechanical properties of solid-state polymers.

We synthesized three polyethylenes (PEs) with narrow MWD (M_w/M_n < 1/3) and M_w of 1.2×10^5, 3.2×10^5, and 25.0×10^5. The synthesized PEs were blended with polydispersed PE ($M_w = 0.6\times10^5$ and $M_w/M_n = 5.3$) with a weight fraction of 5% in boiling xylene at 135 °C followed by participating in cold methanol. The blend PEs were melt-pressed at 210 °C and quenched at 0 °C to prepare sample sheets with a thickness of approximately 0.2 mm. Figure 1 shows the stress–strain curves of all samples. The number attached in the sample code indicates the value of M_w. The stress–strain curve of PE6/PE12 was almost the same as that of PE6, suggesting that the molecular-weight component of 1.2×10^5 has almost no influence on the tensile properties. On the other hand, the strength and strain-hardening modulus were obviously increased by adding PE32 and PE250. Considering that the molecular chains with a molecular weight larger than 3.2×10^5 have a high probability for forming tie molecules connecting more than 6 lamellar crystals[2], the strength and strain-hardening modulus are dominated by the amount of the tie molecules connecting more than six lamellae.

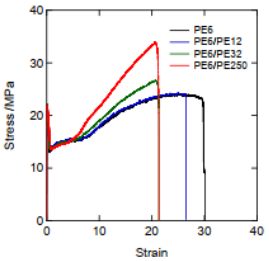

Figure 1. Stress–strain curves of all PE samples.

1. Wu, T.; Yu, L.; Cao, Y.; Yang, F.; Xiang, M., Effect of molecular weight distribution on rheological, crystallization and mechanical properties of polyethylene-100 pipe resins, *J. Polym. Res.*, **20**, 271., 2013.
2. Huang, Y.-L.; Brown, N., The effect of molecular weight on slow crack growth in linear polyethylene homopolymers, *J. Mater. Sci.*, **23**, 3648–3655., 1988.

LINKING MULTISCALE RHEOLOGY TO PERFORMANCE OF HIERARCHICALLY STRUCTURED PEM FUEL CELL CATALYST LAYER

Min-hyung Lee[1], Leonardo Martin-Alarcon[1], and Milana Trifkovic[1]

[1]Chemical and Petroleum Engineering, University of Calgary, Calgary, Canada

ABSTRACT

Fuel cell technology is a rapidly evolving field as alternate energy sources become more crucial for the transition towards sustainable energy. However, the widespread adoption of fuel cells has been hindered by various issues, including the usage of expensive noble metals. Currently, the catalyst layers in a polymer electrolyte membrane (PEM) fuel cell are created from colloidal inks containing platinum-doped carbon nanoparticles (Pt/C) and ionomers suspended in an alcohol/water solvent. Unfortunately, the rapid solvent evaporation during this process results in catalyst layers with little control over their structure, which affects their performance. To improve the efficiency of fuel cells, we focused on hierarchically structuring the catalyst layer using spinodal decomposition of a water and 2,6-lutidine system. Our preliminary results show significant improvements in cell performance, with a 47% higher power density compared to conventional methods. While examining such improvements, rheology tests have demonstrated a significant increase in the storage modulus during spinodal decomposition, indicating a continuous network formation with jammed particles[1]. EDX analysis has further supported the jamming of Pt/C and ionomer chains in the lutidine-rich phase. Microrheology tests have shown that Pt/C and ionomers have a stronger affinity in the lutidine-rich phase, resulting in higher viscosity near the aggregate of Pt/C. This indicates ionomer chains' wrapping around Pt/C aggregates, leading to a higher rate of chemical reaction as it only occurs at boundaries between Pt/C, ionomer, and reactants. In summary, our proposed method for producing catalyst layers represents a significant advancement in fuel cell technology, as it enables greater control over the structure of the catalyst layer, and thereby enhancing the overall performance of cells. Additionally, our multiscale approach enabled gaining fundamental insights into the improved performance, including the formation of bicontinuous channels for better mass transport and the facilitation of ionomer coverage over Pt/C aggregates.

ACKNOWLEDGEMENTS

The authors thank Dr. Kunal Karan's research group for their support in operating the fuel cells.

REFERENCES

1. Kinkead, B., Malone, R., Smith, G., Pandey, A. and Trifkovic, M. Bicontinuous intraphase jammed emulsion gels: A new soft material enabling direct isolation of co-continuous hierarchical porous materials. *Chemistry of Materials*, **31(18)**, 7601-7607, 2019.

INERTIAL FLOW OF IMMERSED ELASTIC CAPSULES THROUGH A CORNER

Damien P. Huet[1], Antoine Morente[1], Guodong Gai[1] and Anthony Wachs[1,2]

[1]Department of Mathematics, University of British Columbia, Vancouver, Canada
[2]Department of Chemical & Biological Engineering, University of British Columbia, Vancouver, Canada

ABSTRACT

The study of immersed elastic membranes enclosing an inner fluid, or capsules, has seen tremendous interest in the past two decades owing to the fact that capsules are a good model to describe a wide range of flowing biological cells, including red blood cells (RBCs), leukocytes and circulating tumor cells (CTCs). The ability to accurately model and numerically simulate flowing capsules can help develop microfluidic "lab-on-chip" devices, used to perform a variety of tasks such as cell segregation and cell characterization based on size, membrane deformability and inner fluid properties[1]. In particular, the inertial-based migration technique has been recently developed and offers the potential to achieve non-destructive blood plasma extraction and enhanced size-based cell segregation[2]. Such microfluidic devices usually include long spiral channels of micrometric widths, as well as several other layers of channels connected together by sharp turns.

Motivated by such devices, we propose to study the deformation of capsules in a model square channel presenting a 90 degrees angle. To this end, we use our open-source adaptive front tracking solver based on the Basilisk software[3]. In this solver, the solid boundaries are represented using the conservative, sharp embedded boundaries method, and the capsule stresses are resolved using a linear finite element method and a paraboloid fitting technique. The flow is controlled by the channel Reynolds number Re and the Capillary number Ca:

$$Re = \frac{\rho U W}{\mu}, \qquad Ca = \frac{\mu U}{E_s},$$

where ρ is the fluid density, U is the average fluid velocity, W is the channel width, μ is the fluid viscosity and E_s is the elastic modulus of the capsule. We show validation results in the non-inertial regime and compare them to those obtained by Zhu & Brandt[4]. As the Reynolds and Capillary numbers vary, we measure the capsule velocity, its area dilatation (a proxy for the capsule potential elastic energy), as well as the general structure of the surrounding flow field. A collection of snapshots is shown in figure 1 for two Capillary and Reynolds numbers. In addition to studying the inertial flow of a solitary capsule, we also introduce a secondary capsule and study its effect on the flow field and the capsule properties as a function of its initial distance from the leading capsule.

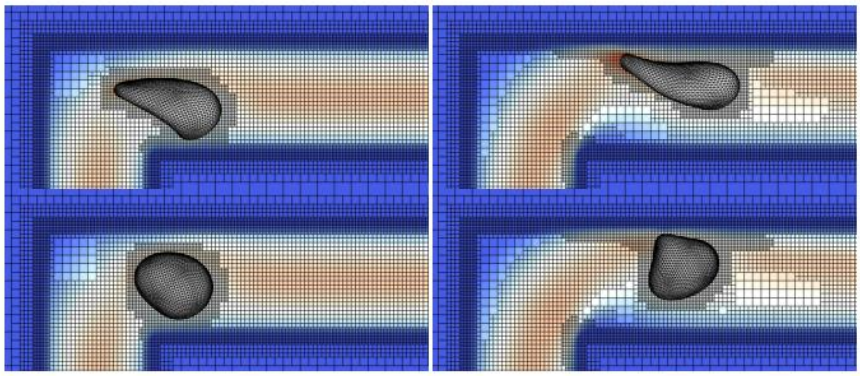

Figure 1: Visualization of the capsule and its surrounding flow field at $Ca = 0.12$ (top) and $Ca = 0.025$ (bottom); as well as $Re = 0.01$ (left) and $Re = 50$ (right). The capsule inlet is located 10 capsule diameters below the corner, and the outlet is located 10 capsule diameters to the right of the corner. The color field represents the norm of the velocity (dark blue is zero and red is max).

ACKNOWLEDGEMENTS

The authors greatly appreciate the financial support of the Natural Sciences and Engineering Research Council of Canada (NSERC) via Anthony Wachs' Discovery Grant RGPIN-2016-06572. This research was enabled by support provided by Compute Canada (http://www.computecanada.ca) through Anthony Wachs's 2021 and 2022 Computing Resources for Research Groups allocation qpf-764-ac.

REFERENCES

1. Emel Islamzada, Kerryn Matthews, Quan Guo, Aline T Santoso, Simon P Duffy, Mark D Scott, and Hongshen Ma. "Deformability based sorting of stored red blood cells reveals donor-dependent aging curves", *Lab on a Chip*, 20(2):226–235, 2020.

2. Yaohui Fang, Shu Zhu, Weiqi Cheng, Zhonghua Ni, and Nan Xiang. "Efficient bioparticle extraction using a miniaturized inertial microfluidic centrifuge", *Lab on a Chip*, 22(18):3545–3554, 2022.

3. Huet, Damien P., Wachs, Anthony. "A Cartesian-octree adaptive front-tracking solver for immersed biological capsules in large complex domains." *arXiv preprint 2211.15814*, 2022. https://arxiv.org/abs/2211.15814

4. Lailai Zhu and Luca Brandt. "The motion of a deforming capsule through a corner". *Journal of Fluid Mechanics*, 770:374–397, 2015.

SLIP BEHAVIOUR AND THIXOTROPY OF KAOLINITE AND MATURE FINES TAILINGS

Jourdain H. Piette[1], and Savvas G. Hatzikiriakos[1]

[1]Department of Chemical and Biological Engineering, The University of British Columbia, Vancouver, Canada

ABSTRACT

The rheological characteristics of kaolinite suspensions and mature fine oil tailings (MFT) were examined in both the linear and non-linear viscoelastic regimes. Both systems exhibited apparent slip, which was suppressed by using sandpaper of grit 80 (200 microns) at the wall of the parallel-plate geometry. The true yield stress with shear-thinning behaviour was determined by fitting the Herschel-Bulkley model. The presence of bitumen remaining in the MFTs (up to 2 wt%) suppressed the apparent slip to a large extent due to the immobilization of the particles at the interface. Ionic surfactants, namely sodium dodecyl sulfate (SDS) and cetyltrimethylammonium bromide (CTAB), were added to both kaolinite suspensions and MFT. SDS was shown to cause thinning and decreasing yield stress, while CTAB caused gelation and increasing yield stress. The yield stress of two MFT suspensions possessing similar volume fractions was found to be similar, however, kaolinite suspensions (formulated to mimic/match the MFT rheology) showed more shear thinning. MFT samples were found to be thixotropic while kaolinite suspensions exhibited antithixotropy. This thixotropy is explored to understand differences in network structure of both suspensions.

Z-SHAPED DEJAMMING PHASE DIAGRAM OF COLLOIDAL GELS

Bin Xia[1], Shoubo Li[1], and Xiaorong Wang[1,2]

[1] School of Chemical Science and Engineering, Tongji University, Shanghai, China
[2] Institute for Advanced Study, Tongji University, Shanghai, China

ABSTRACT

For physically gelled colloidal suspensions, there are two routes that can transform the gel from solid to liquid. One is to raise the temperature, and the other is to increase the shear deformation. In this investigation, we found that the phase boundary of this solid-to-liquid transformation exhibits a surprising Z-shaped curve in the strain-temperature plane. This non-monotonic feature in the phase transition appears to be present in various nanoparticle-filled colloidal gels with significant differences in chemical composition, filler type, structure, particle shape, average diameter and particle size distribution. By applying the Kraus model[1] to the breakage and restoration of filler network and comparing our findings to nonequilibrium glassy behavior, we found that this non-monotonic phenomenon can be theoretically predicted by combining the glassy melting kinetics of filler network at high temperatures with the viscosity-retarded dissociation[2] between particles at low temperatures.

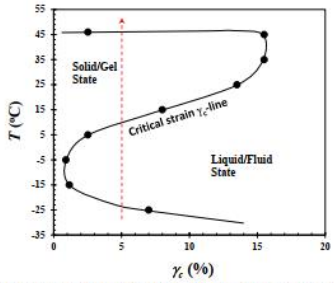

Figure 1: Relationship between critical strain and temperature for a 18 vol% nanoparticle colloidal gel. The data are taken from the crossovers of *G'* and *G"* under strain sweep tests with varying temperature.

REFERENCES

1. G. Kraus, Mechanical losses in carbon-black-filled rubbers, *J. Appl. Polym. Sci.: Appl. Polym. Symp*, 1984, **39**, 75-92.
2. B. Somogyi, F.E. Karasz, L. Trón, P.R. Couchma, The effect of viscosity on the apparent decomposition rate on enzyme-ligand complexes, *J. Theor. Biol*, 1978, **74(2)**, 209-216.

Thursday, May 18, 2023

Plenary Presentations: JNNFM Walters Award Lecture - GEOG 100 (9:00 AM - 10:00 AM)

8TH PACIFIC RIM CONFERENCE ON RHEOLOGY, May 15-19, 2023

VISCOPLASTIC FINGERS AND FRACTURES IN A HELE-SHAW CELL

Thomasina V. Ball[1], Neil J. Balmforth[2]
[1]Mathematics Institute, University of Warwick, UK
[2]Department of Mathematics, University of British Columbia, BC, Canada

ABSTRACT

Radial displacement flows of viscoplastic fluid in a Hele-Shaw cell can give rise to a range of instabilities. Theoretically, the viscoplastic version of the Saffman-Taylor interfacial instability[1] is predicted to occur when the yield-stress fluid is displaced by a Newtonian one. The interface is expected to remain stable, however, if the yield-stress fluid displaces the Newtonian one[2,3].

Experiments using an aqueous suspension of Carbopol show that the Saffman-Taylor instability is observed when the Carbopol is displaced by either air or an immiscible oil, and no instabilities are observed when the displacement is the other way around. However, when water is used in the displacement experiments, other instabilities appear that take the form of localized fractures of the Carbopol over the sections of the interface that are under tension. The fractures arise in both the stable and unstable Saffman-Taylor configurations, leading to a rich range of patterns within the Hele-Shaw cell.

Supported by these experimental observations, we argue that this pattern formation results from the solid-mechanical-like failure of the Carbopol gel. In particular, the fractures result from a reduction of the effective fracture toughness of the suspension when placed in contact with water, also observed in the spreading of Carbopol gravity currents into a shallow layer of water[5].

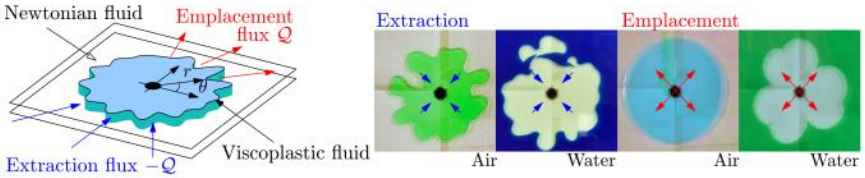

Figure 1: Sketch of the extraction/emplacement of a disk of a viscoplastic fluid with a surrounding Newtonian fluid. Experiments showing the extraction/emplacement of Carbopol when the Newtonian fluid is either air or water. When the Newtonian fluid is water localized fractures appear in both the stable and unstable Saffman-Taylor configurations.

8TH PACIFIC RIM CONFERENCE ON RHEOLOGY, May 15-19, 2023

Controlled Collision of Hele-Shaw Droplets in Extensional Flow Using a Six-Port Microfluidic Device

Aysan Razzaghi[1] and Arun Ramachandran[1]

[1]University of Toronto, Ontario, Canada

ABSTRACT

Collision of two dispersed droplets in the matrix of suspending liquid is the first step toward coalescence. However, to quantify the rate of coalescence, the configuration of the collision should be definable and the force that induces the collision should be measurable. We present a strategy to use the hydrodynamic force in a six-port microfluidic channel to steer two channel-spanning (Hele-Shaw) droplets towards collision.

The analytical solution of the flow field that accounts for the perturbation of the flow due to the hydrodynamic interactions between the Hele-Shaw droplets was developed using the conformal mapping technique. By implementing the analytical solution in the control loop, the flow rates that are required to steer the droplets toward their respective target points can be determined, using a single control parameter, χ^*. The parameter χ^*, is in fact a characteristic time scale that can manipulate the droplets in one of the two manners: 1) by engaging all six ports to create a flow field with two stagnation points ($\chi^* \ll 1$), or 2) by deactivating some of the ports and creating a linear extensional flow through the remaining active ports ($\chi^* \gg 1$). We further determine specific orientations that are more suitable for the collision of Hele-Shaw droplets in the six-port microfluidic channel.

Based on the strategy above, we design and perform controlled head-on and glancing collisions for ~100 μm radius Hele-Shaw perfluorodecalin droplets in silicone oil. The range of the capillary number (ratio of the viscous to interfacial force) that is considered varies from 10^{-3} to 10^{-1}. Coalescence time between two Hele-Shaw droplets undergoing a head-on collision in a dimpled mode was found to be independent of the strain rate of the hydrodynamic flow.

ACKNOWLEDGEMENTS

We acknowledge the funding support from Syncrude Canada Ltd and NSERC Collaborative and Research Development Grant CRDPJ 514675-17.

Bubbles in Yield Stress Fluids: Link between the Rheology and Stability of Bubbles

Masoud Daneshi[1], Ian Frigaard[1,2]
[1]Department of Mathematics, University of British Columbia, Vancouver, Canada
[2]Department of Mechanical Engineering, University of British Columbia, Vancouver, Canada

ABSTRACT

In this work, we study the mechanics of bubbles in a yield stress fluid. This scenario can be found in a wide range of industrial and natural settings including natural and man-made ponds, flooded soils, terrestrial sediments, and other industrial fluid/paste storage scenarios. The original motivation of this work stems from gas emissions from oil sands tailings which is a by-product of the oil sands production process. Microbial degradation of naphtha hydrocarbons and naphthenic acids in the FFT/MFT layers of oil sands tailings ponds leads to the generation of methane and carbon dioxide. The FFT and MFT layers are colloidal suspensions, which behave like viscoplastic fluids with time-dependent rheology. The key feature of a viscoplastic fluid is its yield stress: the material flows only if the imposed stress exceeds the yield stress. This raises questions regarding the stability of bubbles that are trapped in a yield stress fluid, which we try to answer in this research through a series of targeted experiments with model yield stress fluids, Carbopol and Laponite. A vacuum chamber system was used to control the concentration and size of bubbles trapped in the fluid.

A series of experiments have been performed to investigate the growth and stability of bubble clouds in gels with different concentrations. Our objective is to find a link between the rheology of the gel and the maximum gas concentration that can be trapped in the gel and the shape and size of the bubbles at the onset of motion. Our results show increasing the gel concentration, i.e. the yield stress of the gel, improves the capacity for gas retention. In addition, our study confirms that bubble clouds become unstable at a smaller bubble size in comparison with that of a single bubble. This is likely related to the interaction of the stress fields developing around the bubbles or their coalescence. To further investigate this point, we extend our study by looking at more fundamental scenarios, i.e. two or three bubbles at different orientations and separation distances. We examine this problem using both an experimental and a numerical approach to demonstrate how the stress fields around neighbouring bubbles interfere with each other and how this affects their onset of motion in a yield stress fluid.

ACKNOWLEDGEMENT

This research was made possible by funding from NSERC and COSIA/IOSI (project numbers CRDPJ 537806-18 and IOSI Project #2018-10).

PREPARATION AND PROPERTIES OF CONDUCTIVE FOAMS VIA HIGH INTERNAL PHASE EMULSION

Song Hee Lee, Ho Seong Choi and Seong Jae Lee

Department of Chemical and Materials Engineering, The University of Suwon
Hwaseong, Gyeonggi 18323, Republic of Korea

ABSTRACT

A high internal phase emulsion (HIPE), in which the volume fraction of the dispersed phase is higher than the maximum packing volume fraction, forms a polyhedral thin film structure by contacting droplets. The HIPE can be utilized as a template for fabricating microporous structures. When the continuous phase is a monomer, polymerization of the emulsion followed by removal of the dispersed phase results in a microporous foam. The open-cell structure of polyHIPE is formed because the thermodynamically unstable thin film is easily broken, allowing the cells to connect to each other. The cell size of polyHIPE can be controlled by agitation, solvents, emulsifiers, and polymerization conditions. This foam can be used in various fields such as gas storage media, polymer membranes, ion exchange resins, catalyst supports, shape memory resins, tissue engineering scaffolds, and supercapacitor electrode materials. In this study, electrically conductive polystyrene/carbon nanotube (CNT) microporous foam was fabricated using HIPE as a template. CNTs were modified with polypyrrole (PPy), a conducting polymer, to increase chemical affinity with the oil phase of HIPE and improve electrical conductivity of the microporous foam. The effect of PPy-modified CNT (PPy-CNT) was evaluated in terms of rheological properties, morphology and electrical conductivity. The addition of PPy-CNT had a significant effect on the rheological properties of HIPE and the electrical and mechanical properties of polyHIPE. As the PPy-CNT content increased, the yield stress and storage modulus of the emulsion increased, gradually exhibiting solid-like properties. In addition, as the PPy-CNT content increased, the cell size of the microporous foam decreased, and the electrical conductivity and crush strength increased.

REFERENCES

1. Silverstein, M. S. PolyHIPEs: Recent advances in emulsion-templated porous polymers, *Prog. Polym. Sci.*, **39**, 199–234, 2014.
2. Kim, H.; Ahn K. H.; Lee, S. J. Conductive poly(high internal phase emulsion) foams incorporated with polydopamine-coated carbon nanotubes, *Polymer*, **110**, 187–195, 2017.
3. Lee, S. H.; An, J. H.; Kim, Y. J.; Lee, S. J. Electrically conductive foams from high internal phase emulsions with polypyrrole-modified carbon nanotubes: Morphology, properties, and rheology. *Polymer*, **242**, 124600, 2022.

SHEAR-TRIGGERED COALESCENCE

Alireza Mashayekhi[1], Coralie Vazquez[2], John M. Frostad[1]

[1]University of British Columbia, Vancouver, Canada
[2]Chimie ParisTech, Paris, France

ABSTRACT

An emulsion is a fine dispersion of a liquid (dispersed phase) in another one (bulk phase) while two liquids are immiscible. Emulsions are thermodynamically unstable, so over time, droplets of the dispersed phase join together (through coalescence) to form larger droplets until complete phase separation occurs. The terminal desire in such industries as food, cosmetics, and pharmaceuticals is a super-stable emulsion, which is not phase-separated over a long period of time. However, immediate phase separation is critical for oil and gas industries to separate as much dispersed oil as possible from the oily wastewater before discharging it into the environment. That being said, controlling emulsion stability is critical for the various industries mentioned. Prior work has shown that for crude oil emulsions, gentle oscillating shear can dramatically increase the rate of coalescence relative to no shearing. However, the effect has not been rigorously quantified and the physicochemical mechanisms involved require more study to see if this effect can be reproduced in other emulsions. In this study, we present results using a cantilevered capillary force apparatus to precisely manipulate two oil droplets with a range of surfactants and/or nanoparticles, and compare the droplet coalescence time in oscillating shear vs. head-on droplet collisions. We also make bulk emulsions and test them both under shear and at rest to find out how the results compare with the single-droplet results.

A New Instrument for Interfacial Dilational Rheology

Yun-Han Huang[1], John M. Frostad[1]

[1]University of British Columbia, Vancouver, Canada

ABSTRACT

Viscoelastic properties of interface are believed to be important to the stability of foams and emulsions. They also directly influence the functionality of important biological systems, such as the tear film on eyes and alveoli in the lungs. Despite the importance of interfacial rheology, the measurement techniques and mathematical models needed to understand it are still insufficient. In particular, methods for measuring interfacial dilational rheology are still not standardized and there are drawbacks to the instruments commonly used. Here we present a novel design for an interfacial dilational rheometer that can generate purely dilational deformation on a planar interface, which avoids mixed deformations present in other instruments, at frequencies up to approximately 1 Hz and dilational strains down to below 0.001. We verify the rheometer with the measurement of compression isotherm of stearic acid and demonstrate its ability to measure dilational moduli of both soluble and insoluble surfactants.

8TH PACIFIC RIM CONFERENCE ON RHEOLOGY, May 15-19, 2023

RHEOLOGY MODIFICATION OF POLYMERIC NETWORKS VIA LOOP THREADING

Dimitris Vlassopoulos[1,2]

[1]Foundation for Research and Technology Hellas (FORTH)
[2]University of Crete
100 Nikolaou Plastira St., Heraklion 70013, Greece

ABSTRACT

Tailoring the rheological properties of soft composites at molecular level has been a thematic at the forefront of engineering research. A formidable challenge is understanding the role of macromolecular architecture on topological constraints and the resulting network dynamics. Ring polymers represent a unique case because of the absence of free ends that mediate conformational arrangements in a topological entanglement network. It has been shown that these macromolecules exhibit a power-law stress relaxation, in the absence of entanglement plateau. Here, we discuss the rheology of these loopy structures. We show that they exhibit unusual nonlinear response in shear and, especially, in extension because of loop interlocking. Adding small amounts of ring polymers to entangled linear matrices yields a reinforcement effect, which can be understood by invoking the (coherent) constraint release processes on the rings due to the escape (unthreading) of linear chains. The ring-linear molecular weight asymmetry is important and examined in this work. We also consider the addition of a few single chain nanoparticles, which are also (crosslinked) loopy structures, on linear matrices and show that, indeed they exhibit a qualitatively similar reinforcement effect, because of the action of loop threading. The punchline is the emerging ability to selectively tailor the rheological properties of a wide range of polymeric networks with loops and, at the same time, provide insights on the physics of the constraint release process.

ACKNOWLEDGEMENTS

This presentation reflects a large project in collaboration with D. Parisi, K. Peponaki, C. Pyromali (Crete), M. Rubinstein (Duke), V. Mavrantzas, D. Tsalikis (Patras), T. Chang (Pohang), Q. Huang, W. Wang, O. Hassager (DTU), T. O'Connor, G. Grest (Sandia), N. Hadjichristidis (KAUST), G. Sakellariou (Athens). Funding from Hellenic Foundation for Research and Innovation (H.F.R.I.) under the "Second Call of H.F.R.I. for Research Projects to support Faculty members and (Project Number: 4631) is gratefully acknowledged.

Time-Strain Separability and Inseparability in Multiaxial Stress Relaxation of Polymer Gels with Permanent and Transient Crosslinks

Takuro Kimura[1], Takuma Aoyama[1], Masaki Nakahata,[2] Yoshinori Takashima,[2]
Motomu Tanaka,[3] Akira Harada,[2] and Kenji Urayama[4]

[1]Kyoto Institute of Technology, Kyoto, Japan
[2]Osaka University, Osaka, Japan
[3] Heidelberg University, Heidelberg, Germany
[2]Kyoto University, Kyoto, Japan

Introduction of transient physical cross-links into polymer gels with permanent cross-links has attracted much attention as an effective and useful method to enhance the viscoelasticity and mechanical toughness. Indeed, such polymer gels have significant viscoelasticity: they exhibit large degrees of stress relaxation in response to a step strain, a definite relaxation peak in linear dynamic viscoelasticity, and a considerable hysteresis in the stress-strain relationships under loading-unloading cycles. Separability of the time and strain effects on stress is a key to construct the constitutive models of viscoelastic materials, but the time-strain separability is not a rule derived from fundamental laws, it must be assessed experimentally.

We investigate the nonlinear stress relaxation for the two types of polymer gels with permanent and transient cross-links using biaxial stretching with various combinations of two orthogonal strains as an imposed strain. Such general biaxial strain covers a wide range of physically accessible deformations, while conventional uniaxial stretching is only a particular deformation among them. Thus the biaxial stress relaxation data provide a definite basis to access the time-strain separability. We have validated unambiguously the time-strain separability for the dual cross-link poly(vinyl alcohol) (PVA) hydrogels[1)] with covalent bonds and the transient bonds via borate ions.[2)] In contrast, we observe that the time and strain effects are not separable in the supramolecular gels[3)] with permanent rotaxane cross-links utilizing the host-guest interactions as the transient cross-links.[4)] The relaxation is accelerated in a short time region by an increase in the magnitude of strain, whereas it is retarded in a longer time region by an increase in the anisotropy of the imposed biaxial strain.

1. Narita, T.; Mayumi, K.; Ducouret, G.; Hébraud, P., *Macromolecules* 2013, 46, 4174.
2. Kimura, T.; Urayama, K., *ACS Macro Lett.*, 2020, 9, 1.
3. Nakahata, M.; Takashima, Y.; Yamaguchi, H.; Harada, A., *Nat. Commun.*, 2011, 2, 511.
4. Kimura, T.; Aoyama, T.; Nakahata, M.; Takashima, Y.; Tanaka, M.; Harada, A.; Urayama, K., *Soft Matter*, 2022, 18, 4953.

INTRIGUING MELTING BEHAVIOR OF THE NATURAL RUBBER CRYSTAL FORMED BY STRAIN-INDUCED CRYSTALLIZATION

Tomohiro Yasui[1], Ruito Tanaka[1], Yuji Kitamura[2], Katsuhiko Tsunoda[2], Hideaki Takagi[3], Nobutaka Shimizu[3], Noriyuki Igarashi[3], Kenji Urayama[4] and Shinichi Sakurai[1,*]

[1]Department of Biobased Materials Science, Kyoto Institute of Technology, Kyoto, Japan
[2]Bridgestone, Kodaira, Tokyo, Japan
[3]High Energy Accelerator Research Organization, Tsukuba, Ibaraki, Japan
[4]Department of Material Chemistry, Kyoto University, Kyoto, Japan

INTRODUCTION

Natural rubber (NR) is soft and simultaneously robust to meet requirements for exclusive safety of tires of aircrafts. Namely, they should not be broken when momentary stress is applied. Strain-induced crystallization (SIC) is considered to play an important role for the toughening of NR. It is indeed important to recognize the melting behavior of the crystal as formed by the SIC when heating, since temperature of the tires of aircrafts is suddenly elevated upon landing. Since the initiation of the studies on SIC of NR by two-dimensional wide-angle X-ray diffraction (2d-WAXD) 100 years ago [1], temperature dependence of the SIC behavior has been studied. However, few report can be found for the melting behaviors of the SIC crystal upon heating [2]. It was reported that the degree of crystallinity started to decrease gradually at temperature far below the melting temperature. The former behavior is strange as compared to the case of the general crystalline polymers, and hard to be reasonably explained. Furthermore, the changes of the lattice parameters as a function of temperature have never been reported. Therefore, in this study we thoroughly analyzed the quantitative changes of the orthorhombic lattice parameters of NR, the volume of the unit cell, its thermal expansivity, the crystallite size and its volume, the degree of crystallinity, and the degree of orientation of the crystalline lattice as a function of temperature. Then, the detailed and reliable mechanism of the melting of the NR crystal formed upon the SIC can be given based on such quantitative data.

EXPERIMENTAL

The vulcanized NR rubber sheet (vulcanized with 1.4 phr of sulfur; no carbon black included; 0.25 mm thickness) with 10 mm length and 4 mm width was utilized for this study. At room temperature, the sheet specimen was uniaxially stretched 7 fold by slowly elongation with 0.2 mm/sec to form the SIC crystal. Then, temperature of the stretched specimen (keeping the length constant throughout the heating process) was gradually increased up to 380 K with the constant heating rate of 2 K/min. The WAXD measurements during the heating process were performed simultaneously

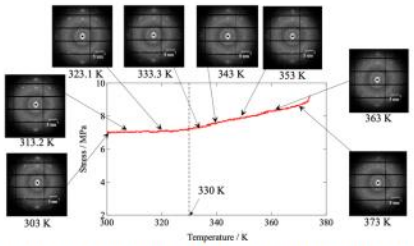

Figure 1: Change in the stress during heating of the stretched and fixed NR specimen at 7 fold elongation. Selected 2d-WAXD patterns are shown together. The elongation direction is horizontal.

with the stress measurements at BL-15A2 of Photon Factory, High Energy Accelerator Research Organization, Japan. The exposure time of the X-ray beam was 5 s for each 2d-WAXD pattern measurement. PILATUS 2M (DECTRIS, Switzerland) was used as a two-dimensional detector. The distance from the specimen to the detector was set to 25 cm.

RESULTS AND DISCUSSSION

Fig. 1 shows the change in the stress as a function of time with selected 2d-WAXD patterns. It is noteworthy that the stress started to increase around 330 K, which can be ascribed to the effect of the entropy elasticity. The reflection peaks were clearly observed for (200), (120), (201), and (002) planes in all 2d-WAXD pattern. To obtain the 1d-WAXD profile, we conducted sector average of the pattern with respect to the scattering vector (***q*** vector) direction where the diffraction spots were observed (within ±5˚sector range). Thus-obtained 1d-WAXD profiles are shown in **Fig. 2** where the intensity was plotted against the magnitude of the scattering vector (q) as defined by $q = (4\pi/\lambda) \sin\theta$ with λ and θ being the wavelength of X-ray (λ = 0.9232 nm) and half the diffraction angle, respectively. The (200) and (120) reflection peaks continuously shifted towards lower q range, while the (002) reflection peak shifted towards higher q range. The (201) reflection peak more or less stayed at constant q position with q = 0.497 ~ 0.500 nm^{-1}. By assuming the orthorhombic lattice, the lattice constants a, b, c values can be evaluated, and evaluated values were plotted in **Fig. 3(a)**. As compared to the reported values a = 1.246, b = 0.889, c = 0.81 nm by Nyburg [3], our results for a and c reasonably coincide but the result of b values are about 28% smaller. The reason is unknown at present. It is noteworthy that the c value decreases as a function of temperature, which suggests the shrinkage of the main chain of NR due to the increased vibration at higher temperature, while the a and b values exhibit the thermal expansion. Note however that the lattice volume ($V = a \cdot b \cdot c$) itself exhibits thermal expansion, as shown in **Fig. 3(b)**. Based on this set of data, temperature dependence of the thermal expansivity, $\alpha = (\partial \ln V/\partial T)_p$, was evaluated and shown together in **Fig. 3(b)**. Here, interestingly it is found to start increasing at 330 K, which coincides with the onset temperature of the change in the stress as shown in **Fig. 1**.

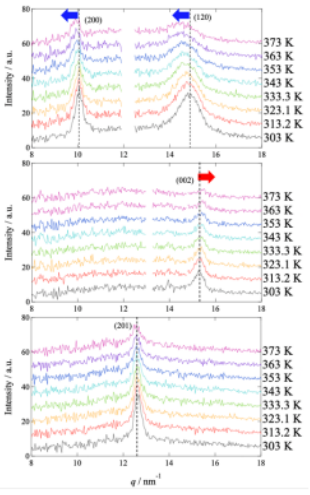

Figure 2: 1d-WAXD to highlight the crystalline reflection peaks.

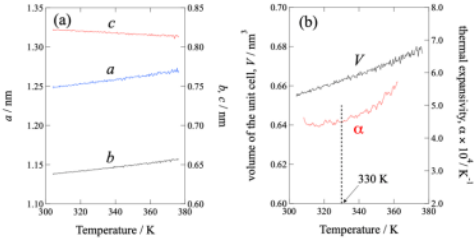

Figure 3: Temperature dependencies of (a) lattice constants, and (b) the volume of the unit cell and the thermal expansivity.

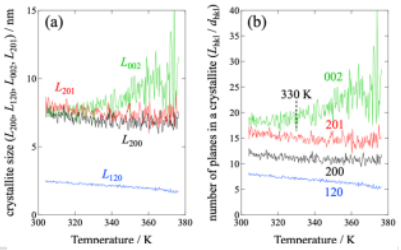

Figure 4: Temperature dependencies of (a) crystallite size, and (b) the number of planes included in a crystallite.

Fig. 4(a) exhibits the change in the crystallite size (L_{hkl}) as a function of temperature for all of the peaks observed in the 2d-WAXD patterns, i.e., (200), (120), (201), and (002) planes, according to the Scherrer's equation from the integral breadths of those reflection peaks. Again interestingly, L_{002} exhibits increasing tendency, while the others show the monotonic decrease with an increase in temperature. Although such increasing tendency of L_{002} implies the growth of crystallites in the c-axis direction (namely in the NR main chain direction), the effect of the c-axis increasing tendency as a function of temperature should be ruled out for the sake of the quantitative discussion. For this purpose, the number of the hkl planes included in a crystallite was estimated by L_{hkl} / d_{hkl}, and shown in **Fig. 4(b)**. Then, more clearly it can be seen that the number for the (002) planes is increased while the others are decreased. Therefore, it can be concluded that crystallites grows in the NR main chain direction, while it is melting off in the other perpendicular directions upon heating. Interesting, the onset of the growth in the c-axis direction is consistent with that of stress increase (**Fig. 1**) and thermal expansivity (**Fig. 3(b)**).

Finally, the change in the degree of crystallinity (χ_c) as a function temperature is shown in **Fig. 5**. It was simply evaluated from the 2d-WAXD patterns by the following equation, $\chi_c = (A_{200} + A_{120} + A_{201} + A_{002}) / (A_{200} + A_{120} + A_{201} + A_{002} + A_{amo})$ where A_{hkl} stands for the integrated peak intensity of the (hkl) plane and A_{amo} does that of the amorphous halo peak, based on the peak deconvolution of the circularly averaged 1d-WAXD profile obtained from the 2d-WAXD pattern. In **Fig. 5**, χ_c clearly exhibits monotonic decrease with temperature, which is somewhat strange because the melting temperature is much higher than the temperature range examined here (about 100 K higher). Can crystallites feel that they should be going to melt? To clearly discuss about this matter, it is important to rule out the possibility of apparent decreasing in χ_c by the shrinkage of crystallites, as expected the decreasing tendency of the crystallite size (**Fig. 4(a)**). Although the crystallite volume is needed to estimate for this purpose, it was impossible to do so accurately because of lack of information of the detailed shape of the NR crystallite. Therefore, we decided to approximate it by the triple product $L_{200} \cdot L_{120} \cdot L_{002}$ (assumption of a rectangular parallelepiped of the crystallite) and shown together in **Fig. 5**. It is then found that the volume of the crystallite decreases with temperature up to 330 K and likely stays constant in the higher temperature range. Furthermore, its decreasing tendency coincides with that of χ_c so that the decreasing tendency below 330 K is not ascribed to the real melting of crystallites but to the shrinkage of the crystallites. However, it is noteworthy here to recognize that the decreasing tendency of χ_c higher than 330 K is still observed in such a temperature range much lower than the real melting temperature, being probably due to the gradual melting of the smaller crystallites which should have a lower melting temperature. As a conclusion, to the best of our knowledge, the clear experimental finding of the shrinkage of the c-axis of the NR crystal with an increase of temperature has never reported before.

ACKNOWLEDGEMENTS

This study was financially supported by JST CREST (Grant No. JPMJCR2091).

REFERENCES

1. Katz, J. R. Ro¨ntgenspektrographische Untersuchungen am gedehnten Kautschuk und ihre mo¨gliche Bedeutung fu¨r das Problem der Dehnungseigenschaften dieser Substanz. *Naturwissenschaften*, **19**, 410-416., 1925.

2. Toki, S., Sics, I., Hsiao, B. S., Tosaka, M., Poompradub, S., Ikeda. Y., Kohjiya, S. Probing the Nature of Strain-Induced Crystallization in Polyisoprene Rubber by Combined Thermomechanical and In Situ X-ray Diffraction Techniques, Macromolecules, **38**, 7064-7073 2005. https://doi/10.1021/ma050465f.

3. Nyburg, S. C. A statistical structure for crystalline rubber. *Acta Cryst.*, **7**, 385-392., 1954. https://doi.org/10.1107/S0365110X54001193.

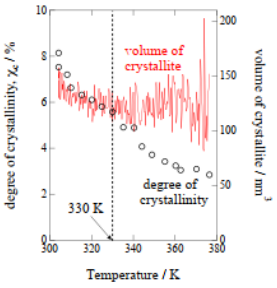

Figure 5: Temperature dependencies of χ_c and the volume of crystallite.

Have you ever listened to the sound of the fluid?

Howon Jin, Seunghoon Kang, Kyung Hyun Ahn

School of Chemical and Biological Engineering, Seoul National University, Seoul, 08826 Korea

ABSTRACT

Conventional rheometry does not help to understand what really happens inside because the flow is highly nonuniform and fluctuating, and it is hardly possible to read the signals from the equipment and sensors. But apparently the fluid tells us how they get stressed and how they feel. To control the process, we need to hear what they say and have to respond. This has never been possible, but we have to find the ways anyhow. Good news is that we now have the tools of machine learning. We have two approaches; one top-down and the other bottom-up. First, we develop the constitutive equation based on machine learning. Second, we understand what the fluid experiences from the signals of whatever. In this talk, I will briefly introduce the heterogenous nature of processing and show what it looks like. Then I will talk about our efforts to communicate with the fluid – small success and big challenges. I will also talk about a few issues and challenges we hopefully share and collaborate.

8TH PACIFIC RIM CONFERENCE ON RHEOLOGY, May 15-19, 2023

RHEOLOGICAL EFFECTS ON PURELY-ELASTIC FLOW ASYMMETRIES IN THE CROSS-SLOT GEOMETRY

Arisa Yokokoji[1], Stylianos Varchanis[1], Amy Q. Shen[1] and Simon J. Haward[1]

[1] Okinawa Institute of Science and Technology, Okinawa, Japan

ABSTRACT

The cross-slot is a canonical geometry for the generation of a planar extensional flow with a free stagnation point. Beyond a critical Weissenberg number *Wi*, viscoelastic flows in the cross-slot geometry are well-known to undergo a transition from a steady symmetric to an asymmetric flow state, ostensibly due to 'purely-elastic' effects.[1] However, some prior work suggests that shear-thinning of the fluid may play an important role.[2] Here, we employ a series of polymer solutions of varying rheology to investigate in detail how the interplay between fluid elasticity and shear thinning affects the onset and development of the asymmetric flow state in the cross-slot. First, we characterize the rheological properties of hydrolyzed polyacrylamide aqueous solutions with and without salt by using standard rotational rheometry and capillary breakup extensional rheometry. We employ micro-particle image velocimetry to obtain velocity fields in the cross-slot device for each of the polymer solutions and to assess the degree of flow asymmetry *I* as a function of *Wi* and the shear thinning parameter *S*.[2] The flow broke symmetry beyond a critical *Wi*, but the degree of asymmetry was found to depend on *S*. Interestingly, for intermediate polymer concentrations, resymmetrization of the flow field occurred above a higher, second critical *Wi*. To understand these trends, we compare our experiments with numerical simulations with the linear Phan-Thien-Tanner model. Finally, we summarize the trends as a flow state diagram in *Wi*-*S*-*I* space, showing the relationship between flow asymmetry and fluid rheological properties. We demonstrate that the degree of both shear thinning and elasticity are important factors for elastic instabilities in the cross-slot geometry.

REFERENCES

1. Arratia, P. E. and Thomas, C. C. and Diorio, J. and Gollub, J. P., Elastic Instabilities of Polymer Solutions in Cross-Channel Flow, Phys. Rev. Lett., 96, 144502, 2006.
2. Haward, S. J. and McKinley, G. H., Stagnation point flow of wormlike micellar solutions in a microfluidic cross-slot device: Effects of surfactant concentration and ionic environment, Phys. Rev. E, 85, 031502, 2012.

FLOW OF A WORMLIKE MICELLAR SOLUTION OVER A LONG CAVITY

Fabian Hillebrand[1], Stylianos Varchanis[1], Simon J. Haward[1] and Amy Q. Shen[1]

[1]Okinawa Institute of Science and Technology Graduate University, Onna-son, Okinawa, Japan

ABSTRACT

Flow instabilities are well known to occur in viscoelastic flows due to the presence of streamline curvature in simple geometries. We investigate the flow of a viscoelastic and shear-thinning wormlike micellar solution over a long cavity, more appropriately described as a sudden one-sided expansion followed by a sudden one-sided contraction. We employ μ-particle image velocimetry to measure the flow field as a function of the applied Weissenberg number (Wi). Experimental data are supplemented by simulations using the Giesekus constitutive model, with parameters corresponding to the measured rheology of the experimental test fluid. We find formation of lip vortices upstream of the expansion and salient corner vortices immediately downstream of the expansion, both of which we quantify against Wi. For the lip vortices we differentiate three regimes: No vortex, steady vortex, and unsteady vortex. Upstream of the contraction, a corner-filling vortex appears, which we attribute to shear-banding. Our results confirm previous numerical studies[1,2] and are in-line with related geometries, such as flow around a sharp bend[3].

REFERENCES

1. Poole, R. J.; Alves, M. A.; Oliveira, P. J.; Pinho, F. T. Plane sudden expansion flows of viscoelastic liquids. *J. Non-Newt. Fluid M.* **2007**, 146 (1), 79–91. DOI: https://doi.org/10.1016/j.jnnfm.2006.11.001.
2. Poole, R. J.; Pinho, F. T.; Alves, M. A.; Oliveira, P. J. The effect of expansion ratio for creeping expansion flows for UCM fluids. *J. Non-Newt. Fluid M.* **2009**, 163 (1), 35–44. DOI: https://doi.org/10.1016/j.jnnfm.2009.06.004.
3. Hwang, M. Y.; Mohammadigoushki, H.; Muller, S. J. Flow of viscoelastic fluids around a sharp microfluidic bend: Role of wormlike micellar structure. *Phys. Rev. Fluids* **2017**, 2, 043303. DOI: https://doi.org/10.1103/PhysRevFluids.2.043303.

EFFECTS OF CHANNEL LENGTH IN EXPANSION PARTS ON FLOW REGIMES OF POLYMER SOLUTION IN CONSECUTIVE ABRUPT CONTRACTION-EXPANSION CHANNELS

Ruri Hidema[1], Yuta Nakamura[1], Francois Lequeux[2] and Hiroshi Suzuki[1]

[1]Kobe University, Kobe, Japan
[2]ESPCI Paris, Paris, France

ABSTRACT

Elastic instability of viscoelastic fluids in microfluidic devices have received lots of attention for the last two decades. Flow regimes of viscoelastic fluids in an abrupt contraction-expansion channel were especially intensively studied, because the channel geometry is related to a flow used in many industrial applications[1]. Reynold number, *Re* [-], and Weissenberg number, *Wi* [-] are usually useful to characterize flow regimes in the channels. However, in the case of the micro channels that consist of consecutive contraction-expansion units mimicking a porous media, variations of flow regimes are affected by other factors in addition to *Re* and *Wi*. For instance, various flow regimes of polymer solution in the same consecutive contraction-expansion channels developed from the inlet to the outlet. In such cases, both polymer deformation-relaxation process and scission of polymers are the key to understand the development in the channel[1, 2]. In this study, we aim to quantify the relative effects of memories of polymer deformation-relaxation and scission of polymers on the flow regimes of polymer solution. We prepared several consecutive abrupt contraction-expansion channels that have different lengths of the expansion part. The channel geometries affect Henky strain and extensional rates in each contraction-expansion unit, which govern the flow development of polymer solutions.

ACKNOWLEDGEMENTS

This study was supported in part by the Japan Science and Technology Agency (JST) FOREST Program (Grant Number JPMJFR203O, Japan).

REFERENCES

1. Hidema, R.; Oka, T.; Komoda, Y.; Suzuki, H. Effects of flexibility and entanglement of sodium hyaluronate in solutions on the entry flow in micro abrupt contraction-expansion channels. *Phys. Fluids*, **31**, 72005, 2019. https://doi.org/10.1063/1.5096781
2. Garrepally, S.; Jouenne, S.; Olmsted, P.D.; Lequeux, F. Scission of flexible polymers in contraction flow: Predicting the effects of multiple passages. *J. Rheol.*, **64**, 601, 2020. https://doi.org/10.1122/1.5127801

Instabilities in immiscible multi-layer viscous shear flows in the presence of interfacial slip

Anna Katsiavria[1], Demetrios T. Papageorgiou[1]

[1]Imperial College London, London, UK

ABSTRACT

Unlike single phase Couette flows, which are known to be linearly stable at all Reynolds numbers, in the case of two superposed, immiscible, viscous fluid layers the interface might be rendered unstable at all non-zero values. For most of the common fluid pairs a no-slip condition is appropriate to describe the liquid-liquid interface and under this assumption both the linear and the non-linear stability of such configurations (including direct numerical simulations and consideration of surfactants) has been extensively addressed [1,2,3].

More recent experimental studies[4,5] on coextruded multilayers of polymer-polymer systems, reveal that presence of slip at the interfaces of such fluids is possible and leads to unexpectedly increased flow-rate measurements. Molecular dynamics simulations[6,7] have also demonstrated the presence of slip at liquid-liquid interfaces for both Couette and pressure-driven flows. The MD simulations also demonstrated that a Navier-slip law is very successful in describing the data.

Attempting to extend the existing studies on multi-layer shear flows[1] by consideration of the aforementioned experimental findings, the present work is a theoretical study of the effects of Navier slip at liquid-liquid interfaces. Following the experiments we focus on Newtonian flows and undertake a comprehensive study of stability of two-fluid Couette flows, where in the presence of slip the basic flow undergoes a slip-length-dependent velocity jump at the interface. Asymptotic solutions are constructed for short and long wave disturbances to isolate the instability mechanisms.

So far, as it has already been presented elsewhere, at the limit of large slip the system has been found to exhibit a novel instability, viscous analogue of the Kelvin-Helmholtz, albeit with a bounded growth rate. In this talk the aim is to focus on arbitrary slip values of order $\mathcal{O}(1)$. Here, analytical solutions are obtained in the form of integrals of Airy functions, and the results are successfully compared with those constructed asymptotically. The effect of each one of the eight parameters involved (viscosity ratio, density ratio, position of the interface, Reynolds number, Froude number, Capillary number, slip length and wavenumber) on the growth rate and the phase speed of the interfacial instability is diligently tracked to reveal that slippage may destabilise all wavenumbers and even trigger a Turing-type instability.

EFFECT OF ULTRASOUND FIELDS ON ASPHALTENE-LADEN W/O INTERFACES: A MICRORHEOLOGY APPROACH

Razie Khalesi Moghaddam[1], Harvey. W. Yarranton[1], Giovanniantonio Natale[1]
[1] Department of Chemical and Petroleum Engineering, University of Calgary, 2500 University Dr., NW, Calgary, AB, T2N 1N4

ABSTRACT

Crude oil emulsions pose significant challenges in the oil and gas industry, leading to pipeline blockages, reduced separation efficiency, and increased operating costs. Ultrasonic waves have been proposed as a promising method for emulsion destabilization, and in this study, we explore their effect on asphaltene-laden interfaces using a microrheology approach. Passive microrheology was used to explore microstructure changes in asphaltene films, while drop size distribution analysis characterized emulsion stability.

The experiments were carried out at various frequencies (20, 40, 50, 80, 120, and 150 kHz) and voltages (20, 30, 40, and 50 V) of ultrasonic fields. Four distinct microrheology regimes were observed based on the motion of the probe particles at the interface: I. no movement, II. slow streaming, III. strong streaming and interfacial cavitation, and IV. bulk cavitation and mixing. The regime encountered depends on the inertial effect of ultrasound on the subphase (Reynolds number) as well as the thermodynamic impact of ultrasonic fields. No significant change was observed in the mechanical behavior of the interface under the ultrasonic field in Regimes I and II. However, a strong disturbance in the asphaltene interfacial film was detected in Regime III, where interfacial cavitation was observed. The linear diffusion of probe particles was observed more frequently, and the interface's elastic shear modulus decreased considerably. In addition, the film's heterogeneity was boosted by increasing the more viscous regions.

Treating the emulsions with the same ultrasonic fields resulted in three categories of behavior: no coalescence, coalescence, and emulsification. There was a strong correlation between emulsion behavior with the microrheology regime. Below the threshold of interfacial cavitation (microrheology Regimes I and II), no change in the emulsions was detected. When interfacial cavitation occurred (microrheology Regime III), the emulsions coalesced significantly, indicating the ability of the cavitation process to break the asphaltene barrier between the droplets. However, increasing the frequency and voltage of the field increased the mechanical effects of the ultrasonic field (microrheology Regime IV) and caused secondary emulsification in the system.

This study highlights the importance of microrheology in understanding the behavior of asphaltene-laden interfaces under ultrasonic fields. The correlation observed between the emulsion behavior and the microrheology regimes suggests that the behavior of emulsions under ultrasonic fields is strongly influenced by the changes in the interfacial rheology. These findings can be used to develop more efficient and targeted ultrasonic techniques for crude oil emulsion management, which can potentially mitigate the problems associated with crude oil emulsions in the oil and gas industry.

8TH PACIFIC RIM CONFERENCE ON RHEOLOGY, May 15-19, 2023

Nonlinear Rheology of Concentrated Poly(vinyl alcohol)/Borax Aqueous Solution

Yanjie Zhang[1,2] Quan Chen,[1,2]* and Hiroshi Watanabe[1,3]*

[1]State Key Laboratory of Polymer Physics and Chemistry, Changchun Institute of Applied Chemistry, Chinese Academy of Sciences, Changchun, China
[2]University of Science and Technology of China, Hefei, China
[3]Institute for Chemical Research, Kyoto University, Uji, Kyoto, Japan

ABSTRACT

Nonlinear rheological behavior was examined for an aqueous solution of poly(vinyl alcohol) (PVA; M_w = 101 kg mol^{-1} and M_n = 67 kg mol^{-1}) mixed with sodium tetraborate decahydrate (borax). In a neat solution with the PVA concentration of w_{PVA} = 15 wt% but without borax, the PVA chains were in a concentrated but barely entangled state. On addition of borax to this solution at a molar concentration of C_{borax} = 15 mM, a well percolated transient network of the PVA chains was formed because of dynamic crosslinks between the chains formed through complexation with the borate ions dissociated from borax. Consequently, this PVA/borax solution showed sticky-Rouse type linear viscoelastic (LVE) relaxation much slower than the relaxation of the neat PVA solution. The PVA/borax solution also exhibited time-flow rate separable damping of the viscosity decay function $\eta_-(t,\dot{\gamma})$ on cessation of fast flow as well as time-strain separable damping of the nonlinear relaxation modulus $G(t,\gamma)$ under large step strain. The electrical conductivity measured together with the stress was found to be very close to that in the quiescent state, which unequivocally indicated that the concentration of the free borate and sodium ions determining the conductivity was hardly affected by the strain/flow. The flow/strain undoubtedly disrupted the percolated PVA network, and the conductivity would have increased if this disruption were to release free borate ions. Thus, the observed flow/strain-insensitive conductivity strongly suggested that the disrupted network was rapidly reformed under flow/strain through the intrinsic Rouse motion of the PVA chains in the disrupted portions of the network. The sticky Rouse model[1-4] applicable to the PVA/borax solution at equilibrium was modified for this flow/strain-induced disruption followed by rapid reformation. This modification simply considered that the fast intrinsic Rouse motion in the disrupted portions averages the orientational anisotropy within those portions; the slow sticky Rouse dynamics itself was not modified in the model. This simple model well captured the features of the PVA/borax solution seen for $\eta_-(t,\dot{\gamma})$ and $G(t,\gamma)$. This success of the modified model in turn demonstrates an importance of a simple but unexplored mechanism of the nonlinearity of associative chains, the conformational averaging of the chain on the network disruption followed by rapid reformation.

HYSTERESES IN ONE-DIMENSIONAL COMPRESSION OF A POROELASTIC HYDROGEL

Zelai Xu[1], Pengtao Yue[2] and James J. Feng[1]

[1]University of British Columbia, Vancouver, Canada
[2]Virginia Tech, Blacksburg, United States of America

ABSTRACT

We investigate theoretically the one-dimensional compression of a hydrogel layer by a uniform fluid flow normal to the gel surface. The flow is driven by a pressure drop across the gel layer, which is modelled as a poroelastic medium. Since the pressure simultaneously drives the Darcy flow through the pores and compresses the gel, the flux-pressure relationship is in general non-monotonic. Most interestingly, we discover hysteresis when the pressure drop is controlled, which are also confirmed by transient numerical simulations. The hysteresis stems from the interplay between the gel compression at the upstream interface and that in the bulk of the gel, and would not be predicted by models that ignore the interfacial compression. Finally, we suggest experimental setups and conditions to seek such hystereses in real gels.

METHODS

Consider the one-dimensional (1D) compression of a layer of hydrogel by a normal ow of the solvent (Fig. 1). The gel layer extends to infinity in y-direction and the uniform flow with the flux Q in x-direction is driven by the prescribed pressure drop across the layer. The downstream surface of the gel layer is fixed in space but allows passage of the solvent, as if by a stiff and highly permeable mesh. The upstream gel surface is displaced by the flow as the layer compacts. The layer of hydrogel is modelled as a poroelastic medium, with volume fractions ϕ_f and $\phi_s = 1-\phi_f$ for the fluid and solid components. We assume Darcy flow inside the gel layer and adopt the same constitutive relation as Hewitt *et al.*[1], which is close to the linear elastic behavior for small strains but diverges as the strain approach to a prescribed maximum value.

In our study, we compared the influence of various permeability models and entry boundary conditions of the layer of hydrogel. Specifically, we investigated the difference between the Kozeny-Carmen model and our own permeability model with a constant drag coefficient. For boundary conditions, we examined two options: the stress-free boundary condition used by Hewitt *et al*[1] and our entry condition based on interfacial permeability η.[2,3] The following results will be in dimensionless variables that have been properly scaled.

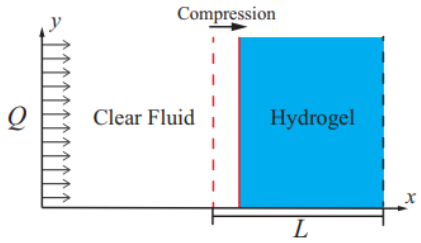

Figure 1: A diagram showing the 1-D compression of a layer of hydrogel. The dashed red line denotes the initial interface between the clear fluid and the hydrogel, and the solid red line the displaced interface under compression. The downstream surface of the gel layer is constrained by a fixed permeable plate (the black dash line), and has zero displacement.

RESULTS

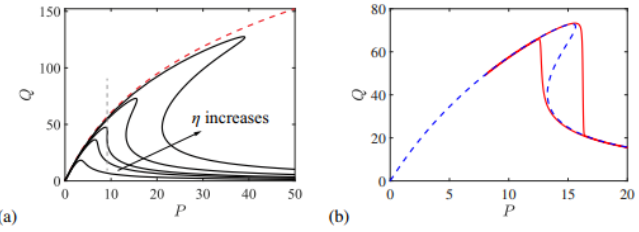

Figure 2: (a) The flux-pressure $Q \sim P$ curve with different $\eta = 1, 2, 2.6, 4, 7$. The gray dashed line marks the vertical segment of the curve at the threshold $\eta \approx 2.6$, and the red dashed line represents the curve at the limit of $\eta \to \infty$; (b) Hysteresis observed by increasing P gradually from $P = 8.2$ to 20, and then decreasing it back to 8.2, at a constant rate $dP/dt = \pm 25$. The red solid lines represent the transient solution whereas the blue dashed lines the steady-state solution corresponding to the $\eta = 4$ curve of (a).

We will present two types of results, steady-state $Q(P)$ relationships that exhibit hystereses, and transient simulations to confirm the hysteretic behaviors expected in an experimental setup. Numerical method is shown in our previous study[4]. Here we present predictions of our entry boundary condition and permeability model. The interfacial permeability η turns out to be a key parameter for the flux-pressure relation. Fig. 2(a) depicts the steady-state flow rate Q as a function of the pressure drop P for a range of η values. Two distinct behavior can be identified. For small η, Q initially increases with P, reaches a maximum, and then declines as P increases further. In this regime, there is a single Q value for each P, and no hysteresis exists. Above a threshold $\eta = 2.6$, the curve overturns as a breaking wave to produce three Q for an intermediate range of the P. Now hysteresis is expected if one varies P in small increments and monitors the reaction of Q. With greater η values, the achievable flow rates are higher, and the curve extends toward the upper-right of the plot, with greater jumps expected for the hysteresis.

The hysteretic behavior, exemplified by η = 4 in Fig. 2(a), is more intricate. We note that the transient solution largely confirms the expectations from the analytical steady solution, with hysteretic jumps when P crosses thresholds while increasing and decreasing. we can rationalize the hysteresis from the dynamics of $Q(P)$ which clearly indicates two distinct states; let us call them "relaxed" and "compressed" for brevity. The hysteresis happens for pressure between two thresholds, $13 \leq P \leq 16.2$. As P increases from below the lower threshold $P_L = 13$, The flux keeps increasing with pressure. The interfacial compression remains small and the upstream portion of the gel layer stays "relaxed", until P reaches the upper threshold of $P_U = 16.2$, when the upstream portion of the gel suddenly becomes "compressed", accompanied by a drop in the fluid velocity. A similar hysteresis occurs when P decreases from above the upper threshold. Note that the hysteretic behaviors can be observed from the flux as well as the thickness of the layer and interfacial volume fraction. We have explained the observed behaviors by analyzing the total pressure drop into two components: interfacial and bulk. Additionally, we discussed the condition of hysteresis in relation to various permeability models and entry conditions.

REFERENCES

.

1. Hewitt, D. R.; Nijjer, J. S.; Worster, M. G.; Neufeld, J. A. Flow-Induced Compaction of a Deformable Porous Medium. Phys. Rev. E 2016, 93 (2), 023116.
2. Xu, Z.; Zhang, J.; Young, Y.-N.; Yue, P.; Feng, J. J. Comparison of Four Boundary Conditions for the Fluid-Hydrogel Interface. Phys. Rev. Fluids 2022, 7 (9), 093301.
3. Feng, J. J.; Young, Y.-N. Boundary Conditions at a Gel-Fluid Interface. Phys. Rev. Fluids 2020, 5 (12), 124304.
4. Li, L.; Zhang, J.; Xu, Z.; Young, Y.-N.; Feng, J. J.; Yue, P. An Arbitrary Lagrangian-Eulerian Method for Simulating Interfacial Dynamics between a Hydrogel and a Fluid. Journal of Computational Physics 2022, 451, 110851.

NONLINEAR RHEOLOGY OF ENTANGLED WORMLIKE MICELLES: A SLIP-SPRING SIMULATION STUDY

Takeshi Sato[1,2] and Ronald G. Larson[3]

[1]Institute for Chemical Research, Kyoto University, Kyoto, Japan
[2]PRESTO, Japan Science and Technology Agency, Saitama, Japan
[3]Department of Chemical Engineering, University of Michigan, Michigan, USA

ABSTRACT

While extensive studies made linear rheological properties of wormlike micelles (WLMs) to be relatively understood, our understanding of nonlinear rheological properties of WLMs is still poor. For deeper understanding of the rheology of WLM solutions, we developed a mesoscopic model to investigate linear and nonlinear rheological properties of entangled WLM solutions.[1] This model is based on the slip-spring (SS) model originally proposed for entangled polymers.[2] To reproduce the dynamics of wormlike micelles, breakage and rejoining events are combined with the polymer-SS model. Furthermore, we address the effects of finite extensibility of springs and stress-induced micelle breakage (SIMB), which are required to reproduce nonlinear rheological properties. After confirming that the micelle-SS model can quantitatively reproduce the linear rheological properties, we used this model to predict nonlinear rheological properties under shear and uniaxial extensional flows. We found that the micelle-SS model can quantitatively predict the shear-rate-dependent viscosity of the WLM solution with a moderate number of entanglements per micelle Z ($Z \leq 7$). Furthermore, the shear rheological properties of the micelle-SS model with moderate shear rates without the remarkable spring stretch can be reproduced by the Giesekus model, which is in agreement with the experimental finding. On the other hand, the extensional properties of the micelle-SS model have not been well tested by comparing with experiments since it is difficult to obtain reliable experimental data for WLM solutions with computationally accessible Z values. Nevertheless, we confirmed that the strain rate dependence of steady extensional viscosity predicted by the micelle-SS model with SIMB shows thickening followed by thinning, which is in qualitative agreement with the experimental observation. We hope to utilize the micelle-SS model to develop a constitutive model.

REFERENCES

1. Sato T.; Moghadam S.; Tan G.; Larson R.G. A slip-spring simulation model for predicting linear and nonlinear rheology of entangled wormlike micellar solutions, *J Rheol*, **64**, 1045-1061, 2020.
2. Likhtman A.E. Single-chain slip-link model of entangled polymers: Simultaneous description of neutron spinecho, rheology, and diffusion, *Macromolecules*, **38**, 6128-6139, 2005.

COUPLING A IONIC SURFACTANT AND A DRUG SALT: EQUILIBRIUM CHARACTERISTIC PARAMETERS & STRAIN HARDENING IN START-UP FLOW

Rossana Pasquino[1], Ilaria Cusano[1], Dganit Danino[2] and Nino Grizzuti[1]

[1]Università degli Studi di Napoli Federico II, Napoli, Italy

[2]Russell Berrie Nanotechnology Institute, Technion, Haifa Israel

ABSTRACT

Surfactant solutions containing Cetylpyridinium Chloride (CPyCl), a classical ionic surfactant, and Sodium Diclofenac (Diclo), a non-steroidal anti-inflammatory drug, were investigated in a wide range of compositions using rheology and Cryo-EM. Solutions were made at three different concentrations of CPyCl, i.e. 5.0, 16.7 and 33.0 mM. The ratio between the salt and the surfactant concentrations, R=CPyCl/Diclo, was within the range $0.4<R<1.4$. Linear viscoelastic rheology was performed at 25°C using a stress controlled DHR-2 Rheometer (TA instruments), equipped with sandblasted 40 mm diameter parallel plates, a Peltier system to control the temperature, and a solvent trap to avoid evaporation. The use of dilute solutions allowed to examine their microstructure via cryo-EM imaging, e.g. avoiding high density of micelles. High-resolution images of vitrified specimens were recorded with a Glacios FEG electron microscope (Thermo Fisher) at 200 kV. Nonlinear rheological experiments were performed at 25°C with a strain-controlled ARES rheometer (TA instruments, USA), using a 50 mm – 0.017rad cone-plate geometry.
We discovered that by tuning R it is possible to achieve completely different microstructures, with variable persistence and contour lengths, and unexpected behaviours in nonlinear start-up flow.

LINEAR RHEOLOGY AND MICROSTRUCTURE

By following the zero-frequency viscosity evolution as a function of Diclo content, it was possible to identify various regions, characterized by a completely different rheological response.

By matching the frequency sweep data with the cryo-EM images, we were able to connect these regions to specific morphological transitions: from spherical micelles to very long and entangled wormlike micelles, to branched networks and eventually well-defined vesicles.
For some systems, we were able to measure the entire spectrum of relaxation times, including the shortest characteristic Rouse time at high frequencies, usually reached only by Diffusive Wave Spectroscopy[1]. This allowed for the evaluation of some important microstructural parameters, such as entanglement, contour, and persistence lengths, taking advantage of available models[2,3]. We were able to quantitatively correlate the above microstructural parameters with the information disclosed by the cryo-EM analysis. A very good quantitative agreement was found between the extracted parameters and the cryo-EM data. The combination of dilute solution rheology and microscopy shed a new light on the role of the binding salt in the morphological transitions of these peculiar micellar solutions.

START UP EXPERIMENTS

For the more entangled systems, the transient behavior in shear flow was investigated through startup measurements, performed at different shear rates so as to cover a wide range of the Weissenberg number, Wi. The long-time response allowed also to build up the flow curves for each sample.
During the transient regime, some samples show flow instabilities and strain hardening phenomena at $Wi > 1$, a phenomenon already detected before on surfactant solutions[4]. Other solutions do not show the same features, behaving like ordinary linear polymers in fast shear flows, that is, exhibiting pronounced overshoots followed by tiny undershoots of the transient shear viscosity, before approaching steady-state[5]. We tried to rationalize this behavior, by identifying the most important parameters, i.e. number of entanglements, characteristic micellar lengths, relaxation times etc., and by clarifying their role in the transient dynamics.
A possible mechanism for the onset of flow singularities is suggested and discussed in terms of a modified rubber network theory, applied recently on similar micellar networks[6].

REFERENCES

1. Oelschlaeger, C.; Schopferer, M.; Scheffold, F.; Willenbacher, N. Linear-to-Branched Micelles Transition: A Rheometry and Diffusing Wave Spectroscopy (DWS) Study. *Langmuir* **25(2)**, 716-723, 2009.
2. Cates, M.E. Reptation of living polymers: dynamics of entangled polymers in the presence of reversible chain-scission reactions. *Macromolecules* **20(9)**, 2289-2296, 1987.
3. Cates, M.E. Dynamics of living polymers and flexible surfactant micelles: scaling laws for dilution. *Journal de Physique* **49(9)**, 1593-1600, 1988.
4. Inoue, T; Inoue, Y.; Watanabe, H. Nonlinear Rheology of CTAB/NaSal Aqueous Solutions: Finite Extensibility of a Network of Wormlike Micelles. *Langmuir* **21(4)**, 1201-1208, 2005.
5. Costanzo, S.; Huang, Q.; Ianniruberto, G.; Marrucci, G.; Hassager, O.; Vlassopoulos, D. Shear and Extensional Rheology of Polystyrene Melts and Solutions with the Same Number of Entanglements. *Macromolecules* **49(10)**, 3825-3835, 2016.
6. Pasquino, R.; Avallone, P.R.; Costanzo, S.; Inbal, I.; Danino, D.; Ianniello, V.; Ianniruberto, G.; Marrucci, G.; Grizzuti, N. On the startup behavior of wormlike micellar networks: The effect of different salts bound to the same surfactant molecule. *Journal of Rheology* **67(2)**, 353–364, 2023.

REFERENCES

1. Saffman P.G., Taylor G.I. The penetration of a fluid into a porous medium or Hele-Shaw cell containing a more viscous liquid, *Proc. Roy. Soc. A*, **245**, (1242) 312-329, 1958.
2. Ball T.V., Balmforth N.J., Dufresne A.P. Viscoplastic fingers and fractures in a Hele-Shaw cell, *J. Non-Newton. Fluid Mech.*, **289**, 104492, 2021.
3. Coussot P. Saffman-Taylor instability in yield-stress fluids, *J. Fluid Mech.*, **380**, 363-376, 1999.
4. Sayag R., Worster M.G. Instability of radially spreading extensional flows. Part 2: Theoretical analysis, *J. Fluid Mech.*, **881**, 739-771, 2019.
5. Ball T.V., Balmforth N.J., Dufresne A.P., Morris S.W. Fracture patterns in viscoplastic gravity currents, *J. Fluid Mech.*, **934**, A31, 2022.

8TH PACIFIC RIM CONFERENCE ON RHEOLOGY, May 15-19, 2023

SQUEEZING OF A CONCENTRATED EMULSION WITH SURFACTANT THROUGH A PERIODIC POROUS MEDIUM

Alexander Z. Zinchenko, Jacob R. Gissinger and Robert H. Davis

Department of Chemical and Biological Engineering
University of Colorado, Boulder, CO 80309-0424, USA

ABSTRACT

This study seeks to explore, through rigorous and accurate hydrodynamical simulations, the fundamental effects of surface contamination by surfactants on emulsion flow of deformable drops through a porous medium. As a prototype problem, high-resolution, long-time 3D simulations are presented for slow, pressure-driven flow of a periodic emulsion of deformable drops through a dense, simple cubic array of solid spheres (one drop and one particle per periodic cell). The drops, covered with insoluble, non-diffusive surfactant, are large compared to pores, and they squeeze with high resistance, very closely coating the solids to overcome surface tension and lubrication effects. The solid volume fraction is 50%, the emulsion concentration c_{em} in the pore space is 36% or 50%, the drop-to-medium viscosity ratio λ is 0.25 to 4. The contamination measure $\beta = R T \Gamma_{eq} / \sigma_0 \le 0.1$ (with the universal gas constant R, absolute temperature T, equilibrium surfactant concentration Γ_{eq} and the clean surface tension σ_0) keeps the linear surfactant model (assumed in most of the work) physically relevant. The boundary-integral solution requires extreme resolutions (tens of thousands of boundary elements per surface) achieved by multipole acceleration with special desingularizations, combined with flow-biased surfactant transport algorithms[1] for numerical stability. The time-periodic regime is typically attained after a few squeezing cycles; the motion period is used in the extrapolation scheme to evaluate critical capillary numbers Ca_{crit} demarcating squeezing from trapping. Due to Marangoni stresses, even light ($\beta = 0.05$) to moderate ($\beta = 0.1$) contaminations significantly reduce the average drop-phase migration velocity (compared to clean drops), especially at small $\lambda = 0.25$. In contrast, Ca_{crit} is weakly sensitive to contamination and levels off completely at $\beta = 0.05$. At $\lambda = 0.25$ and $c_{em} = 0.36$, the average drop-phase velocities are much different for lightly and moderately contaminated emulsions, except for near-critical squeezing when they become the same. Non-linear surfactant models (Langmuir, Frumkin) are used to validate the linear model.

EXAMPLE RESULTS

As one example of the physical trends[2], **Fig. 1** presents the snapshots from the Langmuir model simulation at three close time moments. The time moment $t = 6.74$ corresponds to the peak surfactant concentration $\Gamma = 3.9\Gamma_{eq}$ (i.e. $0.78\Gamma_\infty$) reached in the periodic cycle. The linear model would be clearly inadequate for this Γ. However, such peak concentration in the Langmuir model simulation is observed only on a small portion of the drop surface, and only during a small portion $t = 6.74$ of the periodic cycle. Away from $t = 6.74$, the surfactant concentrations quickly fall to much smaller values on the entire surface, typical of the rest of the periodic regime. The deficiency of the linear model, therefore, does not have a global effect, and both models identically predict the integral flow properties, in particular, strong drop mobility reduction (2.8 times, on the average) due to surfactant.

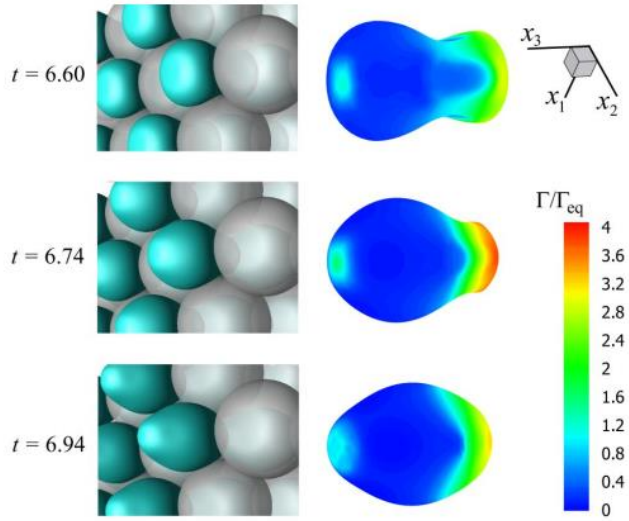

Figure 1: Snapshots of tight emulsion squeezing (left images) and surfactant concentration distribution (right images) for $\lambda = 0.25$, $c_{em} = 0.5$, $\beta = 0.1$ and $E = R\Gamma\Gamma_\infty / \sigma_0 = 0.5$.

REFERENCES

1. Gissinger, J. R.; Zinchenko, A. Z. ; Davis, R. H. Drops with insoluble surfactant squeezing through interparticle constrictions. *J. Fluid Mech.* **878**, 324-355, 2019. https://doi.org/10.1017/jfm.2019.678.
2. Zinchenko, A. Z.; Gissinger, J. R.; Davis, R. H. Flow of a concentrated emulsion with surfactant through a periodic porous medium. *J. Fluid Mech.* **953**, A21, 2022. https://doi.org/10.1017/jfm.2022.951.

The effect of surface viscosity on droplet breakup and relaxation under extensional flow

Vivek Narsimhan[1] and Natasha Singh[1]

[1]Davidson School of Chemical Engineering, Purdue University, West Lafayette, IN USA

ABSTRACT

This study performs boundary-integral simulations to investigate the role of interfacial viscosity on the deformation and breakup of a single droplet in Stokes flow. We model the insoluble surfactant monolayer using the Boussinesq–Scriven constitutive relationship for a Newtonian interface, and simulate the droplet in uniaxial extensional flow. The deformation and breakup results are compared against recently developed small-deformation perturbation theories. The simulations find that the surface shear/dilational viscosity increases/decreases the critical capillary number beyond which the droplet becomes unstable by reducing/increasing the droplet deformation at a given capillary number compared to a clean droplet. We present the relative importance of surface shear and dilational viscosity on droplet stability based on their measured values reported in experimental studies on surfactants, lipid bilayers, and proteins. In the second half of the talk, we incorporate the effect of surfactant transport by solving the time-dependent convection-diffusion equation and consider a nonlinear equation of state (Langmuir isotherm) to correlate the interfacial tension with the changes in surfactant concentration. We explore the coupled influence of Marangoni stresses, surfactant dilution, and pressure-dependent surface viscosity on the droplet deformation and breakup. We conclude by discussing how surface viscosity alters the relaxation of an initially extended droplet in a quiescent external fluid. We note that even small amounts of surface viscosity can alter the thinning behavior towards pinch off, even when surfactant convection (i.e., surface Peclet number) is significant.

ACKNOWLEDGEMENTS

The authors would like to acknowledge support from the Michael and Carolyn Ott Endowment in the Davidson School of Chemical Engineering at Purdue University.

Flow and instability induced by bubbles rising in a two-layer fluid system

M. Zare[1], I.A. Frigaard[1,2], G. Lawrence[3]

[1]Department of Mechanical Engineering, University of British Columbia, Vancouver, BC, Canada
[2]Department of Mathematics, University of British Columbia, Vancouver, BC, Canada
[3]Department of Civil Engineering, University of British Columbia, Vancouver, BC, Canada

ABSTRACT

Buoyancy-driven bubbles crossing horizontal liquid-liquid interfaces are encountered in a variety of engineering applications and natural settings such as wastewater treatment process and methane-emitting lakes. In these two-layer fluid systems, methane bubbles are generated in the lower layer due to biodegradation of organic material. The lower layer exhibits yield stress behaviour and is capped with water. The purpose of this study is to find the effect of the rheology of the lower layer on instability and turbidity driven by rising bubbles. The volume of viscoplastic fluid drawn into the upper layer is a quantity of primary interest. This volume may determine the efficiency of the aeration in the process of wastewater treatment, and the turbidity of the lakes.

Direct numerical simulations employing a volume-of-fluid type formulation combined with a quadtree adaptive mesh refinement technique are performed. The effect of the rheology of the lower layer on the volume of entrained fluid over a range of Archimedes number, density ratio, Bond number and viscosity ratio is explored. Our results show that as the bubble crosses the interface between two liquids tows a column of lower fluid that eventually breaks off into smaller droplets. We define the entrained volume as that of lower fluid located above the position of the initial horizontal interface. This volume consists of fluid trapped in the wake of bubble, the entrained column, and the fluid displaced at the liquid-liquid interface. In cases where either Bond number or Archimedes number is high, a larger volume of entrained fluid gets trapped in the primary/secondary wakes formed behind bubbles, see figure 1. By increasing the viscosity of the upper layer, the major contribution to the entrained volume comes from the region close to the liquid-liquid interface. Finally, the entrainment is categorized into three regimes based on the variation of entrained fluid as the bubble ascends. These were observed to be the ascending, descending, and plateau regimes. The viscoplastic entrainment mainly follows the plateau regime, suggesting that the yield stress of the entrained fluid resists the stress due to density difference between the fluid layers and thus remains unyielded.

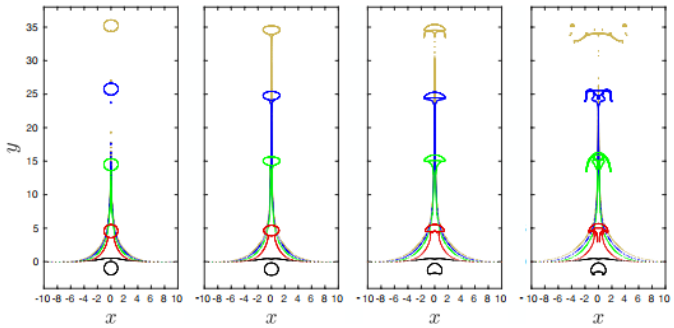

Figure 1: Spatiotemporal images of a bubble crossing the interface between a yield stress fluid (lower layer) and a Newtonian fluid (upper layer). The fluid are iso-dense and the viscosity of the upper layer is 0.1 of the plastic viscosity of the lower layer. The Archimedes number is 5, and the Bond number varies from left to right with values of 0.1, 1, 10, and 50. Since fluids are iso-dense, the Archimedes number varies by a factor of 100 due to the viscosity ratio, as the bubble crosses the interface and the Bond number remains unchanged. By increasing the Bond number, the volume of the lower fluid that bubble entrains increases. It is expected that a combination of strongly sheared and displaced interface, the higher the liquid column entrained and liquid trapped in the primary wake of bubble in the lower layer, contribute to an increase in entrained volume by increasing the viscosity of the upper fluid.

DYNAMICS AND MIXING OF TRAPPED DROPLETS

Gesse Roure[1], Alexander Z. Zinchenko[1] and Robert H. Davis[1]

[1]University of Colorado, Boulder, CO, United States of America

ABSTRACT

The problem of particle trapping and manipulation has a wide range of applications in biotechnology and engineering. Recently, a flow-based, particle-trapping mechanism called the Stokes trap was developed to allow for trapping and control of small particles in microchannels[1]. This mechanism consists of trapping particles in the intersection of multiple branches in a microfluidic channel. The motion of such particles can then be controlled by changing the flow rates in the branches. For deformable particles and vesicles, this mechanism can also be used to perform rheological experiments to determine the viscoelastic response of an emulsion or cell suspension[2]. Besides these applications, the various flow modes produced by the Stokes trap can also be used to manipulate the shape and even induce internal mixing in droplets. In this work, we analyze the dynamics of a droplet in a Stokes trap through boundary-integral simulations[3]. We also explore the response of drop shape with respect to distinct external flow modes, which allow us to perform numerical relaxation experiments such as step strain and oscillatory extension. A linear controller is also used to manipulate drop position, and the drop deformation is characterized by a decomposition of the shape into spherical harmonics. For droplets with small deformation (e.g., small radii and/or capillary number), we observe a linear superposition of harmonics that can be used to manipulate drop shape. We also investigate how the different flow modes may be combined to induce mixing inside the droplets by performing a mixing-number analysis[4]. The transient combination of modes produces an effective chaotic mixing inside the droplet, which can be further enhanced by changing parameters such as viscosity ratio and flow frequency.

PRELIMINARY RESULTS

In this work, we investigate the dynamics of a single Newtonian droplet in the intersecting region between six symmetrically distributed branches of a microfluidic channel with finite depth. To model the branch intersection, we consider a hexagonal prism as our computational domain. The problem geometry, as well as a sample simulation of a deformable droplet in such geometry, can be seen in Figure 1.

Figure 2 shows numerical simulations of mixing inside a droplet undergoing a three-phase extensional external flow mode for $a/H = 0.4, Ca = 0.1, W/H = 1$ and different values of viscosity ratio for different times. The droplet starts with a spherical shape with a passive dye in the lower region. The final configuration of the points is calculated by using the backward Poincaré cell method, where each grid point is traced back to its original position by numerically solving the reverse dynamical

system. As expected from previous works[4], mixing is more effective for less-viscous droplets, as the inner velocity is larger in those conditions.

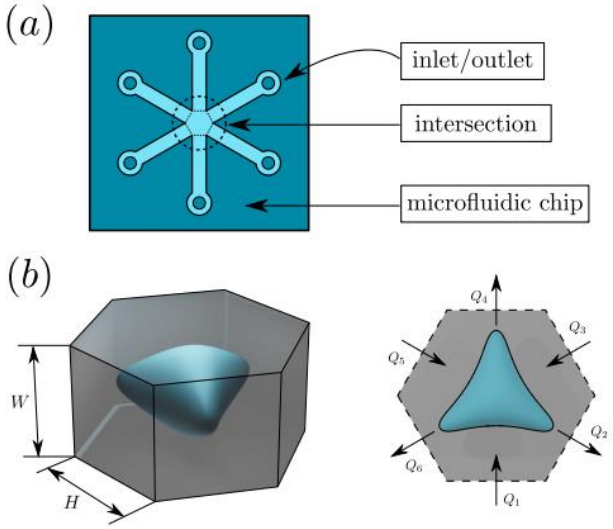

Figure 1: Geometry used for the numerical simulations of a droplet in a Stokes trap. The computational domain shown in (b) is an hexagonal prism corresponding to the intersecting region of the multiple rectangular channel branches, illustrated in (a). The flow velocity at each rectangular panel is given by a Boussinesq velocity profile with prescribed fluxes Q_i, which can be dynamically changed.

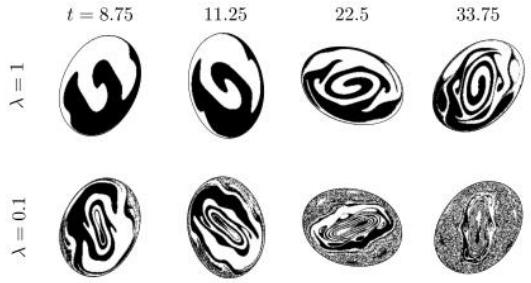

Figure 2: Numerical simulations of mixing inside a droplet undergoing a three-phase extensional flow for $a/H = 0.4$, $Ca = 0.1$, $W/H = 1$ and different values of viscosity ratio for different times. The results are for the midplane $z = 0$. Droplets with a lower viscosity ratio present a better mixing, which is indicated by a smaller mixing number.

REFERENCES

1. Shenoy A., Rao C. V., Schroeder C. M. Stokes Trap for Multiplexed Particle Manipulation and Assembly Using Fluidics. *Proc. Natl. Acad. Sci. U.S.A.* , **113 (15)**, 3976–3981, 2016.
2. Lin C., Kumar D., Richter C. M., Wang S., Schroeder C. M., Narsimhan V. Vesicle Dynamics in Large Amplitude Oscillatory Extensional Flow. *J. Fluid Mech.*, **929**, A43, 2021.
3. Roure G., Zinchenko A. Z., Davis R. H. Numerical Simulation of Deformable Droplets in Complex-Shaped Microchannels. *Phys. Rev. Fluids (under review)*, 2023.
4. Stone Z. B., Stone H. A. Imaging and Quantifying Mixing in a Model Droplet Micromixer. *Physics of Fluids* **17 (6)**, 063103, 2005.

8TH PACIFIC RIM CONFERENCE ON RHEOLOGY, May 15-19, 2023

GAS PROPAGATION THROUGH POROUS MEDIA FILLED WITH YIELD-STRESS FLUID

Ali Pourzahedi[1], Ian Frigaard[1,2]

[1]Dept. of Mechanical Engineering, University of British Columbia, 2054-6250 Applied Science Lane, Vancouver, BC V6T 1Z4, Canada
[2]Dept. of Mathematics, University of British Columbia, 1984 Mathematics Road, Vancouver, BC V6T 1Z2, Canada

ABSTRACT

We use computational methods to study propagation of bubbles inside porous media filled with yield-stress liquid, given the pressure difference across the porous layer. The main motivation for this study comes from the potential for greenhouse gas emissions. In oil sands tailings ponds, the by-products of the extraction of bitumen from oil sands are stored over many decades. The pond slurries, known as Fluid Fine Tailings and Mature Fine Tailings (FFT/MFT) are complex suspensions, rheologically characterised as thixotropic yield-stress fluids. These fluids provide the interstitial liquid within the coarse sand layer that forms underneath, at the bottom of the pond. Anaerobic micro-organisms within the fluid degrade the by-products and create both carbon dioxide and methane. The objective of this research is to provide understanding on how gas generated in the lowest coarse sand layer may propagate to the surface. The underlying research motivation is environmental, i.e. emissions estimation and control.

We use a pore-throat methodology to model the porous media. We develop an algebraic description in the form of a closure law that relates flow rates and displacement efficiency to the fluid properties and applied pressure drop, considering gas motion along an axisymmetric pipe (throat), filled with yield-stress fluid. This is used as the building-block for a meso-scale network model of the coarse sand layer. Gas propagation behaviour is then solved using a gas-liquid hydraulic closure model. This type of model allows us to impose both statistical distributions (e.g., throat size, length, etc.) and background physical variations (e.g. initial conditions for the gas, depth-wise aging of the liquid properties). In this way we can build a picture of the system response of the coarse sand layer, understanding how gas generated in the interstitial liquid might percolate upwards.

Acknowledgement: This research was made possible by funding from NSERC and COSIA/IOSI (project numbers CRDPJ 537806-18 and IOSI Project #2018-10).

Localization of stirring flows: the effect of the yield stress

Mohammad Reza Daneshvar Garmroodi[1], Ida Karimfazli[1]

[1]Dept. of Mechanical, Industrial & Aerospace Engineering Concordia Universiy Montreal, Quebec

ABSTRACT

Viscoplastic fluids (VPFs) are a class of non-Newtonian fluids that behave like solids when the applied shear stress is less than a threshold value called the yield stress ($\widehat{\tau}_y$). When the shear stress exceeds the yield stress, VPFs flow like fluids. Mixing VPF is a ubiquitous problem in many disciplines. Pharmaceutical, polymer, and food processing are examples where mixing plays a vital role in the quality of the final product. We investigate the mixing of a dye in a 2D circular domain of radius $\widehat{R}$ filled with a VPF. The stirring strategy is to move a circular stirrer along a circular path with a constant velocity ($\widehat{r}_o\widehat{\Omega}$, where $\widehat{r}_o$ is the radius of the path and $\widehat{\Omega}$ is constant). The material initially contained in one half of the flow domain is marked by a (passive) dye, described by a concentration field governed by an advection-diffusion equation. The flow domain and the initial condition are illustrated in Fig. 1, where the red and blue colors represent the dyed and dye-free fluid. When the fluid is Newtonian, mixing is enhanced by periodic vortices that spread away from the stirrer. The recirculation zone expands steadily and monotonically (see Fig. 2 for an illustrative example). Keeping the stirring strategy constant, we investigate the effect of viscoplasticity on the evolution of mixing and fluid flow. When the fluid has a yield stress, the kinetic energy decays more rapidly away from the stirrer. Expectedly, the recirculation zone is confined to a finite domain around the stirrer (see Fig. 2 for an illustrative example). We classify the different mixing regimes, characterize the limit cases and discuss the transition between different mixing regimes.

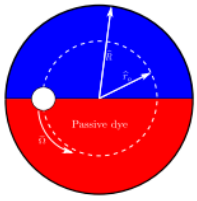

Figure 1: Schematic of the domain geometry and the initial condition

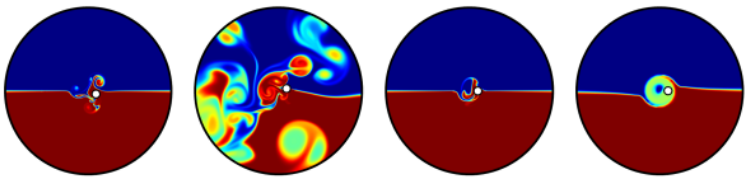

Figure 2: Illustrative examples of the time evolution of the concentration field for a Newtonian fluid (a,b) and a VPF (c,d).

Thin-film flow of a Bingham fluid over topography with a temperature dependent rheology

Miguel Moyers-Gonzalez[1], James Hewett[2], Dale Cusack[3], Ben Kennedy[3] and Mathieu Sellier[2]

[1]School of Mathematics and Statistics, University of Canterbury, New Zealand
[2]Department of Mechanical Engineering, University of Canterbury, New Zealand
[3]School of Earth and Environment, University of Canterbury, New Zealand

ABSTRACT

We consider the flow of a viscoplastic fluid on a horizontal or an inclined surface with a flat and an asymmetric topography. A particular application of interest is the spread of a fixed mass – a block – of material under its own weight. The rheology of the fluid is described by the Bingham model which includes the effect of yield stress, i.e. a threshold stress which must be exceeded before flow can occur. Both the plastic viscosity and the yield stress are modelled with temperature-dependent parameters. The flow is described by the lubrication approximation, and the heat transfer by a depth-averaged energy conservation equation. Results show that for large values of the yield stress, only the outer fraction of the fluid spreads outward, the inner fraction remaining unyielded. We also present an analysis which predicts the threshold value of the yield stress for which partial slump occurs.

Damping of surface waves by a floating viscoplastic plate

Xuemeng Wang[1], Neil J. Balmforth[1]

[1]Department of Mathematics, University of British Columbia, Vancouver, BC, V6T 1Z2, Canada

ABSTRACT

The damping of surface waves by floating material plays an important role in geophysics and engineering. In the marginal ice zone, for example, broken floating ice damps sea waves, with important implications on the maintaince of ice cover and the Arctic climate[1−2].

A theoretical model is presented to explore how surface waves in an inviscid fluid layer are damped by the bending stresses induced in a overlying floating film of yield-stress fluid. The model applies in the long-wavelength limit, combining the shallow-water equations for the inviscid fluid with a theory for the bending of a thin viscoplastic plate described by the Herschel-Bulkley constitutive law. An exploration of the energetics captured by the model suggests that waves decay to rest in finite time, a result that is confirmed using a combination of approximate, numerical and asymptotic solutions to the model equations. In the limit that the plate behaves like a perfectly plastic material, the sloshing motions take the form of triangular waves with bending restricted to narrow viscoplastic hinges.

Fig. 1 shows a sketch of the geometry. The thickness $\mathcal{D}$ of the viscoplastic plate is comparable to the typical depth of the inviscid fluid layer $\mathcal{H}$. Both are much smaller than the characteristic lengthscale $\mathcal{L}$ over which the plate bends.

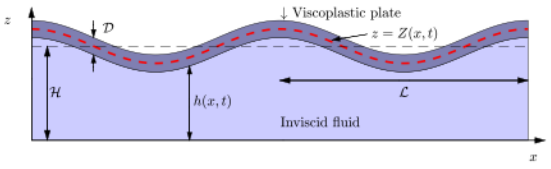

Figure 1: Sketch of the geometry

REFERENCES

1. Squire, V. A. A Fresh Look at How Ocean Waves and Sea Ice Interact. *Philosophical Transactions of the Royal Society A: Mathematical, Physical and Engineering Sciences*, **376**, 2018.

2. Squire, V. A. Ocean Wave Interactions with Sea Ice: A Reappraisal. *Annual Review of Fluid Mechanics*, **52**, 37–60, 2020.

8TH PACIFIC RIM CONFERENCE ON RHEOLOGY, May 15-19, 2023

ADVANCED POLYMER RHEOLOGY BASED ON RHEO-OPTICAL TOOLS AND A DUAL MOTOR DEVICE

Jörg Läuger

Anton Paar Germany
Helmuth-Hirth-Str. 6, D-73760 Ostfildern, Germany
(joerg.laeuger@anton-paar.com)

The simultaneous application of rheological and optical techniques leads to a better understanding of the dependencies between the microstructure and the mechanical properties of complex fluids and especially polymeric materials. Various optical methods such as small angle light scattering, microscopy (polarized, fluorescence, confocal), spectroscopy (NIR, IR, Raman), birefringence and dichroism have been used. A rheo polarized imaging techniques (SIPLI - shear induced polarization light imaging) which measures local stresses by detecting birefringence and Raman spectroscopy are discussed in more detail. By using a parallel-plate geometry with SIPLI, the entire measuring plate is observed and the birefringence can be visualized over the full range of shear rates in a single experiment. To directly relate changes in rheological behavior to chemical changes or phase transition, Raman spectroscopy can be used in situ with rheology.

A rheometer platform based on a combined motor transducer (CMT) rheometer with an electrically commutated synchronous motor on the upper side allows the use of a second motor on the bottom side. The second motor could either be a rotational or a linear drive. When a rotational drive is used, the instrument becomes a separate motor transducer (SMT) rheometer by using one motor as drive and the second as a torque transducer. In addition, the instrument can be operated in a counter-rotation mode where both motors rotate in opposite directions, allowing the creation of a stagnation line in the sample where it is sheared but not moved from its position for rheo-microscopy. The SMT mode has some advantages in terms of sensitivity under certain measurement conditions and allows the use of special tools such as a cone-partitioned-plate (CPP), which allows measurements to be made even when edge fracture would hinder them in standard geometries. Combining the upper rotational motor with a linear drive in the bottom enables new testing possibilities. By using only the linear drive, Dynamic Mechanical Analysis (DMA) is possible on more solid specimens with different geometries like tension, three-point bending, cantilever, or in compression. When using a solid bars geometry, DMA in tension by the linear drive and DMA in torsion with the upper rotational drive are possible on the same specimen, allowing to extract not only the DMA parameters but Poisson's ratio to be determined.

The fast response of the linear motor can be used in combination with a fast visualization setup for capillary breakup rheometry.

UNIVERSAL DIFFUSION OF DENDRIMERS IN SEMIDILUTE SOLUTIONS OF LINEAR POLYMERS

Silpa Mariya[1], Jeremy J. Barr[2], P. Sunthar[3] and J. Ravi Prakash[4]

[1] IITB-Monash Research Academy, Powai, Mumbai, 400076, India
[2] School of Biological Sciences, Monash University, Clayton, VIC 3800, Australia
[3] Department of Chemical Engineering, Indian Institute of Technology, Mumbai, 400076, India
[4] Department of Chemical and Biological Engineering, Monash University, Clayton, VIC 3800, Australia

ABSTRACT

Understanding the diffusion of nanoparticles and macromolecules in biopolymer networks is important for many biological and medical applications[1,2]. For example, elucidating the mechanisms underlying the transfer of macromolecular drugs into living tissue is essential for their use as drug delivery vehicles[3]. The role of the structure of the diffusing species as well as the polymer matrix in determining the physics of the diffusion process has been widely studied experimentally using probe species such as nanoparticles or branched polymers with well defined topologies in semidilute polymer solutions of linear polymer chains[4–7]. The results of these experimental studies have been described by hydrodynamic[8], scaling[9] and computational models[10], which have led to many insights identifying the key length and time scales involved. The theoretical models have however been confined to studying the diffusion of nanoparticles, which are hard spheres. The applicability of these models to situations when the probe diffusing species are soft tenuous particles such as a star polymers or dendrimers is currently unknown. In the present work, a multi-particle Brownian dynamics simulation algorithm, based on a modification of the GPU-accelerated python package HOOMD-blue[11], is used to describe the diffusion of dendrimers of arbitrary topology in a semidilute solution of linear chains. Diffusive and sub-diffusive regimes for the probe dendrimer and the background linear chains are identified and their dependence on the key parameters that determine length and time scales are elucidated. A new scaling law for dendrimer diffusivity as a function of the ratio of its mean size to the correlation length of the semidilute solution is proposed, which differs significantly from previously proposed scaling laws for hard sphere nanoparticles. With the appropriate choice of scaling variables, it is shown that data for dendrimers of different architectures can be collapsed onto a mater curve, independent of architecture. The Gaussian character of normalised particle displacements at various times, as a function of solution concentration, is also examined. It is shown that the central difference between dendrimers and hard sphere nanoparticles, which is responsible for the distinctness of their diffusive behaviours, is the reduction in the mean size of a dendrimer with increasing solution concentration.

REFERENCES

1. Salata, O. V. Applications of nanoparticles in biology and medicine, *Journal of nanobiotechnology*, **2(1)**, 1-6, 2004.

2. Rudramurthy, G. R., Swamy, M. K. Potential applications of engineered nanoparticles in medicine and biology: An update, *JBIC Journal of Biological Inorganic Chemistry*, **23**, 1185-1204, 2018.

3. Jain, R. K., Stylianopoulos, T. Delivering nanomedicine to solid tumors, *Nature reviews Clinical oncology*, **7(11)**, 653-664, 2010.

4. Cheng, Y., Prud'Homme, R. K., Thomas, J. L. Diffusion of mesoscopic probes in aqueous polymer solutions measured by fluorescence recovery after photobleaching, *Macromolecules*, **35(21)**,8111-8121, 2002.

5. de Kort, D. W., Rombouts, W. H., Hoeben, F. J., Janssen, H. M., Van As, H., van Duynhoven, J. P. Scaling behavior of dendritic nanoparticle mobility in semidilute polymer solutions, *Macromolecules*, **48(20)**,7585-7591, 2015.

6. Kalwarczyk, T., Ziebacz, N., Bielejewska, A., Zaboklicka, E., Koynov, K., Szymanski, J., ... , Hołyst, R. Comparative analysis of viscosity of complex liquids and cytoplasm of mammalian cells at the nanoscale, *Nano letters*, **11(5)**, 2157-2163, 2011.

7. Smith, M., Poling-Skutvik, R., Slim, A. H., Willson, R. C., Conrad, J. C. Dynamics of flexible viruses in polymer solutions, *Macromolecules*, **54(10)**, 4557-4563, 2021.

8. Cukier, R. I. Diffusion of Brownian spheres in semidilute polymer solutions, *Macromolecules*, **17(2)**, 252-255, 1984.

9. Cai, L. H., Panyukov, S., Rubinstein, M. Mobility of nonsticky nanoparticles in polymer liquids, *Macromolecules*, **44(19)**, 7853-7863, 2011.

10. Chen, A., Zhao, N., Hou, Z. The effect of hydrodynamic interactions on nanoparticle diffusion in polymer solutions: a multiparticle collision dynamics study, *Soft matter*, **13(45)**, 8625-8635, 2017.

11. Anderson, J. A., Glaser, J., Glotzer, S. C., HOOMD-blue: A Python package for high-performance molecular dynamics and hard particle Monte Carlo simulations, *Computational Materials Science*, **173**, 109363, 2020.

THE EFFECT OF THE SOLVENT DIELECTIC CONSTANT ON THE CONFORMATION AND DYNAMICS OF POLYELECTROLYTES IN SOLUTION

Atsushi Matsumoto[1], Hiroto Osada[2], Ryosuke Ukai[2], Shinji Sugihara[1], and Yasushi Maeda[1]

[1]Graduate School of Engineering, University of Fukui
[2]School of Engineering, University of Fukui
3-9-1 Bunkyo, Fukui-shi, Fukui 910-8507, Japan

ABSTRACT

In this study, we investigated the effect of the solvent dielectric constant ε_r on the counterion condensation for an imidazolium-based polyelectrolyte, poly(1-butyl-3-vinylimidazolium bis(trifluoromethanesulfonyl)imide) (PC_4-TFSI), by measuring the shear viscosity of the PC_4-TFSI in a series of non-ionic good solvents having dielectric constants ranging from 7.9 for tetrahydrofuran to 178 for *N*-methylformamide. We found that for a given molar concentration c_p of the PC_4-TFSI monomers, the specific viscosity η_{sp} decreased significantly with decreasing ε_r. Moreover, the dependence of η_{sp} on c_p in solvents at high ε_r followed the scaling law of η_{sp} for salt-free polyelectrolytes in good solvents, but its scaling relationship gradually shifted to the scaling law of η_{sp} for electrically neutral polymers in good solvents as ε_r was decreased. Thus, we found that PC_4-TFSI could behave as both polyelectrolyte and neutral polymer chains by simply changing the solvent dielectric constant. We further analyzed the viscosity data by estimating the overlap monomer concentration c_p^* as a monomer concentration at which $\eta_{sp} = 1$. The value of c_p^* decreased with increasing ε_r with a power of -3 for $\varepsilon_r < 70$, and asymptotically approached a constant value at higher ε_r. Since the overlap polymer concentration is related to the chain size, i.e., $c_p^* \propto 1/R^3$, the observed result indicates that the chain size increases with increasing ε_r due to the increase in the charge fraction on the PC_4-TFSI caused by the counterion condensation. By applying the Dobrynin blob model for c_p^* of salt-free polyelectrolytes in good solvents[1], we found that the charge fraction f was scaled as $f \propto \varepsilon_r^{7/4}$. The obtained scaling exponent was larger than the value predicted by the classical Manning counterion condensation model[2], i.e., $f \propto \varepsilon_r^1$. Our results provide, for the first time, a valid experimental reference for the study of the counterion condensation process of polyelectrolytes with respect to the varying ε_r.

1. Dobrynin, A. V.; Colby, R. H.; Rubinstein, M. Scaling Theory of Polyelectrolyte Solutions. *Macromolecules*, **28**, 1859–1871., 1995. https://doi.org/10.1021/ma00110a021.
2. Manning, G. S. Limiting Laws and Counterion Condensation in Polyelectrolyte Solutions I. Colligative Properties. *J. Chem. Phys.*, **51**, 924, 1969. https://doi.org/10.1063/1.1672157.

RECENT ADVANCES IN POLYMER VISCOELASTICITY FROM GENERAL RIGID BEAD-ROD THEORY

Alan Jeffrey Giacomin[1,2,3,4] , Mona Kanso[1]
[1]Chemical Engineering Department, Polymers Research Group, Queen's University, Kingston, Ontario, Canada
[2]Mechanical and Materials Engineering Department, Queen's University, Kingston, Ontario, Canada
[3]Physics, Engineering Physics and Astronomy Department, Queen's University, Kingston, Ontario, Canada
[4]Mechanical Engineering Department, University of Nevada, Reno, Nevada, USA

ABSTRACT

One good way to explain the elasticity of a polymeric liquid, is to just consider the orientation distribution of the macromolecules. When exploring how macromolecular architecture affects the elasticity of a polymeric liquid, we find general rigid bead-rod theory to be both versatile and accurate. This theory sculpts macromolecules using beads and rods. Whereas beads represent points of Stokes flow resistances, the rods represent rigid separations. In this way, how the shape of the macromolecule affects its rheological behavior in suspension is determined. Our work shows the recent advances in polymer viscoelasticity using general rigid bead-rod theory, including advances applied on the coronavirus. The coronavirus is always idealized as a spherical capsid with radially protruding spikes. However, histologically, in the tissues of infected patients, capsids in cross section are elliptical, and only sometimes spherical. This capsid ellipticity implies that coronaviruses are oblate or prolate or both. We call this diversity of shapes, pleomorphism. Recently, the rotational diffusivity of the spherical coronavirus in suspension was calculated, from first principles, using general rigid bead-rod theory. We did so by beading the spherical capsid, and then also by replacing each of its bulbous spikes with a single bead. In this paper, we use energy minimization for the spreading of the spikes, charged identically, over the oblate or prolate capsids. We use general rigid bead-rod theory to explore the role of such coronavirus cross-sectional ellipticity on its rotational diffusivity, the transport property around which its cell attachment revolves. We learn that coronavirus ellipticity drastically decreases its rotational diffusivity, be it oblate or prolate.

REFERENCES

1. Kanso, M.A.; A.J. Giacomin; C. Saengow; J.H. Piette, Macromolecular Architecture and Complex Viscosity, *Physics of Fluids*, **31**(8), 087107 (2019).
2. Kanso. M.A.: M. Naime: V. Chaurasia: K. Tontiwattanakul: E. Fried: A.J. Giacomin. Coronavirus Pleomorphism, *Physics of Fluids*, **34**(6), 063101 (2022).
3. Pak, M.C.; R. Chakraborty; M.A. Kanso; K. Tontiwattanakul; K.-I. Kim; A.J. Giacomin, Coronavirus Peplomer Interaction, *Physics of Fluids*, **34**(11), 113109 (2022).

Improvement of Heat Resistance using Physical Aging in Polystyrene Injection Moldings

Kosaku Tao[1,2], Koji Yamada[1], Seiji Higashi[1], Keitaro Kago[1], Shiho Kuwashiro[1], Hiroshi Hirano[1], Hiroki Takeshita[2] and Katsuhisa Tokumitsu[2]

[1]Osaka Research Institute of Industrial Science and Technology, Japan
[2]Department of Material Science, School of Engineering, University of Shiga Prefecture, Japan

ABSTRACT

This work examined the effect of temperature during annealing below glass transition temperature (T_g) on relaxation behavior of amorphous structure and improvement of physical heat resistance in polystyrene injection moldings. The higher the annealing temperature, the faster the rate of the enthalpy relaxation, resulting in that the annealing time required to increase heat distortion temperature (HDT) was shortened. Meanwhile, when the annealing time was longer than 7 hours, it was not that the higher the annealing temperature, the higher the HDT. Then, we investigated the dependence of both the enthalpy relaxation and the increase in HDT on the annealing temperature, using polystyrene with different T_g. As the results, the optimum annealing temperature for the increase in HDT due to the enthalpy relaxation depended on the temperature difference from T_g.

Intorduction

Amorphous resins are widely used in designing components such as automobile parts because amorphous resins are easy to color owing to high transparency. In particular, polystyrene has a high production volume owing to its high versatility.

Injection moldings is a common industrial process because it allows mass production together with high dimensional accuracy. In the injection molding of an amorphous resins such as a polystyrene, the resin is rapidly cooled rom the molten state when it is injected into the mold, so the molecular motion freezes before the intermolecular distance becomes close. It is thought to solidify in an unstable enthalpy state[1)]. When the injection moldings is annealed below T_g, the amorphous structure relax to more enthalpy-stable structure. It is known as physical aging that the various physical properties change with the relaxation of the excess enthalpy[2)]. In our previous studies, we have shown that physical heat resistance [Heat distortion Temperature (HDT)] improves with the enthalpy relaxation in polystyrene injection moldings[3)]. In this study, the annealing temperature dependence of the enthalpy relaxation and HDT was investigated

using polystyrene with different T_g in order to obtain a guideline to annealing condition for increase in HDT of polystyrene injection moldings using physical aging.

Experiment

We used 679 (M_w=237000, M_w/M_N=3.49, T_g=94 °C, PS Japan corp) and HF77 (M_w=240000, M_w/M_N=2.53, T_g=102 °C, PS Japan corp) as general purpose polystyrene.

The test specimen was molded using an injection molding machine (Si-80IV, Toyo Machinery and Metal Co., Ltd.), under the condition included a cylinder temperature of 210 °C, cooling time of 10 s, holding time of 20 s, and overall cycle time of 40 s.

HDT was measured by flatwise method with reference to ISO Test Method 75. The test load was 1.8 MPa. Each specimen was thermally analyzed using differential scanning calorimetry (DSC; DSC 214 Polyma, Netzsch) in temperature-modulated mode, the extent of enthalpy relaxation (ΔH) was quantified on the basis of the area of the endothermic peak near T_g.

Results and Discussion

Fig.1 shows the resuls of the annealing temperature dependence of the enthalpy relaxation and HDT, arranged by the temperature difference (T_g-T_a) between T_g and annealing temperature (T_a), with the annealing time fixed at 336 hours. As shown in Fig. 1, the annealing temperature at which the HDT was maximized was almost the same as in the case of enthalpy relaxation for each polystyrene. Therefore, the increase in HDT and the enthalpy relaxation are considered to be closely related. Inaddition, regardless of the material grade, the enthalpy relaxation and HDT were maximum at the same T_g-T_a. Therefore, the optimum annealing temperature for increaseing HDT using physical aging is thought to depend on the temperature difference from T_g.

The higher the annealing temperaturem, the faster the relaxation rate. Meanwhile, the enthalpy in the equilibrium state is high (that is, the ΔH is small), when the annealing temperature is high. From those balance, it is considered that the optimum temperature for enthalpy relaxation and increase in HDT existed in the annealing for 336 hours.

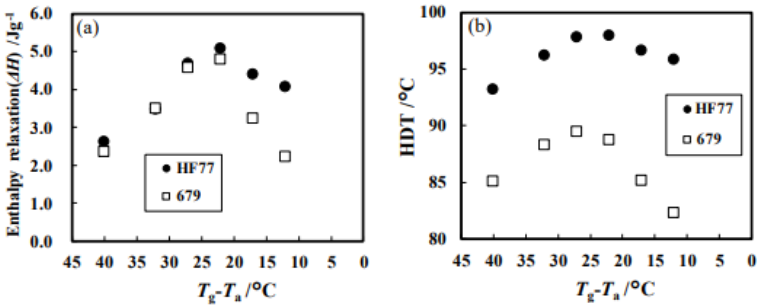

Figure 1: The enthalpy relaxation (a) and HDT (b) as a function of the annealing temperature.

Conclusion

The annealing temperature dependence of the enthalpy relaxation and HDT was investigated using polystyrene with different T_g in order to obtain a guideline for the annealing condition for the increase in HDT of polystyrene injection moldings using physical aging. As the result, the optimum annealing temperature for increasing HDT depends on the temperature difference from T_g. Although the optimum temperature is presumed to differ depending on the time scale, the optimum temperature is considered to be about T_g-25 °C in the heat treatment for 336 hours.

REFERENCES

1. Ho Huu, C.; Vu-Khanh, T. Effects of Physical Aging on Yielding Kinetics of Polycarbonate. *Theoretical and Applied Fracture Mechanics*, **40(1)**, 75-83., 2003. https://doi.org/10.1016/S0167-8442(03)00035-1.
2. Hutchinson, J., M.; Smith, S.; Home, B.; Gourlay, G., M. Physical Aging of Polycarbonate: Enthalpy Relaxation, Creep Response, and Yielding Behavior. *Macromolecules*, **32(15)**, 5046-5061., 1999. https://doi.org/10.1021/ma981391t
3. Tao, K.; Yamada, K.; Hatano, A.; Takeshita, H.; Higashi, S.; Kago, K.; Kuwashiro, S.; Hirano, H.; Tokumitsu, K. Relationship between dynamic viscoelasticity and amorphous structural changes associated with enthalpy relaxation in polystyrene injection moldings. *Journal of the Society of Rheology, Japan*, **50(2)**, 181-187., 2022. https://doi.org/10.1678/rheology.50.181

8TH PACIFIC RIM CONFERENCE ON RHEOLOGY, May 15-19, 2023

EFFECT OF SALT CONCENTRATION AND FLOW RATE ON CLOGGING DYNAMCIS IN THE SINGLE MICRO-PORE

Dae Yeon Kim[1], Seon Yeop Jung[2], Young Jin Lee[1] and Kyung Hyun Ahn[1,*]

[1]School of Chemical and Biological Engineering, and Institute of Chemical Processes, Seoul National University, Seoul 08826, Korea
[2]Department of Chemical Engineering, Dankook University, Yongin-si, Gyeonggi-do, 16890, Korea

ABSTRACT

Clogging is ubiquitous in a wide range of material processing. This undesirable phenomenon causes various flow problems. As a fundamental study of clogging, we investigate the clogging dynamics in terms of the colloidal interaction and hydrodynamics stress in a single-micro pore through microfluidics and image analysis.

Polystyrene suspension with various salt concentrations is used as a feed solution. Microfluidic observation is employed to investigate particle deposition in a contraction microchannel. To quantify particle deposition, particle deposition area is calculated and the pressure drop is also measured.

Dramatic differences in particle deposition were observed. When the colloidal interaction is repulsive, the deposition occurs mostly in the downstream. On the other hand, an opposite deposition behavior is identified when the colloidal interaction is attractive. As the flow rate is changed, more complex deposition behaviors are observed. The difference in particle deposition behavior was explained by the particle flux density and the ratio of the lift force to colloidal force.

Star-polymer-DNA gels showing predictable stress relaxation behavior

Xiang Li[1], Masashi Ohira[1,2], Takamasa Sakai[2] and Mitsuhiro Shibayama[3]

[1]Hokkaido University, Sapporo, Japan
[2]The University of Tokyo, Tokyo, Japan
[3]CROSS, Tokai, Japan

ABSTRACT

Dynamically crosslinked gels are attractive materials for applications requiring time-dependent mechanical responses. DNA duplexes with predictable binding energies are ideal crosslinkers for building such gels. However, the mechanical responses of most DNA gels are unpredictable due to the complications in the gel networks. Here, we designed a DNA gel with a highly homogeneous gel network and well predictable mechanical behaviour using star-polymer strategy. Stress-relaxation tests and dissociation kinetics measurements showed that the macroscopic relaxation time of the DNA gels was approximately equal to the lifetime of the DNA crosslinkers over 4 orders of magnitude from 0.1-2000 s. A series of durability tests show that the DNA gels are hysteresis-free and self-healing after the application of repeated temperature and mechanical stimuli. These results demonstrate the great potential of star-polymer-DNA precursors for building gels with predictable and tunable viscoelastic properties, suitable for applications such as stress-responsive extracellular matrices, injectable solids and soft robotics.

MAIN TEXT

We used a recently proved star polymer strategy [1,2] to improve the homogeneity of the gel network and designed a pair of DNA sequences showing a simple two-state transition as the dynamic crosslinkers[3]. The formed gels responded to multiple stimuli, such as temperature and forces, and were still self-healable and hysteresis-less. The contrast-matched small-angle neutron scattering (SANS) measurements confirmed the high spatial homogeneity of the gel network. UV spectroscopy determined that the two-state transition of the DNA duplexes occurred in the gels, the same as the simulated results from the DNA calculator. In addition, stress-relaxation tests and dissociation kinetics measurements revealed that the macroscopic relaxation time of our DNA gels agreed with the lifetime of the DNA crosslinkers over an extended time range from 0.1–2000 s, which was challenging for most other dynamically crosslinked gels. In combination with the demonstrated star-polymer–DNA gel scheme with the well-established database for DNA thermodynamics and kinetics, we will be able to

fabricate DNA gels with on-demand viscoelastic properties. We envision that highly predictable and tunable star-polymer–DNA gels can boost the fundamental understanding and applications of dynamically crosslinked gels.

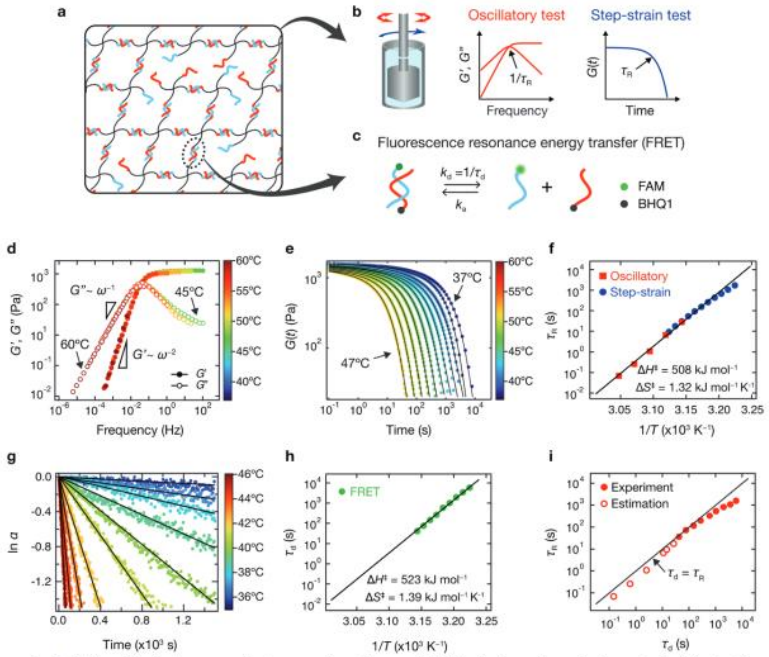

Figure 1: Relationship between gel stress relaxation and DNA duplex dissociation. a) An illustration of the deformed star-polymer–DNA network. b) The viscoelastic properties of the gels were characterized with a rheometer using two different methods: an oscillatory test for fast relaxation at high temperatures and a step-strain test for slow relaxation at low temperatures. c) The duplex dissociation kinetics were evaluated for DNA-only solutions using fluorescence resonance energy transfer (FRET). d) Master curves of G′ and G″ obtained from the oscillatory test for star-polymer–DNA gels over the range of 45–60 °C at intervals of 2.5 °C. The master curves were prepared by the time–temperature superposition treatment, using the curves at 45 °C as reference. e) Stress-relaxation curves of star-polymer–DNA gel obtained from the step-strain tests over the range of 37–47 °C at 1 °C intervals. f) Temperature dependence of the stress-relaxation time of the gels (τR). g) Time variation of the normalized molar concentration of DNA duplexes (α) obtained from FRET measurements over the temperature range of 36–45 °C at 1 °C intervals. h) Temperature dependence of the lifetime of the DNA duplexes (τd). i) Correlation plot of τR with respect to τd. The τd values in the experimentally inaccessible time range were estimated using the Eyring equation and displayed as open circles to distinguish them from the experimentally measured τd values (filled circles). All τR values were obtained experimentally. The solid line denotes a guide for the one-to-one correspondence limit (τR = τd), where the macroscopic stress relaxation is directly linked with the microscopic dissociation of the DNA duplexes. Reproduced from Ref. 3 with permission from the Royal Society of Chemistry.

ACKNOWLEDGEMENTS

This study was supported by Japan Society for the Promotion of Science (JSPS) KAKENHI grants to X.L. (JP17K14536, JP19K15628), M.O. (JP20J22044)). This study was also supported by Japan Science and Technology Agency (JST) grants to X.L. (FOREST Program JPMJFR201Z) and T.S. (CRESTJPMJCR199).

REFERENCES

(1) Sakai, T.; Matsunaga, T.; Yamamoto, Y.; Ito, C.; Yoshida, R.; Suzuki, S.; Sasaki, N.; Shibayama, M.; Chung, U. Design and Fabrication of a High-Strength Hydrogel with Ideally Homogeneous Network Structure from Tetrahedron-like Macromonomers. *Macromolecules* 2008, *41* (14), 5379–5384. https://doi.org/10.1021/ma800476x.

(2) Li, X.; Nakagawa, S.; Tsuji, Y.; Watanabe, N.; Shibayama, M. Polymer Gel with a Flexible and Highly Ordered Three-Dimensional Network Synthesized via Bond Percolation. *Sci Adv* 2019, *5* (12), eaax8647. https://doi.org/10.1126/sciadv.aax8647.

(3) Ohira, M.; Katashima, T.; Naito, M.; Aoki, D.; Yoshikawa, Y.; Iwase, H.; Takata, S.; Miyata, K.; Chung, U.; Sakai, T.; Shibayama, M.; Li, X. Star-Polymer-DNA Gels Showing Highly Predictable and Tunable Mechanical Responses. *Adv Mater* 2022, 2108818. https://doi.org/10.1002/adma.202108818.

OBSERVATION OF FLOW BIREFRENGENCE IN DYNAMIC SQUEEZE FLOW

Manabu Kato[1], Yutaro Akagi[2] and Tsutomu Takahashi[3]

[1]National Institute of Technology, Tsuyama College, Okayama, Japan
[2]National Institute of Technology, Tsuyama College 5th grade, Okayama Japan
[3]Nagaoka University of Technology, Niigata, Japan

ABSTRACT

In this study, it is visualized the flow birefringence of an aqueous surfactant solution, which forms wormlike micelles and has strong viscoelastic properties, in a dynamically oscillating two-dimensional squeezed flow over the entire flow field. Strong flow birefringence was observed in the direction of elongation and a phase difference between the birefringence and the strain was confirmed. This result indicates that viscoelastic properties in extensional flow can evaluate from the birefringence measured by image immediately after cessation of the squeeze motion.

INTRODUCTIN AND PURPOSE

In aqueous surfactant solutions, surfactant molecules aggregate above a concentration called critical micelle concentration to form micelles. Micelles are known to take various shapes depending on a surfactant concentration and a salt concentration. The surfactant solution forming wormlike micelles exhibit strong viscoelasticity, and their rheological properties have long been the subject of research. Wormlike micelles change their macrostructure under strong shear deformation. This is called the shear-induced structure (SIS), and it leads to the occurrence of opaque, shear thickening, and inhomogeneous flow in rheometric flow have been reported[1)]. However, those relationship is not fully understood.

On the other hand, there have been efforts to investigate elongation-induced structures (EIS). The Capillary Breakup Elongational Rheometer (CaBER, Thermo Scientific HAAKE) and stagnation point flow are used for those study. Studies using stagnation point flow have reported that EIS occur at a lower strain rate and strain than SIS[2,3)]. In study using CaBER, micelle structures and EIS were reported based on the relationship between the shape change of filaments and the ratio of relaxation times between shear and elongational flow[4)]. These reports suggest that important findings about macrostructure of micelles can be obtained from elongational flow, where micelle are stretched and occurred orientation in only one direction.

In this study, we propose a method to visualize micelle motion in dynamically fluctuating squeeze flow. The flow birefringence of the entire squeeze flow field is observed, and the rheological properties of a surfactant solution in the elongational flow are clarified from the relationship between the birefringence and the squeeze motion.

EXPERIMENTAL APPALATUS AND SAMPLE FLUID

Fig. 1 shows the experimental apparatus used for the flow birefringence observation. From the direction of observation, circular polarizer, squeeze flow cell, circular polarizer, and the light source are arranged in this order. A video camera capable of shooting at 120 fps was used to capture images from the start of flow to relaxation. **Fig. 2** shows a schematic diagram of the squeeze channel and drive system. The squeeze channel consists of a reservoir (80.0 mm × 30.0 mm × 10.0 mm) with an optical glass window (φ30.0 mm) for observation to visualize the flow birefringence caused by the squeezing motion. The upper and lower parts of the flow channel are fixed to a movable stage, which is moved by rotating a ball screw with a stepping motor. The ball screw is divided into a right-hand thread and a left-hand thread, and the stage moves symmetrically up and down when the axis is rotated. The gap between the plates in the squeeze region H changes according to cosine wave. In this experiment, the amplitude A, the squeeze frequency ω, and the initial gap H_0 were used as variables.

CTAB/NaSal aqueous surfactant solution with surfactant concentration 10mM and salt/surfactant ratio 3.00 was used as the test fluid.

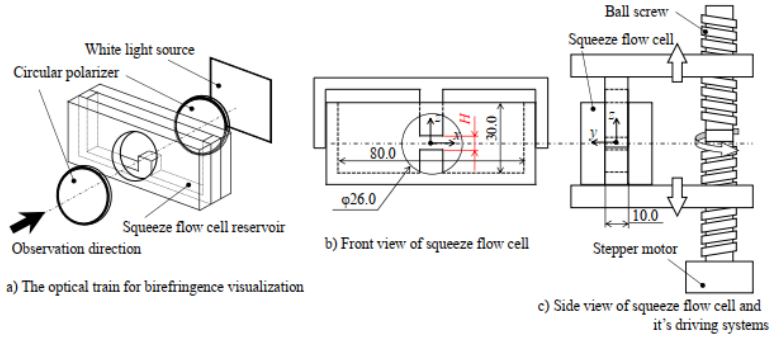

Figure 1 : The experimental apparatus and it's coordination system.

EXPERIMENTAL RESULTS AND DISCUSSION

Flow birefringence immediately after the start of squeeze motion

Fig. 2 shows a visualization of flow birefringence under the squeezing motion at an initial gap H_0=2.0 mm, amplitude A=2.0 mm, and frequency f=1.0 Hz. The image shows one cycle of squeeze motion divided into ten segments. **Fig. 2(a)** shows the image before the start of the flow, and **Fig. 2(k)** shows the state in which the squeeze plates return to its initial position. The dark background in **Fig. 2(a)** shows no birefringence. **Fig. 2(b)** and after show the results during the squeeze motion, and the change in color indicates the measure of birefringence. Squeeze motion begins in the direction which H increases. Therefore, the fluid is deformed in the z-axis direction from **Fig. 2(b)** to **(e)**. **Fig. 2(f)** is the top dead center, and the fluid is deformed in the x-axis direction from **Fig. 2(g)** to **(j)**. **Fig. 2(k)** is the initial position. Flow birefringence due to the deformation was observed very strongly in the z-axis direction from the stagnation point immediately after the start of flow. The birefringence around the stagnation point reached a maximum at **Fig. 2(e)** and entered a decreasing process at **Fig. 2(f)**. From **Fig. 2(g)** to **(j)**, the

fluid is deformed in the x-axis direction, but no strong birefringence is observed in the x-axis direction. It indicates that the flow birefringence that occurred in the z-axis direction is relaxing during this period. Birefringence is also observed in **Fig. 2(k)**, which returns to the initial position. Furthermore, the birefringence in **Fig. 2(k)** is larger than that in **Fig. 2(j)**, confirming the phase difference to the variation in the strain.

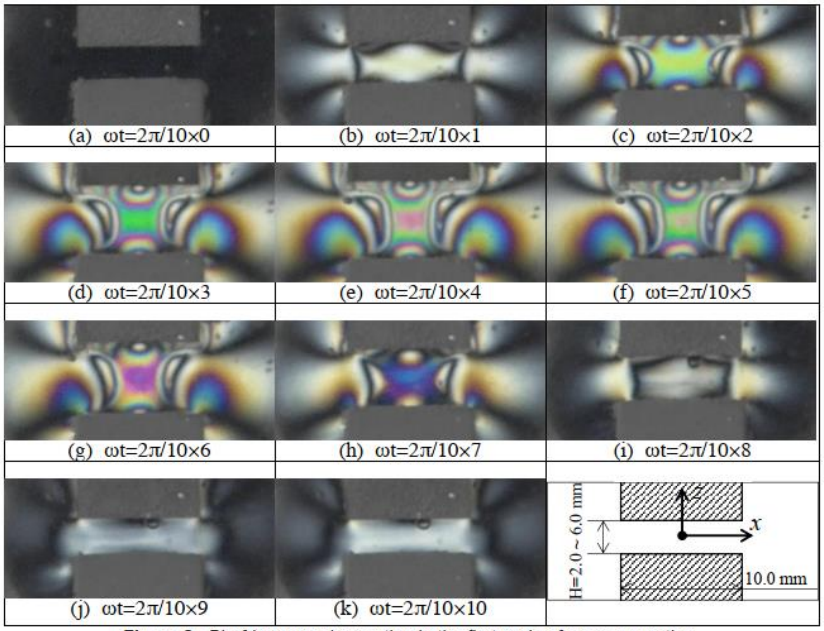

Figure 2 : Birefringence observation in the first cycle of squeeze motion.

REFERENCES

1. Kato, M., Takahashi T., and Shirakashi M., Influence of planar elongation strain on flow-induced structure and flow instability of CTAB/NaSal aqueous solution, *Trans. Jpn. Soc. Mech. Eng. Ser. B*, **72**, 1935–1942, 2006. https://doi.org/10.1299/kikaib.72.1935
2. Takahashi, T., and D. Sakata, Flow-induced structure change of CTAB/NaSal aqueous solutions in step planar elongation flow, *J. Rheol.*, **55**, 225–240, 2011. https://doi.org/10.1122/1.3528042
3. Sachsenheimer, D., Oelschlaeger, C., Müller,S., Küstner, J., Bindgen,S., and Norbert Willenbacher, N., Elongational deformation of wormlike micellar solutions, *J. Rheol.*, **58**(**6**), 2017-2042, 2014. https://doi.org/10.1122/1.4897965
4. Ito M., Yoshitake Y., Takahashi T., Shear-induced structure change in shear-banding of a wormlike micellar solution in concentric cylinder flow, *J. Rheol.*, **60**, 1019-1029 (2016). https://doi.org/10.1122/1.4961034

SAXS, SANS and Spectroscopy Study on High Tunability of a Block Copolymer by Strongly Selective Solvents

Shigeru Okamoto[1], Akifumi Matsushita[1]

[1]Nagoya Institute of Technology, Japan

ABSTRACT

Block copolymer copolymers (BCPs) generally form periodic structures on the order of tens of nanometers. The morphology and the dimension are determined by the volume fractions of the blocks, the segregation power described by the Flory-Huggins interaction parameter (χ), the molecular weight, and the molecular architecture.

The aim of this study is to control dimensions of microphase-separated structures, i.e., domain spacings for potential application of BCPs to photonic crystals with high tunability of wavelengths. BCPs are expected to play an important role in the development along this strategy because they form structures by self-assembly at less energy cost. Many researches on controlling domain spacings have been conducted by temperature change, constructive or destructive change of hydrogen bonding, compositional change in blend systems of BCPs.

In this study, we demonstrate the control of domain spacings by exposing diblock copolymers to solvents with selectivity to one or both constituent blocks; lamella-forming symmetric polystyrene-b–polyisoprene, PS-b-PI, diblock copolymers and three kinds of solvents were employed: dimethyl phthalate (DMP) selective for PS, n-tetradecane (C14) selective for PI, and dioctyl phthalate (DOP) as a neutral solvent. DMP and C14 selectively swell PS and PI, respectively, resulting in the enhancement of the segregation power between PS and PI and the increase in the domain spacing, while DOP shields the segregation power resulting in the decrease in the domain spacing[1-4].

METHODS AND MATERIALS

Two kinds of polystyrene-b-polyisoprene (PS-b-PI), designated SI-60 and SI-655, were synthesized by anionic living polymerization. SI-60 has weight averaged molecular weight (M_w) of 60.1k with M_w/M_n =1.03, where M_n is number averaged molecular weight, and has f_{PS} of 46.7 vol.%. SI-655 has M_w of 655k with M_w/M_n =1.09, and f_{PS} of 37.9 vol.%. DMP, C14 and DOP were used as described above. Small-angle X-ray scattering (SAXS) was measured with in-house apparatus, Nanoviewer (Rigaku), and at BL-40B2 at SPring-8. Reflection spectra measurement was conducted with Multispec-1500 (Shimadzu corp.), measurement wavelength of which ranges from 190nm to 800nm.

A diblock copolymer used for Small-angle Neutron Scattering was poly(styrene)-block-poly(methyl meth-acrylate) with a molecular weight of 2.4×10^5 g/mol. The volume fraction of PS was 0.43. We used two combinations of solvent mixtures ((i)tetrahydrofuran (THF) / water and (ii)toluene / methanol as a good and non-solvent, respectively). Small-angle Neutron

Scattering (SANS) measurement was conducted at 40M SANS Beamline in HANARO, Korea to evaluate the spatial distribution of the solvent molecules by the contrast variation method using the mixtures of protonated and deuterated solvents.

RESULTS AND DISCUSSION

By combination of protonated and deuterated solvents, the scattering length densities of block copolymer solutions were varied for the SANS experiments. From the primary peak intensities, the spatial distributions of the solvents were evaluated. THF and Toluene were mainly distributed into PS phase. However, Toluene was slightly selective for PS chain. From theoretical calculation on the basis of SCFT, THF and water were mainly distributed into PMMA phase and behaved as a single solvent. In the case of toluene and methanol mixture, however, toluene was mainly distributed into PS phase and methanol was inversely distributed into PMMA phase. These phenomena resulted in the increase in the segregation power in solutions.

We prepared various ratios of SI/DOP/DMP/C14 mixtures of SI-60 and SI-655. Each solution has different concentrations of the polymers and/or different ratios of DOP in the solvent mixture (DOP, DMP and C14). The volume ratios of DMP to C14 are fixed at 47:53 for SI-60 solutions, and 39.2:60.8 (50:50 by weight) for SI-655 solutions. Solutions at the volume ratio of DOP from 0 to 100% were prepared for SI-60. However, as for SI-655, at least ca. 28 vol.% of DOP was required to dissolve the polymer into the mixture. In Figure 1, the domain spacing of SI-60 solutions are shown as a function of the DOP ratio. We studied the solutions at the polymer concentration of 20, 30, 40 vol.%. Domain spacing was calculated from the first SAXS peak position by $2\pi/q_{max}$, where q_{max} is the first peak position. The SAXS profiles of the solutions at the lower ratio (0 to 40%) of DOP showed multiple scattering peaks. The ratios of the peak positions confirmed that the structure is lamella. The solutions at the higher ratios (50 to 100%) of DOP showed only one peak, from which it is difficult to identify the morphology. However, the morphology is most probably lamella in the weak segregation regime, because volume ratio of PS:PI and DMP:C14 are nearly 50:50. As shown in Figure 1, we successfully controlled domain spacing by adjusting the ratio of the selective solvents to the neutral solvent. As for the solution at the polymer concentration of 20 vol.%, the domain spacing varied from 28.8 to 107.9 nm, while that of neat SI-60 is 34.8 nm. In Figure 2, the reflection peaks of SI-655 is 34.8 nm.

In Figrue 2, the reflection peaks from the SI-655 solutions are shown. We observed the reflection peaks varying from 342.2 to 770.9 nm. In the past study, Urbas et al. conducted reflection wavelength control by blending PS and PI into SI. In their report[5], the reflection peak was ranged from c.a. 340 to 610 nm, and the full width at half maxima of those were ca. 70 nm at narrowest. In our study, the use of solvent mixture successfully yielded wider range and narrower peak width. From Figures 1 and 2, we can see the different behavior of the shift of domain spacing against the polymer concentration, e.g. SI-60 at 30% of DOP and SI-655 at 29% of DOP. They have almost the same concentration of DOP, although the rise of polymer concentration increase the domain spacing of SI-655 solution, while it decreases that of SI-60 solution. We consider that SI with the larger molecular weight (SI-655) has higher segregation power that was shielded in the solvent mixture with 29% of DOP by a so-called dilution effect while it increases for the lower molecular weight one (SI-60). As a conclusion, the effect of solvent mixture depends on the magnitude of the segregation power of the diblock copolymers.

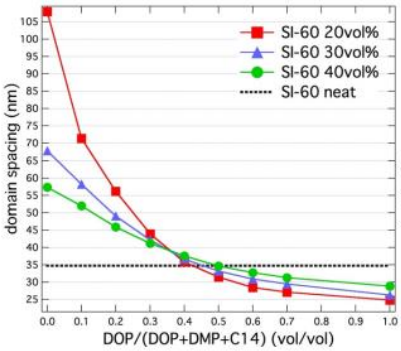

Figure 1: Domain spacing as a function of DOP ratio of SI-60 solutions at the polymer concentration of 20, 30 and 40 vol.%

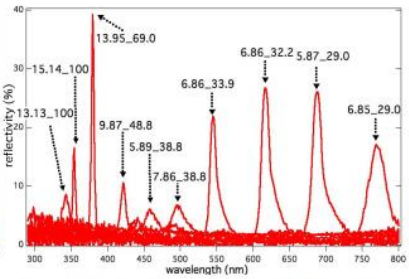

Figure 2 Reflection peaks from SI-655 solutions as a function of wavelength. Attached numbers represent polymer concentrations and DOP ratios in the solutions.

CONCLUSIONS

We prepared solutions of SI-60 and SI-655 with various ratio of PS-selective solvent (DMP), PI-selective solvent (C14) and a neutral solvent (DOP). In the SI-60 solution, we obtained lamella structure with the domain spacing varied from 28.8 to 107.9 nm by adjusting the neutral solvent ratio, while that of neat polymer is 34.8nm. The reflection peaks of SI-655 solutions shifted over the whole range of visible wavelength (342.2 to 770.9 nm). In brief, we found that domain spacing can be controlled over quite a large range by using solvent mixture.

ACKNOWLEDGEMENTS

The SAXS measurements were performed at the BL40B2 of SPring8 with the approval of the Japan Synchrotron Radiation Research Institute (JASRI) (Proposal No. 2011B1502, 2012B1476, 2013B1236). This work was supported by JSPS KAKENHI Grant No. 21550208 and 20K05603. SANS measurements were conducted at 40M SANS Beamline in HANARO, Korea.

REFERENCES

1. Fuse C.; Okabe S.; Sugihara S.; Aoshima S.; Shibayama M. *Macromolecules*, **37**, 7791-7798, 2004.
2. Ando K.; Yamanaka T.; Okamoto S., et al. *IOP Conf. Ser.: Mater. Sci. Eng.*, **14**, 012012, 2010.
3. Ando K.; Yamanaka T.; Okamoto S., et al. *J. Phys.: Conf. Ser.*, **247**, 012040, 2010.
4. Matsushita A.; Okamoto S. *Macromolecules*, **47**, 7169-7177, 2014.
5. Urbas A.; Sharp R.; Fink Y.; Thomas E. L., et al., *Advanced Materials*, **12(11),** 812-814, 2000.

Friday, May 18, 2023

Plenary Presentations: GEOG 100 (9:00 AM - 10:00 AM)

SUBSTRATE COLONIZATION BY AN EMULSION DROP PRIOR TO SPREADING

Arun Ramachandran[1]

[1]Department of Chemical Engineering and Applied Chemistry, University of Toronto, Canada.

ABSTRACT

In classical wetting, the spreading of an emulsion drop on a surface is preceded by the formation of a bridge connecting the drop and the surface across the sandwiched film of the suspending medium. However, this widely accepted mechanism ignores the finite solubility of the drop phase in the medium. We present experimental evidence of a new wetting mechanism, whereby the drop dissolves in the medium, and nucleates on the surface as islands that grow with time. Island growth is predicated upon a reduction in solubility near the contact line due to attractive interactions between the drop and the surface, overcoming Ostwald ripening. Ultimately, wetting is manifested as a coalescence event between the parent drop and one of the islands, which can result in significantly large critical film heights and short hydrodynamic drainage times prior to wetting. This discovery has broad relevance in areas such as froth flotation, liquid-infused surfaces, multiphase flows and microfluidics.

ACKNOWLEDGEMENTS

NSERC Discovery program (Grant #402005), Discovery Accelerator Supplement (RGPAS-2018-522652), Canada Research Chair (File # 950-231567), the Ontario Early Researcher Award (Grant #ER13-09-138)

REFERENCES

1. Borkar, S; Ramachandran, A. Substrate colonization by an emulsion drop prior to spreading *Nature Communications*, **12 (3)**, 5734, 2021. https://www.nature.com/articles/s41467-021-26015-2.

8TH PACIFIC RIM CONFERENCE ON RHEOLOGY, May 15-19, 2023

RHEOLOGY-DRIVEN CONTINUOUS IN-MELT SEPARATION OF PET/PE BLENDS AND LAMINATES: A NOVEL APPROACH TO RECYCLING

S. Vecchi, E. Kone, L. Hampton, H. Ghassemi, D. Schiraldi and J. Maia

Case Western Reserve University, Cleveland, USA

ABSTRACT

Multilayer, multicomponent films are widely used for their barrier properties, with more than 40 million tons of all plastic being produced annually being composed of multilayer polymer systems. This creates an enormous challenge as recycling of these multilayer systems is not technically feasible at large scales. In fact, the component plastics often have differing recycling pathways which prevents these films from being recycled. This work is aimed at developing a novel chemical-mechanical approach that leads to achieving in-process melt separation of polyethylene/polyethylene terephthalate (PE/PET) blends in twin-screw extrusion for posterior individual recycling. Herein, we pursue two strategies to achieve this goal:

1) We use various levels up to 1.00% w/w of pyromellitic dianhydride (PMDA) as a PET chain extender at 260 °C and demonstrate that significant chain-extension occurs up to 0.5% w/w/ of PMDA, while chain-branching becomes dominant above this PMDA level. The corresponding increase in PET viscosity, and consequently blend viscosity ratio, induces coalescence of the PET droplets, which can then be mechanically filtered out of the main PE melt stream. This work further studies the coalescing ability of the chain-extended PET vs. that of branched PET and determines the optimal PET modification levels to maximize droplet coalescence within the typical processing window in twin-screw extrusion of 2-3 minutes.

2) We use various levels up to 8% w/w of ethylene glycol (EG) to depolymerize PET at 260 °C and demonstrate that significant chain depolymerization occurs with a reduction of PET molecular weight (MW) greater than 95%. The corresponding decrease in PET MW allowed for the PET to be depolymerized to a level that was extractable with the aid of SC CO2. The resulting PET wax separated from the PET/LLDPE film was further depolymerized into monomeric form with the aid of zinc acetate. This work further studies the effect EG%, time, temperature, screw design, feed rate, and screw speed have on the depolymerization in a twin screw extruder. Two different reagents EG and BHET (Bis(hydroxyethyl)terephthalate) were used to look at the depolymerization efficiency, with EG being the more efficient depolymerization reagent.

Experimental Validation of Viscosity Homogenization Treatment System for Waste Plastic Recycling

Hiroki Endo[1], Takeharu Isaki[2], Takeru Yamamoto[1], Yasunori Sato[1] and Tsutomu Takahashi[1]

[1]Dept. of Mechanical Engineering, Nagaoka University of Technology,
1603-1 Kamitomioka, Nagaoka, Niigata 940-2188, Japan
[2]Polymers and Composite Materials Lab., R&D Center, Mitsui Chemicals, Inc.,
580-32 Nagaura, Sodegaura, Chiba 299-0265, Japan

ABSTRACT

Waste plastics are often a mixture of plastics in various states depending on the recycling process, which consists of sorting, washing, drying, and melt-blending, and making them into pellets[1]. Waste plastics are known to have reduced mechanical properties[2], and recycled plastics are often used by blending with virgin plastics. In molding processes, high-precision moldings in extrusion molding and injection molding rely on the uniformity of the flow characteristics of the plastics. Therefore, it is required that the viscosity is uniform even in the recycled pellets of waste plastic.

In this research, we developed the Viscosity Homogenization Treatment System[3] of waste plastic recycling and verified it experimentally. The system consists of two extruders, the lab-made in-line viscometer, and a control PC. To general verification, virgin plastics (polypropylene, PP) with different flow curves were used. For the target viscosity of the recycled plastic was reached, the volume fraction of the two virgin resins used as adjusting agents was controlled considering the transient viscosity change of PP measured by an in-line viscometer. Then melt-blending was carried out using a second extruder. As a result, the viscosity of the obtained recycled plastic agreed well with the target viscosity, demonstrating the system's effectiveness.

REFERENCES

1. Ito M. and Tsunekawa M. Recent Developments in plastic-plastic separation techniques. *Shigen-to-Sozai (The Mining and Materials Processing Institute of Japan)*, **122**, 142-149., 2006. https://doi.org/10.2473/shigentosozai.122.142.
2. Yao S.; Tominaga A.; Fujikawa Y.; Sekiguchi H.; Takatori E. Inner Structure and Mechanical Properties of Recycled Polypropylene. *Nihon Reoroji Gakkaishi (J. Soc. Rheol. Jpn.)*, **41**, 173-178., 2013. https://doi.org/10.1678/rheology.41.173
3. Isaki T.; Endo H.; Sato Y.; Takahashi T. Viscosity Homogenization Treatment of Waste Plastic Recycling, Development of Process and Control Methods. *Nihon Reoroji Gakkaishi (J. Soc. Rheol. Jpn.)*, **50**, 269-274., 2022. https://doi.org/10.1678/rheology.50.269

DEVELOPMENT OF COMPOSITE VIA SECONDARY POLYMER-INDUCED PARTICLE AGGREGATION AND DESTRUCTION OF ITS PARTICLE AGGREGATION DURING 3D PRINTING

Ji Hwan Kim, Joung Sook Hong,* Kyung Hyun Ahn

School of Chemical and Biological Engineering and Institute of Chemical Processes, Seoul National University, South Korea

ABSTRACT

The performance of polymer composite is determined depending on several parameters. Among them, particle dispersion and percolation structure control are the most important. In this study, poly(lactic acid) (PLA) composite was fabricated through a secondary polymer-induced particle aggregation. Particle dispersion was manipulated through the addition of secondary polymer with high-affinity to particles and analyzed corresponding changes in electrical conductivity and moduli. Through rheological scaling analysis of percolation structure, it was found that the addition of a small amount of secondary polymer induces diffusion of particle to form aggregates of high-order structure against interaction between particles. A ternary composite of PLA, poly(caprolactone) (PCL) and carbon black (CB) exhibited the PCL-induced CB aggregation when the amount of the PCL was comparable to that of particles. Particle percolation with a high-order structure improves the performance of composite like high storage modulus, high dielectric loss, and negative-positive switching of dielectric constant at high frequency (~ 100 Hz). Most of all, it induced a brittle-ductile transition to PLA. However, during 3D printing process of this ternary composite, CB aggregates were rearranged and percolation structure was disrupted under the given flow, resulting in a decrease in the modulus of the composite and lower electrical conductivity. Under high shear through nozzle, assemblies of CB aggregates could not remain close enough to maintain the percolation structure

ACKNOWLEDGEMENTS

This work was supported by the National Research Foundation of Korea(NRF) grant funded by the Korea government(MSIT) (No. 2020M3H7A1098305, No. 2021R1A2C1004746)

REFERENCES

1. Kim, J. H.; Hong, J. S.; Ahn, K .H. Secondary polymer-induced particle aggregation and its rheological, electrical, and mechanical effects on PLA-based ternary composites. *J. Rheol. Acta*, **66 (2)**, 275-291, 2022. https://sor.scitation.org/doi/abs/10.1122/8.0000366.
2. Ahn, Jung Hyun; Kim, Dahong; Park, Su A; Hong, Joung Sook; Ahn Kyung Hyun. Variation of the Electrical Conductivity of PLA-based Composites with a Hybrid of Graphene and Carbon Black During 3D Printing, Macromolecular Materials and Engineering, 2200145, 2022. https://onlinelibrary.wiley.com/doi/abs/10.1002/mame.202200145 8/79843-ms.

ANALYSIS OF OPERATING LIMITS OF VACUUM-ASSISTED SLOT DIE COATING OF HERSCHEL-BULKLEY FLUIDS

Myungjae Lee[1], Kyounghun Shin[2], and Jaewook Nam[1,*]

[1]Seoul National University, Seoul, Republic of Korea
[2]SAMSUNG SDI, Suwon, Republic of Korea

ABSTRACT

Shear-thinning and yield stress are two important rheological properties in the industrial using coating liquid, such as battery slurries. In this study, we use the Herschel-Bulkley constitutive equation to describe coating liquid flow. We develop a simple model by applying HB constitutive equation to the 1-D viscocapillary model. Additionally, the visualization experiment is performed using a custom-made apparatus that mimics all essential industrial-grade slot coater features to detect the location of gas/liquid interfaces and contact lines.

All of the coating windows obtained through experiments and modeling were depicted on the dimensionless space. The shape of dimensionless coating windows obtained from various dimensionless numbers is similar. The effect of yield stress is insignificant in Bi (Bingham number) about 0.1. However, when the Bi and Rgt (gap-to-thickness ratio) become larger, the yield stress effect should be considered. The effect of shear-thinning changes the dimensionless coating window dramatically. In high Rgt cases, the shear field under the die lip drastically deviates from the simple shear flow, and the shear thinning effect becomes more considerable.

REFERENCES

1. Tsuda, T. Coating flows of power-law non-Newtonian fluids in slot coating. *Nihon Reoroji Gakkaishi*, **38(4_5)**, 223-230, 2011
2. Lee, J., & Nam, J. A simple model for viscoplastic thin film formation for coating flows. *Journal of Non-Newtonian Fluid Mechanics*, **229**, 16-26, 2016

8TH PACIFIC RIM CONFERENCE ON RHEOLOGY, May 15-19, 2023

Effect of local relaxation time on drag reduction in turbulent boundary layer flow of viscoelastic fluids

Shinji Tamano[1], Hiromi Osawa[1], and Masakazu Muto[1]

[1]Nagoya Institute of Technology, Nagoya, Japan

ABSTRACT

We performed direct numerical simulations (DNSs) of a zero-pressure-gradient turbulent boundary layer flow of viscoelastic fluids with variations of solution concentration and temperature in order to investigate the effect of local variation in the relaxation time on the drag reduction. To this end, we proposed a new constitutive equation model based on the FENE-P model, c-T-FENE-P model, in which the FENE-P model was coupled with the scalar equations of solution concentration and temperature. In this study, DNSs for 6 cases of increasing and decreasing relaxation times with temperature were performed.

INTRODUCTION

As reported in recent reviews,[1] numerous DNS studies of wall-bounded turbulent flows of viscoelastic fluids can predict some experimental findings such as the steeper gradient of mean velocity profile in wall-units and more suppression of turbulence structures with the amount of the drag reduction. In the minimal channel flow, Xi & Graham[2] found that the instantaneous levels of polymer stretching and drag reduction were anticorrelated in time. Tamano et al.[3] also revealed that what occurs temporally in the minimal channel[2] was similar to what occurred spatially in boundary layer flow, and the streamwise profile of drag reduction ratio shifted downstream, as the Weissenberg number, i.e. the relaxation time became larger. However, the effect of local variation in relaxation time on the drag reduction still remains unknown in wall-bounded turbulent flows of viscoelastic fluids, since the relaxation time is constant in space and time in previous studies based on the FENE-P model. In this study, the effect of the local relaxation time on the drag reduction in wall-bounded turbulent flows is investigated by coupling the FENE-P model with equations of solution concentration and temperature.

NUMERICAL METHOD AND CONDITIONS

The non-dimensional governing equations for the incompressible viscoelastic flow are continuity and momentum equations:

$$\frac{\partial u_i}{\partial x_i} = 0, \frac{\partial u_i}{\partial t} + \frac{\partial u_i u_j}{\partial x_j} = -\frac{\partial p}{\partial x_i} + \frac{1-\beta}{Re_{\theta_0}}\frac{\partial E_{ij}}{\partial x_j} + \frac{\beta}{Re_{\theta_0}}\frac{\partial^2 u_i}{\partial x_j \partial x_j}, \quad (1)$$

where u_i is the velocity component, p is pressure, x_i is a spatial coordinate, t is time, and E_{ij} is the viscoelastic stress component. In this paper, x_1 (x), x_2 (y) and x_3 (z) directions are streamwise, wall-normal and spanwise, respectively. $\beta = \eta_s/\eta_0$ is the ratio of solvent viscosity η_s to zero shear rate viscosity of solution η_0. In the present study, the inflow condition for the boundary layer is given by the Lund's method,[4] so that the computational domain is divided into the main and driver parts in which the inflow condition for the main part is obtained. In Eq. 1, the momentum-thickness Reynolds number Re_{θ_0} is defined as, $Re_{\theta_0} = \rho U_e \theta_0/\eta_0$, where U_e is the free-stream velocity, θ_0 is the momentum thickness at the inlet plane of the driver part, ρ is density. The non-dimensional FENE-P constitutive equation for conformation tensor C_{ij} for inhomogeneous polymer solutions is as follows:[4]

$$\frac{\partial C_{ij}}{\partial t} + u_k \frac{\partial C_{ij}}{\partial x_k} - \frac{\partial u_i}{\partial x_k} C_{kj} - \frac{\partial u_j}{\partial x_k} C_{ik} = -nE_{ij}. \tag{2}$$

The viscoelastic stress component is related to the conformation tensor, $E_{ij} = (fC_{ij} - \delta_{ij})/Wi$, where f is the Peterlin function $f = L^2/(L^2 - Tr(C_{ij}))$, and L represents the maximum extension of polymer. The Weissenberg number Wi is defined as, $Wi = \lambda U_e/\theta_0$, where λ is the relaxation time.

In Eq. 2, n is the number of density, i.e. the polymer concentration which is described by the following equation:[4]

$$\frac{\partial n}{\partial t} + u_j \frac{\partial n}{\partial x_j} = \frac{1}{Pe_n} \nabla^2 n, \tag{3}$$

where $Pe_n = ScRe_{\theta_0}$ is the Péclet number for concentration. In this study, the Schmidt number is set at $Sc = 1$ for the computational limitation. We called this type of FENE-P model[4] coupled with the concentration equation "c-FENE-P model". In this model, the relaxation time is constant ($\lambda = \lambda_0$), so that Wi is the same as the setting Weissenberg number $Wi_0 (= \lambda_0 Ue/\theta_0)$.

In this study, moreover, we introduced the equation of the non-dimensional solution temperature T as follows:

$$\frac{\partial T}{\partial t} + u_j \frac{\partial T}{\partial x_j} = \frac{1}{Pe_T} \nabla^2 T, \tag{4}$$

where $Pe_T = PrRe_{\theta_0}$ is the Péclet number for temperature. In this study, the Prandtl number is set at $Pr = 1$ for simplicity. Here, it is assumed that the relaxation time λ is the simple function of the solution temperature, $\lambda(T) = \lambda_0 T^{\pm 0.5, \pm 1.0, \pm 2.0}$, so that the Weissenberg number is rewritten as,

$$Wi = \frac{\lambda(T) Ue}{\theta_0} = \frac{\lambda(T)}{\lambda_0} Wi_0. \tag{5}$$

We name this type of constitutive equation model "c-T-FENE-P model."

The second-order accurate finite difference scheme on a staggered grid is used. The semi-implicit time marching algorithm is used where the diffusion term in the wall-normal direction is treated implicitly with the Crank-Nicolson scheme, and the third-order Runge-Kutta scheme is used for all other terms. The setting momentum-thickness Reynolds and Weissenberg numbers are $Re_{\theta_0} = 670$ and $Wi_0 = 50$, respectively. The viscosity ratio is $\beta = 0.9$. The maximum extension of the polymer L is 100. The size of the computational domain for the present simulations is equal to $(L_x \times L_y \times L_z)$ $= (300\theta_0 \times 30\theta_0 \times 20\pi\theta_0/3)$ in the streamwise, wall-normal, and spanwise directions, respectively. The grid size is $(N_x \times N_y \times N_z) = (384 \times 64 \times 64)$. The concentration inlet boundary condition is given by the constant Gaussian profile.[4] The inflow temperature is constant ($T = T_{in}$), and the isothermal heated wall boundary condition ($T_w = 4T_{in}$) is imposed.

RESULTS

The streamwise variation in the drag reduction ratio DR is shown in Fig. 1. $DR(x)$ is defined as,

$$DR(x) = \frac{C_{f_{\text{Newtonian}}}(x) - C_{f_{\text{Viscoelastic}}}(x)}{C_{f_{\text{Newtonian}}}(x)}, \tag{6}$$

where $C_{f_{\text{Newtonian}}}(x)$ and $C_{f_{\text{Viscoelastic}}}(x)$ are the skin friction coefficients for Newtonian and viscoelastic fluids, which are functions of the streamwise position x and are evaluated at the same x. For the case of increasing relaxation time with temperature (open symbols), the DR of the c-T-FENE-P model is smaller than that of the c-FENE-P model ($\lambda = \lambda_0$), while it is larger for the case of decreasing relaxation time with temperature (closed symbols).

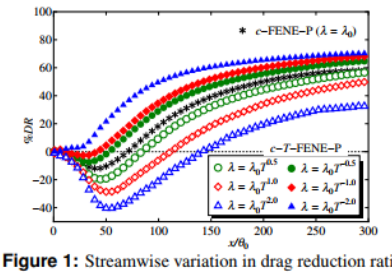

Figure 1: Streamwise variation in drag reduction ratio

CONCLUSIONS

Direct numerical simulations of the zero-pressure gradient drag-reducing turbulent boundary layer of viscoelastic fluids were performed using the proposed c-T-FENE-P model. The effect of local variation in the relaxation time on the drag reduction ratio was discussed.

ACKNOWLEDGEMENTS

This work was supported by a Grant-in-Aid for Scientific Research (JP15H03918, 20H02065) from Japan Society for Promotion of Science.

REFERENCES

1. Xi, L. Turbulent drag reduction by polymer additives: Fundamentals and recent advances, *Phys. Fluids*, **31**, No. 121302, 2019.
2. Xi, L., Graham M.D. Active and hibernating turbulence in minimal channel flow of Newtonian and polymeric fluids, *Phys. Rev. Lett.*, **104**, No. 218301, 2010.
3. Tamano, S., Graham, M.D., Morinishi, Y. Streamwise variation of turbulent dynamics in boundary layer flow of drag-reducing fluid, *J. Fluid Mech.*, **686**, 352-377, 2011.
4. Dimitropoulos, C.D., Dubief, Y., Shaqfeh, E.S.G., Moin, P. Direct numerical simulation of polymer-induced drag reduction in turbulent boundary layer flow of inhomogeneous polymer solutions, *J. Fluid Mech.*, **566**, 153-162, 2006.

TURBULENT DRAG REDUCTION WITH FLEXIBLE AND RIGID POLYMER SOLUTIONS: FROM LOW TO MAXIMUM DRAG REDUCTION

Rodrigo S. Mitishita[1], Gwynn J. Elfring[2], Ian A. Frigaard[1,2]

[1]Department of Mathematics, University of British Columbia, Vancouver, Canada
[2]Department of Mechanical Engineering, University of British Columbia, Vancouver, Canada

ABSTRACT

We present an experimental study of turbulent drag reduction with flexible and rigid polymer solutions in a 2:1 aspect ratio rectangular channel. The experiments are carried out at low drag reduction (LDR, $\%DR < 40$), high drag reduction (HDR, $\%DR > 40$) and maximum drag reduction (MDR, where the velocity profile U^+ roughly matches Virk's asymptote), with partially hydrolyzed polyacrylamide as a flexible polymer, and xanthan gum as a rigid polymer[1]. The rheology of the polymer solutions is characterized with a Malvern Kinexus Ultra+ Rheometer. We measure velocity profiles, streamwise and wall-normal Reynolds stresses and power spectra of streamwise velocity fluctuations with a Laser Doppler Anemometry (LDA) setup.

Our results[2] show similar effects of both polymeric additives on the velocity and Reynolds stress profiles, provided that the Reynolds numbers and $\%DR$ are also similar. At both HDR and MDR, the power spectral densities of streamwise velocity fluctuations of both XG and HPAM flows show a power-law decay near -3 instead of $-5/3$ in the inertial range. This slope was recently interpreted as evidence of elasto-inertial turbulence (EIT) in polymer jets[3]. At concentrations near 100 ppm, we observe that flexible polymer solutions are more effective at reducing drag, while XG can only reach MDR at very high concentrations. Therefore, we hypothesize that the formation of polymer aggregates with high concentrations contributes to increase viscoelasticity and $\%DR$ in rigid polymer solutions.

REFERENCES

1. Pereira A. S., Andrade R. M., Soares E. J., Drag reduction induced by flexible and rigid molecules in a turbulent flow into a rotating cylindrical double gap device: Comparison between Poly (ethylene oxide), Polyacrylamide, and Xanthan Gum, *J. Non-Newtonian Fluid Mech.*, **202**, 72–87, 2013.

2. Mitishita R. S., Elfring G. J., Statistics and spectral analysis of turbulent duct flows with flexible and rigid polymer solutions, *J. Non-Newtonian Fluid Mech.*, **311**, 104952, 2023.

3. Yamani S., Keshavarz B., Raj Y., Zaki T. A., McKinley G. H., Bischofberger I., Spectral universality of elastoinertial turbulence, *Phys. Rev Lett*, **127**, 074501, 2021.

RELATING ELASTOINERTIAL TURBULENCE TO THE PHENOMENOLOGY OF POLYMER DRAG REDUCTION

Lu Zhu[1] and Li Xi[1]

[1]Department of Chemical Engineering, McMaster University, Hamilton, Ontario, Canada

ABSTRACT

A small amount of flexible polymer additives may cause drastic reduction in turbulent friction drag. The rich dynamics of polymer-turbulence interplay behind the drag reduction (DR) phenomenon is reflected in the transitions in turbulent phenomenology between several distinct stages as the fluid becomes more elastic (higher Weissenberg number Wi)[1].

Starting from the Newtonian limit, there is initially no DR (NDR) until Wi reaches its onset level $\mathrm{Wi}_{\mathrm{onset}}$. As Wi further increases, the flow enters the low-extent DR (LDR) stage, where DR effects are contained in the turbulent buffer layer only[2]. Transition to the high-extent DR (HDR) stage is manifested by several distinct markers in flow statistics, especially those in the log-law layer[2]. There are still ongoing debates about conflicting observations in the HDR stage[1]. Finally, at sufficiently high Wi, the level of DR converges to the maximum DR (MDR) limit, whose full mechanism remains unexplained.

Recent discovery of the so-called elastoinertial turbulence (EIT), a distinct type of high-Wi flow instability where polymer elasticity feeds into, rather than suppressing, turbulent fluctuations, sparked much interest among researchers. We focus on building the connection between EIT and the phenomenology of DR, especially the multistage transitions in turbulent dynamics as described above. Several interesting findings arose during our investigation. First, although EIT has been widely associated with MDR, we found that MDR cannot be described by the simple convergence to a single EIT state[3]. Second, EIT shows up a lot earlier than MDR does. Its rise to dominance marks a previously unknown transition, which would explain the seemingly contradictory observations in HDR[4]. Third, opposite to the prevailing view, transition to EIT is triggered by a new linear instability[5], which is also a sharp contrast to the laminar-turbulent transition in Newtonian fluids.

On the numerical side, EIT dynamics cannot be captured with spectral methods because its sharp stress shockfronts would be smeared by the artificial diffusion term required for numerical stability. This has cast doubt over the general reliability of spectral methods in viscoelastic fluid simulation. We show that although artificial diffusion is detrimental to EIT structures, it has minimal impact on the traditional inertia-driven turbulence (IDT), provided that the numerical diffusivity is chosen at a proper magnitude[4,6]. Therefore, artificial diffusion can not only still be used in IDT, it also provides a way for us to separate the two types of turbulent dynamics by selectively removing EIT.

ACKNOWLEDGEMENTS

The authors acknowledge the financial support from the Natural Sciences and Engineering Research Council of Canada (NSERC; Nos. RGPIN-2014-04903 and RGPIN-2022-04720) and the allocation of computing resources awarded by the Digital Research Alliance of Canada (alliancecan.ca). The computation is made possible by the facilities of the Shared Hierarchical Academic Research Computing Network (SHARCNET: sharcnet.ca).

REFERENCES

1. Xi L, Turbulent drag reduction by polymer additives: Fundamentals and recent advances, *Phys. Fluids*, **31**, 121302, 2019.
2. Zhu L, Xi L, Distinct transition in flow statistics and vortex dynamics between low- and high-extent turbulent drag reduction in polymer fluids, *J. Non-Newton. Fluid Mech.*, **262**, 115–130, 2018.
3. Zhu L, Xi L, Nonasymptotic elastoinertial turbulence for asymptotic drag reduction, *Phys. Rev. Fluids*, **6**, 014601, 2021.
4. Zhu L, Xi L, The role of elastoinertial turbulence in the multistage transitions of viscoelastic turbulent channel flow, *in preparation*.
5. Zhu L, Xi L, Direct transition to elastoinertial turbulence from a linear instability in channel flow, arXiv:2211.09366, 2022.
6. Zhu L, Xi L, Inertia-driven and elastoinertial viscoelastic turbulent channel flow simulated with a hybrid pseudo-spectral/finite-difference numerical scheme, *J. Non-Newton. Fluid Mech.*, **286**, 104410, 2020.

8TH PACIFIC RIM CONFERENCE ON RHEOLOGY, May 15-19, 2023

Modular material properties in bimodal blends of amine functionalized polyolefins

Benjamin M. Yavitt[1,2,3], Ziyue Zhang[2], Damon J. Gilmour[3,4], Laurel L. Schafer[3], Savvas G. Hatzikiriakos[2]

[1]Department of Chemical Engineering, University of Cincinnati, Cincinnati, OH, USA
[2]Department of Chemical and Biological Engineering, University of British Columbia, Vancouver, B.C., Canada
[3]Department of Chemistry, University of British Columbia, Vancouver, B.C., Canada
[4]a2o Advanced Materials Inc., Vancouver, B.C, Canada

ABSTRACT

The rheological properties of associating polymers are driven by a combination of entanglements and dynamic intermolecular interactions between chains. Binary mixtures of aminopolyolefin associating polymers with low and high molecular weight (M_w) were prepared at systematic mass fractions. The ability to tune rheological, mechanical, and adhesive properties was investigated. A transition from viscoelastic liquid to elastic solid is traversed between the limits of low and high M_w by controlling the ratio of the two components. As the fraction of high M_w increases, the mechanical properties (Young's modulus, tensile strength) increase. Transitions between cohesive and adhesive bonding to low surface energy substrates are also observed, while the peel and lap shear strength can be tuned by the molecular weight distribution. Due to the high density of polar amine groups, recoverable adhesion on poly(tetrafluoroethylene) is facilitated by the inherent self-healing ability of the associating polymers. The adhesion strength recovers monotonically with healing time. Controlling the ratio of low and high M_w could be used to accurately control material properties from two simple component feedstocks, replicating the behavior of an individual monomodal sample.

ACKNOWLEDGEMENTS

NSERC, MITACS and CREATE Sustainable Synthesis are gratefully acknowledged for funding. The work was supported in part by the Canada Research Chairs program.

LINEAR VISCOELASTIC PROPERTIES OF COMB-SHAPED RING POLYSTYRENES

Yuya Doi[1]

[1]Nagoya University, Nagoya, Japan

Ring polymers with no chain ends and their derivatives (having both ring and linear units in their structures) are known to exhibit characteristic viscoelastic properties.[1] Thus, it is important to correctly understand their properties through experiments using model samples with well-defined structures and analyses based on molecular models. This study examined linear viscoelastic properties in melt of a series of comb-shaped ring (RC) polystyrene samples with different branch chain length, i.e., the molecular weight of the ring backbone M_{bb} ($\simeq 4M_e$ where M_e is the entanglement molecular weight) and linear branch chains M_{br} ($\simeq M_e$, $2M_e$ and $4M_e$), with the average number of branch chains $f \simeq 20$.[2,3] Even for the RC sample with the shortest branch chains, a plateau region of the dynamic modulus $G^*(\omega)$ was observed in the middle angular frequency ω regime. The longer the branch chains of the RC samples, the wider plateau region became, suggesting that intermolecular branch chain entanglement occurs. In the ω region between the plateau and terminal region, $G^*(\omega)$ with a weaker ω dependence than the terminal relaxation was observed. This behavior at low ω was more pronounced for the corresponding linear comb (LC) sample than the RC one. Moreover, the obtained $G^*(\omega)$ data were analyzed by two models: the comb-Rouse in which the structure of the RC/LC molecules is considered by graph theory,[4] and the Milner-McLeish model for entangled star-shaped polymers.[5] The former model qualitatively described the terminal relaxation behavior of $G^*(\omega)$ at low ω, but failed to reproduce the plateau in the middle ω range. In contrast, the latter model described the entanglement plateau in the middle ω, but the difference in the terminal relaxation regime between the RC/LC samples, which was seen in the comb-Rouse model as well as in the data, was disappeared.

1. Doi, Y. Rheological Properties of Ring Polymers and Their Derivatives. *Nihon Rheoroji Gakk. (J. Soc. Rheol. Jpn.)*, **50 (1)**, 57–62., 2022. https://doi.org/10.1678/rheology.50.57.

2. Doi, Y.; Iwasa, Y.; Watanabe, K.; Nakamura, M.; Takano, A.; Takahashi, Y.; Matsushita, Y. Sythesis and Characterization of Comb-Shaped Ring Polystyrenes. *Macromolecules*, **49 (8)**, 3109–3115, 2016. https://doi.org/10.1021/acs.macromol.6b00208.

3. Doi, Y.; Kitamura, J.; Uneyama, T.; Masubuchi, Y.; Takano, A.; Takahashi, Y.; Matsushita, Y. Viscoelastic Properties of Comb-Shaped Ring Polystyrenes. *Polym. J.*, **54 (12)**, 1267–1277, 2022. https://doi.org/10.1038/s41428-022-00686-0.

4. Nitta, K. A Graph-Theoretical Approach to Statics and Dynamics of Treelike Molecules. *J. Math. Chem.*, **25(2–3)**, 133–143, 1999. https://doi.org/10.1023/A:1019176215208.

5. Milner, S. T.; McLeish, T. C. B. Parameter-Free Theory for Stress Relaxation in Star Polymer Melts. *Macromolecules*, **30 (7)**, 2159–2166, 1997. https://doi.org/10.1021/ma961559f.

APPLICATION OF A ROBUST SELF-HEALING EXPERIMENTAL PROTOCOL FOR ASSOCIATING POLYMERS

N. Moradinik[1], B.M. Yavitt[1,2], Z. Zhang[1], N. Kuanr[2], D.J. Gilmour[2], E. Mohammadi[2], L.L. Schafer[2], and S.G. Hatzikiriakos[1]

[1] Department of Chemical and Biological Engineering, University of British Columbia, Vancouver, B.C, Canada, V6T 1Z3

[2] Department of Chemistry, University of British Columbia, Vancouver, B.C, Canada, V6T 1Z4

ABSTRACT

Catalytically synthesized amine-containing polymers have been reported to possess enhanced rheo-mechanical adhesion and self-healing properties. While the rheo-mechanical and adhesive properties can be consistently and reliably measured using well established experimental protocols, self-healing behavior requires further investigation to gain a better understanding of critical parameters to be considered for a consistent evaluation. In this study, we developed a self-healing protocol for a class of newly synthesized amine-functionalized polyolefins. A dynamic mechanical analyzer is used to determine the impact of critical time scales such as the waiting time before the damaged pieces are brought together, the healing time, characteristic relaxation times of the polymers (reptation and lifetime of associations) and the contact force to critically evaluate the self-healing rate of the materials under examination.

To achieve a good healing performance at room temperature, we also combined hydrogen and ionic bonding, two different types of dynamic interactions, in aminated polyolefins. This combination results in high toughness along with a relatively fast self-healing rate.

8TH PACIFIC RIM CONFERENCE ON RHEOLOGY, May 15-19, 2023

RHEOLOGICAL CHARACTERIZATION OF SUSPENSIONS GENERATED FROM COPPER ORES O VARYING MINERALOGICAL FEATURES AT GRINDING CONDITIONS

Leopoldo Gutiérrez[1,2], Andreés Ramirez[1], and Luver Echeverry[1]

[1]Department of Metallurgical Engineering, Universidad de Concepcion, 4070371 Concepción, Chile
[2]Water Research Center for Agriculture and Mining (CRHIAM), University of Concepcion, 4070411 Concepción, Chile

*Correspondence: lgutierrezb@udec.cl

ABSTRACT

An important stage of copper processing is grinding as it is responsible for more than 60% of the energy consumption as well as of plants production. All the grinding phenomena strongly depend on the rheological behavior of the slurries generated from the mixture of the fine particles generated in the process, and water. The operational results of grinding circuits indicate that one of the variables that has significantly impacted its performance is associated with the rheological behavior of the treated suspensions. Additionally, it is observed that the rheological behavior varies significantly depending on the mineral blends processed.

The objective of this work was to analyse the effect of the ore type on the rheological behavior of the suspensions generated from 7 ore samples of varying mineralogical characteristics using seawater. Rheological flow curves were obtained by using the *infinite gap approach* technique in a Haake VT-550 rheometer. The effect of pH, solids content, sodium hexametaphosphate and sodium silicate on the rehological behavior of the resulting suspensions was studied.

The results indicated a wide range of rheological behaviors that are strongly influenced by the type of mineral. The results clearly show that the solids content of the suspensions has an important effect on the yield stress. This result is very important for mining operations since minor variations in the control of the solids content in the secondary grinding circuit can have important effects on the pulp transport in the mills. The results also show that lime addition generates an increase in the yield stress of suspensions, which is associated with the precipitation of magnesium and calcium hydroxyl-complexes in seawater. These compounds generate particles aggregation and an increase in the yield stress and viscosity of the pulp. This conclusion is a relevant precedent to be considered in other operations that also use seawater. Finally, sodium hexametaphosphate and sodium silicate showed no significant effects on the rheological behavior of the suspensions.

Rheological characterization of suspensions generated from copper ores o varying mineralogical features at grinding conditions

Acknowledgments: We thank Centro CRHIAM Project ANID/FONDAP/15130015, project ANID/FSEQ/210002 for financial support. L.G. thanks projects ANID/ FONDECYT /1211705 and ANID/ACT210030.

QUANTIFYING THE EFFECTS OF FINES AND CLAYS ON MINERAL TAILINGS DEWATERING

Anthony D. Stickland, Yuxuan Luo, Sajid Hassan, Nilanka I. K. Ekanayake and Peter J. Scales

ARC Centre of Excellence for Enabling Eco-Efficient Beneficiation of Minerals
Department of Chemical Engineering, The University of Melbourne, Parkville, Australia

ABSTRACT

Mineral beneficiation produces tailings, which is finely ground waste rock. Tailings undergo dewatering via thickening and filtration to increase solids content and recycle process water. However, there can be substantial clay and fine particles in tailings. This causes poor dewatering that can reduce plant throughput, increase additive dosage, or decrease final solids content. In practical terms, mineral processors are keen to understanding the allowable amounts of fines or clay before catastrophic impacts to process performance.

Compressive Rheology[1], uses the compressive yield stress, $p_y(\phi)$, to describe network strength or compressibility, and the hindered settling function, $R(\phi)$, to describe the fluid-liquid drag or permeability. In this work, we measure the compressibility and permeability of a range of synthetic tailings suspensions using filtration[2] and sedimentation[3] methods. The synthetic tailings are calcium carbonate of various sizes with kaolin added to some. Fine particles and clay are usually detrimental to both compressibility and permeability, although there are some subtle effects on compressibility where small particles can sit in the interstices of large particles. Since suspension composition can affect both compressibility and permeability, there is not a single number to describe the effects of fines and clays on solid-liquid separation processes. Therefore, this work uses the measured solid-liquid separation properties of the synthetic tailings suspension in models of filter presses[4] and thickeners[5] to quantify the dewatering performance. The results show that fines and clays are always detrimental to filter and thickener performance. Mineral processing must either reduce output solids concentration to maintain throughput or reduce throughput to maintain final solids concentration.

REFERENCES

1. Buscall R, White LR. The consolidation of concentrated suspensions. Part 1.-The theory of sedimentation. *J Chem Soc, Faraday Trans 1*. 1987;83(3):873-891.
2. de Kretser RG, Usher SP, Scales PJ, Boger DV, Landman KA. Rapid filtration measurement of dewatering design and optimisation parameters. *AIChE J*. 2001;47(8):1758-1769.
3. Lester DR, Usher SP, Scales PJ. Estimation of the hindered settling function R(ϕ) from batch settling tests. *AIChE J*. 2005;51(4):1158-1168.
4. Stickland A, De Kretser R, Scales P, Usher S, Hillis P, Tillotson M. Numerical modelling of fixed-cavity plate-and-frame filtration: Formulation, validation and optimistion. *Chem Eng Sci*. 2006;61(12):3818
5. Usher SP, Scales PJ. Steady state thickener modelling from the compressive yield stress and hindered settling function. *Chemical Engineering Journal*. Aug 2005;111(2-3):253-261.

MODELLING HIGH-PRESSURE DEWATERING ROLLS FOR MINERAL TAILINGS

Nilanka I. K. Ekanayake[1,2], Sajid Hassan[1,2], Dalton J. E. Harvie[1], Robin J. Batterham[1], Peter J. Scales[1,2] and Anthony D. Stickland [1,2]

[1]Department of Chemical Engineering, The University of Melbourne, Parkville, Australia
[2]ARC Centre of Excellence for Enabling Eco-Efficient Beneficiation of Minerals, Australia

ABSTRACT

Mineral tailings are solid-liquid suspensions that contain finely ground waste rock particles and processed water. To ensure safe storage and disposal of tailings and minimise water usage, it is crucial to increase the solid concentration of the suspension and recover water through various dewatering techniques. A novel filtration technology, coined High Pressure Dewatering Rolls (HPDR) designed and developed at the University of Melbourne[1], is currently being investigated through experiments and modelling to utilise as a secondary dewatering stage following the thickening process.

To understand the flow dynamics and cake formation inside the HPDR, a modified two-fluid framework[2] that accounts for multi-particle effects is used in this study. The model includes material-dependent functions describing suspension compressibility, permeability, and a solid volume fraction-dependent viscosity model partitioned between the solid and liquid phases. On application of a vacuum pressure to the permeable rolls, preliminary results show filter cake formation on the rolls and an increase of cake thickness along the roller surface. The cake is forced through the gap between the rollers, exposing it to a high compressional load. Further, simulations show that the part of the formed cake near the top surface of the roll is swept away as the feed suspension falls on top of the cake (see Fig 1). Shifting the feed location to the bottom of the HPDR shows no disturbance to the cake formation, suggesting the possibility of utilising the simulation results in optimising the HPDR design and throughput.

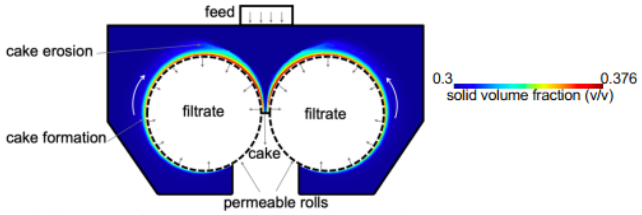

Figure 1: Filter cake formation inside the HPDR in a 2D transient simulation.

REFERENCES

1. Scales, P. J.; Tordesillas, A.; Stickland, A. D.; Batterham, R. J. Separation of liquid from a material. AU patenet 283684, October, 4, 2017.
2. Harvie, D. J. E. An implicit finite volume method for arbitrary transport equations. *ANZIAM Journal*, **52**, C1126-C1145, 2010.

Influence of fluid type in the transition from spray to roping in hydrocyclones

Fernando Betancourt[1], Pablo Cornejo[2], Daniel Reyes[1]

[1]Department of Metallurgical Engineering, University of Concepción, Chile
[2]Department of Mechanical Engineering, University of Concepción, Chile

ABSTRACT

Water recovery in mineral processing operations has been proven that depends strongly on the performance of the classification equipments. Hydrocyclones are widely used as the main classification operations in the copper industry in Chile and their understanding is crucial for any effort in the optimization of water consumption. In this work, we perform an experimental study of roping in hydrocyclones[1,2] using as a base, a Bingham-type fluid, and another Pseudo-plastic that follows a power law[3]. In particular, the transition from spray to roping was analyzed based on the parameters that characterize the constitutive equations of the different fluids. A strong dependence was found between the hydrocyclone discharge angle and the fluid rheology for both types of fluids.

The authors acknowledge the support of ANID/FONDAP/15130015

REFERENCES

1. Pérez, D., Cornejo, P., Rodríguez, C., & Concha, F. (2018). Transition from spray to roping in hydrocyclones. Minerals Engineering, 123, 71-84.
2. Daza, J., Cornejo, P., Rodriguez, C., Betancourt, F., & Concha, F. (2020). Influence of the feed particle size distribution on roping in hydrocyclones. Minerals Engineering, 157, 106583.
3. Tavares, L. M., Souza, L. L. G., Lima, J. R. B. D., & Possa, M. V. (2002). Modeling classification in small-diameter hydrocyclones under variable rheological conditions. Minerals Engineering, 15(8), 613-622